Design and Development of Configurational Biomimesis

Molecularly Imprinted Polymer Nanoparticles for

Clinical Analysis of Chiral Drugs

Sirirat Rakkit

A Thesis Submitted in Partial Fulfillment of the Requirements for the

Degree of Doctor of Philosophy in Pharmaceutical Sciences

Prince of Songkla University

2017

Thesis Title   Design and Development of Configurational Biomimesis Molecularly Imprinted Polymer Nanoparticles for Clinical Analysis of Chiral Drugs

Author   Miss Sirirat Rakkit

Major Program   Pharmaceutical Sciences

Major Advisor

....

(Assoc. Prof. Dr. Roongnapa Srichana)

Examining Committee:

....Chairperson

(Assoc. Prof. Dr. Suwipa Ungphaiboon)

....Committee

(Asst. Prof. Dr. Chutima Jantarat)

....Committee

(Assoc. Prof. Dr. Roongnapa Srichana)

....Committee

(Dr. Neeranuch Phusunti)

The Graduate School, Prince of Songkla University, has approved this thesis as partial fulfillment of the requirements for the Doctor of Philosophy Degree in Pharmaceutical Sciences.

....

(Assoc. Prof. Dr. Teerapol Srichana)

Dean of Graduate School

This is to certify that the work here submitted is the result of the candidate's own investigation. Due acknowledgement has been made of any assistance received.

…………................................Signature

(Assoc. Prof. Dr. Roongnapa Srichana)

Major Advisor

…………................................Signature

(Miss Sirirat Rakkit)

Candidate

I hereby certify that this work has not been accepted in substance for any degree,

and is not being currently submitted in candidature for any degree.

………..…………...Signature

(Miss Sirirat Rakkit)

Candidate

ชื่อวิทยานิพนธ์   การออกแบบและการพัฒนาของพอลิเมอร์ที่มีรอยพิมพ์ประทับโมเลกุลชนิด
นาโนพาร์ทิเคิล ที่มีความจดจำแบบคอนฟิกุเรชันนอลไบโอมิเมซิสและการ
ประยุกต์ใช้สำหรับการวิเคราะห์ทางคลินิกของอิแนนทิโอเมอร์ของยาไครัล
ผู้เขียน   นางสาวศิริรัตน์ รักกิจ
สาขาวิชา   เภสัชศาสตร์
ปีการศึกษา   2559

บทคัดย่อ

วัตถุประสงค์ของงานวิจัยนี้เพื่อศึกษาและออกแบบการสังเคราะห์พอลิเมอร์ที่มีรอยพิมพ์
ประทับโมเลกุลขนาดนาโนพาร์ทิเคิล (Molecularly Imprinted Polymer Nanoparticles; MIPs
nanoparticles) ซึ่งพอลิเมอร์มีรอยพิมพ์ประทับโมเลกุลแบบสามมิติซึ่งอยู่ในรูปของอนุภาคขนาดนาโน
ที่จำเพาะนั้น ถูกออกแบบโดยใช้โมเลกุลตัวพิมพ์คือ อาร์- หรือ เอส-ทาลิโดไมด์ (*R*)- หรือ (*S*)-
thalidomide   พิมพ์ประทับโมเลกุลขนาดนาโนพาร์ทิเคิลแบบสามมิติ โดยใช้วิธี multi-step-
swelling polymerization โดยใช้มอนอเมอร์ฟังก์ชั่นสองชนิดคือ methacrylic acid (MAA) และ
1-vinyl-2-pyrrolidone (NVP) ซึ่งมีหมู่ฟังก์ชันเฉพาะที่เกิดอันตรกิริยาอย่างเหมาะสมกับโมเลกุล
ตัวพิมพ์ โดยมอนอมอร์ที่เป็นตัวเชื่อมโยงคือ *N,N'*-(1,2-dihydroxyethylene)   bisacrylamide
(DHEBA) เกิดปฏิกิริยาพอลิเมอร์ไรเซชั่นในตัวทำละลายโทลูอีน (toluene)   นอกจากนี้การปรับ
สัดส่วนระหว่างมอนอเมอร์และตัวพิมพ์จะช่วยทำให้การเกิดอันตรกิริยาดีขึ้นในขบวนการพอลิเมอร์ไร
เซชัน เพื่อให้การสร้างรอยพิมพ์ประทับในระดับนาโนมีความจำเพาะที่สูง จากนั้นมีการศึกษา
คุณสมบัติทางกายภาพของพอลิเมอร์ที่มีรอยพิมพ์ประทับโมเลกุลขนาดนาโนพาร์ทิเคิลของอาร์- หรือ
เอส-ทาลิโดไมด์โดยใช้เทคนิคฟูเรียร์ทรานสฟอร์มอินฟราเรดสเปคโตรสโคปี (FT-IR) กล้องจุลทรรศน์
อิเล็กตรอนแบบส่องกราด (SEM) เครื่องวัดอนุภาคขนาดนาโนพาร์ทิเคิล (zeta nanoparticle)
นอกจากนี้ได้ตรวจประเมินคุณสมบัติพื้นผิวของพอลิเมอร์ที่มีรอยพิมพ์ประทับโมเลกุลด้วยกล้อง
จุลทรรศน์แรงอะตอม (AFM)   และตรวจวัดแรงกระทำที่พื้นผิวร่วมกับการตรวจรามานสเปกตรา
ศึกษาประสิทธิภาพของการจดจำต่ออิแนนทิโอเมอร์ของทาลิโดไมด์โดยใช้เทคนิคการสกัดด้วยวัฏภาค
ของแข็ง (SPE) โดยมีเรซินเป็นเฟสของตัวดูดซับของแข็งเพื่อศึกษาผลของการทำให้เข้มข้นและการ

แยกระหว่างคู่อิแนนทิโอเมอร์จากราซิมิคของยาทาลิโดไมด์ จากตัวทำละลายอะซิโตไนไตรท์ที่มีน้ำ
และเลือด จากผลการทดลองพบว่าการประยุกต์ใช้ของพอลิเมอร์ที่มีรอยพิมพ์ประทับโมเลกุลขนาดนา
โนพาร์ทิเคิลของอิแนนทิโอเมอร์ของทาลิโดไมด์กับเรซิน สามารถที่จะแยกคู่อิแนนทิโอเมอร์และสารที่
เชื่อมโยงกับทาลิโดไมด์

นอกจากนี้ได้ทำการเตรียมตัวตรวจวัดที่เตรียมจากพอลิเมอร์ที่มีรอยพิมพ์ประทับโมเลกุลบน
นาโนพาร์ทิเคิลของตัวพิมพ์อิแนนทิโอเมอร์ โดยองค์ประกอบของพอลิเมอร์ได้มีการตรวจสอบ
คุณสมบัติจนเหมาะสำหรับนำไปเคลือบบนตัวแปลงสัญญาณอินเตอร์ดิจิเตทคอนดักโตเมทตริก
อิเล็กโทรด (IDC) เพื่อพัฒนาเป็นเครื่องมือที่มีความไวและมีประสิทธิภาพสูงสำหรับตรวจสัญญาณ
ความต้านทานของเซ็นเซอร์ต่ออิแนนทิโอเมอร์ทั้งสอง สัญญาณความต้านทานการตรวจวัดสอดคล้อง
กับความเข้มข้นของทาลิโดไมด์ที่เพิ่มขึ้น และสามารถตรวจวัดสัญญาณความต้านทานที่ระดับความ
เข้มข้นต่ำของทาลิโดไมด์ และปรากฏสัญญาณที่คงที่ขึ้นกับสูตรของพอลิเมอร์ และได้มีการทดสอบ
การตรวจวัดทั้งในสภาวะในตัวทำละลายและจากการเติมสารชีวโมเลกุลได้แก่ เซราไมด์ (ceramide),
คอเลสเตอรอล (Cholesterol), และโปรตีนอัลบูมิลวัว (bovine serum albumin) ในเลือดซึ่ง
สามารถตรวจทาลิโดไมด์ได้ในระดับที่ต่ำถึง 6.4 ng mL^{-1} [ในช่วงความเข้มข้นระหว่าง 0.025-100 µg
mL^{-1}] เซ็นเซอร์ที่เตรียมได้เมื่อใช้ MIP เป็นตัวตรวจวัดสัญญาณจะมีความไวและความเลือกจำเพาะสูง
จากนั้นตรวจวิเคราะห์เพื่อยืนยันตำแหน่งเฉพาะที่ของตัววิเคราะห์อิแนนทิโอเมอร์ โดยใช้เทคนิคกล้อง
จุลทรรศน์แรงอะตอม (AFM) และรามานอะตอมมิคฟอดไมโครสโครปี (Raman-AFM) เพื่อตรวจ
สภาพผิวของอิเล็กโทรดหลังสัมผัสกับสารชีวโมเลกุลและอันตรกิริยาที่เกิดขึ้นระหว่างทาลิโดไมด์
อิแนนทิโอเมอร์ บนรอยพิมพ์ประทับโมเลกุลและผลของสารชีวโมเลกุลในเลือดต่ออิแนนทิโอเมอร์ ที่
สามารถแยกความแตกต่างของแรงดึงดูดของ (*R*)-thalidomide (100 nN) ขณะที่แรงลดลงอย่างมาก
ของ (*S*)-thalidomide (0.01 nN) สอดคล้องกับแรงกระทำบนผิวของอิเล็กโทรดซึ่งแตกต่างกันอย่าง
ชัดเจนระหว่างอิแนนทิโอเมอร์ทั้งสองบนพอลิเมอร์ที่มีรอยพิมพ์ประทับโมเลกุลในเลือดและมี
ประโยชน์ในการประเมินของการนำส่งยาโดยกล้องจุลทรรศน์แรงอะตอมที่ทำให้แยกความแตกต่าง
ของบริเวณเฉพาะที่ได้ดีขึ้นในระดับ 1-2 Å เมื่อตรวจด้วย SERS spectra และจากผลการศึกษาทำให้
สามารถที่จะออกแบบอุปกรณ์การตรวจวัดในสภาวะที่มีเลือดและสารชีวโมเลกุล ซึ่งการออกแบบการ
ตรวจวัดเพื่อให้เกิดความจำเพาะกับอิแนนทิโอเมอร์เป้าหมายที่มีฤทธิ์ทางชีวภาพ สมบัติทางสเตอริโอ
เคมี และอันตรกิริยาที่เกิดขึ้นระหว่างทาลิโดไมด์ในปริมาณที่ต่ำมากกับการเพิ่มความแตกต่างในการ

ตรวจวัดของแรงที่สำคัญของอิแนนทิโอเมอร์ด้วยความแตกต่างของลักษณะผิวที่ระดับนาโน ที่สามารถ
ตรวจด้วย MIP-SPE และการใช้ MIP เป็นเซนเซอร์สำหรับตรวจการนำส่งยาและใช้เป็นแนวทาง
สำหรับการประเมินผลการวิเคราะห์ทางคลินิก

Thesis Title Design and Development of Configurational Biomimesis Molecularly Imprinted Polymer Nanoparticles for Clinical Analysis of Chiral Drugs

Author Miss Sirirat Rakkit

Major Program Pharmaceutical Sciences

Academic Year 2016

ABSTRACT

In this study, it was to develop molecularly imprinted polymer nanoparticles (MIPs nanoparticles) for selective recognition to (*R*)-, and (*S*)-thalidomide for assessment of chiral drugs in blood. The selectivity of these materials that enable them to selectively bind the (*R*)-thalidomide and (*S*)-thalidomide was created using either as a core shell and non-core shell polystyrene. Firstly, the MIP microspheres were produced using a mixture of methacrylic acid (MAA) and 1-vinyl-2-pyrolidone as a mixed functional monomer that was then cross-linked using *N,N'*-(1,2-dihydroxyethylene) bisacrylamide (DHEBA), followed by high pressure homoginization. The amounts of the added monomers required to prepare the resultant MIP nanoparticles were optimized. To ensure that the imprinting affect its suitability for the combination of MIPs and other ingredients into a nanosized scale was examined. The performances of the thalidomide imprinted nanoparticles were characterized using Fourier Transform Infrared Spectroscopy (FT-IR), scanning electron microscope (SEM) and a zeta nanosizer. In addition the atomic force microscopy images of the molecularly imprinted nanoparticles were obtained to

examine the surface behaviors and force curve analysis. They were mixed with the resin to study the recognition ability by the different MIPs solid-phase extraction for enrichment the two enantiomers and racemic compounds followed by their detection by HPLC. It was shown that each of the enantiomers was recognized by the appropriate MIP and enriched it in the presence of the other biomolecules into the blood.

These molecularly imprinted nanoparticles were then attached to a glass substrate and used to form an interdigitated capacitive electrode to develop a highly sensitive and specific sensor to detect each of the enantiomeric drugs. In the preparation processes the monomer ratios were optimized to favor complexation with the crosslinking monomer during the polymerization process. The imprinted thin-films supported on the interdigitated capacitance electrode (IDC) allowed for a rapid binding the individual thalidomide enantiomer after sensing and reaction on the surface. Upon sensor measurement, the resistance signals were gradually increased when increase the concentration of thalidomide, but at a low concentration the resistance signal reached plateau or even reduced which depended on the MIP formulation, because of the release of the thalidomide from the MIPs. They provided the resistance signal with linearity (R^2) > 0.990 in the range of 0.025 to 100 μg mL^{-1}. The MIP-based IDC showed high sensitivity and selectivity at low concentration detection for thalidomide down to 6.4 ng mL^{-1} in the presence of biological matrix. This led to interactions between the imprinted nanoparticles and the enantiomers from bovine serum albumin, associated with cholesterol and ceramide that were the interfacial regions on the films. Atomic force microscopy (AFM) and surface enhanced Raman spectroscopy (SERS) were used to examine the nanometered

topographical surface onto the surface of the electrode after exposure to the matrix. The results revealed that, the interaction forces on the surface of 100 nN for (*R*)-thalidomide, but a very low surface force (0.1 nN) for (*S*)-thalidomide with a high hysteresis and confirmed the interaction of the localized thalidomide enantiomers into the blood component enabled of distinguishing different local regions, better special resolution in the depth detection of 1 Å with the SERS spectra.

Thus, the developed MIP nanoparticles with various chemical functional precursors on the films of polymer yielded adjusting in low detection limit of the analyte in blood sample. Taking sensor together with the detection of significant force of enantiomers and SERS images, we can measured the amount of thalidomide relevant within particular biological component exposed to whole blood, that can manipulate the mechanism of molecule interaction of both enantiomers. The MIPs for recognition of (*R*)- and (*S*)-thalidomide can be used for enantiomer separation and they have highly potential for the evaluation of efficient drug delivery and the approach to design the assessment for clinical effect.

ACKNOWLEDGEMENTS

I would like to thank all staff of the Drug Delivery System Excellence Center, Faculty of Pharmaceutical Sciences, Prince of Songkla University for their guidedance kindness.

Finally, I would like to say thanks you my family for their support, understanding and encourage when I got discourage.

Sirirat Rakkit

CONTENTS

Page

CONTENTS (CONTINUED)

CONTENTS (CONTINUED)

CONTENTS (CONTINUED)

CONTENTS (CONTINUED)

CONTENTS (CONTINUED)

CONTENTS (CONTINUED)

CONTENTS (CONTINUED)

LIST OF FIGURES

LIST OF FIGURES (CONTINUED)

LIST OF FIGURES (CONTINUED)

LIST OF FIGURES (CONTINUED)

LIST OF FIGURES (CONTINUED)

LIST OF FIGURES (CONTINUED)

LIST OF FIGURES (CONTINUED)

LIST OF FIGURES (CONTINUED)

LIST OF FIGURES (CONTINUED)

LIST OF FIGURES (CONTINUED)

LIST OF FIGURES (CONTINUED)

LIST OF FIGURES (CONTINUED)

LIST OF FIGURES (CONTINUED)

LIST OF FIGURES (CONTINUED)

LIST OF FIGURES (CONTINUED)

LIST OF TABLES

LIST OF TABLES (CONTINUED)

LIST OF SCHEME

LIST OF ABBREVIATIONS AND SYMBOL

AFM	Atomic Force Microscopy
AIBN	2,2´-azobisisobutyronitrile
°C	Degree Celsius
D_0	Diffractive coefficient of the water-vapor-air mixture (2.5×10^{-5})
DHEBA	N,N'-(1,2-dihydroxyethylene) bisacrylamide
f	Frequency (60,000 Hz)
FT-IR	Fourier-Transforms Infrared Spectroscopy
R	Gas constant (R = 8.314 JK^{-1} mol^{-1})
h	Hours
HPLC	High Performance Liquid Chromatography
IDC	Interdigitated capacitance electrode
M	Molecular weight of the thalidomide molecule (M = 258 g/mol)
µg/ mL	Microgram per milliliter
µm	Micrometer
mg	Milligram
mL	Milliliter
min	Minute
MAA	methacrylic acid
M	Molar
MIP	Molecularly imprinted polymer

LIST OF ABBREVIATIONS AND SYMBOL (CONTINUED)

MW	Molecular weight
D	Molar mass of diffractivity of the thalidomide enantiomer (m^2/s)
NIP	Non-imprinted polymer
NVP	1-vinyl-2-pyrrolidone
nm	Nanometer
PDB	Protein data blank
%	Percent
pH	Potential of hydrogen ion
r^2	Regression coefficient
C	Resistance from IDC electrode
rpm	Revolutions per minute
P_{sat}	Saturated vapor pressure, Pa (7.21 mmHg)
SEM	Scanning Electron Microscope
TEM	Transmission Electron Microscope
T	Temperature, K
s	Second(s)

CHAPTER 1

INTRODUCTION

1.1 Overview and general introduction

1.1.1 Chirality and importance of chirality in drug action

Chirality is property of the matters that has the mirror images, same chemical composition and has 2 dimensions. This phenomenon is found in the biological system, such as amino acids, carbohydrates, lipids and nucleic acid. However, in chiral environments such as the receptors and enzymes in the body, that they can behave differently because in the living system are chiral. Enantiomers of a chiral drug play different chemical and pharmacological activities in *in vivo*. The difference between 2 enantiomers of a drug on its binding site represent in biological process is illustrated in Figure 1. The difference in 3-dimensional structure allows the active enantiomer to bind and have a biological effect. The 3-dimensional structure also prevents the inactive enantiomer from having a biological effect at the binding site (McConathy *et al.*, 2003). The chiral drug has about 50% in the market. So, the stereoselectivity of the racemic therapeutics, are of important interesting in pharmaceuticals and biomedical applications. The use of single-enantiomer drugs is established that offered selective pharmacologic profiles and decreased drug interactions. Consequently, the use of the single enantiomer would provide a superior medication and may be preferred over the racemic form of the drug. The choice

between single enantiomers (homochiral drugs) and composite chiral drugs (mixtures of stereoisomers) relies on the therapeutic advantages, such as enantiomeric separation or purification, possible adverse side effects and development costs. Therefore, it is necessary for studying the interaction and evaluation of chiral drugs either in solution or biological matrix.
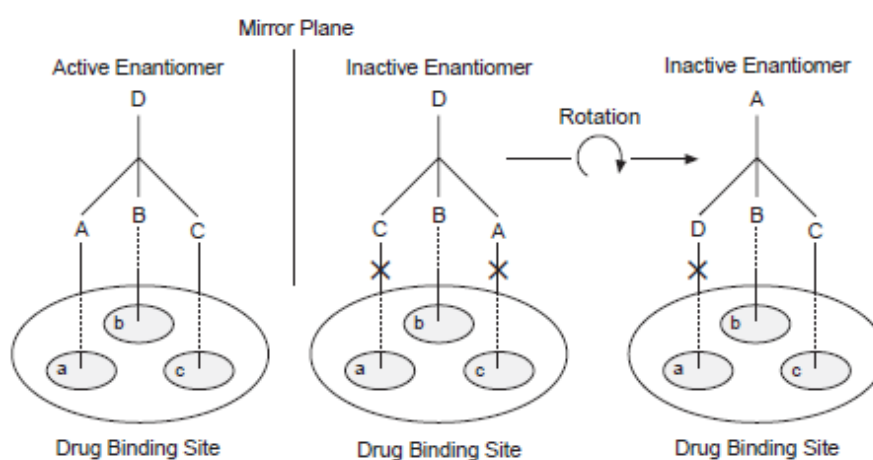
Figure 1.1: The hypothetical interaction between the 2 enantiomers of a chiral drug and its binding sites (McConathy *et al*. 2003).

Biomolecular interactions play an important role in many biological and physiological processes (Hinterdorfer and Dufrene, 2006). It has importance for screening of the active drugs exposed to a target site for ligands binding due to the stereoconfigurations have different interactions in the biological recognition processes. Molecular recognition has an essential role in the biological processes. The use of biomimetic approach by molecular imprinting, that is the powerful technique to generate the molecular recognition with a high selectivity inside the polymer matrix. As the non-covalent imprinting approach was developed by Arshady and Mosbach

(Arshady and Mosbach, 1981) and this has increased the attraction for scientific research because its simplicity production and mimic biological recognition materials. The specificity for target binding of small organic compounds comes from a combination of non-covalent interactions, such as hydrogen bonds, hydrophobic interactions, dipole interactions or π- π interactions (Owens *et al*., 1999). In the molecularly imprinted sites can selectively recognize and rebind the original template molecule by an ability to memorize structure of stereoisomers molecules mimicking to natural one. It is well known that different configurations lead to the stereoisomers to have different interactions with natural receptors, enzymes and other binding molecules that contribute to the diversity of biological responses. Over the last year the application of molecular imprinting has been used in many fields of research such as drug delivery (Kryscio *et al*., 2009), diagnostics (Sergey *et al*., 2006), analytical application (Fuchs *et al*., 2012), environmental science (Calisto *et al*., 2011) and biomimetic sensor (Wangchareansak *et al*., 2013). However, chemical recognition is important for a selective material based on biomimetic system to stabilize the chiral molecules when expose into the biological conditions and studied the mechanism of the enantiomer drug.

A biosensor provides a method that can detect a biologically relevant compound. Development of a biosensor relies on the effect of different polymerization processes. The biosensors are useful for monitoring specific molecules, for detecting therapeutics, or for evaluating the activity of small organic molecules such as drugs and chiral compounds. This method allows for a rapid and sensitive alternative means for biosensing and creates robust and long-life sensing for the active molecules. In addition, constructing biomimetic materials use for

application in biomedicine and drug delivery system based on molecular imprinting that give the recognition with the binding sites. Therefore, the use of MIPs micro/nanoparticles has ability to control the enantiomer on solid surface interactions with the imprint of the original template. We have initiated new imprinting techniques to enable identification of biologically active entities and the molecular structure of a targeted drug of thalidomide enantiomer. The use of MIP-based configurational biomimetic system receptors for identification of a molecular target can lead to screening compounds with appropriate activities and optimizing them for better specificities with and without the relevant biological component.

1.2 Thalidomide

Thalidomide was first introduced in the 1950s as a sedative and antinausea medicine for pregnant women but severe teratogenic effects to a human fetus were observed. These included a high number of miscarriages and most importantly fetal malformations of newborns (McBride 1997) thus it was withdrawn from the market in the early 1960s (Ahuja *et al*., 1997). Thalidomide has been reported to be remarkably effective for the treatment of the debilitating and disfiguring lesions associated with erythema nodosum leprosum and myelodysplastic syndrome. Inhibition of immune and inflammatory responses and angiogenesis by thalidomide is related through inhibition of cytokine-induced nuclear factor κB (NF-κB), tumor necrosis factor-α (TNF-α), vascular endothelial growth factor (VEGF) (Eriksson *et al*., 1992; Sampaio *et al*., 1991; Li *et al*., 2003; Fujita *et al*., 2001) . So, thalidomide brought back to use because of the important role of thalidomide as an anticancer agent (Kumar *et al*., 2004). Thalidomide is made and used as racemic mixture. The (*R*)- and (*S*)-thalidomide enantiomers provide different pharmacological effects (Eriksson *et al* 2001; Teo *et al* 2004). (*R*)-thalidomide is responsible for the sedative properties, while (*S*)-thalidomide has teratogenic and immunomodulatory properties. However, individually enantiomers will rapidly racemize in *in vivo*. The (*R*)-thalidomide undergoes a fast-rate bidirectional chiral inversion in basic condition and after treatment in humans oral or intravenous doses, which (*S*)-thalidomide can be found in blood when administering as pure (*R*)-thalidomide (Eriksson *et al*., 2001). In this work, we consider the (*R*)-thalidomide and (*S*)-thalidomide as a model drug of this study (Figure 1.2).

(*R*)-thalidomide
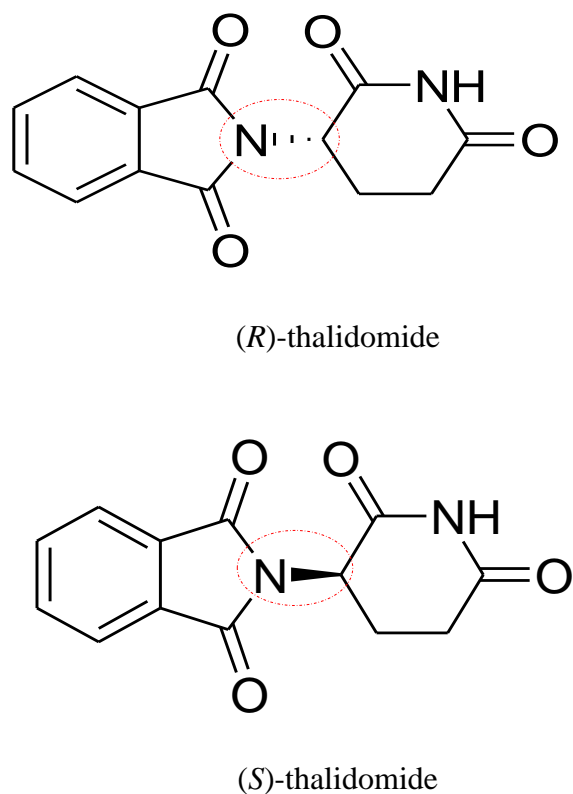
(*S*)-thalidomide

Figure 1.2: The structure of (*R*)-thalidomide and (*S*)-thalidomide.

Thalidomide (α-phthalimidoglutarimide), which is drug of interest, has been shown to have potential as an immunomodulating agent and is an efficient inhibitor of tumor necrosis factor-α (TNF-α) as an angiogenic agent. The drug has a chiral center and in clinical practice is used as a racemate of the (*S*)-(-)- and (*R*)-(+)- enantiomers. A method for separation and analysis by sensor measurement of thalidomide enantiomers exposed to the biological matrix such as whole blood samples has been studied. This can be achieved by generation for a recognition site in the polymeric matrix using non-covalent imprinting approach. Therefore, the preparation of MIP nanoparticles is made to create the recognition site for selectivity toward both (*R*)-and

(*S*)-thalidomide with in polymeric networks, which subsequent apply as a stamp to procedure selective pattern of the chiral template with a gold electrode on the coated thin-film.

1.3 Principal of molecularly imprinted polymer (MIPs)

Selective recognition onto the supporting electrode requires selective and sensitive recognition of the target analyte. The biological systems such as antibodies, receptor or enzyme for selective recognition are limitation. Those are ruggedness, high mechanical properties and cost effectiveness. To overcome this problem, synthetic materials have been interested in many application areas (Haupt *et al*., 2000; Haupt *et al*., 2003; Poma *et al*., 2013). Molecular imprinting is an alternative technique to produce the artificial recognition materials. This technique was established in 1972 by Wulff and Sarhan. Molecular imprinting is an emerging methodology for the creation of selective recognition sites in synthetic polymers (Mosbach *et al*., 1996). This technique involves the polymerization of functional monomers in the presence of a chosen template, and cross-linking monomer that interact in the template molecules by non-covalent or covalent bonds in a porogenic solvent. The template is then extracted, which will remain cavities with binding site that are complementary in size, shape and chemical functionality to the template. (Arshady *et al*., 1981; Wulff *et al*., 2013). Figure 1.3 summarized the principle of molecular imprinting.

Molecularly imprinted polymers (MIPs) are artificial recognition materials with recognition sites capable of rebinding a target molecule. It obtained by

polymerizing of functional monomers and cross-linking monomers around a template molecule, leading to a three-dimensional network polymer. The monomers are selected by interaction with the functional groups of the template molecule. The polymerization has produced; the template molecule is then extracted that provided the binding sites with size, shape and functionalities complementary to the target analyte are established. The resulting MIPs maintain the selectivity inside the molecules after the template removal.
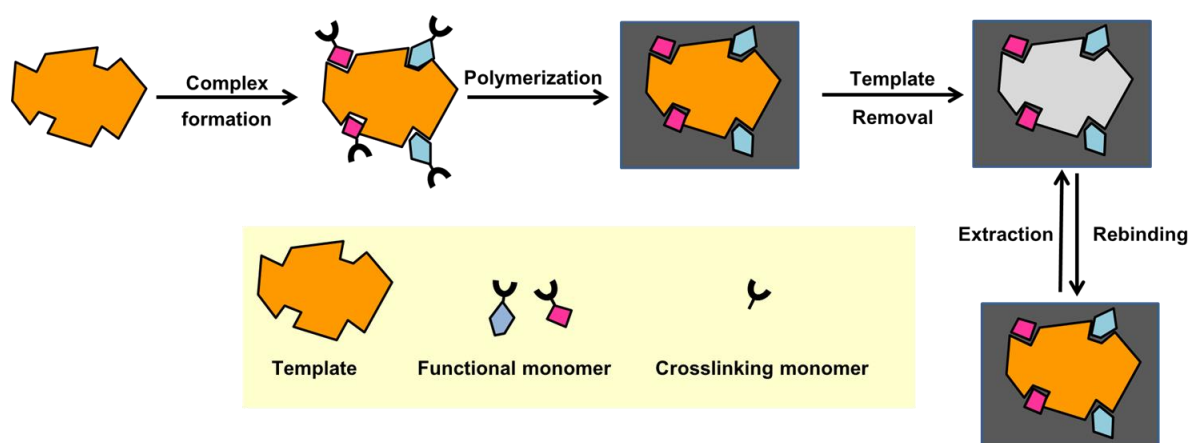
Figure 1.3: General processes of molecular imprinting: Template molecule, functional monomer and crosslinking monomer are dissolved into the porogenic solvent. Then, polymerization process between the template and functional monomer by self-assembly process. The binding sites and recognition cavities was produced by template extraction.

Molecularly imprinted polymers exhibited many advantages such as thermal and chemical stability, low cost, ease of preparation, high stability (Vlatakis *et al*., 1993). A wide range of analytes can be applied to synthesis for electrochemical sensor application by using molecular imprinting techniques from the subnano to microlevel

such as drugs (Suksuwan *et al*., 2015), herbicides (Sambe *et al*., 2007; Mirzajani *et al*., 2107), peptides (Hoshino *et al*., 2008) viruses (Birnbaumer *et al*., 2009; Schirhagl *et al*., 2010; Findeisen *et al*., 2012), erythrocytes (Ghosh *et al*., 2016) or immunoglobulins (Schirhagl *et al*., 2010), also volatile organic compounds (Liu *et al*., 2006; Mustafa *et al*., 2014) or ions (Latif *et al*., 2011), cell or yeast (Polreichova *et al*., 2011), protein (Hoshino *et al*., 2010) or 2,4-dichlorophenol (Liu *et al*., 2016).

The advantages of MIPs led to the development of several of MIP applications in sensor (Sontimuang *et al*., 2011; Bajwa *et al*., 2012; Jungreuthmayer *et al*., 2012; Mustafa *et al*., 2014; Wackerlig *et al*., 2015; Oberländer *et al*., 2105), solid phase extraction (Nestora *et al*., 2016), separation (Meyring *et al*., 2000; Gao *et al*., 2013), capillary electrophoresis (Weinz *et al*., 1995), catalysis (Kirsch *et al*., 2009), and sensor of environmental compounds (Suedee *et al*., 2004).

1.4. Synthesis and characterization of MIPs

1.4.1 Polymer composition of MIPs

1.4.1.1 Monomer

Methacrylic acid (MAA) and 1-vinyl-2-pyrrolidone (NVP)

In the preparation procedure of MIPs, functional monomers are responsible for the binding interactions in the imprinted binding sites. The monomers are usually used in excess moles ratio of template to produce the template-functional monomer assemblies. The functional group of monomer could interact with the functional group of the template. Hydrogen bond is responsible for the molecular recognition interaction of molecularly imprinted polymers. Methacrylic acid have carboxyl group functions exhibit as a hydrogen donor and a hydrogen acceptor. The non-covalent interactions are easily extracted by using acid or base. 1-vinyl-2-pyrrolidone is responsible for hydrophobic interaction. In order to increase the complex formation between functional monomer and template could be achieve by using co-monomer to maximize the non-covalent interactions.
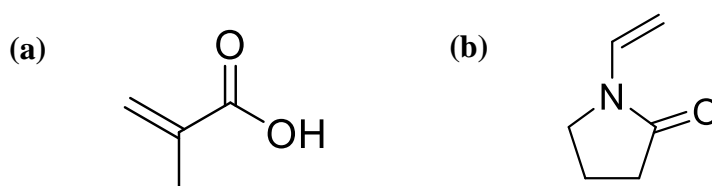
Figure 1.4: The structure of methacrylic acid (MAA) (a) and 1-vinyl-2-pyrrolidone (NVP) (b).

1.4.2.1 Cross-linker

N,N'-(1,2-dihydroxyethylene) bisacrylamide (DHEBA)

The cross-linker has an importance to stabilize the imprinted polymer, the morphology and stabilize the imprinted binding site of the obtained MIP. Moreover, cross-linker responsible for the generation of porous materials and maintaining the stability of the recognition sites. High amount of cross-linking supports the three-dimensional structure corresponding with size, shape and chemical functionality of the template after template removal.
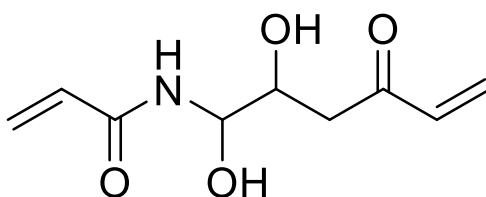
Figure 1.5: The structure of *N,N'*-(1,2-dihydroxyethylene) bisacrylamide (DHEBA).

1.4.3.1 Porogenic solvent

Toluene

Porogenic solvents play an important role to produce the macroporous polymers and effects to polymer morphology of MIP materials. It also stabilizes the strength of non-covalent interactions. The important criteria of formation for MIPs is

the choice of porogenic solvent for the polymerization processes. First of all, template molecule, initiator, monomer and cross-linker have to be soluble in the porogenic solvents. Then, the porogenic solvents related to make the polarity during complex formation that affect to selectivity of MIP.

1.4.4.1 Initiator

2,2´-Azobisisobutyronitrile (AIBN)

The 2,2´-azobisisobutyronitrile (AIBN) is available to make radicals molecules the initiation in the polymerization process that occurred by photolysis (UV) or thermolysis. In the preparation process, purging the monomeric mixture with inert gas of nitrogen is needed to remove the oxygen that influence the rates of propagation process.
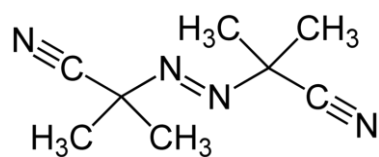
Figure 1.6: The structure of 2,2´-azobisisobutyronitrile (AIBN).

1.5 Molecularly imprinted polymerization process

The polymerization method used for the making of MIPs can be classified by the nature of the interactions between the template and the functional monomer throughout the polymerization process. The interactions can be either covalent or non-covalent interactions. Three different approaches for the synthesis of MIPs have been reported: covalent, semi-covalent and non-covalent. The covalent approach, introduced by Wulff and Sarchan (Wulff and Sarchan 1972), involves the formation of covalent bonds between template and monomers before polymerization processes. Then, the template is removed from the polymer by cleavage of covalent bonds. It produced the highest stability between the template-monomer interactions that reduced the non-specific binding sites. The advantages of the covalent approaches were no excess of functional monomer during the synthesis of the MIP. It could be produce the homogeneous binding sites. Nevertheless, it is very difficult to extract the template molecules because of the requirement of an acid hydrolysis procedure to cleave the covalent bonds.

The semi-covalent approach is considered as an alternative approach to synthesize MIP (Sellergren *et al*., 1990; Whitcombe *et al*., 1995). In this method, the template-monomer is covalently bound before polymerization step, and then the template extraction is done by non-covalent interactions. Self-assembling approach is related to the biological recognition systems, that uses non-covalent forces, such as hydrogen bonds, Van der Waals forces, and hydrophobic interaction. The non-covalent was introduced by Arshady and Mosbach (Arshady *et al*., 1981), based on the non-covalent interactions of hydrogen bonding, electrostatic interactions between

template molecule and functional monomers and the other monomer before the cross-linking polymerization. In the polymerization processes, the special binding sites are formed by the self-assembly process between the template and monomer. The non-covalent imprinting approach is related to the interaction of biological compounds. This process is easily to find the monomers that able to interact with template and provide high affinities of binding sites. The non-covalent approach is generally used to produce MIPs. Several approaches have been used to synthesize MIPs.

1.5.1 Bulk polymerization

Molecularly imprinted microparticles have been synthesized via solution polymerization method that was easily to prepare by grinding the imprinted polymer monolith. The MIP particles used as a chromatographic stationary phase. However; the bulk polymers requires time-consuming processes for sieving and then led to irregular particles sizes, low packing quality for separation. Thus, they have to be sieved to favor the desired particle size for the application (Silvestri *et al*., 2005; Ye *et al*., 2000). Therefore, it required straightforward method and commonly produces MIP particles in narrow size distribution with high yield.

1.5.2 Emulsion polymerization

The preparation processes of emulsion polymerization approaches were prepared with a cross-linker, functional monomers and the templating as the organic phase as a porogen. The aqueous phase were prepared by containing surfactant and stabilizer, cross-linker as the aqueous phase to produce the stable emulsion and homogeneous size (Vaihinger *et al*., 2002). The resulting MIP nanoparticles could improve the homogeneous binding properties of the imprint sites. The mini emulsion polymerizations were applied to detect the lysozyme. The lysozyme imprinted (MIP) nanoparticles were prepared by mini-emulsion polymerization then dropping of nanoparticle solution to the gold surface and dried at 37 ˚C for 6 h onto the QCM. It shows the monolayer onto the surface and provided the high selectivity and sensitivity in the aqueous solutions (0.2-1500 µg/mL) and natural sources (egg white) (460-1500 ng/mL) (Sener *et al*., 2010). In addition, the imprinted nanoparticle of lysozyme was prepared for the attachment of surface plasmon resonance (SPR) sensor that showed the lowest concentration at 32.2 nM (Sener *et al*., 2011). It using of sodium dodecyl sulfate (SDS) for emulsion polymerization which it was toxic to cells and cannot be completely removed (Schirhagl *et al*., 2010) and the protocol requires many synthesis steps to produce the nanoparticles.

1.5.3 Precipitation polymerization

Precipitation polymerization was first synthesized in 1999 to obtained MIP nanoparticles (Ye *et al*., 1999). Precipitation polymerization is done by cross-linking polymerization in highly diluted monomer solutions containing the template in the monomeric mixture. This continuous phase is a non-solvent for the formed polymer. This method provided the cheap syntheses of monodisperse spherical particles in high purity and could be obtained the nanoparticles product. Gao and coworker prepared the surface imprinting nanosphere by using covalent template immobilization for the MIP shell around the core (Gao *et al*., 2013). The peptide MIP-based NPs also could be synthesized by using precipitation polymerization technique in the absence of solvent media (Hoshino *et al*., 2008). In the precipitation polymerization processes is no need to add emulsifier or suspending reagent to the reaction system. Precipitation polymerization has been produced spherical imprinted particles in a single preparative step, and it is a particularly convenient method for MIP synthesis. The advantages of precipitation polymerization to produce the uniform size distribution of imprinted nanoparticles are significantly increasing the surface to volume ratios when compare with the monolith particles, low consumption of reagents during polymerization and help to improve purity of the nanoparticles. However, a higher amount of solvents is required to obtain the desirable sizes of the nanoparticles (Yoshimatsu *et al*., 2007).

1.5.4 Multi-step swelling polymerization

Many researchers used the multi-step swelling polymerization method to produce the spherical particles. Sambe and coworker prepared uniformly-sized, molecularly imprinted polymers (MIPs) by using multi-step swelling and polymerization method for determination of methythioltriazine herbicides in river water. The MIP could be used for selective pretreatment and enrichment of trace amounts of methylthiotriazine herbicides with real time analysis (Sambe *et al*., 2007) Yand and coworker synthesized amphiphilic nonspherical SPS/PS composite particles by multistep swelling polymerization that can be used as solid surfactants (Yang *et al*., 2014). The solvent effect of toluene to the surface of the nanoparticles leads to the larger internal surface areas due to increased porosity (Li *et al*., 1998; Yoshimatsu *et al*., 2007).

1.6 Molecularly imprinted polymer nanoparticles

The major challenges involved with the development of the selective recognition materials (Bajwa *et al*., 2012). The molecular imprinting technique provided the possibility to produce the recognition element that was biomimetic receptor and used as a recognition layer of sensor. Molecularly imprinted nanoparticles (MIN) possess had an advantage of high surface area, good accessible of template to the analyte binding and improve the binding performance (Mustafa *et al*., 2012; Lian *et al*., 2012; Singh *et al*., 2011). When compared with monolithic imprinted particle because of high-affinity of binding site, imprinted nanoparticles provided the potential for adsorption-desorption processes that contributed the high sensor responses signal and easily integrated with electrochemical sensor (Wackerlig *et al*., 2015). The nanoparticles are used as recognition layers in chemical sensor. Kriz and coworker used the MIP as a fiber optic sensing device (Kriz *et al*., 1995). The nanoparticles have been interested due to the high sensitivity and specificity for the molecules when compared with the other nanostructured material (Han *et al*., 2001). Gold surface are used for sensing because of good interaction with thiol or disulphide-terminated molecules (Christopher *et al*., 2005). The synthetic immunoglobulin based on non-covalent binding, such as hydrogen bonds or hydrophobic interactions has been successfully for immune recognition on a molecular level (Schirhagl *et al*., 2010). The imprinted nanoparticles could be used to increase two time sensitivity when compared with thin films (Lieberzeit *et al*., 2007; Lieberzeit *et al*., 2007). The sensitivity and selectivity depend on the affinity on the interfacial layer and interaction of analyte. The preparation of MIP by using imprinted nanoparticles as a

stamp onto the supported thin-films is a simple method which can directly prepare rigid, uniform, and compact MIPs film on the electrode surface. Moreover, MIPs film could improve the sensitivity and selectivity of sensors. Consequently, in this work we would like to apply molecularly imprinted nanoparticles onto the coated thin films of IDC electrode because higher surface-to-volume ratio, the geometric features provide the better accessibility of the analyte to the recognition sites and expected to improve the binding kinetics.

1.7 Molecularly imprinted polymer solid phase extraction (MIP-SPE)

Pretreatment and enrichment processes are necessary for trace analysis in biological samples because of high levels of much interference. The extraction techniques of solid-phase extraction (SPE) had low selectivity, and the matrix compounds were eluted with the target analytes. The application of MIPs as adsorbent materials had purpose for selective enrichment of specific enantiomers and sample pre-treatment before determination. Consequently, molecularly imprinted polymer used in SPE, it is so called molecularly-imprinted polymer solid phase extraction (MIP-SPE). However, the most of bulk MIP-SPE had some drawbacks in preparing and slow mass transfer. Therefore, MIP with PS as a core shell with proper size, shape and surface area are produced by multi-step swelling polymerization (Hosoya *et al*., 1996) have been used for the preparation of MIPs for SPE of a wide variety of analytes in biological samples (Haginaka *et al*., 1999; Haginaka *et al*., 2000; Sanbe *et al*., 2003) and environmental samples (Tamayo *et al*., 2003; Cacho *et al*., 2003; Tamayo *et al*., 2005; Zhang *et al*., 2006). Solid-phase extraction (SPE) is now

frequently used. For the conventional SPE sorbents, such as C18, ion-exchange and size-exclusion phases are lacking in selectivity to target analytes. In order to overcome this problem, molecularly imprinted polymers (MIPs) had advantages such as, easy preparation and high stabilities. Therefore, MIPs are expected as an alternative affinity SPE sorbent so, we have developed a uniformly sized MIP using a multi-step swelling and polymerization method (Haginaka *et al*., 1998; Sambe *et al*., 2007). Molecularly imprinted polymers (MIPs) have been used for pre-concentration, cleaning of the sample and also selective extraction of the target analyte, which is important for quantification of analytes inside the complex samples (Martín-Esteban 2013; Terzopoulou *et al*., 2016). The molecularly imprinted solid phase extractions were applied for direct assays of drugs in blood following by using HPLC. Furthermore, it has been reported that it could be effective for removal of the interferences present in the blood sample. In this study, focusing on the determination of enantiomers drugs in aqueous sample, so the purposes of sample preparation were to remove the interferences, increased the concentration of analytes, and improved selectivity in extraction before further the analytical step.

1.8 Atomic force microscopy

Atomic force microscopy (AFM) was established in 1986 (Binning *et al.*, 1986) to be used for topographical imaging and force measurements. Topographical imaging involves with scanning of the cantilever/tip across the sample surface. A laser beam is deflected off the back of the cantilever, and changes in deflection are monitored with a photodiode detector as shown in Figure 1.7. The Atomic Force Microscope (AFM) has been increasing the attention in the field of physical and biological sciences due to its useful for imaging to study in physiological conditions of soft biological materials. It can also be used to probe the mechanical properties of receptor-ligand interactions. The AFM has numerous advantages over electron microscopy in the study of physical and biological materials, including the ability to image in liquid with minimal sample preparation and characterize the surfaces of sample that is limited by the diffraction limit of light. Moreover, AFM provides the high-resolution imaging and able to measure forces in piconewtons range. This feature provides the ability to determine the mechanical properties for example; analyzing the protein structure (Dufrene 2009) and probing the molecular interaction (Kasas *et al.*, 2008).
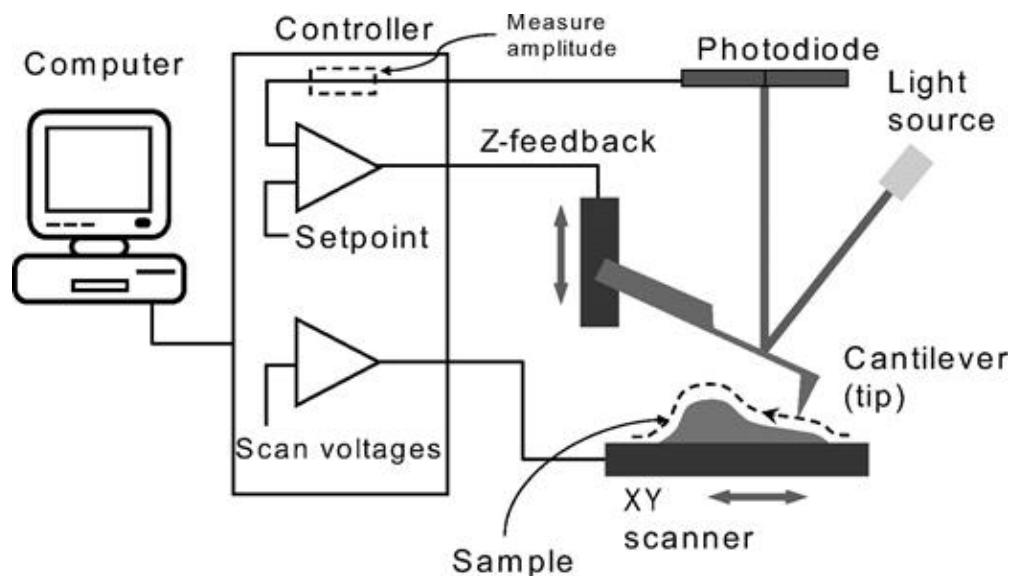
Figure 1.7: Schematic of the operation of the AFM (Last *et al.*, 2010).

The operations of AFM are divided into three modes in: contact, tapping, and force mode. In contact mode, AFM tip contact with the surface of sample. When the tip attaches across the hole or height on the surface, the deflection of the cantilever increases, and the cantilever is returned back. Very small forces are produced between the probe and the surface. The deflection of the cantilever is called "stiffness of cantilever" (Fotiadis *et al.*, 2002). The contact mode of AFM and operation providing very fast scanning (typically 0.1–0.5 second per scan line), but the tip can stretch or even damage the surface. Tapping mode was introduced, the tip are oscillates up and down very fast lateral scanning. This mode decreases the sample deformation. It is important for soft samples materials that related to the properties of the surface material. Because of its nondestructive scanning, tapping mode is an optimal for soft biological surfaces (spring constants in the range of 1 Nm^{-1} and above). In addition,

AFM mode is force mode to measure the interaction by using AFM tip at a specific point sample. The scanner goes up and down, elevating and approaching the cantilever to the surface, the image shown in Figure 1.8. The force occur when the tip approaching to the sample. The force curve recorded when the sample is retracted down is known as the tip-retracting curve. During retraction the surface may possibly display elastic properties and occur the hysteresis between the approaching and retracting curves. The adhesion force can be appeared due to weak short-range forces (such as van der Waals forces) between the tip and surface.
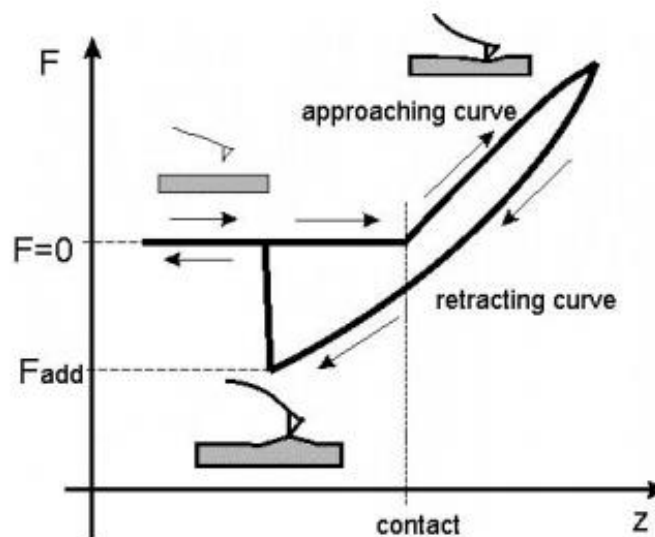
Figure 1.8: Force-distance curve recorded by AFM in force mode (Sokolov 2007).

AFM has benefits to gain information nanometer resolution surfaces properties of materials and to sense small forces values in the characterization of materials. Muller used the AFM to scan the interaction between lipid bilayer and drug. Force spectroscopy can also be used to probe the local elasticity, chemical groups, and receptor sites of live cells (Muller, 2008). Atomic force microscopy is

used to study the adsorption of hen egg-white lysozyme onto mica under acidic conditions. It appeared the conformational changes due to the adsorbed proteins and able to study the phenomenon when the surface is sparsely covered at low bulk protein concentrations.

1.9 Biosensor

A chemical sensor is a device that transforms from a chemical reaction of the analyte, ranging from the concentration of a specific sample component to total composition analysis, into an analytically useful signal (Hulanicki *et al*., 1991). The natural systems have the limitation, such as degradation in harsh environments and limited life time, stability and strong interaction between antibodies bind to antigens. Consequently, the recognition system has been generated by mimicking the naturally derived receptors. The interactions between the analyte and matrix play a key role in controlling the recognition ability of the material (Xu *et al*., 2011). The artificial materials have been used to detect numerous of analyte. Normally, antigen and antibody detection has been used to detect the interaction of analyte. Nevertheless, antigen and antibody has the weakness of pore binding site recognition leading to decreased sensitivity and reusability (Hall, 2002). Molecularly imprinted polymers as an alternative material was used for the sensing layer that providing high robustness and reproducibility (Haupt *et al*., 2000; Mayes *et al*., 2005). The greatest properties of MIP nanoparticles compared to bulk materials, for example amplified the signal, response time, selectivity, chemical reactivity, binding capacity, large amount of imprinted. This makes them are attractive for recognition with a range of transducers

leading to many different chemical sensors (Chang *et al*., 2013). The electrochemical technique has the advantages of low cost, high sensitivity and short time analysis but, the most of electrochemical techniques has low affinity and specificity. The development of molecular imprinting technique has been applied for electrochemical determination of analytes due to the biomimetic materials providing high affinity to the desirable molecule.

The artificial recognition materials provided the highly selective by using the non-covalent intermolecular interactions. The molecularly imprinted polymers nanoparticles showed high affinity between the analyte-layer interactions, particularly with nanostructured layer leading to high signals in mass-sensitive detection by quartz crystal microbalances (Bajwa *et al*., 2012). Recently, molecularly imprinted polymers (MIPs) based electrochemical sensors have received considerable attention such as high sensitivity, selectivity, simple operation, rapid response, and portable sensor for on-site detection regarding to the interdigitated sensor (Li *et al*., 2011; Reddy *et al*., 2011). Lab-on-a-chip (LOC) has extended increased of the high interest for the detection of pathogens (Mairhofer *et al*., 2009). The advantages of microfluidic systems were used the small volumes of analytes and easily to operate (Yager *et al*., 2006). The surface plasmon resonance (SPR) and mass-sensitive sensors, such as quartz crystal microbalances (QCM), are popular due to their selectivity and sensitivity. In the this work, the development of a lab-on chip integrated with imprinted nanoparticles as a stamp on IDC to detect thalidomide enantiomers. The application of MIPs is used to support the specific recognition of each enantiomer.

1.10 Aims and objectives of this thesis

It would be has an advantage to study the selective recognition of the specific form of the enantiomers drug. One method involve with the development of biomimic materials that could beneficial apply to study the interaction of the activities of drugs when exposed to the physiological condition. The optimal layer on IDC is used as a recognition layer for analytical detection.

This research was concerned with the development of the molecular recognition materials by imprinting technique onto the IDC for application as recognition element for biosensor. The main objective was to investigate their use as sensor coating layer in terms of different polymer composition of MIP formation. This involved the specific binding interaction of MIP compositions on the transducer surface with the target of enantiomer drug and characterization in physicochemical properties of the obtained sensor coating to the electrical signal. The objectives were:

1. To develop chirally imprinted polymer. The selectivity of MIPs, which made by utilizing the (*R*)- and (*S*)-thalidomide enantiomer as a template. The imprint pattern was formed in a different polymerized mixture during the polymer synthesis using methacrylic acid (MAA) and 1-vinyl-2-pyrrolidone (NVP) as a mixed functional monomer with different mole ratios and a crosslinker, *N, N'*-(1,2-dihydroxyethylene) bisacrylamide (DHEBA) in toluene as a porogenic solvent. The configurational biomimetic imprinting of these components can be designed to specifically interact with the template enantiomer under an optimized polymerizing

reaction, and thus provide for the three-dimensional, stereospecific binding site formed in the polymer with high recognition capability in an aqueous medium and physiological condition.

2. To examine the chemical and physical properties of the obtained MIP by using the attenuated total reflection (ATR-FTIR) spectroscopy. The morphology of all the polymer was achieved by scanning electron microscopy (SEM) as well as for analysis of the particle size of the resultant micro/nanoparticles determined with a zeta nanosizer.

3. To study the selective enrichment of the synthesized MIP materials by batch binding experiment and investigate the effect of the enantioselective recognition, for their binding affinity of the thalidomide enantiomers with distilled water, solvent of acetonitrile/phosphate buffer pH 5.5.

4. To develop molecularly imprinted solid-phase extraction (MISPE) for the selective enrichment and determination of a sample of human blood spiked with thalidomide enantiomers. The MIPs allowed for an effective selective extraction and also a simple method for the determination of thalidomide.

5. To investigate and characterize the thalidomide enantiomer imprinted nanoparticles and their use for films layer obtained by the surface imprinting approach with a polymer system as stamp by AFM.

6. To identify the template-MIP interaction on the various MIPs nanoparticle embedded films with Raman AFM. The surface-imprinting thin film based on the stamping procedure by using thalidomide imprinted nanoparticles as stamp for chiral separation applications.

7. To develop the thalidomide imprinted nanoparticles as a recognition layer onto the sensor system which would be able to improve the efficiency of recognition of the chiral drugs. Thereafter, AFM and Raman-AFM were applied to confirm the enantiomer drug interaction to the imprinted cavities.

The MIPs have been exploited as the recognition system on IDC sensor that can provide high specific sensitivity to the target analyte. A method for separation and analysis by IDC sensor measurement of thalidomide enantiomers exposed to the biological matrix such as whole blood samples were investigated. The application of lab-on-chip sensor measurements due to diffusion pathway and template accessibility to the imprint site can provide for interaction of MIP-template complex in the one of thalidomide transfer into imprints to both original stereoisomers of thalidomide. Applications of combining MIPs and surface micropatterning technology have been proposed the high selectivity and affinity for selective binding in order to analyze from a biological mixture containing of structurally similar compounds. Thin-films of imprinted polymer were produced as layer coating onto IDC electrode that used to improve the imprinting properties or the ability of the materials for analysis of binding to the template enantiomer in the presence of biological fluids and whole blood.

CHAPTER 2

SYNTHESIS AND CHARACTERIZATION OF THALIDOMIDE IMPRINTED POLYMER

2.1 Introduction

Biomaterial strategies have been tailored at a micro and nanoscale to be used in medicine. Microparticles (MPs), defined as particles whose size ranges from 1 to 1000 μm (Lockman *et al*., 2002). Nanoparticles (NPs) are regarded as nano sized scale of material whose size ranges from 10 to 1000 nm (Hamidi *et al*., 2008). This chapter is involved with the synthesis of the (*R*)-, (*S*)-thalidomide enantiomers molecularly imprinted polymer micro/nanoparticles was produced by non-covalent interactions using methacrylic acid (MAA) and 1-vinyl-2-pyrrolidone (NVP) (see structure in Figure 2.1) as single and mixed functional monomers by the multi-step swelling polymerization method (Hosoya *et al*., 1994). Thalidomide has functional groups of imide moieties available for interactions with the carboxylic acid of methacrylic acid (MAA) and the weak/neutral functional 1-vinyl-2-pyrolidone (NVP) monomers that provide for the formation of hydrogen bonding to recognize the thalidomide. In addition, thalidomide is sensitive to light, which may result in denaturation, conformational changes or aggregation (Vargesson *et al*., 2015). Strategies for thalidomide imprinting can be carried out by the surface imprinting technique (Ding *et al*., 2014). This method is known to produce surface with a

covering of binding sites, which are close to the surface, consequently, this make the binding site more accessible, the specific target molecules can fit more easily into the imprinted site. Initially, the obtained MIP spherical particles were characterized by scanning electron microscope, atomic force microscopy and contact angles. In this case, the polymerization medium was water, that interfered with the non-covalent interaction between the template and the functional monomers, such was carried out in toluene as the porogen, that the preparation of the uniformed size of the molecularly imprinted nanoparticles (Mayes *et al*., 1996). DHEBA was chosen as a cross-linking agent (see structure in Figure 2.1) because it had strong supporting properties so the imprinted site would not be collapsed after the template was removed. The cross-linker is important to control the morphology of the imprinted polymer and to stabilize the imprinted binding site. Moreover, the amount of cross-linker should be high enough to maintain the stability of the recognition sites. In addition nanoparticles had been prepared either with or without the polystyrene seed as a core-shell configuration. The biocompatible polymer including poly (vinyl alcohol) or PVA and poly carprolactone-trial were employed (PCL-T) as the stabilizer during the suspension polymerization to stabilize the imprinted polymer solution.
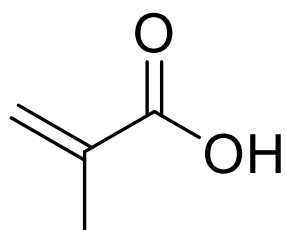
Methacrylic acid (MAA)   1-vinyl-2-pyrolidone (NVP)
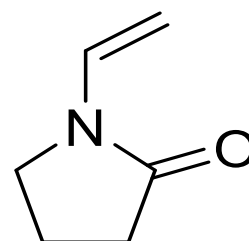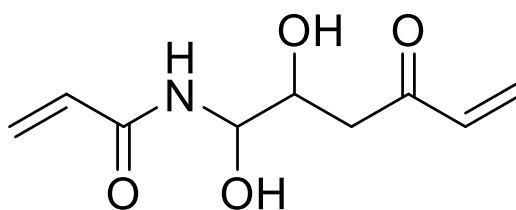
N, N'-(1, 2-dihydroxyethylene) bisacrylamide (DHEBA)

Figure 2.1: Structure of the functional monomers (MAA and NVP) and cross-linkers (DHEBA) used in this study.

2.2 Objectives of this study

The objectives of this study were to prepare the (*R*)-or (*S*)-thalidomide imprinted polymer micro/nanoparticles, that *R*-, and *S*-thalidomide was used as a template for use in selective recognition. [Characterization of the physicochemical properties of the thalidomide imprinted polymer micro/nanoparticles has been focused on the effect of the ratio of the two functional monomers and the macromolecular polymer as stabilizer that the enantioselective property of the imprinted sites would be expected for resultant MIPs to both enantiomer templates.] The thalidomide imprinted polymer micro/nanoparticles were characterized *via* scanning electron microscopy (SEM), transmission electron microscopy (TEM), the zeta nanosizer, fourier transformed infrared spectroscopy (FT-IR) and contact angle.

2.3 Experimental

2.3.1 Chemical and reagents

Styrene, methacrylic acid (MAA), 1-vinyl-2-pyrrolidone (NVP)*,* *N,N′*-(1,2-dihydroxyethylene) bisacrylamide (DHEBA), sodium lauryl sulfate (SDS), styrene, disodium ethylenediaminetetraacetic acid (EDTA), (*S*)-(-)-thalidomide, (*R*)-(+)-thalidomide and racemic (±)-thalidomide were from Aldrich Chemical Company (Milwaukee, WI, USA). 2,2´-Azobisisobutyronitrile (AIBN) was obtained from wako company (Japan) and some of gift from Prof. Peter A. Lieberzeit, University of Vienna for which many thanks. Dibutyl phthalate, potassium peroxidisulfate and

polyvinyl alcohol (PVA) were from Fluka Chemie (Buchs, Switzerland). MAA was purified by distillation under reduced pressure before use to remove the hydroquinone inhibitor. All other solvents used were of analytical reagent grade and used without further processing.

2.3.2 Equipment for characterization

The structures of the MIPs were determined with a 1720X FTIR spectrometer (Perkin-Elmer, Beaconsfield, U.K.) using a Spectra Tech ATR-flow cell and a 45° ZnSe crystal. The surface morphology of the polymers was obtained using a JSM-5800 LV electron microscope (Jeol, MA, USA). The mean particle size of the samples was determined by a Zetasizer Nano ZS (Malvern Instruments, Malvern, U.K.). The water contact angle were determined at room temperature using a OCA40 contact angle goniometer (Dataphysics, OCA40, Germany) (see in Figure 2.2). A deionised water droplet of 1μL was placed on the specimens using an automatic droper and the receding contact angle was obtained by the removal of the liquid. A charge coupled device camera was used to capture the image of the water droplets for the determination of the contact angle. The angle was changed by x-ray irradiation. Contact angles were determined using the software modules SCA 20 and SCA 24 (Filderstadt, Germany).
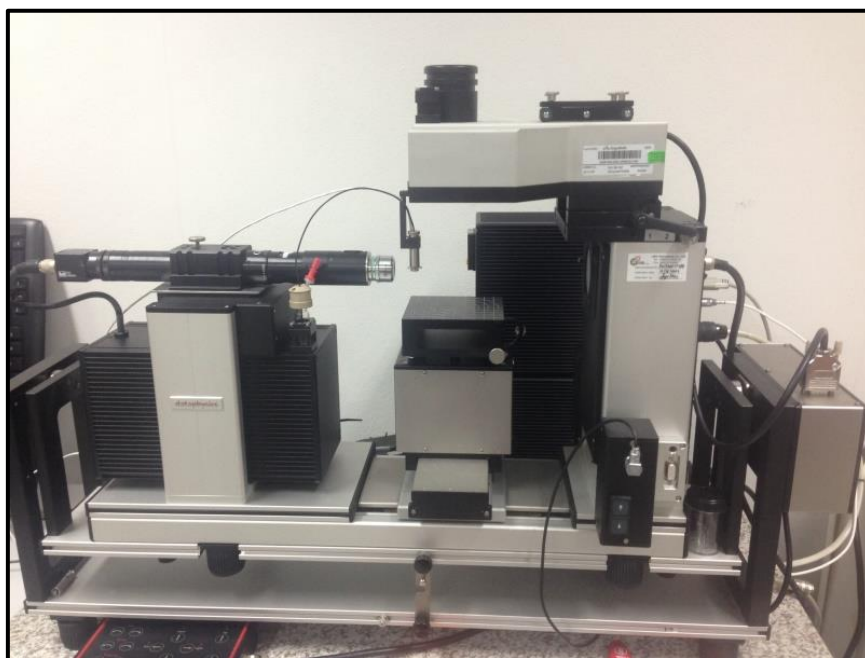
Figure 2.2: Contact angle (Dataphysics, OCA40, Germany).

2.3.3 Methodology

2.3.3.1 The preparation of MIP microparticles/nanoparticles

Molecularly imprinted polymers selective for (*R*)-thalidomide and (*S*)-thalidomide were prepared by a multi-step swelling polymerization process that was previously reported but with a slight modification (Hosoya *et al*., 1994). In a typical preparation for the imprinted polymers, first, AIBN was added to a pre-polymerized reaction mixture consisting of a cross-linking agent and monomers. This was followed by a second swelling step in the presence of the pre-polymerizing mixture that

contained the template [(R)-thalidomide or (S)-thalidomide] and the functional monomer assemblies in toluene that was used as the porogen solvent. Subsequently the hardening process of the outer shell of the core with a selective polymer layer was carried out by a thermal polymerization method, thus allowing for the assembly of functionalized assemblies of template and all the monomers to produce the polymer matrix. The polystyrene seeds were produced by the polymerization of the purified styrene and potassium peroxidisulfate that were mixed and heated at 75°C for 24 h. In a typical MIP preparation, 1.0 g of polystyrene particles (approximately 0.96 μm in diameter of polystyrene) were mixed with 0.6 mL of dibutyl phthalate, 0.02 g of sodium lauryl sulfate, and 6 mL of distilled water. Subsequently, this suspension was stirred (125 rpm) at room temperature (25±1°C). After the polymerization for 20 h, 6 mL of toluene was added to the mixture. Then 12.0 mL of distilled water was admixed, along with 10 mL of a 4.8% PVA or 4.8% PCL-T solution. The mixture was kept stirring at room temperature for 2 h. A mixture of 0.006 g of DHEBA, 0.697 mol of MAA (0.060 g), 0.02 g sodium lauryl sulfate, 12.0 mL of distilled water, and 10 mL of 4.8% PVA was added into the mixture to ensure dispersion of the powder in the toluene. The mixture was kept overnight while being stirred at 50 °C under a stream of nitrogen. The particle suspension was centrifuged at 13,500 rpm for 10 min. The resulting polymer particulates were washed with 3 x 250 mL portions of 10% v/v acetic acid in methanol, and finally with 3 x 250 mL portions of methanol. Complete extraction of the template molecule from the polymer was confirmed by the absence of the template(s) in the methanol rinses of the polymer, as verified using a stereospecific HPLC method. A non-imprinted polymer (NIP), that was included as the control, was prepared in the same way as the MIP beads, but with no added

template. The monomeric mixture was prepared from the components of the polymerization reaction (Table 2.1). The supernatant liquid was homogenized at 1,000 bar for 1 h to obtain the imprinted polymer nanoparticles. The template was removal from the obtained nanoparticle by a skin dialysis method using Snake skin® Dialysis Tubing (Thermo Fisher Scientific Inc., USA). In the next step, the nanoparticles were incubated with the original template for 24 hours and thus the amount of template absorbed was characterized before the preparation of the nanoparticle embedded films. All the experiments were performed at room temperature (25±1°C). The mean value of the contact angle from three measurements of each polymer was recorded.

Table 2.1: The composition of the polymer of molecularly imprinted polymers.

Polymer	Template (mol)	PS (g)	MAA (mol)	NVP (mol)	DHEBA (mol)	AIBN (mmol)
MIP1	0.025	1.0	0.43	0.17	0.03	0.73
MIP2	0.025	1.0	0.35	0.35	0.03	0.73
MIP3	0.025	-	0.43	0.17	0.03	0.73
MIP4	0.025	-	0.35	0.35	0.03	0.73

2.4 Results and discussions

2.4.1 Synthesis of the (*R*), (*S*)-thalidomide imprinted micro/nanoparticles

The arrangement of the functional groups in the binding cavity on polymerization reaction was examined by a study of the IR spectroscopy is illustrated in Scheme 1. The recognition process occurs through specifically localized hydrogen bond complexes. The results revealed that the MIPs and NIPs both exhibited the crosslinking polymerization of double bond because of the MAA, NVP functional monomers and cross-linker and the formation of binding groups that were complementary to the template molecules (see Scheme 1). In general, for the formation of the molecular imprints, the self-assembly processes around the template in the presence of a flexible polymer for pre-polymerization, and followed by the templating process that added more stable and chemical functional groups of the monomeric reactants into the polymeric environment. These polymer components provided a spatial three-dimension cavity within the imprinted polymer and were able to provide a specific recognition site for thalidomide enantiomers. After formation of the imprinted spherical polymer microparticles in the presence of a surface-stabilizing polymer the template can be recovered by extraction from the matrix with an appropriate solvent in the study. Such imprinted materials have been successfully prepared using methacrylic acid (MAA) and 1-vinyl-2-pyrrolidone (NVP) as a mixed functional monomer in the presence of the template during the polymerization and templating processes. In the protocol for template removal, the total amount of the template in the extraction medium was directly dependent on the amount of the

enantiomer incorporated and with the polymerization reaction. Two sets of MIP were prepared one with and the other without PS and each formed a core-shell and a non-core shell format for the MIP. Two types of imprinted polymers were formed in this study by the use of different amounts of the two functional monomers at the surface layer on the polystyrene and were called MIP1 and MIP2 whereas the MIP3 and MIP4 were prepared with the same polymeric compositions as MIP1 and MIP2, but without any polystyrene.
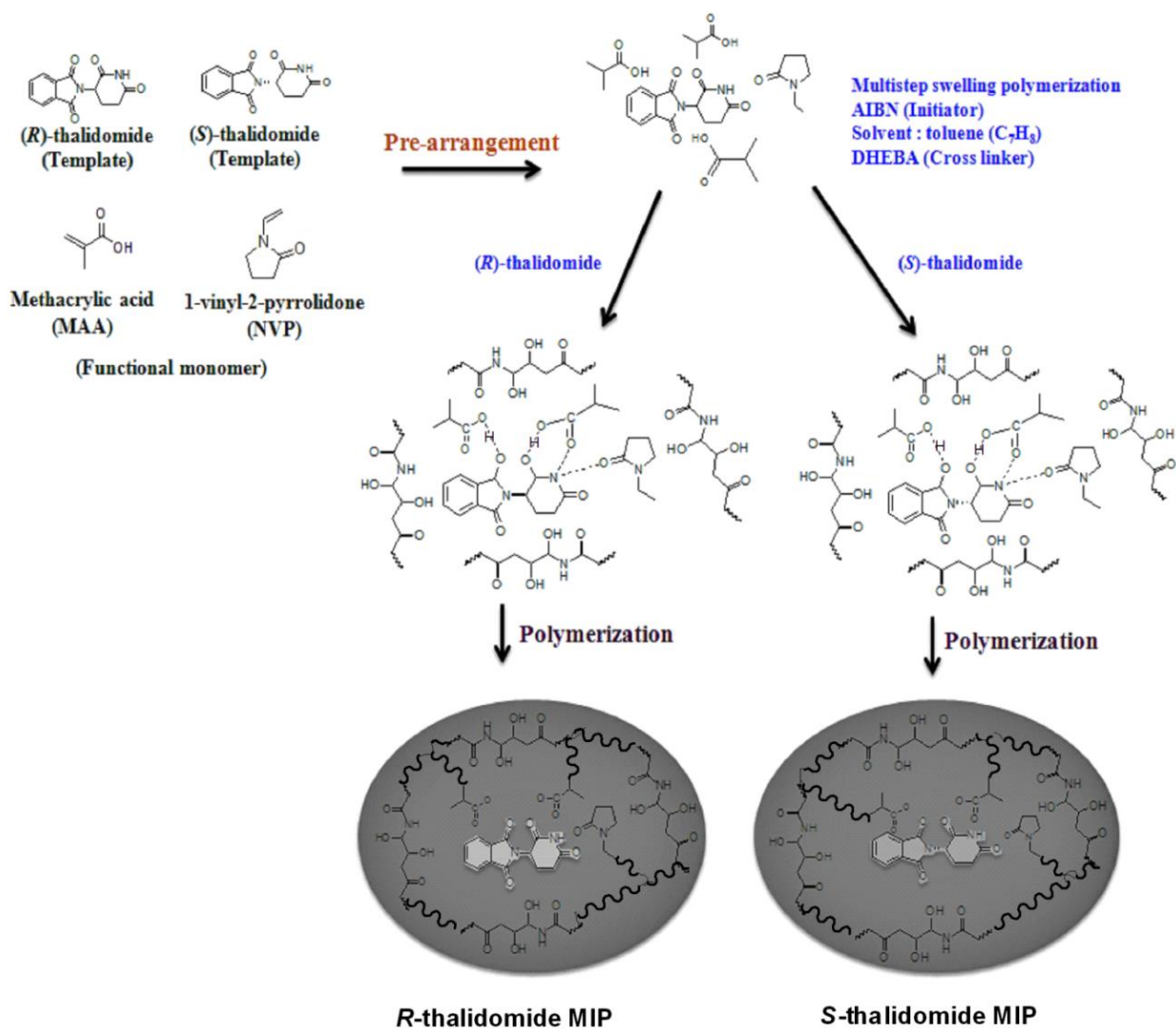
Scheme 1: Schematic diagram showing the generation of an (*R*)-thalidomide and (*S*)-thalidomide.

2.4.2 Studying the effect of the polymer composition

2.4.2.1 Scanning Electron Micrographs

The characterization of nanoparticles to support measurements of the mirco- and nano-particles obtained in this study and study of polymerizing protocol optimizing the ratio of the functional groups that yield the resulting synthetic polymer particles. Figure 2.3.1 shows the surface morphology of the MIPs for each of the core-shells (MIP1 and MIP2) or the non-core-shell (MIP3 and MIP4) types of particles. These MIP materials induced the enantiomer molecules to orient themselves in a specific imprint pattern so as to form a surface for the (*S*)-thalidomide that was distinguishable from the (*R*)-thalidomide, in the particulate MIP3. The characteristics of the binding sites in the imprint provided for the interaction between the template and the functional monomer to occur to form the MIP. The SEM image indicated that the porogenic solvent toluene had a significant effect on the morphology of the polymer particles and showed an interdigitated phase throughout the surface that covered the synthesized product. In contrast for the MIP4 for both the thalidomide enantiomer imprints, the SEM images had the same binding structure of the cavities on the surface of a resultant MIP microsphere. It was of interest that the MIP3 in particular using (*S*)-thalidomide as a template showed surface rearrangements and the hierarchically nanostructured polymer became entirely attached to the assembled spherical polymer. After removal of the template, in part, also it was accounted for the nature of the cavities that were formed when the polymer changed to a collapsed state as a function of time during which the MeOH solvent gradually decreased. It was

important to examine the interactions of the template with the functional monomers, so that the core-shell and non-core-shell MIP particles were produced by optimizing the ratio of the two functional monomers in the reactants that formed the synthesized product.
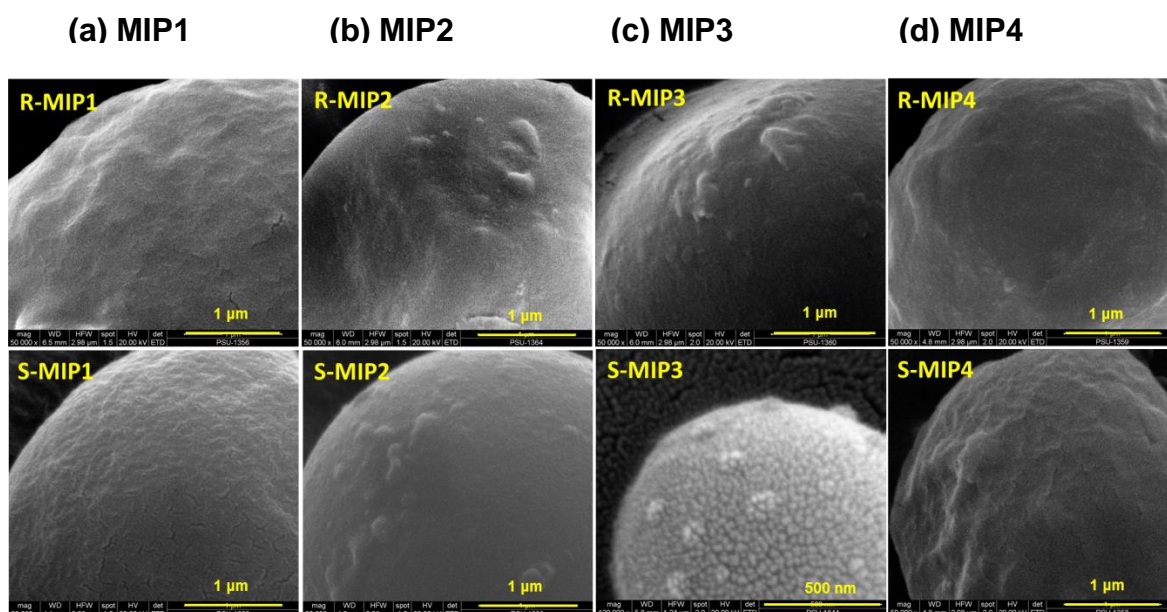
Figure 2.3.1: SEM image of the (*R*)- and (*S*)-thalidomide poly (MAA-*co*-NVP)-MIPs prepared using different ratios of functional monomers and a fixed amount of the DHEBA crosslinker after homogenization showing the patterns of the (*R*)-thalidomide and (*S*)-thalidomide imprints onto the surface of the particles (a) in the presence of poly(styrene) MAA:NVP ratios of 0.43:0.17 (MIP1); (b) 0.35:0.35 (MIP2); (c) in the absence of poly(styrene) at a MAA:NVP ratio of 0.43:0.17 (MIP3); (d) 0.35:0.35 (MIP4).
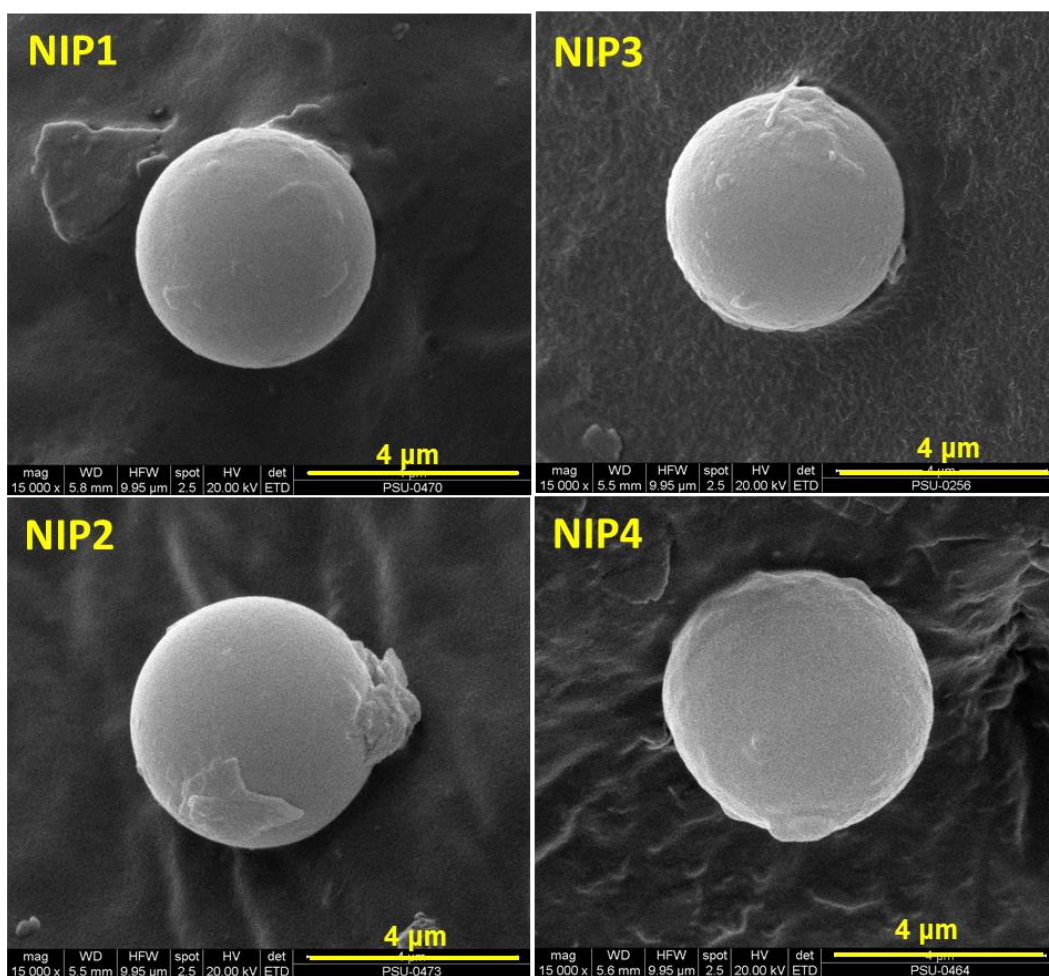
Figure 2.3.2: SEM image of the poly (MAA-*co*-NVP)-NIPs prepared using different ratios of functional monomers and a fixed amount of the DHEBA crosslinker after homogenization (a) in the presence of poly(styrene) MAA:NVP ratios of 0.43:0.17 (NIP1); (b) 0.35:0.35 (NIP2); (c) in the absence of poly(styrene) at a MAA:NVP ratio of 0.43:0.17 (NIP3); (d) 0.35:0.35 (NIP4).

2.4.2.2 Zeta nanosizer

The particle size and size distribution of the imprinted particles with PVA and PCL-T stabilizers were investigated. Two sets of MIP were taken with and without PS. Figure 2.4 shows a bar graph of the particle size and the size distribution of the (*R*), and (*S*)-thalidomide imprinted particles with PVA and PCL-T stabilizers that were investigated before and after high pressure homogenization by using the zeta nanosizer. The macromolecular polymers of PVA and PCL-T were used to enhance the physical stability. The use of the PCL-T stabilizer showed the reduction of the size of the MIP beads after homogenization with the smallest size of 1 μm or the submicron size for prepared of IDC sensor, so the resultant MIPs microsphere had a size range of between 15-20 μm before being homogenized depending on the polymer composition. After the use of the PVA stabilizer, the particles sizes of all the microparticles after homogenization were significantly reduced (1-5 μm) compared to the initial particle size of 20-30 μm, that will be used for MIP-SPE for efficient separation. Significant differences were recorded by the particle size analysis with smaller particles produced in the presence of the PVA stabilizer. No differences were seen on the particles with PCL-T stabilizer before and after homogenization. Polydispersity Index (PDI) is dimensionless and scaled such that values smaller than 0.05 are monodisperse of the particles size distribution and values greater than 0.7 indicated that the sample has a very broad size distribution or heterogeneity (Lynd *et al*., 2005). The synthesized of the obtained MIP showed the PDI values 0.5 that ascribed for heterogeneity size distribution of the imprinted polymer. The PVA was used as a stabilizer because the synthesis of the MIP and its compatibility with PVA,

significantly improved the stiffness and ductility of the resultant polymer composite (Piperno *et al*., 2010). As a result of the core-shells this led to the MIPs having better mechanical properties and improved robustness. The formation of a spherical MIP composite was ensured, because the polystyrene acted as the core polymer component and this governed the surface chemical properties.
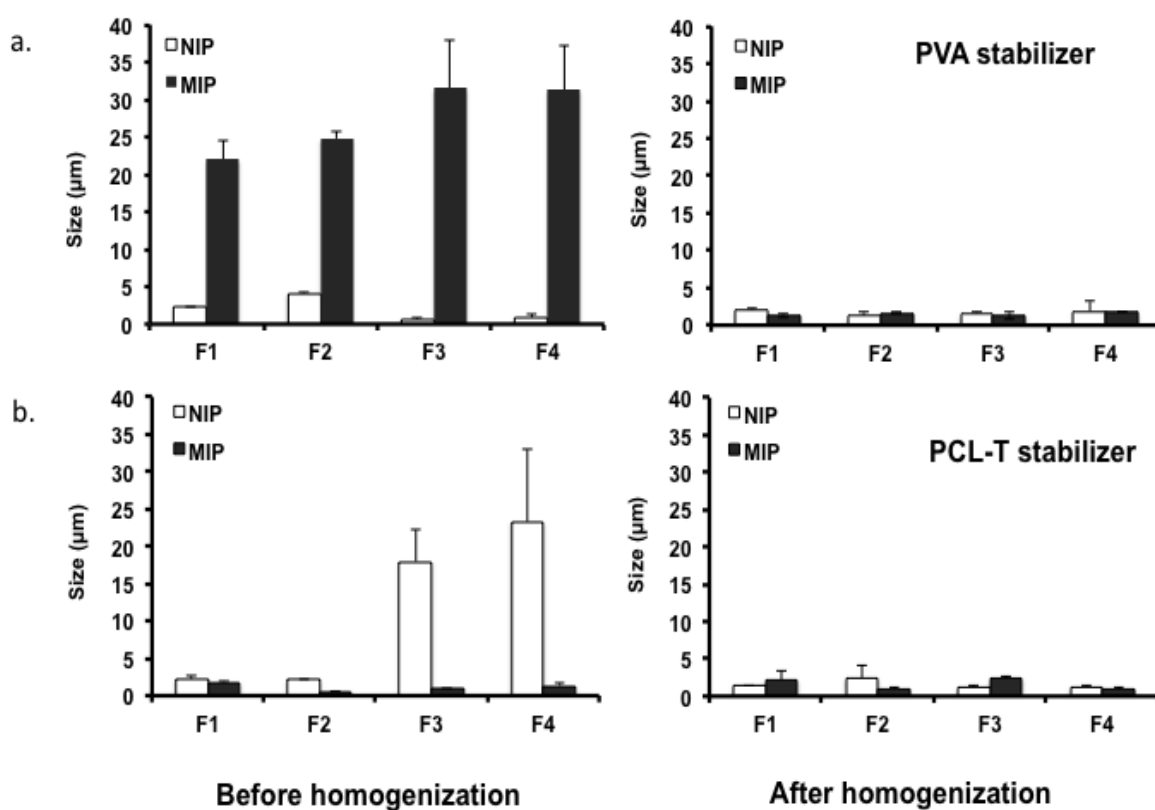
Figure 2.4: Particle size and size distribution of the (*R*), and (*S*)-thalidomide imprinted particles with PVA (a) and PCL-T (b) stabilizers were investigated before and after high pressure homogenization as determined by using the zeta nanosizer.

2.4.2.3 Fourier transforms infrared spectroscopy (FT-IR)

The determination of the optimized amount of functional monomers and the process of the polymerization of the MIPs to bind the (*R*)-thalidomide and (*S*)-thalidomide in the presence of macromolecular polymers was carried out. Figure 2.5 shows the FT-IR spectrum of polystyrene seeds, (*R*)-thalidomide, and (*S*)-thalidomide. The standard (*R*)-thalidomide and (*S*)-thalidomide show the sharp peaks at 3200 cm^{-1} belonging to NH group of the thalidomide and carbonyl peak at 1708 cm^{-1}. The polystyrene seed shows the intensity peaks at 2921 cm^{-1} according to the aromatic C-H stretching and aliphatic C-H stretching on the main PS chain. The peak at 3025 cm^{-1} is the C-H stretching vibration of benzene ring. The peaks at 1492 cm^{-1} and 1600 cm^{-1} are the characteristic bands of C-C stretching vibration of benzene ring. The peaks at 756 cm^{-1} and 697 cm^{-1} are the bands of aromatic C-H out-of-plan bending vibration and overtone between 1800-2000 cm^{-1}. The polystyrene seed shows the intensity peaks at 2922 cm^{-1} according to the aromatic C-H stretching and aliphatic C-H stretching and overtone between 1800-2000 cm^{-1} (Sun *et al*., 2017). In all of the FT-IR spectroscopy results of the RMIPs (Figure 2.6) and SMIPs (Figure 2.7) nanoparticles and non-imprinted control polymers presented four common peaks: a broad peak about 3400 cm^{-1} was produced by the stretching vibrations of (O-H) belonging to the hydroxyl group; a weak peak at about 2940 cm^{-1} was caused by the C-H stretching and a weak peak at about 1720 cm^{-1} is assigned for carbonyl group and strong peaks at 1420 and 1270 cm^{-1}, which are attributed to an ester group. FT-IR study confirmed the successful of MIPs because the MIPs and NIPs exhibited a crosslinking polymerization as that the absence of vinyl group of MAA, NVP at 1680

cm^{-1} and the appearance of aliphatic C-H replacement, as shown in the Figure 2.6 & 2.7. In addition, the imprinted polymer of (R), and (S)-thalidomide or MIP1 and MIP2 contained the poly(styrene) used as a core shell. The FT-IR spectra showed that the functional monomer and template propagated around the core shell that covered the complete poly(styrene) seed particles. The results provided the spectrum of the interaction between COOH groups of MAA to interact with the functionality of the thalidomide enantiomers.
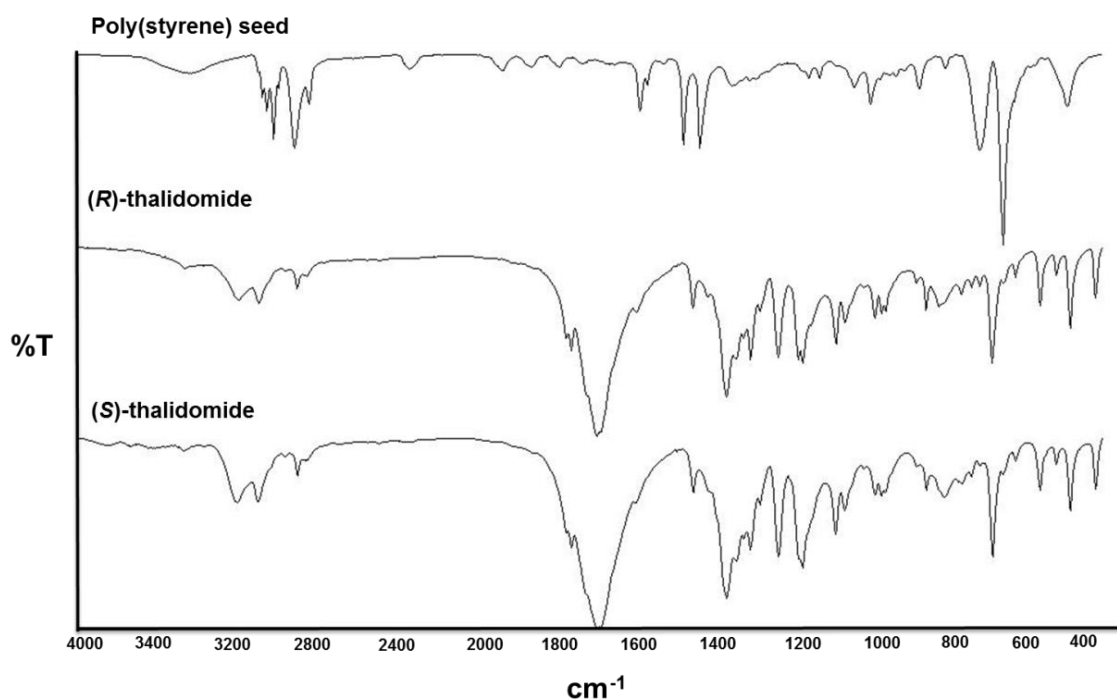
Figure 2.5: FT-IR spectrum of the polystyrene seeds, (R)-thalidomide, and (S)-thalidomide, respectively.
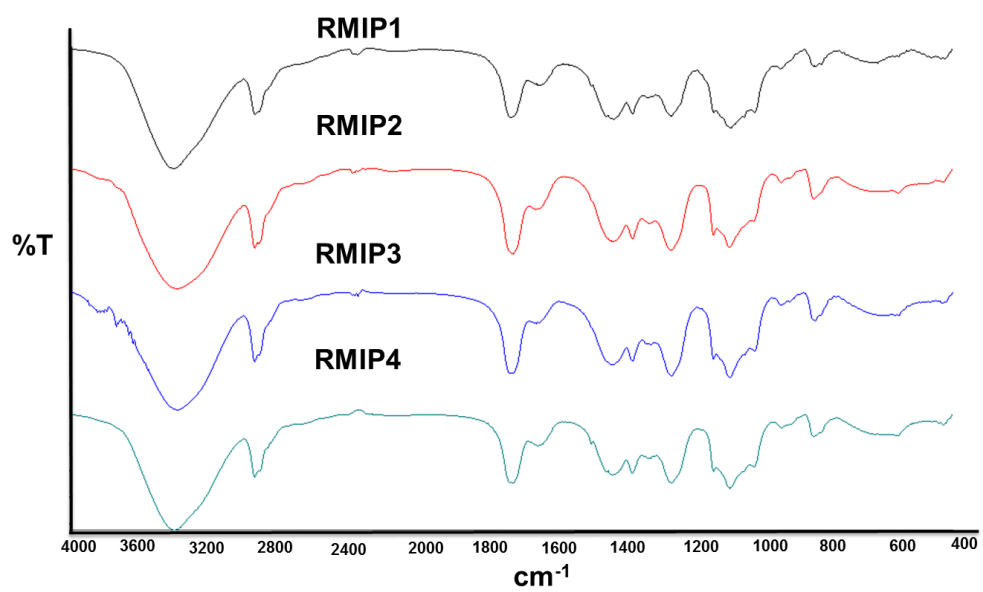
Figure 2.6: FT-IR spectrum (*R*)-thalidomide imprinted polymer (RMIP1, RMIP2, RMIP3 and RMIP4).
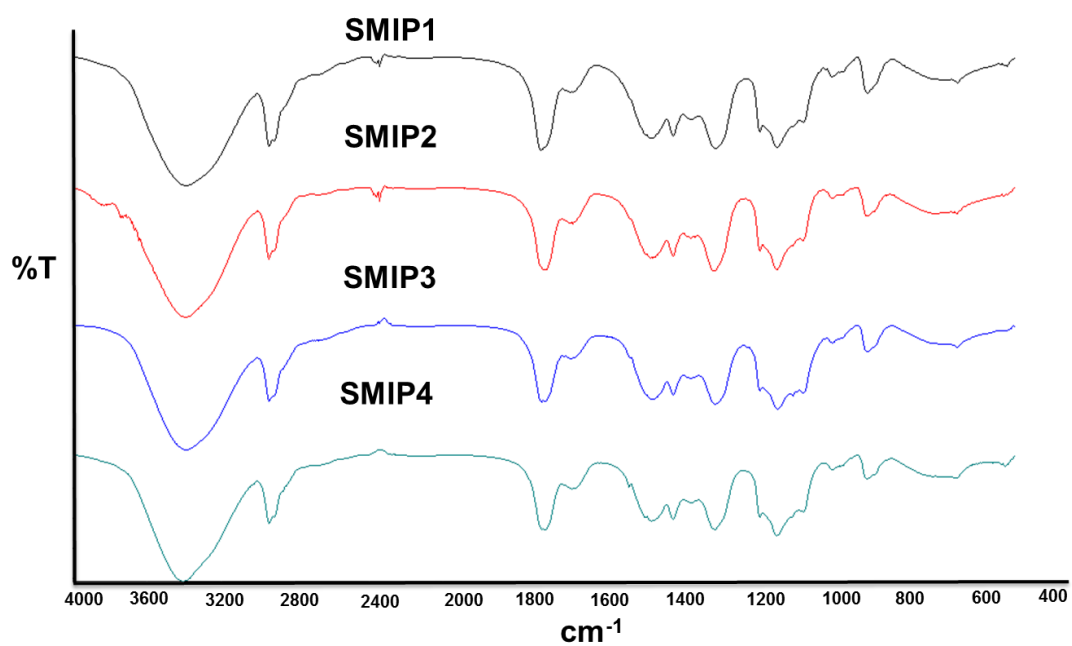
Figure 2.7: FT-IR spectrum of (*S*)-thalidomide imprinted polymer (SMIP1, SMIP2, SMIP3 and SMIP4).

2.4.2.4 Zeta potentials

Table 2.2 illustrates the average zeta potential values for both the (*R*)- and (*S*)-thalidomide imprinted polymers and the non-imprinted polymers. In particular, it was found that, by using a different polymer composition and with a macromer for the polymerization process for both the non-imprinted and imprinted polymers. It was shown that all the particles that were dispersed in the suspension had low zeta potential values and positive charges; hence there was no force to prevent the particles coming together and flocculating. So, the zeta potential data of an imprinted (MAA-NVP)-polymer bead using different monomeric components indicated the appearance of the surface charges on the particles. Also, a comparison of the zeta potentials of the MIPs obtained using either of the two stabilizers is illustrated in Table 2.2. It was of interest, that when the amount of MAA and NVP in the MIP2 was equal, the net surface charge became positive for the polymerization and this in turn reduced the electrostatic interaction of the (*R*)-thalidomide on the particles surface. However, it can be seen that there was an increase in the hydrophobic property with the addition of the poly(styrene) for the polymerization process, in the MIP2 compared with a greater number of negatively charged MAA functional group using either of the thalidomide enantiomers in the MIP1. In contrast, the hydrogen bonding of the COOH groups in the protonated form was also responsible for the interactions in the template-monomer assembly as the overall surface charge became negative when the reaction of the monomeric mixtures had more NVP monomer in the porogenic solvent because that increased the hydrogen bond network that was formed between the polymerized layer and the template assembly at the interface of an aqueous

environment. These results obtained in this work provided knowledge on the effects of the synthesis of the MIPs on the interfacial properties of the MIPs obtained between the PVA and PCL-T as a stabilizer and confirmed the binding sites of the obtained MIPs after polymerization.

Table 2.2: The zeta potential data of non-imprinted polymers and imprinted polymers obtained by different polymeric macromolecules with various functional precursors.

Formulations	Zeta potentials (mV)					
	PVA			PCL-T		
	NIPs	RMIPs	SMIPs	NIPs	RMIPs	SMIPs
F1	1.73 ± 0.95	2.51 ± 1.87	6.38 ± 1.12	-4.57 ± 1.31	2.57 ± 1.81	5.94 ± 2.29
F2	4.27 ± 1.02	-2.39 ± 1.08	1.49 ± 2.04	-1.29 ± 0.58	4.12 ± 3.71	3.50 ± 2.52
F3	-1.10 ± 2.17	-0.52 ± 1.13	-0.83 ± 1.03	3.04 ± 3.95	2.11 ± 1.86	-2.43 ± 3.44
F4	1.59 ± 1.15	-0.44 ± 1.00	0.83 ± 1.43	-1.29 ± 0.58	2.46 ± 2.28	3.56 ± 2.41

2.4.2.5 Contact angle

In this section, the interaction of the imprinted polymers for either nanoparticles and supported onto the glass substrate, and also the MIP films exposed to the thalidomide enantiomers were examined along with the corresponding NIPs by using the contact angle. Figure 2.8 shows the contact angle of the (*R*) and (*S*)-thalidomide imprinted nanoparticles, NIP films, (R)-MIPs and (S)-MIPs films. According to the results in Figure 2.8, the contact angle values were comparable between the nanoparticles, for the NIP and MIP films using the (*R*),-(*S*)-thalidomide enantiomer. Formulations of the MIP2, MIP3 and MIP4 for the (*R*)-thalidomide enantiomer provided different values for the contact angles. The contact angle values (θ_A) of 56.57° for the RMIP1 and 55.24° for the RMIP2 were obtained that was comparable to the RMIP3 ($\theta_A = 59.32°$) and RMIP4 ($\theta_A = 60.67°$). In the case of the S-imprinted polymer only the SMIP3 show different contact angles values between the SMIPs film and NIP-film. A contact angle value of 70 means that there was a hydrophilic interaction of the nanoparticles and the films onto the glass substrate, for which the MIP1 for both templates showed the lowest values of contact angles. The contact angle values of the NIP, MIP nanoparticles, and MIP films were different because the contact angle values were affected by the surface properties and positioning of the cross-linked chains and that would depend on the chemical polymerization process. This approach helped to facilitate to understand the specific interactions between the template and the imprinted sites and the other non-specific adsorption with the polymer matrix and the film polymer.
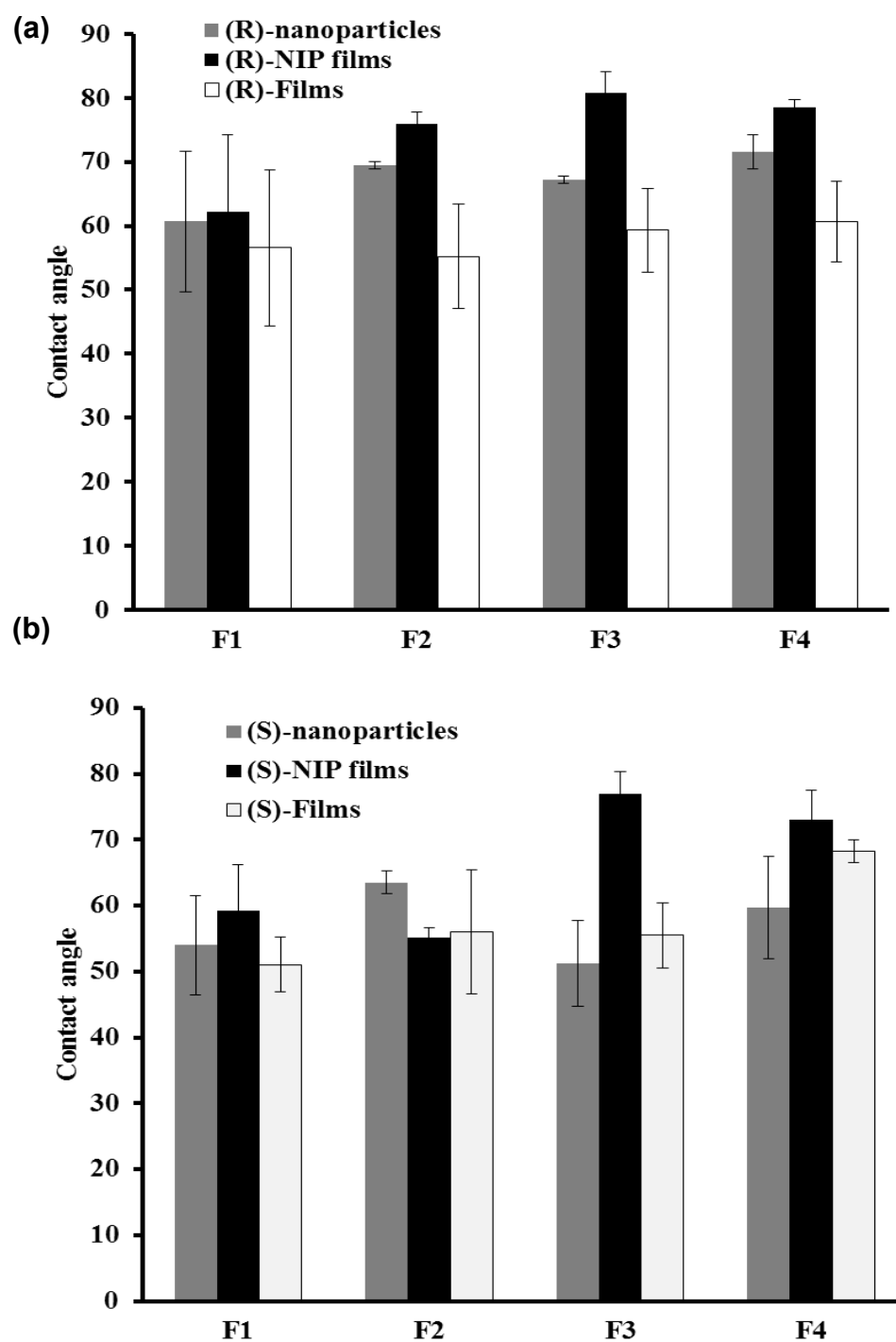
Figure 2.8: Contact angles of the (*R*) and (*S*)-thalidomide imprinted nanoparticles, NIP films, (R)-MIPs and (S)-MIPs films.

2.4.2.6 SEM micrographs of the imprinted films onto glass substrate

The effect of the polymer surface onto the MAA-NVP-crosslinked DHEBA-polymer pre-polymer layer was examined with the focus of the measurement of morphology for RMIP1 and RMIP2. Figure 2.9 shows the SEM micrographs of the imprinted films consisted of the (*R*)-thalidomide imprinted nanoparticles that represent the recognition materials by using the films layer as supporting coating on the glass substrate, RMIP1 and RMIP2 in the presence of the thalidomide template. The RMIP1 films showed the spherical morphology of the nanoparticles. In the case of the RMIP2 provided numerous pore onto the thin films were clearly observed in SEM images because the porogen is attributed to porous material. The characteristic of the surface properties, the non-imprinted nanoparticle thin films were assessed, which they had smaller sized spherical particles on the surface. The particles were embedded inside the thin films so, the remaining specific site with an ability to recognize the analyte was less. The pore on the imprinted thin films can be achived that make possible the interactions with template enantiomers.
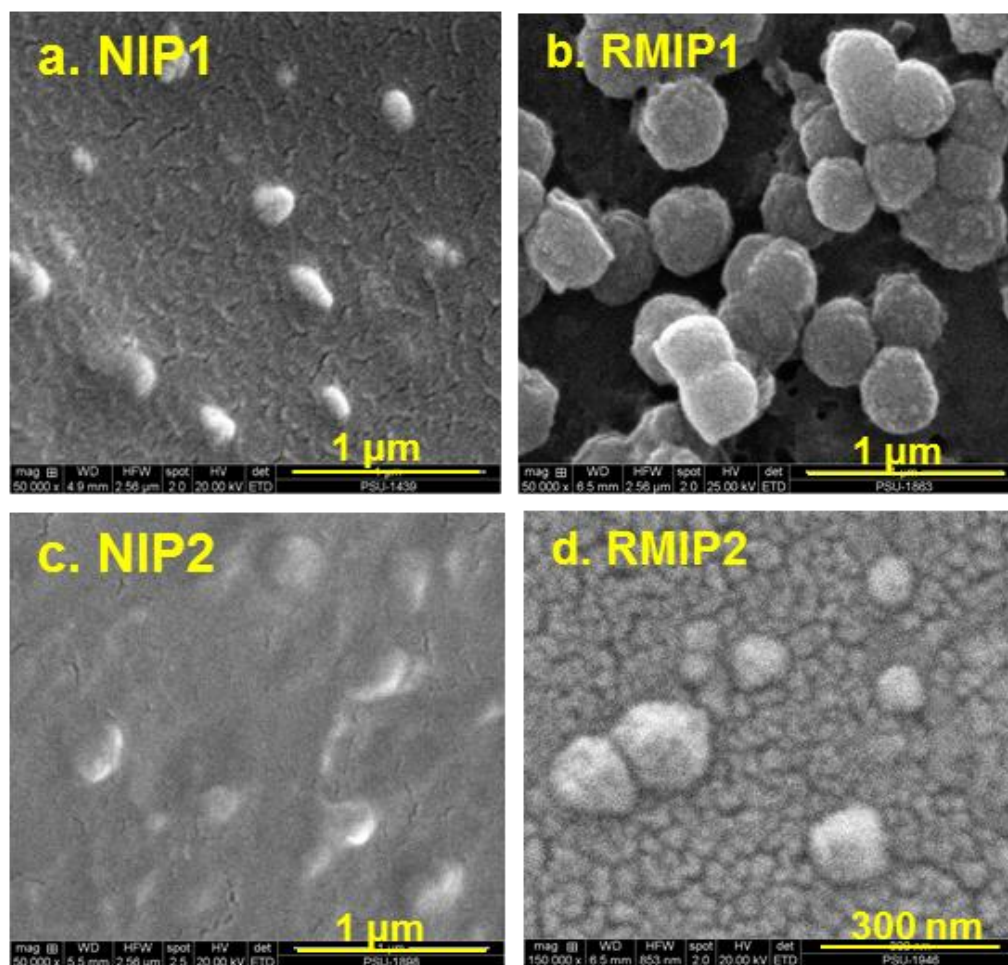
Figure 2.9: SEM images of the imprinted films that were coated with (*R*)-thalidomide imprinted nanoparticles; RMIP1 (MAA-co-NVP 0.43:0.17) and RMIP2 (MAA-co-NVP 0.35:0.35) in the presence of the thalidomide templates.

2.5 CONCLUSION

The objective of the second chapter was to synthesize molecularly imprinted polymer micro/nano particles. The preparations of MIP with MIP micro/nano particles have been successfully prepared using both (*R*)-thalidomide and (*S*)-thalidomide as a template upon the polymerization processes. The presence of polystyrene as a core shell particles in the polymerization reaction from the mixed functional monomer MAA and NVP and DHEBA as the crosslinking agent in toluene as the porogen, followed by high-pressure homoginizer. The characterization and physical properties of the obtained MIPs nanoparticls were investigated by SEM, zeta nanosizer, FT-IR and contact angle. The template removal was performed with methanol and 10% acetic acid in methanol solvents and completed extraction of thalidomide enantiomers template was shown imprinted cavities after washing off. The obtained MIPs particles exhibited a crosslinking polymerization that confirmed by using FT-IR. The stabilizer of PVA and PCL-T could enhance the physical stability of the obtained MIPs that prevented the aggregation of the suspension solution. The use of the PVA stabilizer, the particles sizes of MIPs products was 20-30 µm. and reduced in the sub-micron sizes (1-5 µm) after homogenizing method in using of PVA. The component of the monomeric mixture had effect to the net charge of the solution that occur the interface between thalidomide templates and the imprinted site.

CHAPTER 3

THE STUDY OF MOLECULARLY IMPRINTED POLYMER-SOLID PHASE EXTRACTION (MIP-SPE)

3.1 Introduction and objectives

The recognition ability of the prepared molecularly imprinted polymers is important to identify which MIPs would be effective for binding the Anti-tumor Necrosis Factor Alpha (anti-TNF-α) agent. For this purpose, (*R*)-thalidomide and (*S*)-thalidomide molecularly imprinted polymers were employed in screening experiments in which the two single enantiomers of thalidomide were used in the presence of their related MIP and their non-imprinted control polymers. The determination of the template binding interactions of the obtained MIPs has been carried out by batch binding experiments. Molecularly imprinted polymers were used as a selective agent for the chiral enantiomers. Molecularly imprinted solid phase extraction was used for evaluation of the recognition ability of the analyzes in the presence of the biological components of blood sample, using a polymer material as a support system (MISPE). Moreover, the chiral recognition sites of the MIP micro/nanoparticles helped to facilitate the concentration and %age recovery of transformation and the chiral inversions of thalidomide enantiomers in blood using molecularly imprinted solid phase extraction (MISPE). MIPs can provide a strong selectivity and sensitivity of analytical methods.

The adsorption could be occurred through the processes of selective imprinted sites, the enantiomer extraction where on sorbent bed of thalidomide imprinted micro particles during enrichment process only selected enantiomers were retained while the non-adsorption enantiomer was not retained on the MIP selective adsorbent. Then, the impurities were rinsed through with PBS pH 5.5 that were strong enough to remove unbound thalidomide enantiomer. The selective elution of enantiomers adsorbed into the imprinted sites was eluted in a solvent. The % recovery was calculated by using equation (3.1).

$$\% \text{ enrichment (recovery)} = \frac{\text{Detected amount} \times 100}{\text{Actual amount}} \quad \text{------------ (3.1)}$$

Actual amount was obtained through the HPLC chiral column and measured from equation (3.2).

$$\text{Actual amount} = \frac{\text{Weight of solution} \times \text{concentration of standard}}{\text{Density of solution} \times \text{volume}} \quad \text{------- (3.2)}$$

The first question of the investigation of this chapter was addressed to the examination of the chiral conversion in blood of the thalidomide enantiomers by using the molecularly imprinted polymer micro particles as a sorbent mixed with the resin. MISPE used to extract and clean up a sample before using a chromatographic method to quantify the amount of enantiomers in the sample.

3.2 Experimental

3.2.1 Materials and equipment

Biored® resin sodium form (Bio-Red Laboratories, Inc., California), Chiral-CBH column (Chromtech, UK). NIPRO Disposable Syringe, Sterile, 1 ml, Nipro Co.,Ltd (Phra Nakhon Si Ayutthaya, Thailand). VertiPure™ NYLON Syringe Filters with a pore size of 0.45 μm, and diameter of 4 mm were from Vertical Chromatography Co.,Ltd (Ladyao, Jatujak, Thailand).

3.2.2 The binding experiments

The recognition ability of the template by all the MIPs was examined using different media: distilled water, acetonitrile and pH 5.5 phosphate buffer, for different periods of time (15, 20 and 24 hour) by the batch dissolution tests. A control experiment was performed with the corresponding non-imprinted polymers under the same conditions. In a typical batch binding experiment, 25 mg of polymers were added into 10-80 μg mL^{-1} of a pure (*R*)- and (*S*)-thalidomide solution (2.5 mL) that was added separately, after the required incubation period the amounts of the (*R*)-thalidomide and (*S*)-thalidomide enantiomers in the samples were determined by reference to a standard solution calibration curve obtained using separation by a column that separated the chiral enantiomers. In order to enhance the specific molecular recognition within the imprinted polymer network that was performed in the preliminary study, a 24 h period was selected. The amount of bound drug was

obtained by subtracting the amount of free drug from the total amount of the drug added. All experiments were performed in triplicate. In addition, an amount of 10-80 μg mL^{-1} of R)-thalidomide was incubated for a period of up to 6 months. The bound polymer was washed with distilled water and dried in air before analysis of the enantiomer by stereospecific HPLC. The AFM images of the particle surfaces of the non-imprinted polymer, and (R)-thalidomide and (S)-thalidomide imprinted polymer were taken after incubating the chiral print molecules in distilled water.

3.2.3 The selective property studies of thalidomide enantiomers

The selective recognition of the synthetic materials was evaluated in an aqueous solution, of acetonitrile and 10 mM phosphate buffer solution pH 5.5 (50:50, v/v) using a batch binding assay. A control-imprinted polymer (NIP) was used as the reference material. In a typical binding experiment, the polymer particulate (50 mg) was added to 5 mL of the solvent containing 10-80 μg mL^{-1} of the (R)-or (S)-thalidomide. The polymer solution was stirred for 24 h at room temperature (28 ± 1°C). The polymer particles were then filtered, and the filtrate analyzed for their content of the thalidomide enantiomers by the stereospecific HPLC. The quantity of the drug enantiomer in the solution was determined by reference to a calibration curve. The ability for recognition by the MIPs was defined as the ratio of the amount of the drug released by the MIP to that released by the NIP. All experiments were performed in triplicate.

3.2.4 Molecularly imprinted polymer-sorbent assays (MIP-SPE)

The adsorption affinity achieved by the MIP and NIP nanoparticles packed in cartridges was performed for the individual enantiomer and racemic thalidomide solution before use and in the presence of heparinized human blood plasma at a concentration that ranged from 5-200 μg mL^{-1}. A 50 mg sample of the MIPs or NIPs were mixed with the sodium form of the Biored$^{®}$ resin to support the MIP and NIP nanoparticles (Bio-Red Laboratories, Inc., California) were packed into an empty SPE cartridge column (1 mL) (Figure 3.1), that supported the nanoparticles (less than 30 nm) during MIP-SPE for an efficient separation. The pH of the collected blood obtained at Songklanagarind hospital, which had been dispensed in glass tubes filled with carbon dioxide-oxygen at the ratio 95:5 for control of pH 7.4, then sealed, and incubated at 37°C in a water bath. An equal volume of 0.025 M citrate buffer solution (pH 1.5) was added to stop the reactions and samples were stored at -4°C until analyzed. The sample of human blood was then passed through the solid-phase at a flow rate of about 1.0 mL/min for 10 min. The combined fractions were filtered through a 0.45 μm PTFE membrane and analysis of the enantiomer in the eluent was determined by the stereospecific HPLC method. They were analysed for milligram amounts of the unbound drug of the (*R*)-isomer from each of the MIPs divided by the (*S*)-isomer (amount/time).
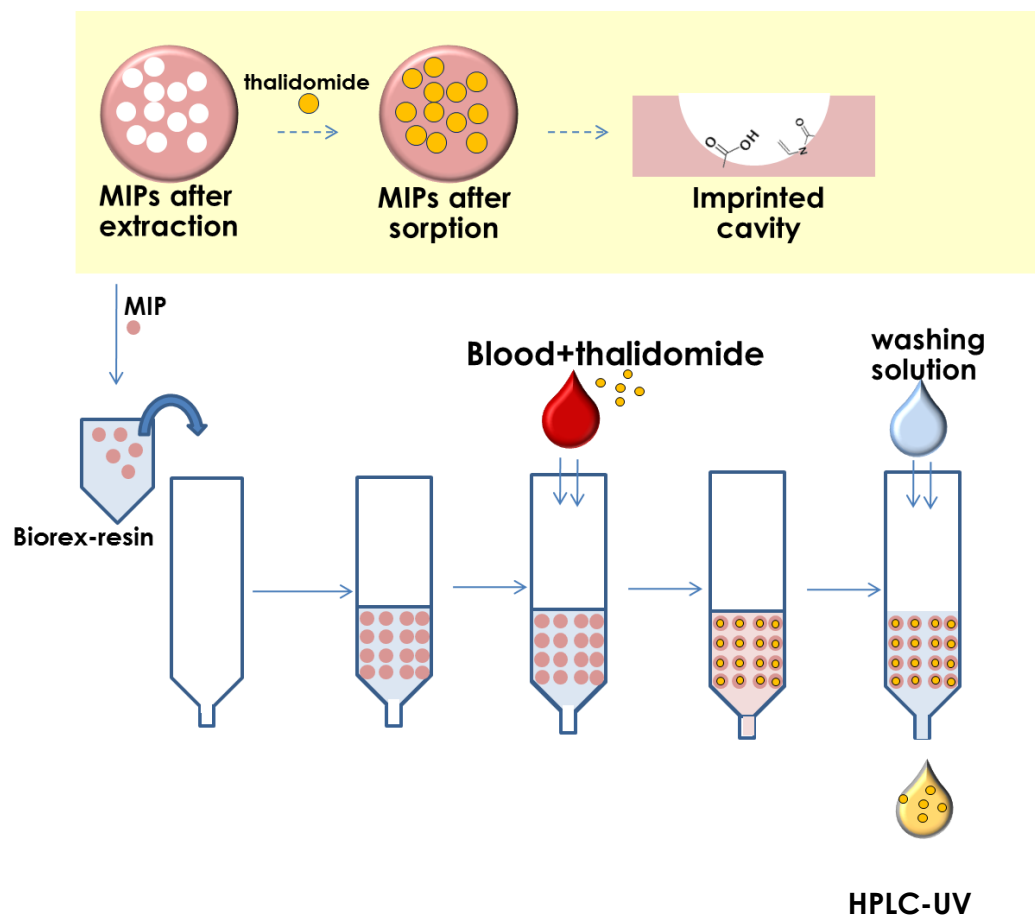
Figure 3.1: Schematic diagram of MISPE for investigation of the recognition properties of thalidomide exposed to aqueous solutions and human blood samples.

3.2.5 Enantioselective HPLC analysis

The amount of the thalidomide enantiomers in the sample solutions was examined by HPLC using a chiral CBH column. The chromatographic system comprised a Thermo HPLC system, equipped with a variable wavelength UV detector. A 150 x 4 mm Chiral-CBH column (Chromtech, UK) was used. The detection wavelength was 225 nm and separation was performed at ambient

temperature. The flow rate was set at 0.9 mL/min for every analysis. The mobile phase was 10 mM phosphate buffer (pH 5.5) containing 50 mM disodium EDTA and 2 % (v/v) acetonitrile. Correlation coefficients for the calibration curves of the (*R*)- and (*S*)-thalidomide enantiomers in the range 1-10 µg mL^{-1} were greater than 0.990. The sensitivity of the detection for both thalidomide enantiomers was about 1 µg/mL and the reproducibility of the peak areas of analytes was more than 95%.

3.2.6 Statistical analysis

All results are shown as means ± standard deviations. Statistical analysis was performed with the excel software program version 2010 was applied to assess the variances between the groups, followed by the *t*-test (p ≤ 0.05) that showed significant difference between the means.

3.3 Result and discussions

3.3.1 The evaluation of chiral recognition for the MIPs

3.3.1.1 The effect of time to achieve equilibrium

The recognition site of the molecularly imprinted polymer that had a flexible structure should provide the ability to differentiate between the stereo-chemical entities of the enantiomers of thalidomide in an aqueous solution. The recognition ability for the binding of the enantiomer template to the (*R*)- and (*S*)-thalidomide

imprinted (MAA-co-NVP)-polymer were investigated. This was important in order to assess the release of the desired enantiomer after the adsorption process at a suitable reaction site by using dissolution studies. Figure 3.2 shows the effect of the concentration of the template and non-template on the binding efficiency of MIP2 as a function of time when incubating with each of the pure single enantiomer at 15, 20, and 24 h. The enantiomer release was calculated from detected amount of the thalidomide enantiomers divided by actual amount of the standard thalidomide enantiomers and multiply by 100. The optimum time required for the production of the imprinted polymer with the chiral recognition property. As shown in Figure 3.2 (a-c), after incubation for 15 h, it was clearly observed that addition of the pure single (R)-enantiomer of thalidomide to the imprinting polymer in an aqueous solution produced some changes to the opposite (S)-enantiomer as racemization of the thalidomide enantiomer occurred. Both imprints were now present in the same polymer. Nevertheless, an identical enantiomer concentration of the enantiomerically pure (S)-thalidomide enantiomer, led to desorption of the (S)-enantiomer from the imprint towards the (S)-thalidomide enantiomer but only in an aqueous solvent with the same selectivity profile throughout the incubation for 24 h. These observed differences can be explained by the kinetics of conversion of thalidomide enantiomers that occurred by either the imprinted and non-imprinted enantiomers from both the (S)-enantiomer imprint and the (R)-enantiomer imprint, that were loaded with the pure single (R)-thalidomide enantiomer. In the case of the non-imprinted polymer this led to almost a total desorption of thalidomide enantiomer with the same profile after 15 h, to indicate a non-specific effect on the polymers under the same conditions with regard to both stereoisomers. The correlation of the time required for the enantiomer

binding to reach equilibrium was dependent on two additional factors, the diffusion of the template from the bulk solution through the pores in the polymers to the binding sites and the actual binding kinetics between the template and the imprint. However, the measurements performed using the MIP spherical particles showed there was a high rate of adsorption of the corresponding thalidomide enantiomers in aqueous solution. After 20 h, the increase of the template enantiomers released from either of the MIP beads incubated with either of the pure thalidomide enantiomers demonstrated a gradual increase in the amount of the enantiomer that was permeated with time. The rate of diffusion of the non-templated enantiomer was much faster than that of the template enantiomer so the target recognition was stronger than for the non-target enantiomer. The cross-reactivity of the (S)-form of the thalidomide was lower than that for the (R)-thalidomide enantiomer. Therefore, the inclusion of the (R)-enantiomer to the latter polymer was being spatially hindered and the conformation of the imprint enantiomer was preserved during the rebinding of the template. The current studies have indicated that the imprint of the (R)-thalidomide as template that produces a complex results in a diminished adsorption and racemization at every concentration in an aqueous environment which undergo a slow conformation change to produce a fitted complex. At 24 hour showed the optimal binding of the thalidomide enantiomers because it showed the optimal amount bound to the imprinted sites and the enantiomers was not changed.

(a) 15 h
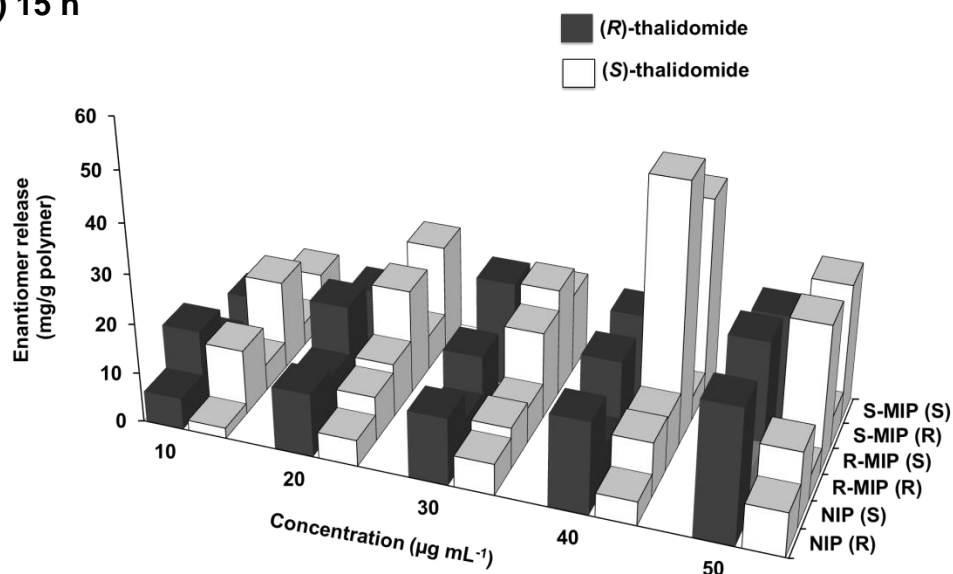
(b) 20 h
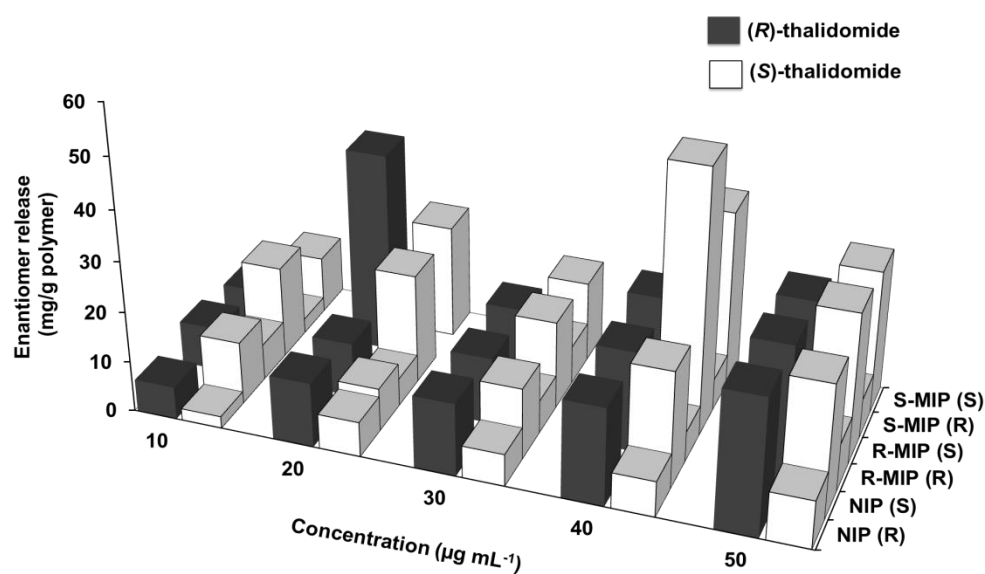
Figure 3.2: The effect of time 15 hour (a) and 20 hour (b) for the equilibrium binding of the template enantiomer on the (*R*)- and (*S*)-thalidomide imprinted (MAA-*co*-NVP)-polymer that had been produced in the presence of the additional poly(styrene) with a 0.35:0.35 mole ratio MAA/NVP.

(c) 24 h
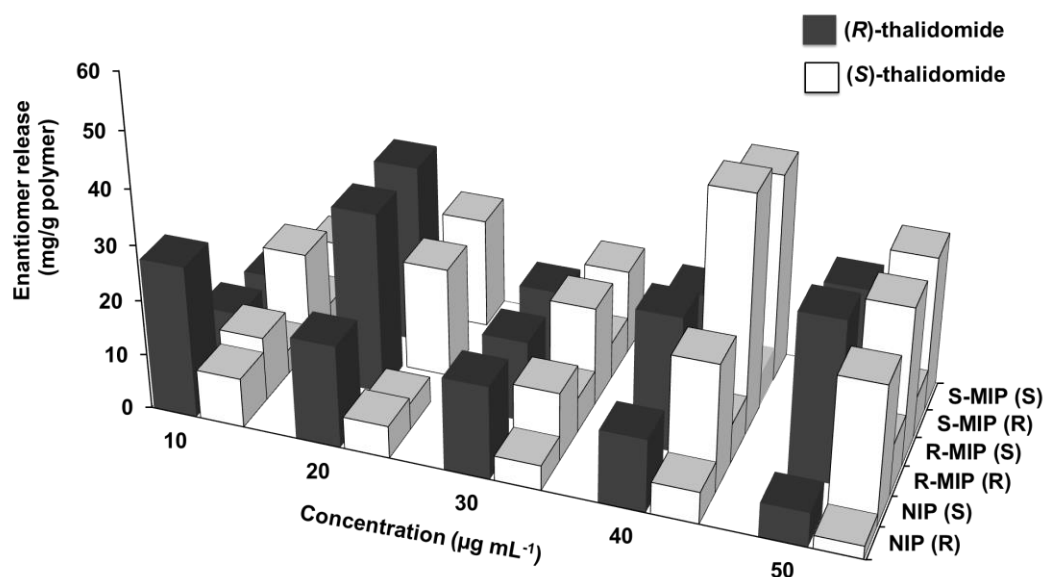
Figure 3.2: The effect of time 24 hour (c) for the equilibrium binding of the template enantiomer on the *R*)- and the(*S*)-thalidomide imprinted (MAA-*co*-NVP)-polymer that were produced in the presence of the additional poly(styrene) with a 0.35:0.35 mole ratio for the MAA/NVP.

3.3.1.2 The effect of the enantiomer concentrations

Figure 3.3 illustrates the effect of the (*R*),-(*S*)-enantiomer concentration on the binding capacities of the thalidomide imprinted polymer and the control polymers after incubating for 6 months. For the (*R*)-thalidomide imprinted polymer only the (*R*)- enantiomer was obtained in the extract but there was a lower amount of the enantiomer in the extract than for the (*S*)-enantiomer imprint. When the corresponding NIP, were used both the (*R*)- and the (*S*)-enantiomer were recovered after incubation with the pure single enantiomers to show that there was a high non-specific adsorption at most of the concentrations studied. During the 6 months the amount of the enantiomers bound to the specific particles did increase and no racemization occurred. This indicated that the template diffused into the polymer and bound to the MIPs. When each of the latter polymers was incubated with the imprint and non-imprint enantiomer separately. The analyte was found to increase in the solution as the added concentration increased but the increase in the amount of the non-imprint (*R*)-isomer released in the (*S*)-enantiomer MIP was greater than the increase of the concentration of non-imprint release (*S*)-isomer in the (*R*)-enantiomer MIP. In contrast, the MIP4 showed that the entire amount of both the (*R*)- and (*S*)-enantiomers of the thalidomide had in this case disappeared because the MIP4 was able to adsorb the thalidomide enantiomers inside the imprinted site. We tested the stereoselectivity of the different imprinted DHEBA-polymer materials with variable functionalities for the polymerization process to examine the enantioselective recognition characteristics of the resulting synthetic polymers. This provided important information such as an imprinting factor, and a factor for selectivity was obtained.

(a) MIP1
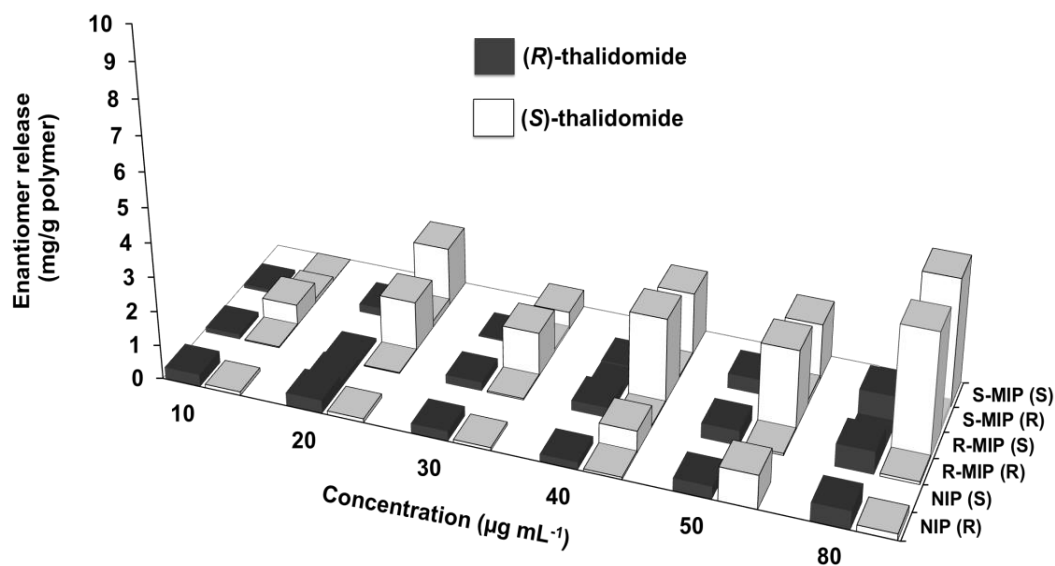
(b) MIP2
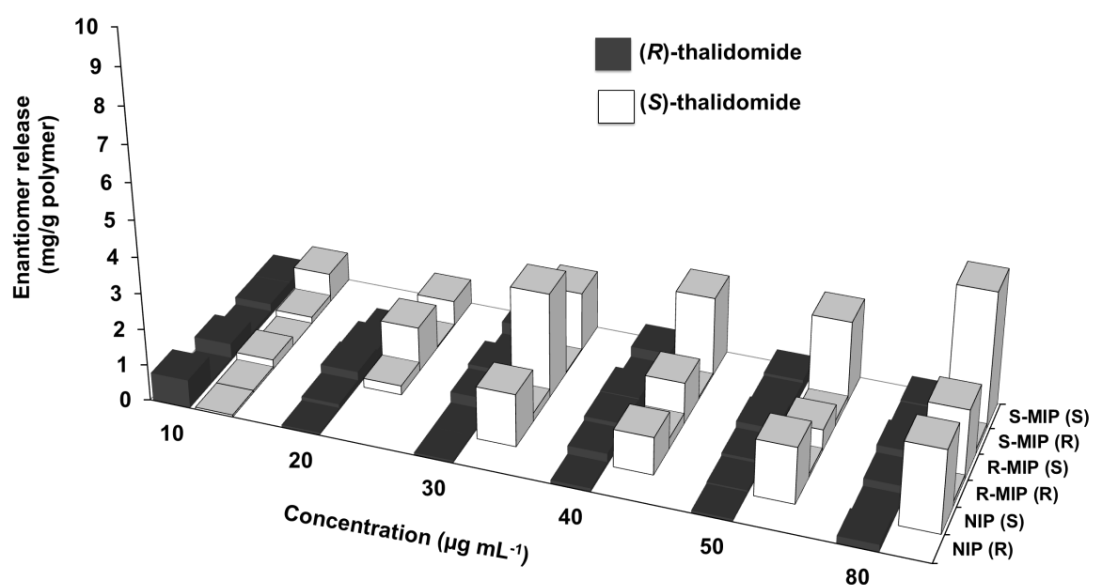
Figure 3.3: The effect of the (*R*), -(*S*)-enantiomer concentrations on the binding capacities of the thalidomide imprinted polymer and the control polymers in an aqueous solution for 6 months from their formation.

(c) MIP3
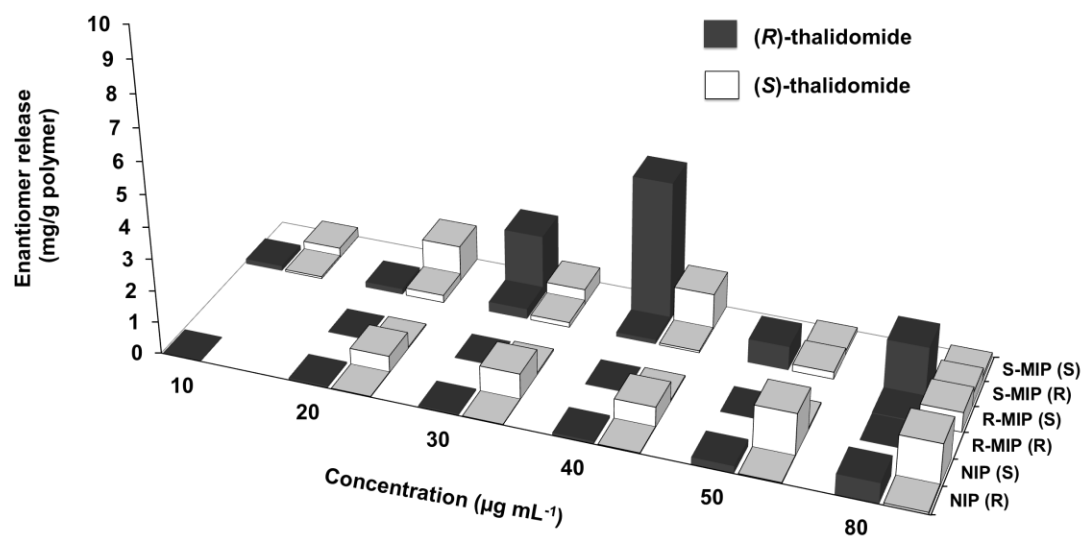
(d) MIP4
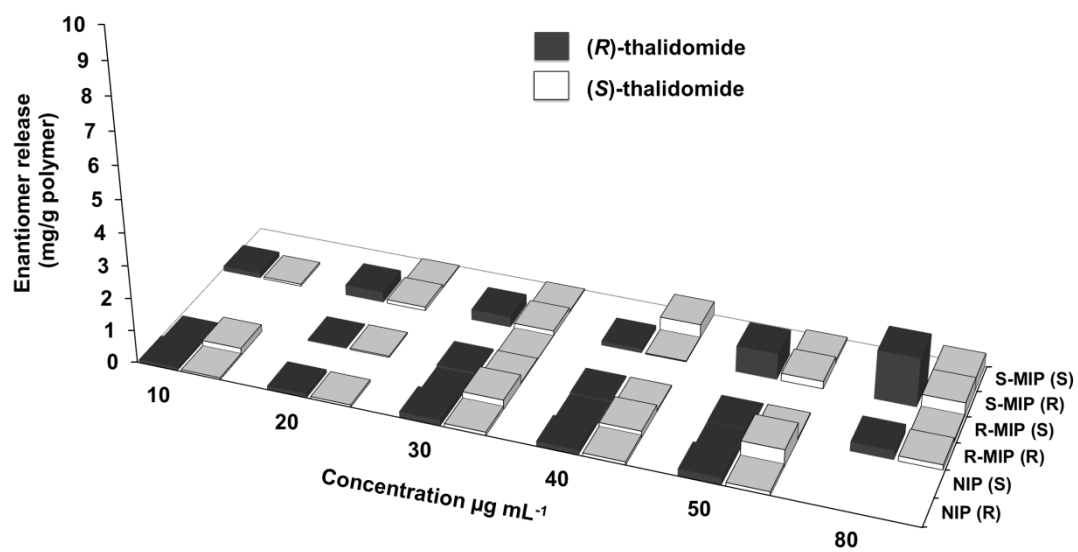
Figure 3.3: The effect of the (*R*), -(*S*)-enantiomer concentrations on the binding capacities for the thalidomide imprinted polymer and the control polymers in an aqueous solution 6 months after their formation.

3.3.2 The characterization of the surface behavior by MIP-SPE

3.3.2.1 The effect of aqueous solution

To evaluate if the obtained molecularly imprinted polymer were selective to the imprinted sites; the rebinding of the imprinted polymer was investigated, following by enantioselective chromatography. The enantioselective separation of thalidomide in an aqueous solution was carried using the CBH chiral column. Figure 3.4 shows the chromatograms of the (*Rac*)-thalidomide to show the performance of the enantioseparated chromatogram. Separation of the enantiomers had an optimal pH of pH ~5.5. To evaluate the recognition properties of the imprinted polymer, the (*R*)-imprinted polymer (RMIP1) and (*S*)-imprinted molecularly polymer (SMIP1) were incubated with their individual template of (*R*)-thalidomide and (*S*)-thalidomide. As can be seen by the chromatograms for the RMIP1 (Figure 3.4 II) the thalidomide underwent hydrolysis degradation at the higher pH (Lyon *et al*., 1995). Consequently, the molecularly imprinted polymer had a specific recognition site to memorize the thalidomide enantiomer.
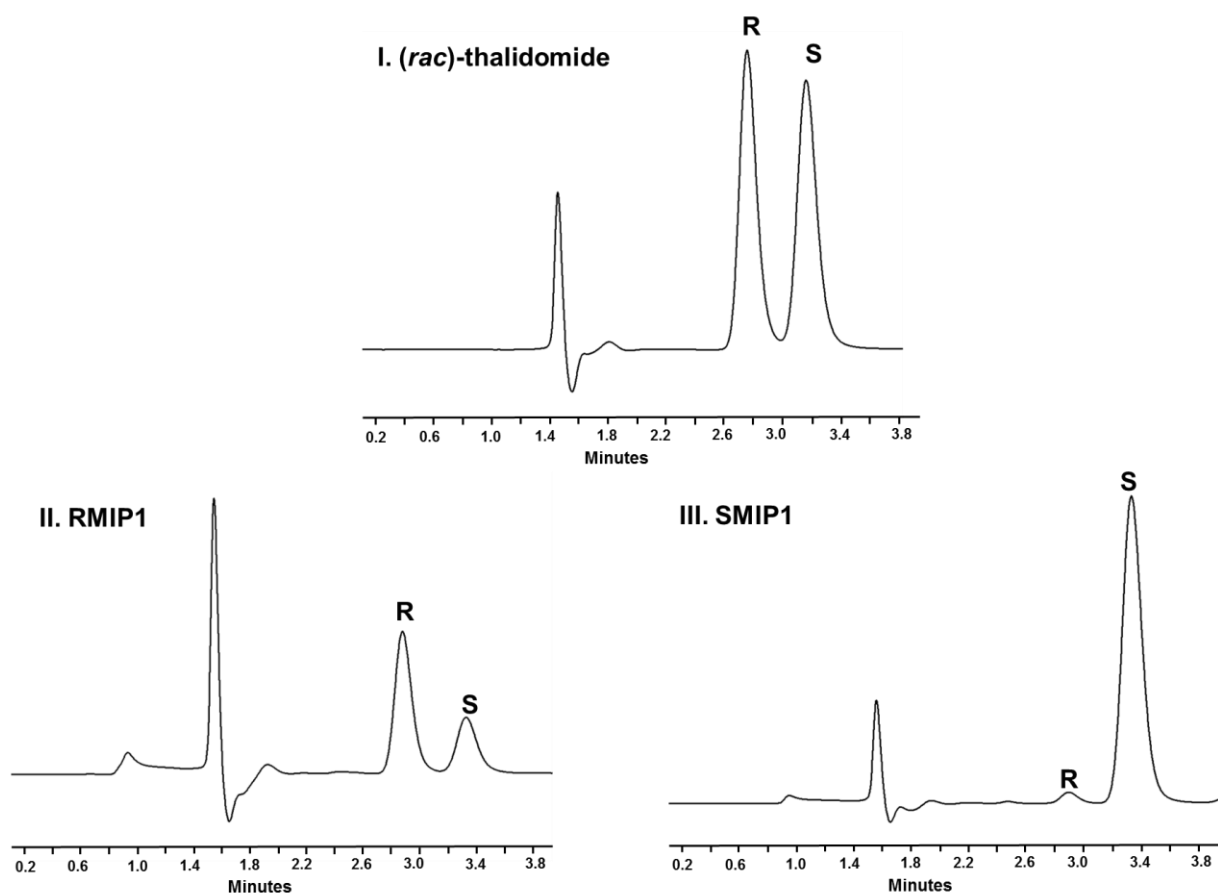
Figure 3.4: Chromatograms of the individual thalidomide enantiomers at 10 μg mL^{-1} on (I). RMIP1 were incubated with (*R*)-thalidomide in the water at a concentration of 50 μg mL^{-1} (II). SMIP1 was incubated with (*S*)-thalidomide in the water at a concentration 50 μg mL^{-1} (III). Chromatograms of the (*R*)-isomer and the (*S*)-isomer of thalidomide in a solution.

3.3.2.2 The effect of solvent media

The separation of the thalidomide enantiomer under the solvent conditions was carried out because the stability of thalidomide in acetonitrile (ACN) is the most important parameter of concern to ensure the reliability of the assay. (*R*)-, (*S*)-imprinted polymer were incubated with their template enantiomers into the ACN:PBS pH 5.5 to evaluate the recognition ability of the synthesize MIPs. Figure 3.5A illustrates the chromatograms of the RMIP2 that were incubated with (*R*)-thalidomide (I). SMIP3 was incubated with (*S*)-thalidomide (II) in the ACN:PBS pH 5.5 (1:1) solvent to provide enantioselective separation of the (*R*)-isomer, (*S*)-isomer, *R/S*-isomer and (*rac*)-isomer of MIPs. The corresponding retention times of the RMIP2 were incubated with (*R*)-thalidomide at the concentration of a 80 µg mL^{-1} as shown in Table 3.1 under the ACN with PBS of pH 5.5 that provided a good enantioselective separation for the R-MIP and the S-MIP.
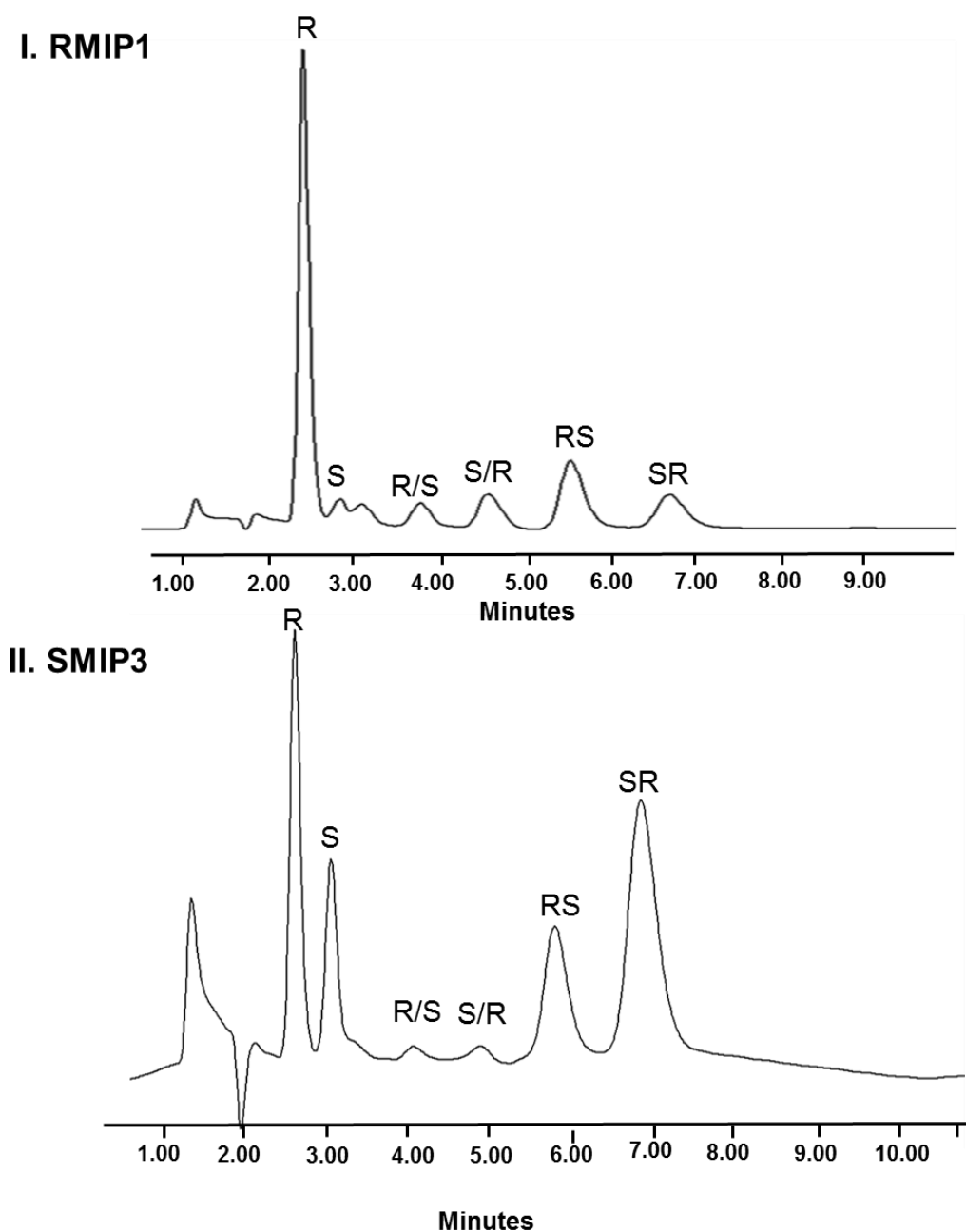
Figure 3.5A: Chromatograms of the individual thalidomide and various isomers of thalidomide after extraction on MIP-SPE. RMIP1 that had been incubated with (*R*)-thalidomide (I). SMIP3 were incubated with (*S*)-thalidomide into the ACN:PBS pH 5.5 at 80 μg mL^{-1} (II) showing the stereoisomers of thalidomide and a mixture of enantiomer separated on the MIP.

3.3.2.3 The incubation of blood with other component mixture

Figure 3.5B shows enantioselective chromatograms of the RMIP2 that had been incubated with the (*R*)-thalidomide and blood sample (III). SMIP4 was incubated with (*S*)-thalidomide and a blood sample (IV). The racemization between the enantiomers of thalidomide now occurs at physiological pH in a biological matrix and underwent a rapid spontaneous hydrolysis. However, the isomers of thalidomide were clearly separated even from the blood sample.
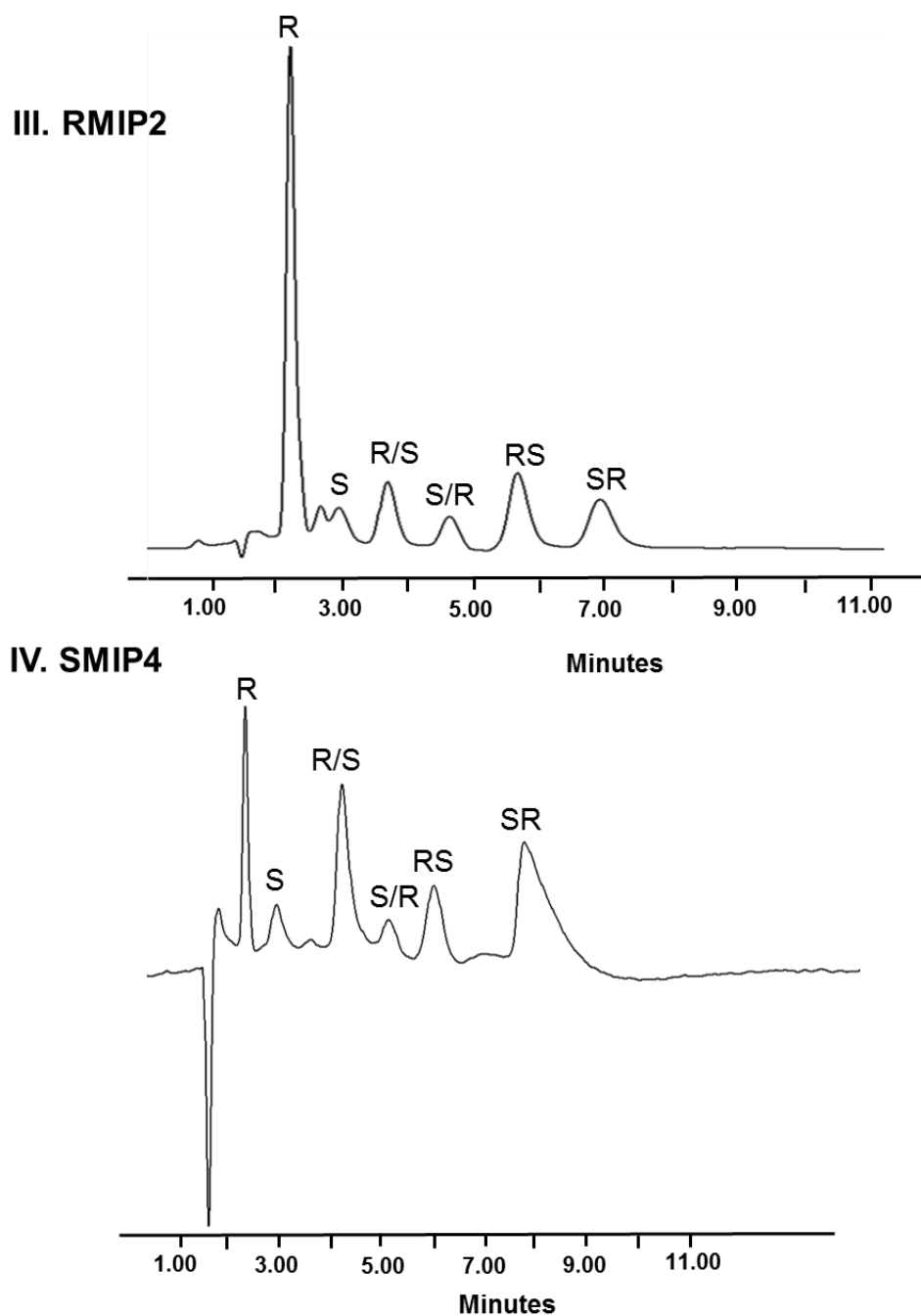
Figure 3.5B: Chromatograms of the individual thalidomide and various isomers of thalidomide after extraction on MIP-SPE. RMIP2 were incubated with (*R*)-thalidomide and blood sample at 80 μg mL^{-1} (III). SMIP4 was incubated with (*S*)-thalidomide and blood sample at 150 μg mL^{-1} (IV), showing the stereoisomers of thalidomide and a mixture of enantiomer separated on the MIP (II).

Table 3.1: The chromatographic retention time of the thalidomide enantiomers from MIP-SPE in different solvent media.

Incubation system	MIPs	Thalidomide enantiomer					
		(*R*)-isomer	(*S*)-isomer	*R/S*-isomer	*S/R*-isomer	(*RS*)-isomer	(*SR*)-isomer
Aqueous solution	RMIP1	2.80	2.90	-	-	-	-
	SMIP1	3.30	3.40	-	-	-	-
ACN:PBS pH 5.5	RMIP2	2.50	2.9	3.90	4.80	5.80	6.90
	SMIP3	2.80	3.10	4.00	5.00	5.80	7.00
Blood	RMIP2	2.40	2.9	3.80	4.60	5.80	7.00
	SMIP4	2.80	3.00	4.20	5.00	6.00	8.20

3.3.2.4 The characteristic of MIPs mixed with resin

SEM was applied to evaluate the characteristics of the imprinted polymer and resin that was packed inside the column. Figure 3.6 show a scanning electron micrograph showing the morphology of the RMIP1 with the resin. The images had an irregular morphology (like microparticles with small cavities). The pore structure of the imprinted polymer mixed with resin was due to the combined material as shown in Figure 3.6, after extraction, the size of the particles was 300 nm and this provided a high surface area for attachment of the analytes.
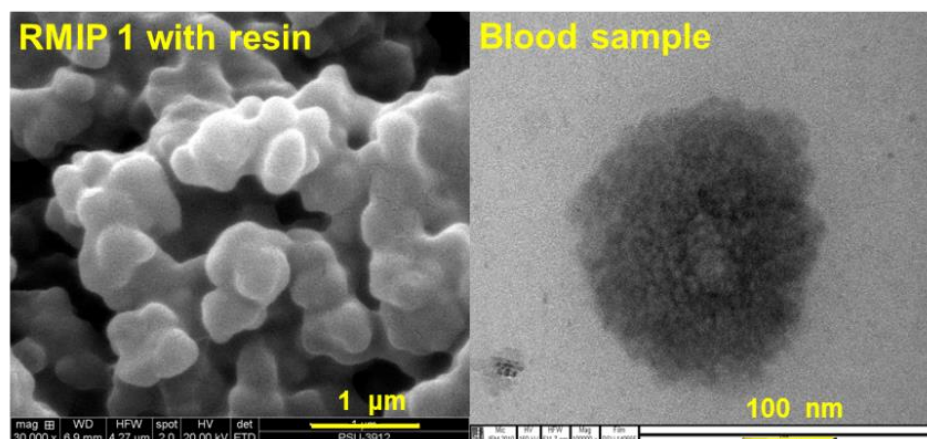
Figure 3.6: SEM of the RMIP1 (30,000x magnification) with resin when exposed to the enantiomer of thalidomide in the blood (100,000x magnifications).

3.3.3 The extraction by MISPE

Figure 3.7 shows the amount of thalidomide bound to the imprinted site from the MISPE using the four MIP formulations for both enantiomers. The results showed that the amount of thalidomide bound to the RMIP was much higher in comparison to its corresponding NIP. This indicated that a large number of (R)-thalidomide specific binding sites had been produced during the polymerization processes. The adsorption of the (R)-thalidomide template bound to the RMIP2 was greater than the (R)-enantiomer released from the SMIP2. However, the same amount of the enantiomer was released from the RMIP2 and SMIP2 when they were incubated with the racemic-thalidomide. However, at low concentrations an amount of the template was released from the RMIP3 into the solution while when the (S)-thalidomide imprinted polymer was incubated with (R)-thalidomide, it was more easily released than from the non-template molecules. The RMIP3 or SMIP3 facilitated more binding of the (R)-thalidomide when incubated with the (RS)-thalidomide. The (R)-thalidomide from the RMIP4 and SMIP4 had a lower release of (R/S) and (S/R). However, the adsorption of the (S)-thalidomide to the RMIP4 and the SMIP4 provided only the (R)-thalidomide. A non-specific binding of the (RS)-thalidomide was observed in the RMIP4 and SMIP4. This study indicated that, the amount of the bound thalidomide for the (R)-isomer was much higher than for the other isomers. Consequently, the RMIP1 showed the lowest selective enrichment of the unbound drug for the (R)-thalidomide because the (R)-thalidomide had access to the specific site for the (R)-thalidomide imprinted polymer MIPs. The selectivity was indicated in that the imprinted polymer would be specific to the enantiomer template used in the

polymerization. In this study, the use of the MISPE for measuring the MIPs and either of the two enantiomers can be used to assess the amount and the concentration of conversion of the thalidomide enantiomer in the solution and the blood.
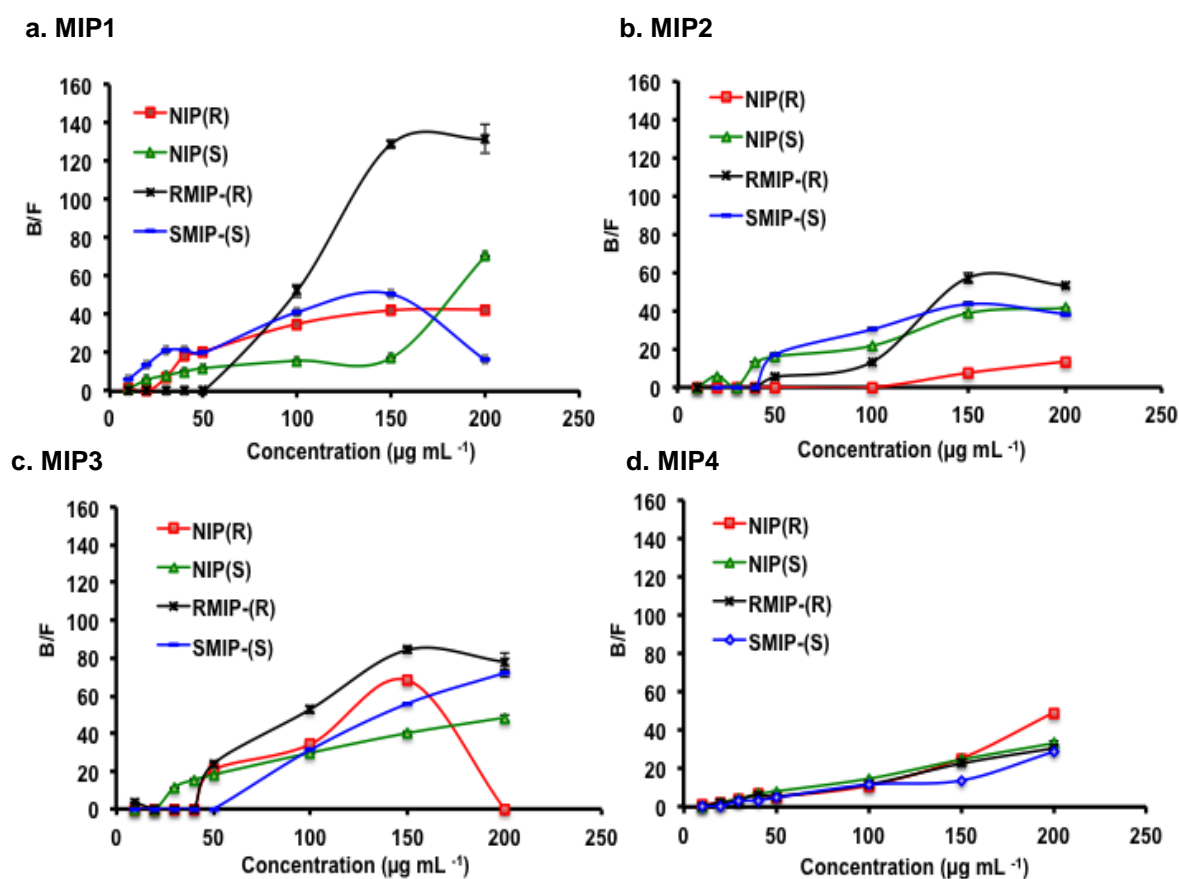
Figure 3.7: The concentration of the thalidomide bound to the imprinted site of the MIP1, MIP2, MIP3, and MIP4 when incubated with the individual enantiomers and racemic thalidomide by the MISPE.

3.3.4 Chiral conversion of thalidomide enantiomer in the various solvents

Table 3.2 shows the rate of the thalidomide conversion for both the RMIP4 and SMIP4 at 50 µg mL^{-1}. The lowest chiral inversions were observed in the absence of a polystyrene seed for the (*R*)-enantiomer MIP3 and MIP4 that was incubated with the (*R*)-enantiomer. Complexation within the imprinted polymer beads was low and the (*R*)-thalidomide did not easily desorb from the polymer bead by itself but it diffused in the presence of either the MIP1 or the MIP2, whereas the mass transfer of the alternative enantiomer was low in an aqueous medium at the ambient temperature and it had a similar pattern with either of the imprinting polymers over a 24 h period.

Table 3.2: Chiral conversion of thalidomide enantiomers for the MIPs on phase extraction in different solvents and blood.

Polymer	Analyte	Rate $\times 10^{-4}$ (mg min^{-1})*							
		Water	ACN:pH 5.5 without incubation			pH 5.5 with incubation in blood		
		R,S-isomer	R,S-isomer	R/S isomer	Rac-isomer	R,S-isomer	R/S isomer	R,S-isomer
RMIP	Template	4.10±0.22	1.49±0.04	3.91±0.09	330.0±37.9	0.01±0.46	-	-
	Non-template (enantiomer)	-	0.99±0.05	119.70±18.20	9.36±0.19	4.01±0.75	6.31±1.40	2.29±0.17
	Non-template (racemic)	-	-	-	-	6.63±0.45	2.55±0.52	2.29±0.17
SMIP	Template	-	28.0±2.05	6.97±0.04	914.19±169	12.3±1.91	6.74±1.28	2.36±0.32
	Non-template (enantiomer)	12.30±0.68	0.85±0.02	21.9±7.16	7.35±3.33	21.9±1.11	1.68±0.11	-
	Non-template (racemic)	-	-	-	-	5.40±0.48	-	-

* Mean ± s.d., n=3

3.3.5 The %age recovery of the extraction and solvent effect

3.3.5.1 The effect of an aqueous solution

The ability to adsorbe the thalidomide enantiomers on the MISPE after incubation with the thalidomide enantiomers and the racemic mixture for the study of their chiral conversions in aqueous solvents. The effect of the initial thalidomide concentration on the adsorption process was evaluated at a specific concentration (20 μg mL^{-1}), and this was used to evaluate the recovery of the extraction for the thalidomide enantiomers. Figure 3.8 illustrates the %ages and the enrichment of the unbound drug to the binding site of the imprinted pattern into the water. The selective enrichment of the unbound drug from the *R*-thalidomide MIP was below 60% while the *S*-thalidomide provided for a 100% enrichment for both the enantiomers inside the aqueous environment. The aqueous environment therefore had a significant effect on the re-binding of the thalidomide. The MIP4 had excellent imprinting factor values when compared with the control polymer compared to all the other MIPs (The imprinting factors (IF) were calculated from the microgram of the unbound drug of the MIPs divided by the NIP compared with one gram of the imprinted polymer). In the case of the SMIP4 it had the highest imprinting factor (IF of SMIP4 = 13.19). Also, the SMIP4 incubated with (*R*)-thalidomide showed a higher enantioselectivity than did the RMIP4 incubated with (*R*)-thalidomide in an aqueous solvent.

a. (*R*)-thalidomide imprinted polymer
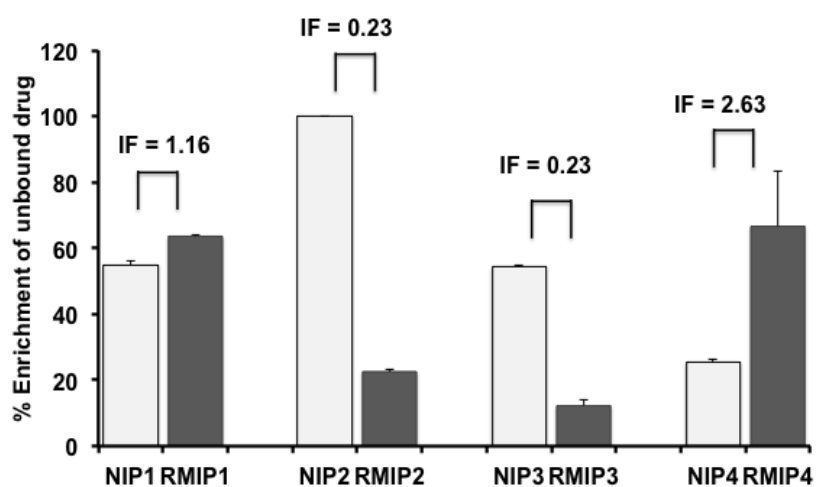
b. (*S*)-thalidomide imprinted polymer
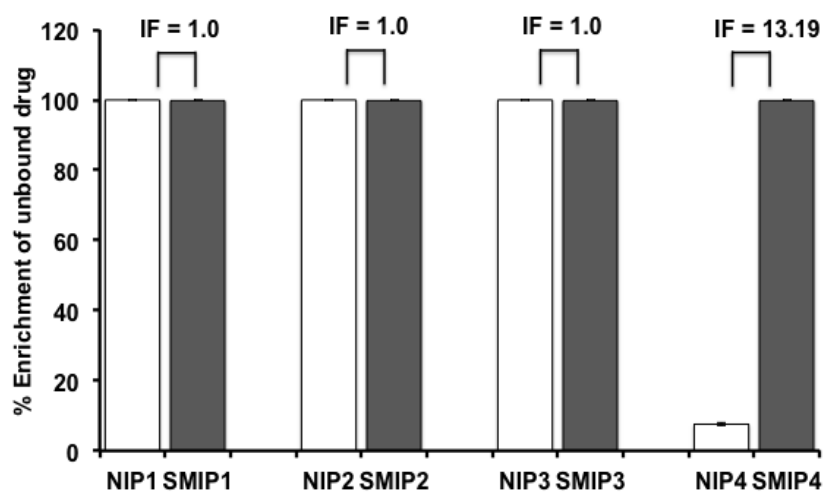
Figure 3.8: % Enrichment of the (*R*)-thalidomide MIPs (a) and (*S*)-thalidomide MIPs (b), and control polymer (NIPs) into water. The imprinting factors (IF) were calculated from the microgram of the unbound drug of the MIPs divided by the NIP compared with one gram of the imprinted polymer.

3.3.5.2 The effect of an organic solvent

The influence of the organic solution on the adsorption of the thalidomide enantiomer and the recognition ability of imprinted binding site in MISPE was also investigated. The particles of RMIP and SMIP were incubated with (*R*)-thalidomide, (*S*)-thalidomide in PBS at a pH 5.5 with the addition of ACN. Figure 3.9 shows the effect of the addition of acetonitrile into the PBS pH 5.5 mixture (50:50) on the selective enrichment of (*R*)-thalidomide and (*S*)-thalidomide. This reduced both the selective enrichment and the imprinting factor with an increase of non-specific adsorption, especially in the core-shell for the *S*-thalidomide in contrast to that of the non-core-shell for (*R*)-thalidomide. The enantioselectivity of the RMIP and SMIP were calculated from the selectivity for the (*R*)-isomer for each of the MIPs divided by the selectivity of the (*S*)-isomer. The chiral inversion of the RMIP was decreased when compared to the chiral inversion of the SMIP (see Figure 3.5A). The observed differences of the chromatograms between the RMIPs and SMIP could be attributed to the changing of the conformation of the template after exposure to an aqueous medium. The results indicated that the rebinding ability of the prepared MIP was influenced by the effect of the ACN. The RMIP2 provided for a high %age enrichment of the unbound single isomer of the drug that had an imprinting factor value = 1.03, while for the RMIP3 the amount of the (*R*)-enantiomer was lower than the amount of the racemate thalidomide in the MIP cartridge. In the presence of acetonitrile the hydrophobic interaction decreased, so the selectivity of the RMIP3 was lower than that of the RMIP2 in this solvent. Although, the NIPs were used for both the (*R*)- and (*S*)-enantiomers, after incubation with both pure single enantiomers,

a low non-specific adsorption was obtained, which showed that some concentration of the thalidomide enantiomer was adsorbed with a low enantioselectivity. The RMIP1 and RMIP2 that was bound to the preferential template released much less enantiomer into the solution than the other formulations. As expected, the lowest selectivity was observed in the non-imprinted polymer. The obtained SMIP3 exhibited the highest re-binding ability and showed high imprinting values (IF = 6.45). Both the SMIP1 and SMIP2 showed that a high amount of thalidomide was adsorbed and then released into the solution. The SMIP3 and SMIP4 showed higher interactions in the adsorption process towards the template enantiomer than the SMIP1 and SMIP2. The surface area of these MIP nanoparticles was enhanced, and had cavities that were specific for a target enantiomer and were able to distinguish the stereochemical entities of the enantiomers of thalidomide, and then play a role for an enhanced enantioselectivity.

a. (*R*)-thalidomide imprinted polymer
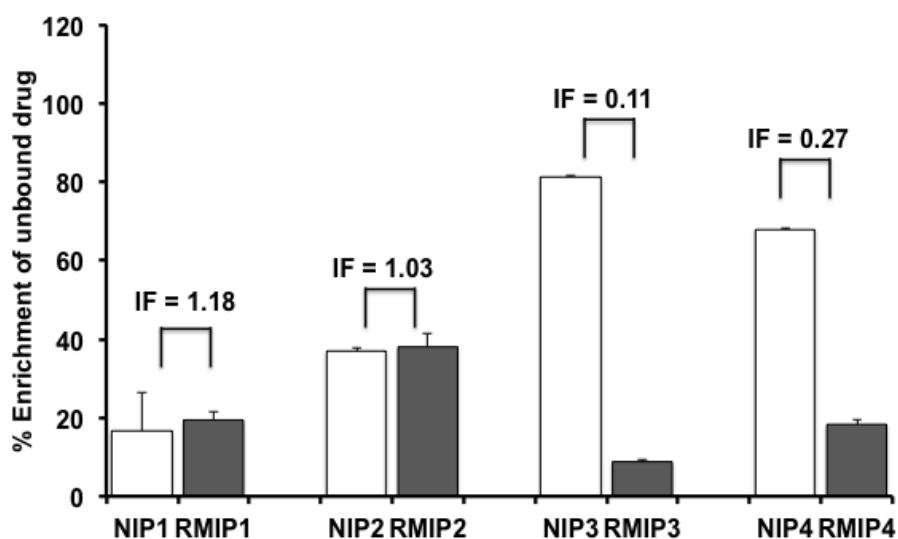
b. (*S*)-thalidomide imprinted polymer
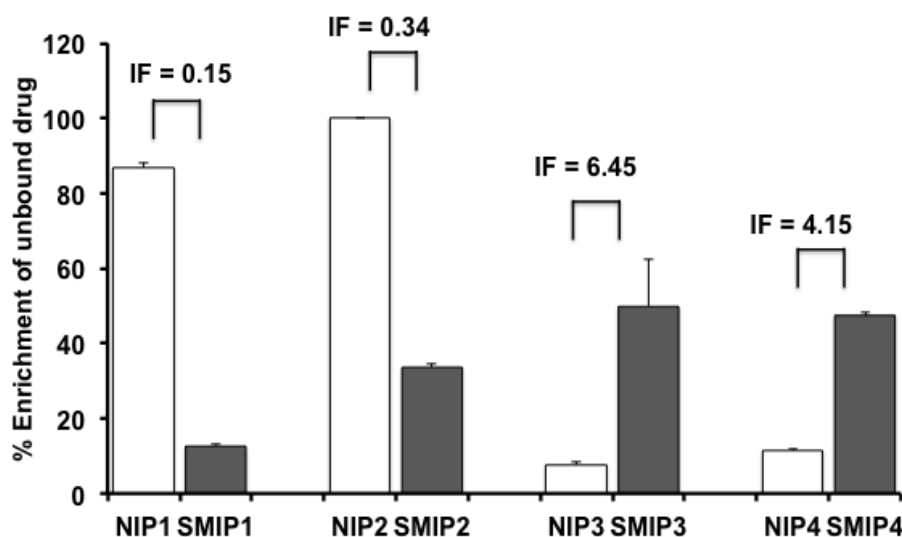
Figure 3.9: % Enrichment of the (*R*) thalidomide MIPs (a) and the (*S*) thalidomide MIPs (b) and control polymer (NIPs) into the phosphate buffer solution (pH 5.5); and the mixture with the ACN (50:50). The imprinting factors (IF) were calculated from the microgram of the unbound drug of the MIPs divided by the NIP compared with one gram of the imprinted polymer.

3.3.5.3 Incubation with the blood mixture

The % enrichment in the ACN:PBS pH 5.5 and the whole blood mixture were investigated for all the MIPs and both the thalidomide enantiomers. Figure 3.10 shows the % age enrichment of the template after incubation with the non-template (racemic thalidomide) for which the imprinting factor of the MIPs was indicated between the two enantiomers for each of the formulations of the MISPE. The highest IF values for both imprints of the RMIP1 and SMIP1 formulation towards the (*RS*)-thalidomide enantiomer produced the highest values for the imprinting factor (IF of RMIP1 = 38.36, and the IF of SMIP1 = 7.65). This result indicated that the interaction between the thalidomide enantiomer and the functional monomers of the MIP binding site was strong when there was a higher molar ratio of methacrylic acid than NVP in the cavity, and this more easily developed enantioselectivity for the binding of the plasma protein. Hence the development of racemic thalidomide in the blood sample assay was possible. Consequently, the MIPs could discriminate by recognizing different stereochemical properties of the enantiomers from any interference by the matrix did not disturb the specific recognition for the MIP. The studies in this chapter have indicated that the surface chemistry of a molecular imprinted polymer prepared by combination with the thalidomide enantiomers could be attributed to an enantiormorph related structure and the presenting surfaces for protein binding and other components in the blood environment on the MISPE.
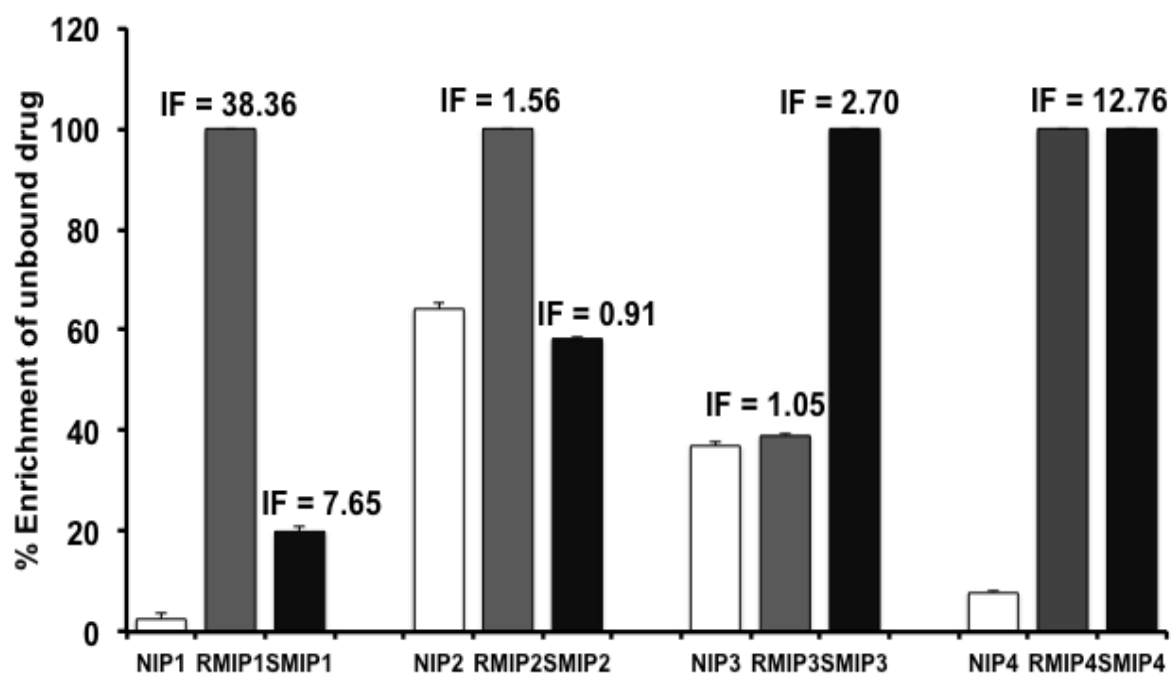
Figure 3.10: % Enrichment of the (*R*)- , (*S*)-thalidomide MIPs after incubation with (*RS*)-thalidomide on the MISPE and blood mixture. The imprinting factors (IF) were calculated from the microgram of the unbound drug of the MIPs divided by the NIP compared with one gram of the imprinted polymer.

3.4 CONCLUSIONS

The evaluation of recognition ability for the synthesized materials on MISPE represents the adsorption process of the enantiomers and racemic thalidomide have been carried out with and without the human blood mixture revealed the MIP micro particles used as a sorbent mixed with the resin had been successfully extracted and cleaned up a sample before using HPLC method to measure the amount of stereoisomer species in the sample. The molecularly imprinted polymer could protect and show configuration change of two enantiomers in an aqueous environment and the effect of solvent as well as the cells in blood. Moreover, MISPE was used to quantity the amount and the concentration of conversion of the thalidomide enantiomer in the solution and the blood sample. Consequently, the racemization between the enantiomers of thalidomide happens at the physiological pH in a biological matrix and underwent a rapid spontaneous hydrolysis. However, the isomers of thalidomide were clearly separated even from the blood sample.

CHAPTER 4

CHARACTERIZATION AND FORCE ANALYSIS OF THE MIP NANOPARTICLES SUPPORTED BY A FILM-LAYER

4.1 Introduction

4.1.1 Atomic Force Microscopy (AFM)

Atomic force microscopy (AFM) is used to observe the topographical surfaces on a nanometer scale. AFM has the ability to determine the morphology of a polymer coated onto a substrate and also to study any interaction of the analytes by using force spectroscopy as a dynamic analytical technique (Hugel and Seitz, 2001). The mechanism of the AFM is based on the detection of forces between an AFM tip, fabricated from silica or silicon nitride, and the surface of the substrates (Fotiadis *et al*., 2002). The interactive forces between the nanoparticles and the film of the polymer that covers the MIPs would be detected between the probe and the surface by passing through the probe via the surface, and these forces will enable the AFM system to record the deflection of the cantilever. These analytical methods using AFM and force analysis are used to enable the production of data for making decisions about the formation of the MIPs and identification of the template interactions on surfaces while forming a coating operation in ambient conditions.
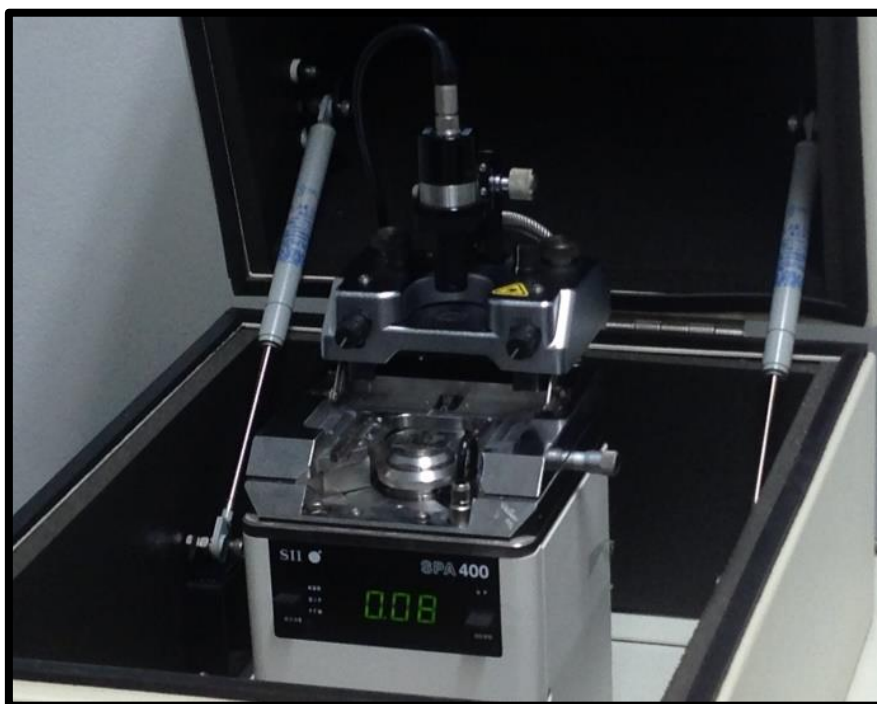
Figure 4.1: Atomic Force Microscopy (SPA400, SEIKO Inc., Chiba, Japan).

4.1.2 Confocal Raman Spectroscopy

The Raman Spectroscopy technique is involved in the selective absorption of a small amount of the irradiating light by the molecule's functional group, which allows for chemical information of the test compound in a solid–state phase (Robert Allen Carton., Pharmaceutical microscopy). Raman spectra results from the oscillations of atoms in molecules due to vibrational transitions and yields information about the molecular vibrational energy levels. They also provide data from molecular conformations, structure, intermolecular interactions, and chemical bonding in organic compounds. Most light irradiating from a reflective, opaque object will be reflected with no change in energy and is referred to as Rayleigh scattering. Most

Raman experiments utilize Stokes scattering. Since the loss or gain of energy is relative to the energy of the irradiation light, then the x-axis of the Raman spectrum should properly be in Δcm^{-1}, although it is common to drop the delta sign and just label the x-axis as reciprocal centimeters. Raman spectroscopy provides advantages for biomedical applications as it requires minimum samples and the Raman spectrum covers the spectral range between 4000 cm^{-1} and 100 cm^{-1}, it can also be used to identify isomers. Experimental Raman spectroscopy was used to determine the vibrations of the thalidomide molecular structures. Figure 4.2 shows the Confocal Raman Spectroscopy technique for the study of Raman spectra and structure of the molecules that interact on surfaces.
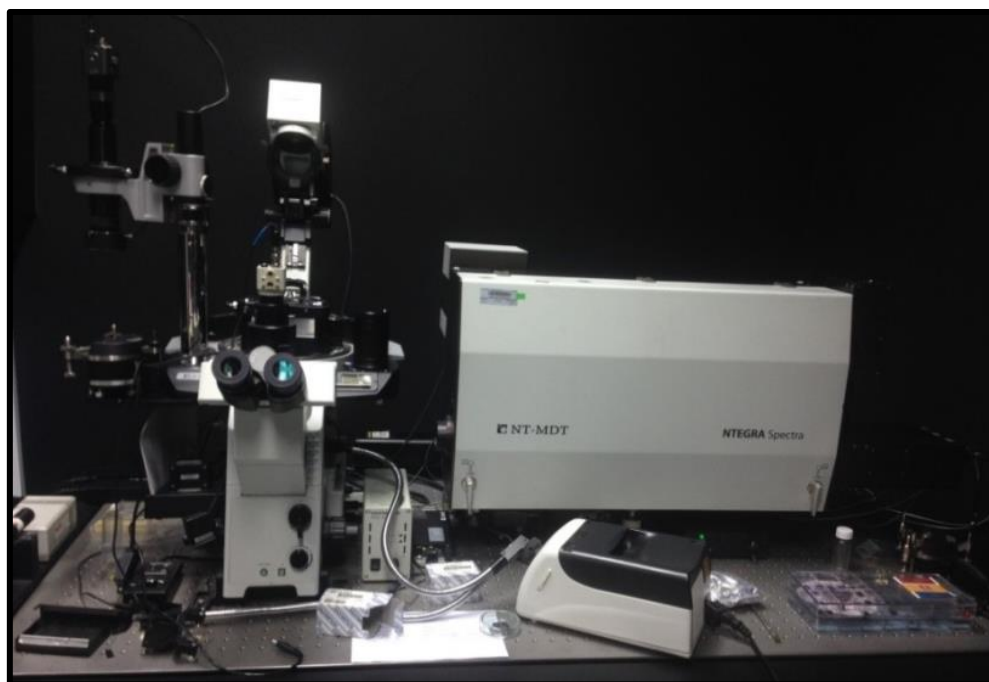
Figure 4.2: Confocal Raman Spectroscopy (NT-MDT, NTEGRA Spectra, Russia).

4.2 The objective of the study

The characterization of the MIPs and the use of Atomic Force Microscopy were used to determine the morphology and to study the interactions between the thalidomide and the imprinted thin films in ambient conditions. Confocal Raman Spectra were obtained for the reaction of the thalidomide enantiomer onto the imprinted nanoparticles films that can be examined on the same sample by AFM.

4.3 Experimental

4.3.1 Chemical and materials

(R)-(+)-thalidomide (98.0%) and (S)-(-)-thalidomide (99.0%) were from Aldrich Chemical Company (Milwaukee, WI, USA).

4.3.2 Equipment

4.3.2.1 Atomic force microscopy (AFM) and force analysis

A non-contact mode AFM (SPA400, SEIKO Inc., Chiba, Japan), and images were used to determine the morphology of the imprinted nanoparticles and the surface patterning in air at room temperature (25 ± 1°C). The AFM tip consisted of a pyramidal Si_3N_4 (typical radii: 10 nm for etched Si tip). A silicon cantilever was used with a typical spring constant of 20 N/m in the tapping mode and a scan speed of 1

Hz. The resulting images were analysed using the software, Nano Navi SPA400 (DFM). The distinct forces on the obtained nanoparticle-MIP films were determined in the force microscope mode using a HA-NC ETALON cantilever with 110-190 kHz resonance frequencies and a constant force in the range of 2.5-10 Nm^{-1} with an AFM (SPA400, SEIKO Inc., Chiba, Japan).

4.3.2.2 AFM with Confocal Raman microscopy (Raman-AFM)

The Raman spectra were obtained using an NTEGRA Spectra system with tip-enhanced Raman spectra (TERS) (NT-MDT, NTEGRA Spectra, Russia). The Raman system consisted of a 35 mW He–Ne excitation source of 632.8 nm and a power of 10–12 mW during the Raman and TERS, with a spot size of 1 μm. The Stokes-shifted Raman scattering was recorded using a 1200 grove min^{-1} grating and a Peltier-cooled charged-coupled device (CCD, Andor Technology PLC, California, USA). The Raman mapping spectra of the sample films were obtained from 1×1 μm at 3 areas. Multiple spectra were acquired with exposure times of 10 s, using an accumulated time 12 N under ambient conditions. We focused on a fingerprint region of approximately 200–1900 cm^{-1}, where most of the characteristic vibrational bands of the thalidomide enantiomers drug on the coated film of the nanoparticles layer were found.

4.4 Result and discussions

4.4.1 Nanoanalysis

4.4.1.1 Characterization of the MIP nanoparticles by AFM imaging

The atomic force microscope images were also employed for surface analysis and measurements of the macromolecular interactions between the imprints with the template at the surface of the nanoparticles that were used as a stamp. Figure 4.3 shows the AFM images from the non-imprinted and imprinted nanoparticles with various monomeric mixtures. The RMIP1 and RMIP2 nanoparticles showed imprint cavities with reversible binding to the template enantiomer on the surface. The enantiomer drugs were easily accessible to the binding site of the imprint. Formulation 2 (F2) of the RMIP shows that some visible droplets or clouding of the drops was observed in the chiral imprinted polystyrene beads formed from the functional precursors. Consequently; the association increased the aggregated growth on the (*R*)-thalidomide imprinted polymer. However, the polymerization of the RMIP3, RMIP4, and the SMIP-imprinted nanoparticles showed only small values for the nanotopography that would provide for a greater amount of the enantiomer to be adsorbed onto the surface. The polymerized (*R*)-imprinted nanoparticles showed a high value for the height of the nanotopography that provided for a greater amount of the enantiomer to be released. Therefore, the RMIP2 nanoparticles provided for greater accessibility of the enantiomer to the particular sites of the imprint cavities, and this indicated that the RMIP2 would provide a high selectivity. This was in

comparison to the NIP that was prepared without the template molecules. The patterns of the NIP nanoparticles showed only small individual ridges (data of the particle dimension of the ridge are shown in the Table 4.1). Therefore, the enantiomer templates had been adsorbed only onto the surface, and had not been adsorbed into any specific cavity. Consequently, the AFM studies have indicated that there is a definite binding of the chiral template to the cavities of the enantioselective molecularly imprinted polymers and even less so for the NIPs. The results can be clearly explained in that the rebinding of the thalidomide enantiomers to the chirally imprinted sites allowed for specific adsorption and the selective release predominantly at the structured surface of the nanoparticle (Joshi *et al*., 2000). The AFM has demonstrated the direct assemblies of the template (*R*)-thalidomide and (*S*)-thalidomide into three-dimensional structures on a solid particle within an organic compound environment, as well as a spatial dimension for the growth and aggregation due to the response to surface topography of the different imprinted polymers. The effects of the hydrophobicity and the surface charge distribution play a crucial role in orienting the template-MIP assembly in the polymer materials. Finally, the template could be reversibly lost so the specific cavity has an ability for rebinding the template under these conditions. The thickness of the nanoparticles supported onto glass substrate was 4-15 nm that used for the recognition of the enantiomers.
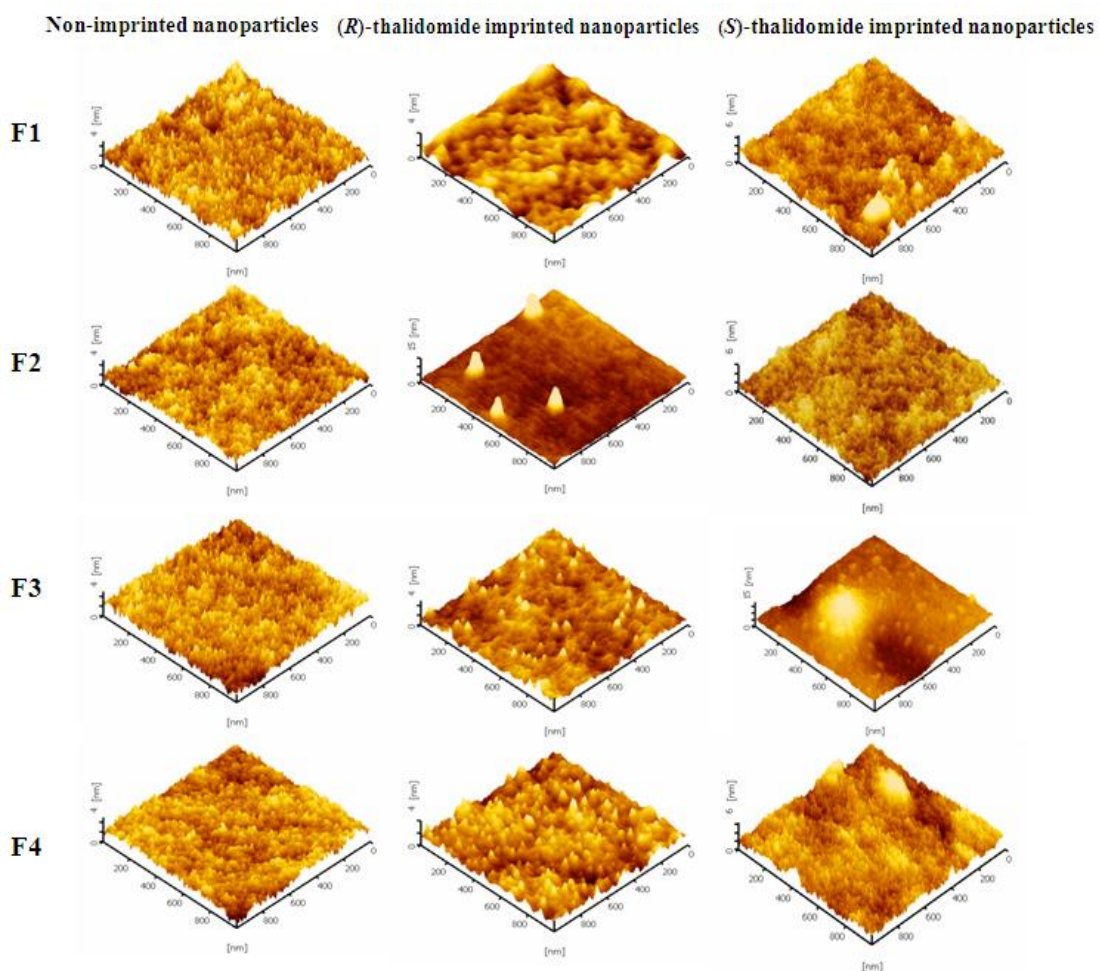
Figure 4.3: Images obtained by non-contact mode atomic force microscopy of the molecularly imprinted (*R*)- and (*S*)-thalidomide enantiomers and the non-imprinted nanoparticles. Molecularly imprinted nanoparticles showed the self-organized nanostructure of assembled MIP-nanoparticles.

4.4.1.2 Force measurements of the molecularly imprinted

nanoparticles

AFM was also a powerful tool that was used to study the interactions and the physical properties of the nanoparticles and the thin-film layers. A study of the interactive forces with the AFM applying the force to the cantilever, so when the tip touched and pressed the sample it was able to probe the small interaction area (constant force in the range 2.5-1000 Nm^{-1}) and provided the high sensitivity of a small force, while the pull-off tip provided the adhesion force between the tip and the surface materials. This was because the force experiment by the cantilever onto the surface provided information about the short-range interaction of the van der Waals forces. Figure 4.4 shows the force values of the molecularly imprinted nanoparticles when they were re-binding with their template enantiomers. The data plots show the movement of the cantilever onto the surface against the deflection of the cantilever and provided the force values. The force values for the RMIP1 were the lowest at 200 nN compared to 300 nN for the RMIP2 that was comparable with the RMIP3 600 nN and RMIP4 500 nN, but the (*S*)-thalidomide had a force value of about 1 nN for all the cases of the MIPs. The adhesion force provided on the layer surface of the nanoparticles was due to the presence of thalidomide that fixed on the surface and showed the interaction between the tip and surface of the molecularly imprinted nanoparticles..
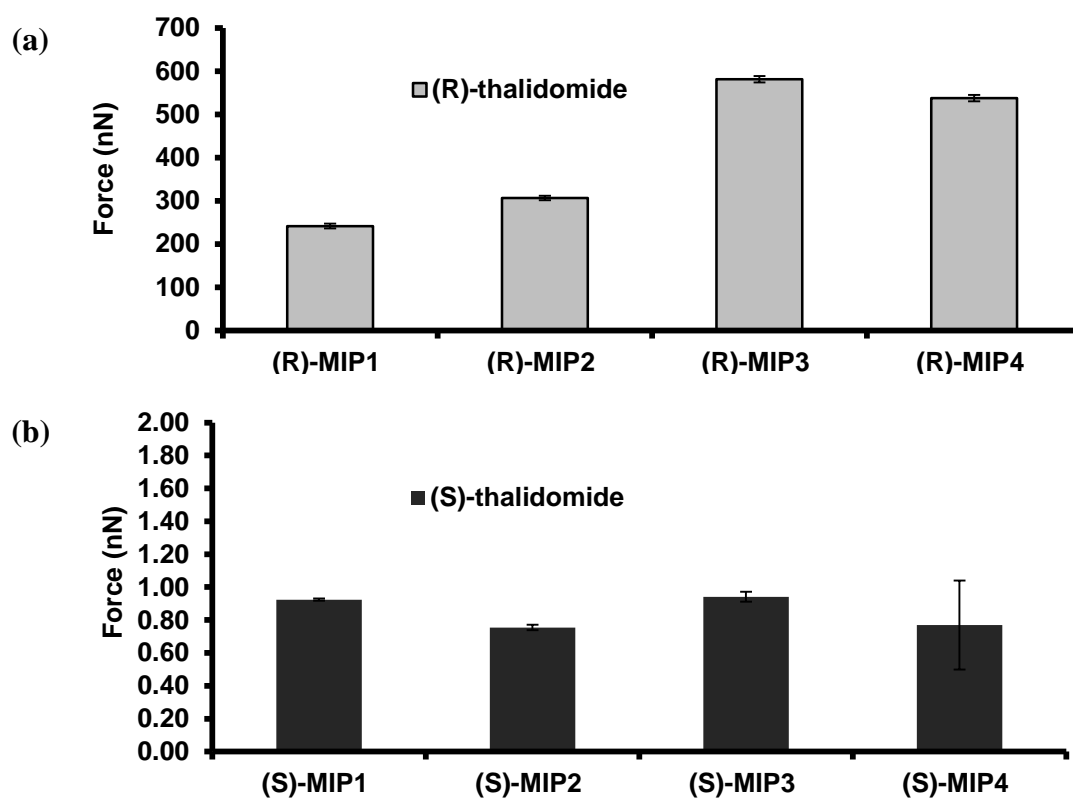
Figure 4.4: The force values of molecularly imprinted nanoparticles produced by using (*R*)-thalidomide and (*S*)-thalidomide as template molecules were coated onto stamped glass substrate nanoparticles.

4.4.1.3 The characteristics of the MIP nanoparticles supported onto

the thin-film

After studying the characteristic of the imprinted nanoparticles that were coated onto the glass substrate by micropatterning of the film polymer. The imprinted nanoparticles were used to print onto the pre-polymer layer of the glass substrate. Figure 4.5 shows the topography image and the 3D images obtained with the tapping mode atomic force microscopy of the non-imprinted polymer, (*R*)-thalidomide imprinted and (*S*)-thalidomide imprinted films. The insert images were the magnified part of the imprinted nanoparticles-coated layer. The variations of the functionalities of the monomeric components with an increasing amount of the NVP, showed that the surface roughness of the selective materials was observed with dissolution of both the thalidomide enantiomers during the incubation in distilled water, and this demonstrated the coverage of the surface and the specific organization of the site. The observed different surface morphologies and surface topography of the polymers may be a consequence of the different chemical functionalizations of the molecular imprinted sites during the dissolution process. This was attributed to the intermolecular interactions between the water and the selective materials that led to a differentiation of the molecular chiral entities of the two enantiomers of thalidomide. The RMIP2 provided the larger size of the particles with a high nanotopography (51.03 nm). The SMIP and RMIP nanoparticles also occurred by a self-assembly process, however, the RMIP3, R-MIP4 and S-MIP nanoparticles among all the MIPs showed only small nanotopography. This means that a greater amount of the enantiomer template was adsorbed onto the surface, and this provided for a lower

release of the enantiomer. It was expected that the RMIP2 nanoparticles provided the best accessibility for the enantiomer drug to the site of the imprint cavity and showed a high selectivity. The imprinted site of the RMIP2 decreased the drug against racemization into the solution when compared with the non-imprinted polymer have the interaction on surface polymer. The topographical images of the control polymer and the imprinted nanoparticles showed largely different surface topographies and allowed for the information of the function of the MIPs. The topography in the AFM images allowed for the opportunity for the study of the rebinding from the imprinted sites onto the nanocomponent film.
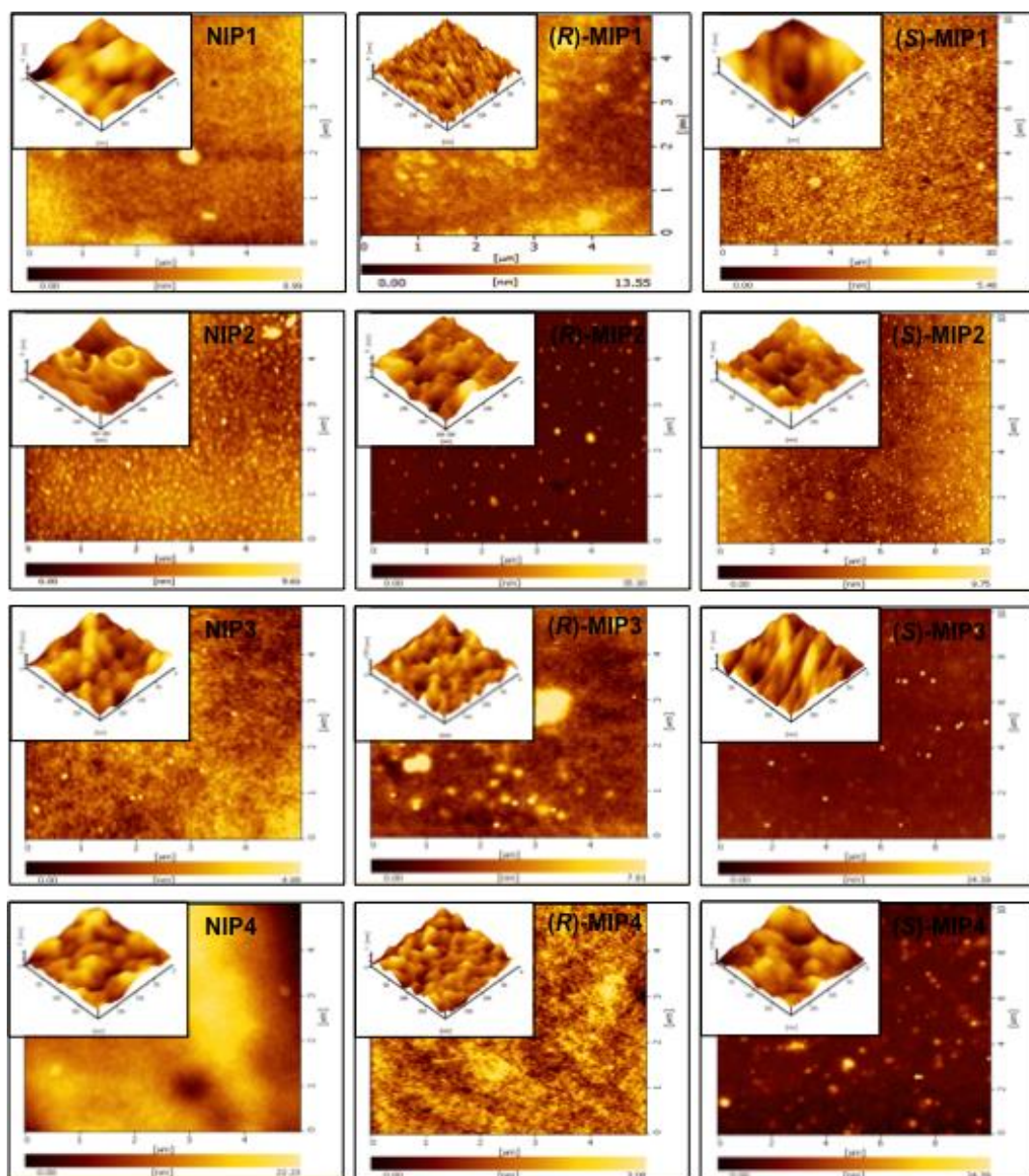
Figure 4.5: A tapping mode atomic force microscopy image of the non-imprinted polymer, (*R*)-thalidomide imprinted and (*S*)-thalidomide imprinted films. Insert: The AFM image of the surface on a polymer-coated layer for the NIPs, RMIPs and SMIPs as a stamp that was formed into the MIP nanocomposite layer or the coated MIP nanopattern that remained on the film after removal of the template.

4.4.1.4 The roughness values

The roughness (R_a) values of the imprinted nanoparticles and the thin film layers that were produced by using nanoparticles as a stamp are shown in Figure 4.6. The summarized data about the dimensions of the particles, the layer thickness, nanotopography and the separation distance upon the formation of the passivated surface layer are shown in Table 4.1. The R_a values for the imprinted nanoparticles were reduced by the formation of the core-shell that had a poly(styrene) seed and thus could allow for variations to the surface height in the outer layer among the four formulations of the nanoparticles. However, the SMIP3 had a high roughness value because the surface of the SMIP3 nanoparticles showed the nanotopography. The nanotopography showed that the integrated gold layer that was coated onto the electrodes produced high values for the roughness. The thin films of the MIP3 and MIP4 in the absence of polystyrene provided for a higher separation distance of the nanoparticles and also showed better nanotopography. The results indicated that the effect of the nanotopography on the thin-films of MIP3 and MIP4 provided for a greater amount of the drugs to be adsorbed but a lower amount of the drugs to be released. Then, the MIP1 and MIP2 films could allow for the transport of the thalidomide from the binding site within the MIP easier, and increased the porosity of the MIP due to the reduction of the surface defects from the rapid fabrications of the coated layer. This promoted the diffusion pathway from the templating nanoparticles into the passivated surface layer. The experimental data shows that the dimensions of the particles of the NIPs were larger than those of the imprinted films. The small particle dimensions provided for a high surface area and a better accessibility to the

analyte matrix in the blood samples assay more than for the NIP, and the appropriate interspace along the surface of the nanoparticles could increase its dependence on the sensitivity toward nanotopography for all the MIPs. Evidently, the selectivity of the imprinted polymer changed, during the 6 months that it took for the templates to be fully released. The recognition ability of the imprinted molecules to those of the binding behavior of the polymer particles were accessed by the batch rebinding experiments (Figure 4.7). The MIP2 on the polymer surface allowed for the highest nanotopography height that would provide for the adsorption processes and for a release of a high amount of the drug enantiomer. This was attributed to the carboxylic acid of the MAA that was capable of forming electrostatic and hydrogen bond interactions with the imide moieties on the phthalimide and glutethimide of the thalidomide. The NVP functional monomer provided for the formation of the H-bonding when compared with the other formulations. We assumed that the integration of the monomer mixtures were into the macromolecular networks instead of using the functional monomer(s) for the (*R*)-thalidomide imprinted polymer, that allowed for an optimization of the steric fit and the accessibility to the imprinted sites. Despite the minor differences in their surface morphology, the absence of the PS during the polymerization process led to the disappearance of the droplets in the F3 of the (*S*)-thalidomide imprinted nanoparticles but aggregates of the particles were observed in the AFM images of the F2 of the (*R*)-thalidomide imprinted nanoparticles (see Figure 4.8) as compared to the corresponding NIP. This illustrated that some of the possible variations that occurred, with the imprinting was related to van der Waal forces.
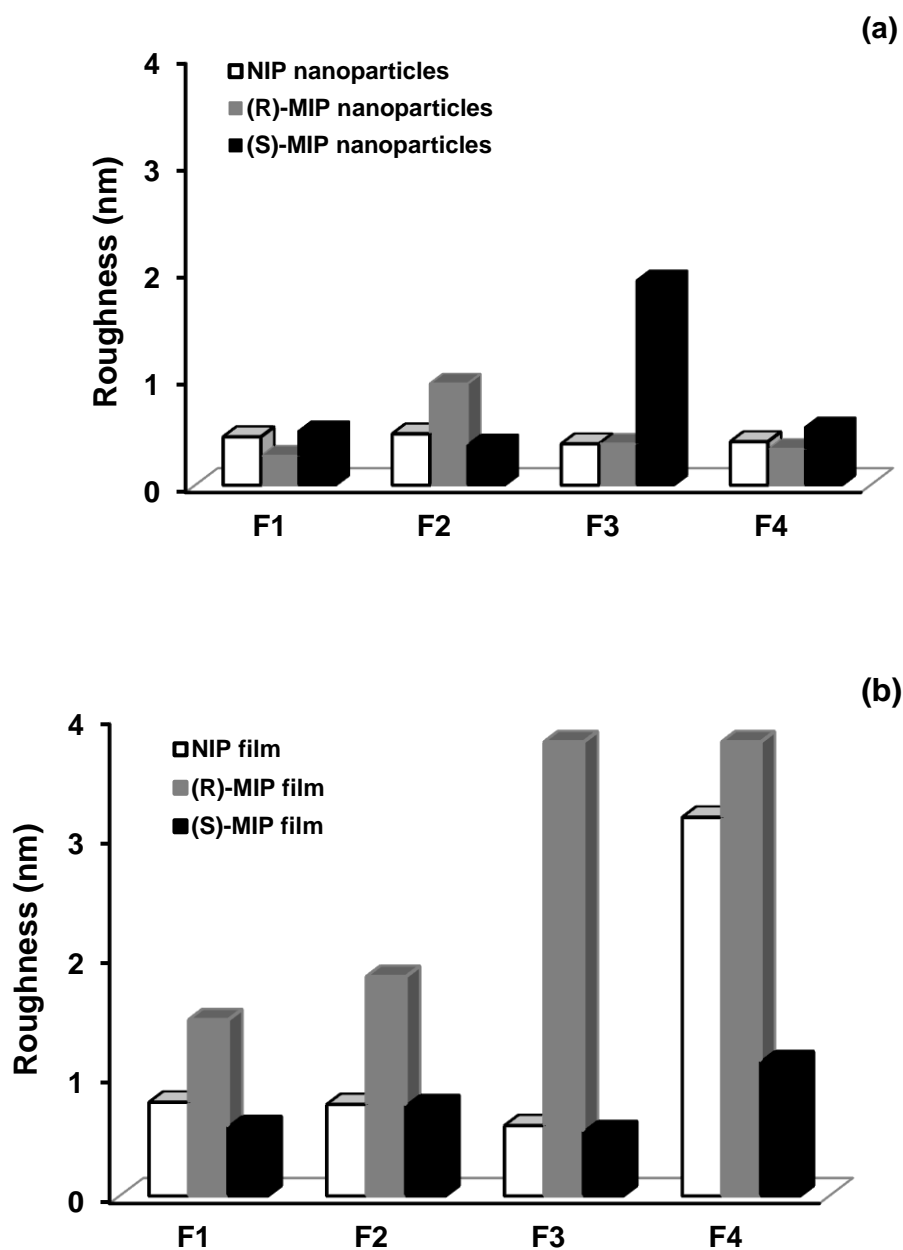
Figure 4.6: The roughness values of the NIPs and MIPs prepared by using (*R*)-thalidomide and (*S*)-thalidomide as the templates and various monomer functionalities for core-shell and non-core-shell (a) onto the thin film coated IDC (b).

Table 4.1: Data of the reproducibility of the control polymer, the (*R*)-thalidomide imprinted polymer and the (*S*)-thalidomide imprinted polymer from the surface-imprinting processes.

Polymer	Particle dimension (nm)	Layer thickness (nm)	Interspaces dimension (nm)	Ridge (nm)
NIP1	37.15	1.26	30.30	37.65
R-MIP1	18.90	0.83	12.95	16.45
S-MIP1	67.40	0.24	26.21	39.38
NIP2	56.07	0.88	58.08	18.74
R-MIP2	17.78	0.62	16.76	51.03
S-MIP2	11.89	0.57	19.22	17.89
NIP3	40.25	0.25	50.57	34.92
R-MIP3	12.24	0.24	13.94	15.75
S-MIP3	28.19	0.27	18.86	25.25
NIP4	23.08	0.36	19.92	30.25
R-MIP4	12.37	0.28	14.74	18.80
S-MIP4	19.50	0.06	14.01	35.22

4.4.1.5 Force measurements of the imprinted thin films

The analysis of the forces of the MIPs coated onto the glass slide were carried out to determine the interaction of the nanoparticles at the interfacial surface on the coating layer. Figure 4.7 shows the force curves obtained from the AFM images of the RMIPs. The subtle differences of the separation distances for the retraction of the force-distance curve at the affected area was similar for the outer layer of the three RMIPs, and showed hysteresis in most RMIPs, except for the RMIP1 where the separation distance was narrow. Also, the SMIPs led to layer hysteresis for all of the SMIPs (Figure 4.8). The results indicated that the indentation depth and the stresses were related to the mechanical forces and an intermolecular interaction of the interacting surfaces. This was noticeable for the hysteresis in these RMIPs and also the SMIPs during the retraction of the force distance curve. The R-MIP1 with no hysteresis must have the same interactive surface because of the van der Waals forces between the intermolecular interactions and the large adsorption on the embedded film of the polymer nanoparticles. It was likely to act as an adsorbed substrate as a result of the dissolution of the hydrophobic drug (*R*)-thalidomide itself as the templates grew in a controlled manner that could minimize the structural defects. So the mechanical force measurement did distinguish the surface characteristics of these RMIPs.
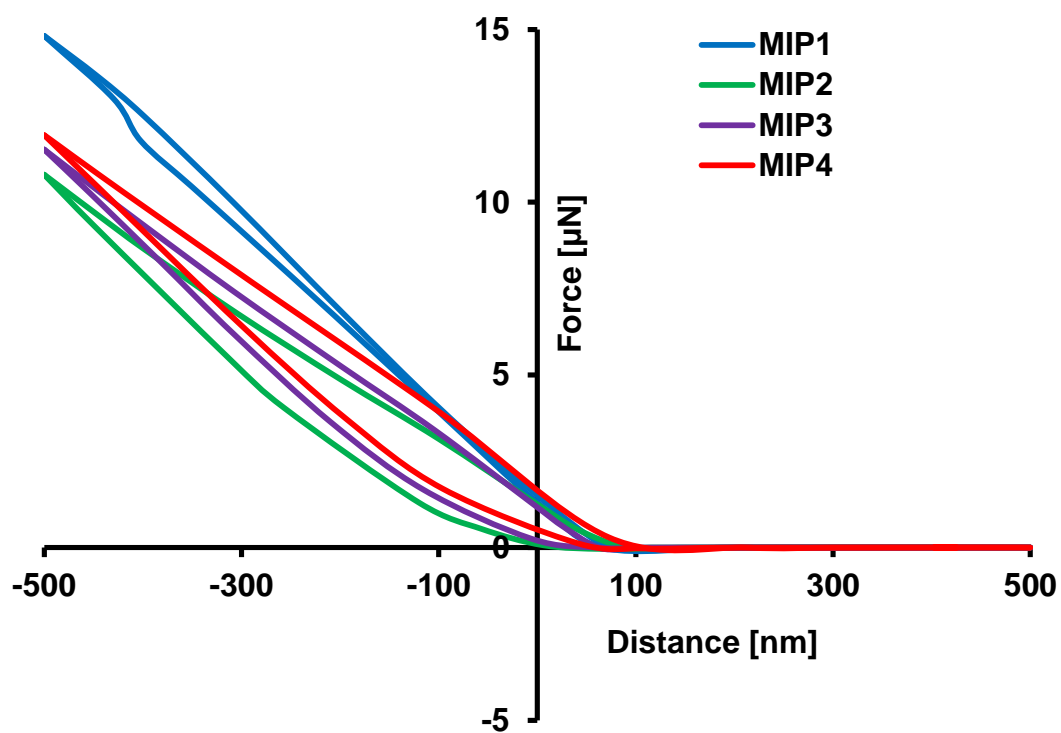
Figure 4.7: The force curves of the RMIP1, RMIP2, RMIP3, and RMIP4 films that were produced by using the poly(MAA-*co*-NVP)-crosslinked with the DHEBA polymer.
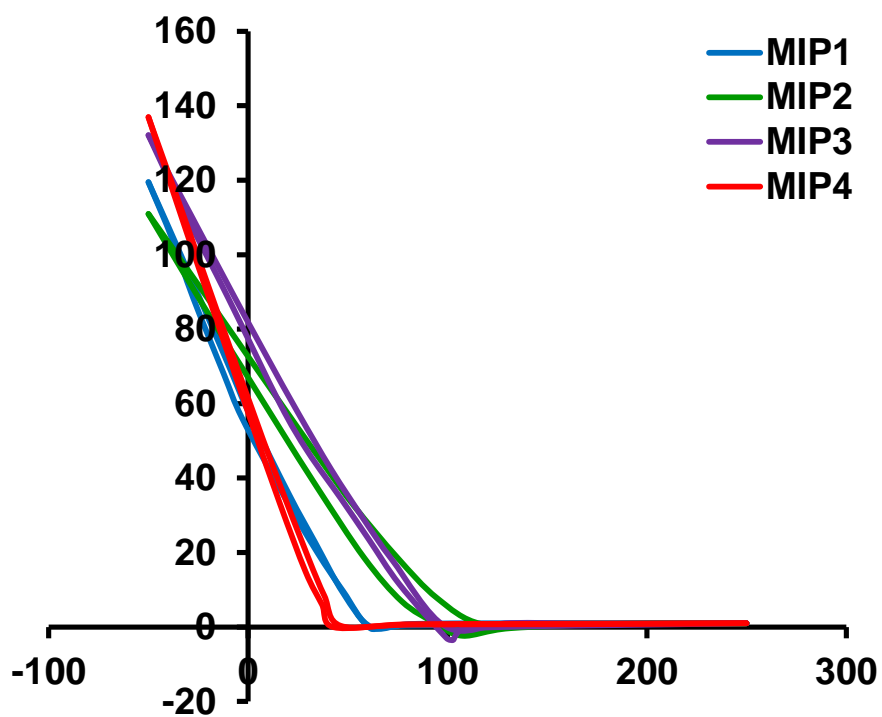
Figure 4.8: The force curve of the SMIP1, SMIP2, SMIP3, and SMIP4 films were produced by using poly(MAA-*co*-NVP)-crosslinked with the DHEBA polymer.

4.4.1.6 The characteristic of the RMIP films after washing out the

template

We have utilized the contact mode AFM to confirm the characteristics of the enantiomers after washing out the template by using distilled water onto the imprinted site of the imprinted films. Figure 4.9 shows the Raman-AFM images of the RMIP3 and RMIP4, and showed the different surface orders and arrays of the nanoparticle-films. The adsorption sites of the nanoparticle on the adjacent particles appeared to influence the final patterned particles to adsorb close to the adjacent particles. The RMIP3 showed the presence of the adsorbed particles onto the surface of the imprinted thin-films. In the case of the RMIP4 the enantiomer drugs that provided the imprinted cavity of the enantiomer drug were removed. The enantiomer can be adsorbed onto the adsorbed sites by weak forces, of van der Waals interactions because of the drug attached to the imprinted site onto the glass slides. The AFM images can be used to confirm the characteristics of the binding sites of imprinted polymer based on the MIP nanoparticles as the stamp in the polymer coating.
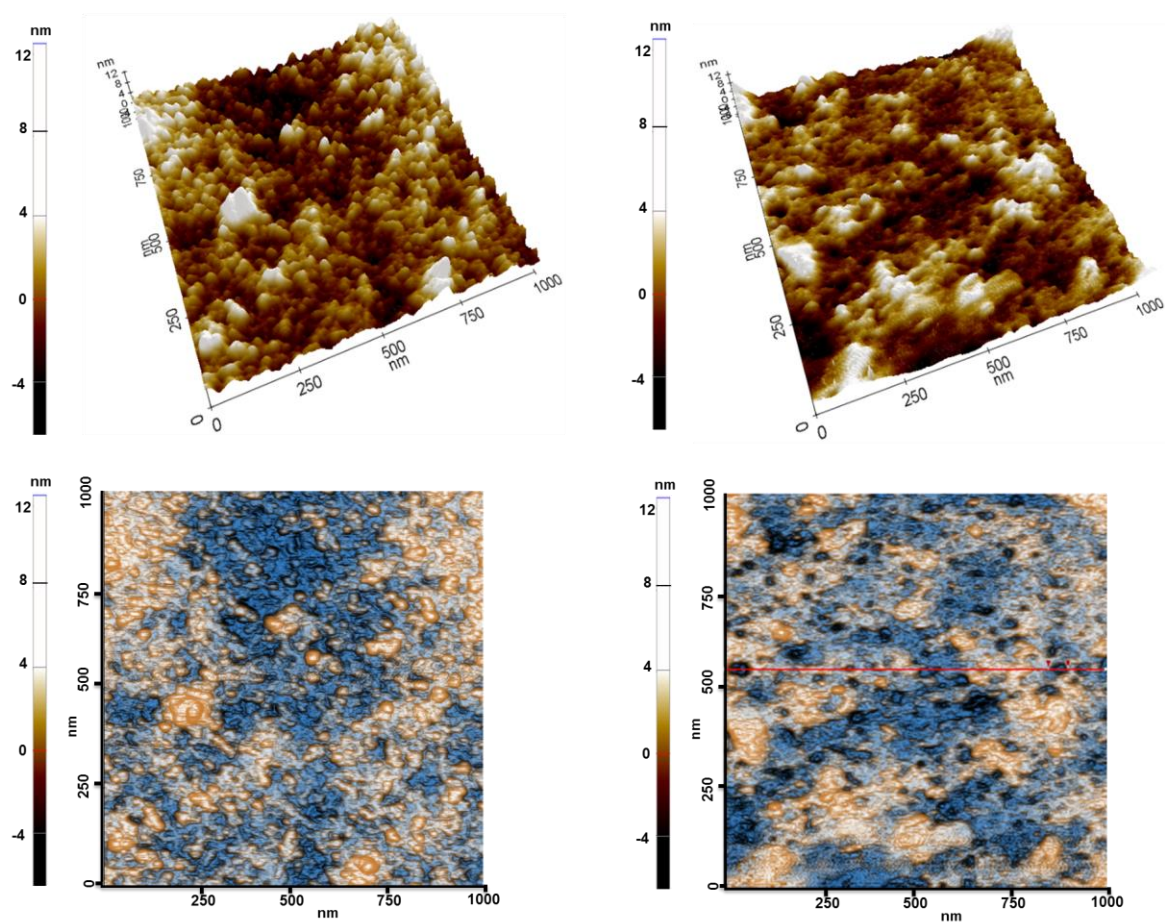
Figure 4.9: The three-dimensional AFM images and topographical image of the (*R*)-thalidomide imprinted nanoparticles of the RMIP3 and RMIP4 both of which were stamped onto the respective film layers of the polymer after it was washed out.

4.4.2 Surface enhanced Raman scattering (SERS)

SERS was used to study the interactions of the enantiomer template onto the coated films containing the RMIPs and SMIPs at the thalidomide concentrations of 50 µg/mL using the Raman-AFM with the hybrid method. It was found that the detection sensitivity was increased by the MIP layer on the Au-coated IDC. The higher sensitivity was because of the amplification of the electromagnetic field by the SERS substrate.

4.4.2.1 (R)-thalidomide imprinted thin film

After the extraction on the MIP-SPE the Raman spectroscopy was utilized on the outer layer of the MIPs nanoparticle-film layers that provided for a lower release of the drug template. Figure 4.10 demonstrated the Raman spectrum of the (*R*)-thalidomide standard and imprinted films by using the nanoparticles of the (*R*)-thalidomide as a stamp after washing out the template. The slower rate of the thalidomide enantiomers on the RMIP3 and RMIP4 nanoparticles agreed with the intensity of the imprint of the Raman spectra of the *R*-thalidomide of between 1500-1800 cm^{-1} upon exposure to the blood. According to the rapid transport of the enantiomers onto the R-MIP1 and R-MIP2, they showed only a very slight intensity of the Raman spectra over the film which indicated a thinning of the layer coating and the total extraction of the enantiomer template from the imprinted films. The substantially tighter nanotopography on the surface-coating, in the cases of the RMIP3 compared to the RMIP4. (Figure 4.10) was most likely due to the interaction

of the drug-MIP within the imprinted cavities. There was also an additional peak at 1445.83 cm^{-1} in the spectrum of RMIP3, and RMIP4 belonging to the C-H bend and the cyclic C-C stretching. There were also the vibrations of the substituted-benzene portions of the molecule at the 800-400 cm^{-1} regions.
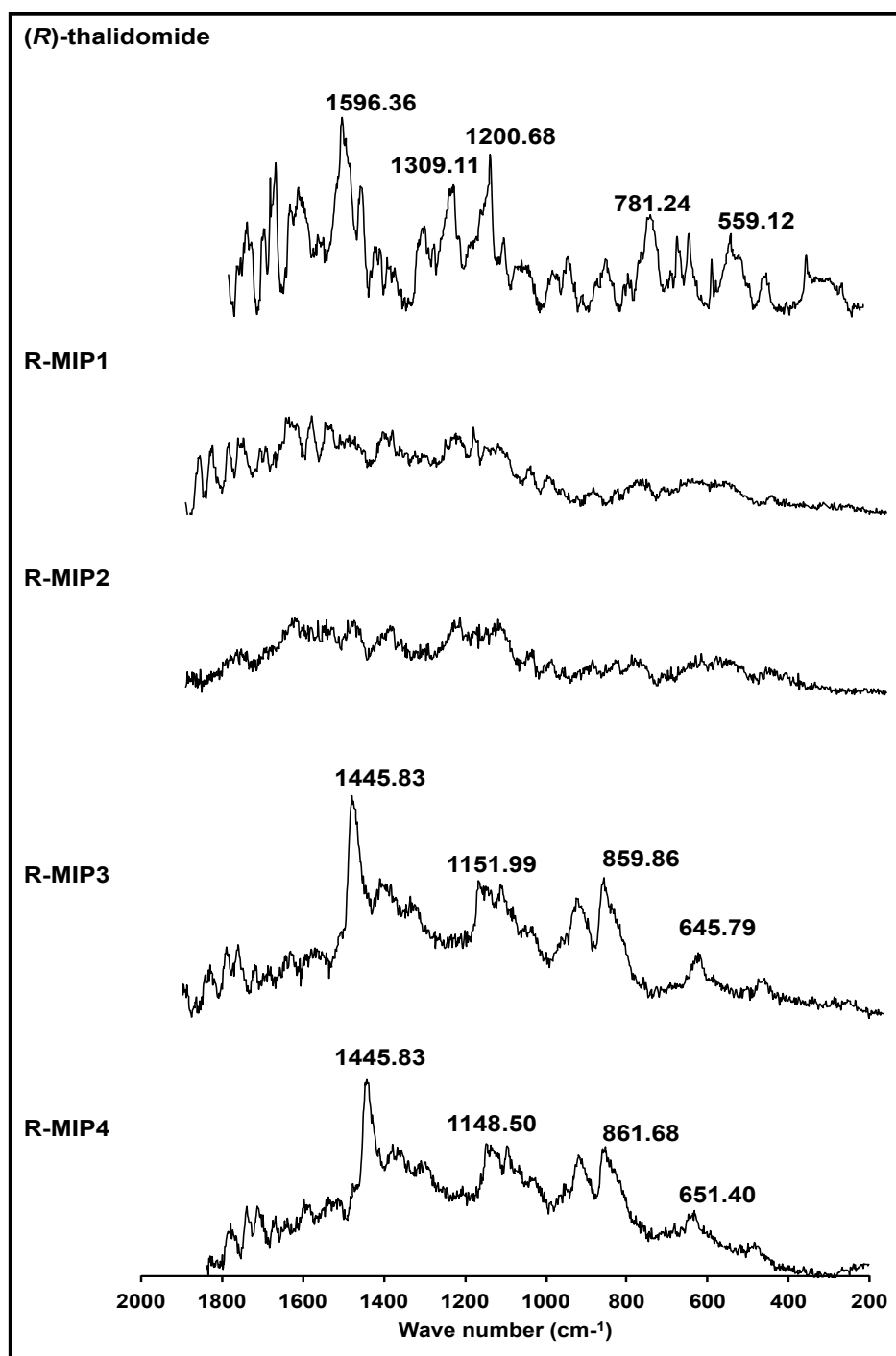
Figure 4.10: Raman spectra of the (*R*)-thalidomide and the (*R*)-thalidomide imprinted

films (RMIPs) as a stamp after washing out, showing some of remained template onto

the sample of the polymer.

4.4.2.2 (S)-thalidomide imprinted thin film

Figure 4.11 shows the Raman spectra of the (S)-thalidomide enantiomers and the (S)-thalidomide imprinted thin films after washing out the template. There was a low intensity in the $1500–1800$ cm^{-1} region and the SMIP1 and SMIP4 that were comparable to the standard solution of (S)-thalidomide, but the strongest intensities of the thalidomide enantiomer was found for the SMIP3 because of the interaction after the self-organization in the mesoporous pores. Obviously, only the SMIP2 showed the Raman shift at the $1100–1200$ cm^{-1} region that was the Raman vibrational modes for the benzene and was similar to those that occurred for the RMIP3 and RMIP4. The bands at 1445.91 and 1599.63 cm^{-1} might be assigned to the in-phase shift of the carbonyl (C=O) stretching of the imide group on the thalidomide structure, particularly in the SMIP2. The SMIP3 showed the strongest intensity bands between $1200–1450$ cm^{-1} that included 1249.03 and 1317.53 cm^{-1} that was accounted for by the highest roughness of the nanoparticles of this material (see Figure 4.6), while it had a reduced nanotopography of the film cast as compared to the other MIPs. These Raman peaks were attributed to the CH_2 deformations or a C-N-H stretch-band. The low intensity bands occurred in the $1300–1400$ cm^{-1} range that may be assigned to the C-O and the C-N-C stretching. These results demonstrated the ability of the Raman to distinguish between the differences of the transport behavior of each of the thalidomide enantiomers on these MIPs. These results provided key information of the interactions of the chiral pharmaceutical compounds in the recognition system of the solid materials.
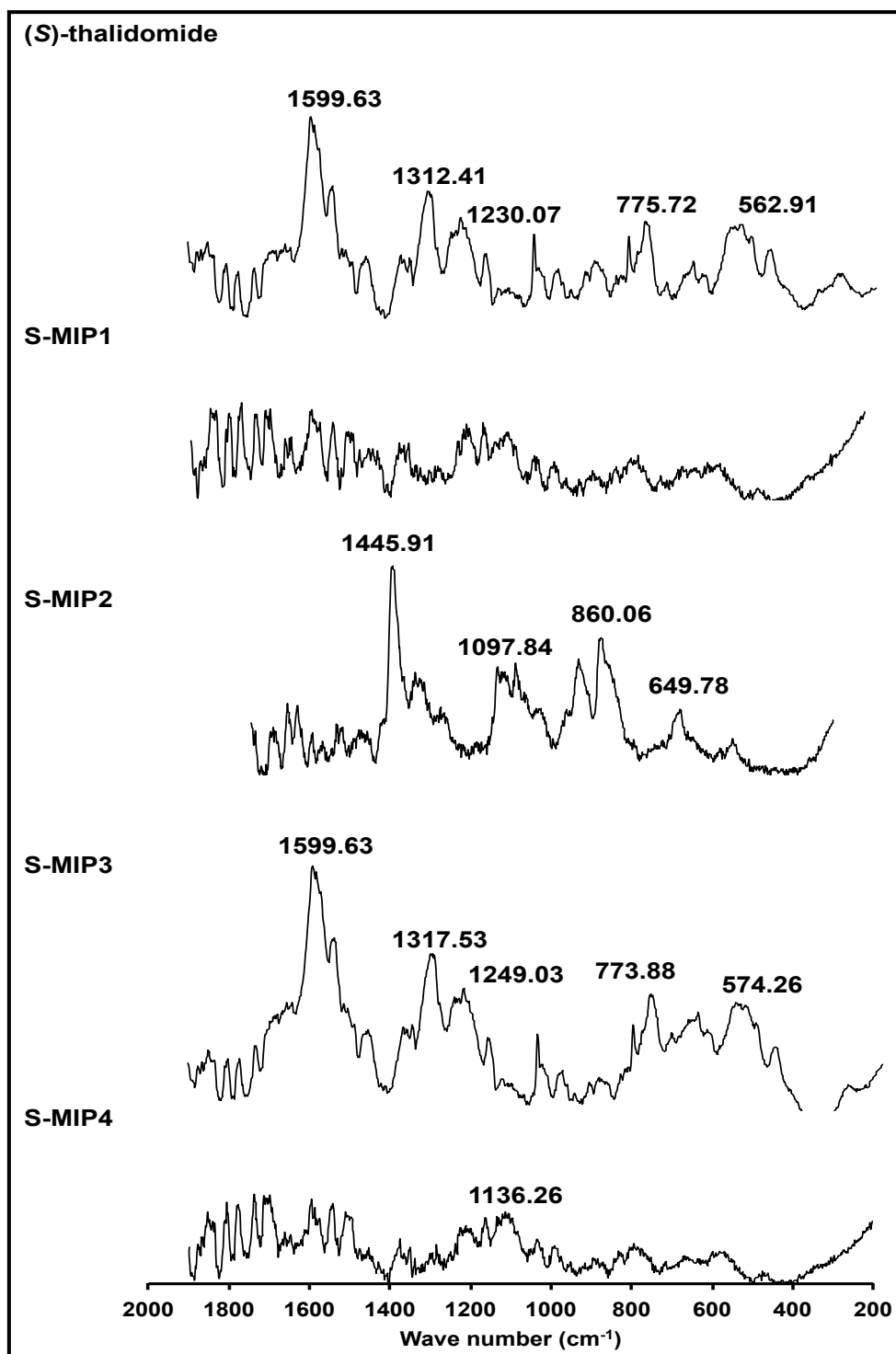
Figure 4.11: Raman spectra of the (*S*)-thalidomide alone and the (*S*)-thalidomide imprinted films embedded with the SMIPs as a stamp after washing out the template.

4.4.2.3 Study of the interaction of the biological compound with the

thalidomide enantiomer in the imprinted nanoparticle stamped film

All of the MIPs after exposure to the enantiomer were adsorbed onto the imprinted films and washing off the enantiomers of thalidomide was inspected by the Raman intensity peaks using the confocal Raman-AFM. The biological system consisted of CER, cholesterol and BSA that were admixed separately with the thalidomide enantiomer to study the effect of these biomolecules on the chemical properties of the thalidomide enantiomer. The blood component mixture containing the human serum albumin, cholesterol and ceramide were mixed at (w/w) 1:1:1 ratio. The Raman spectrum of the biological sample incubated with the imprinted nanoparticles and the (*R*)-thalidomide and (*S*)-thalidomide enantiomer as a template at 50 μg mL^{-1}, were as shown in Figure 4.12&4.13. The Raman AFM image showed that the adsorbed layer of the biological component had a complexity in the organization of the thin surface. The RMIP3, RMIP4, SMIP3 and also SMIP4 showed a high binding and a rapid saturation following incubation of the coated film on the glass-substrate that contained the non-core shells. The MIP3 and MIP4 showed the intensity shift of the Raman spectra of the (*R*)-thalidomide and (*S*)-thalidomide on the imprints at 900 and 450 cm^{-1}, so they were assigned to cyclic C-C-C bending and N-C-O bending. These intensity shifts can be explained by the reversibility of the enantiomers that was reduced in this material, and reflected the protein binding of the thalidomide enantiomers. These results were achieved because of the fine-tuning of the molecular recognition and the more selective stabilization of the template enantiomer over the non-templated enantiomer between the imprinting polymers and

the respective enantiomer template as compared to the non-imprinted control polymer. This also prevented the occurrence of bidirectional racemization. Because of the influence of the solid surface on the thalidomide enantiomers that had been exposed to the macromolecular environments that were probed by the surface chemistries of these two imprinted polymers. Also the mechanical force parameters were probed and were correlated to the molecular imprinting protocols to generate the selective binding of the thalidomide enantiomers. The concern over the deposition of the biological system on the interfacial binding surface being overcome by the cast films is for masking the protection and that a film coat can be utilized for the separation and drug delivery of the thalidomide enantiomer, that have been mostly investigated at ambient conditions. Based on the MIP-SPE results and the Raman spectroscopy based on the synthesized material it was highly appropriate for the application to diagnose and the sensor that was relevant to the recognition ability of the MIP upon the spatial deposition and imprinting processes. The thickness of the film cast played an role on the migration of the substrates and the detection of the thalidomide enantiomers through the adsorption process, and this has been an important consideration in the design of the affinity phases for separation.
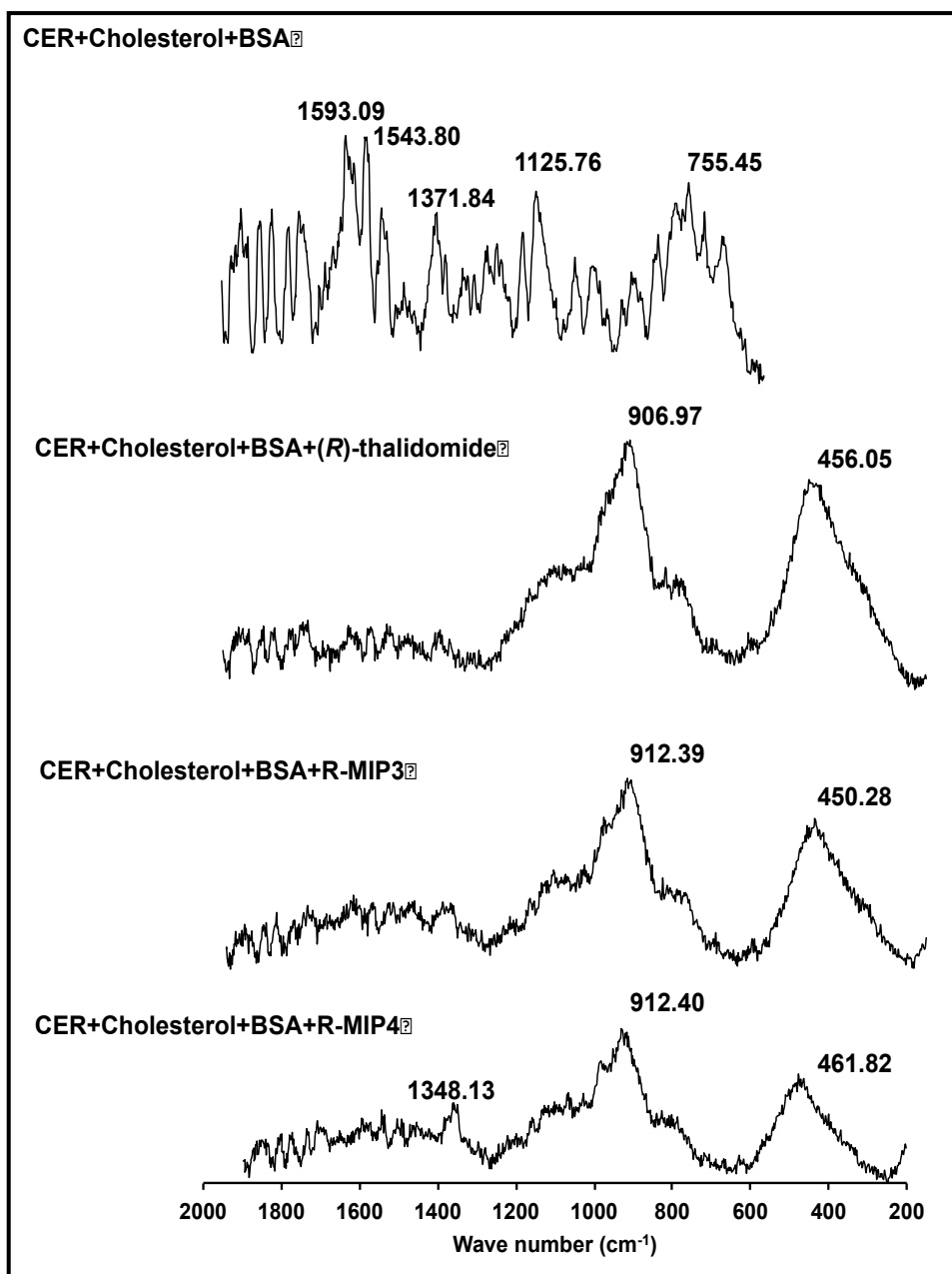
Figure 4.12: The characteristics of the Raman spectroscopy of the ceramide (CER), cholesterol, and bovine serum albumin (BSA) mixture and the incubated mixture with the (*R*)-thalidomide on the adsorption of the imprinted nanoparticles, when the concentration of the (*R*)-thalidomide was 50 μg mL^{-1}.
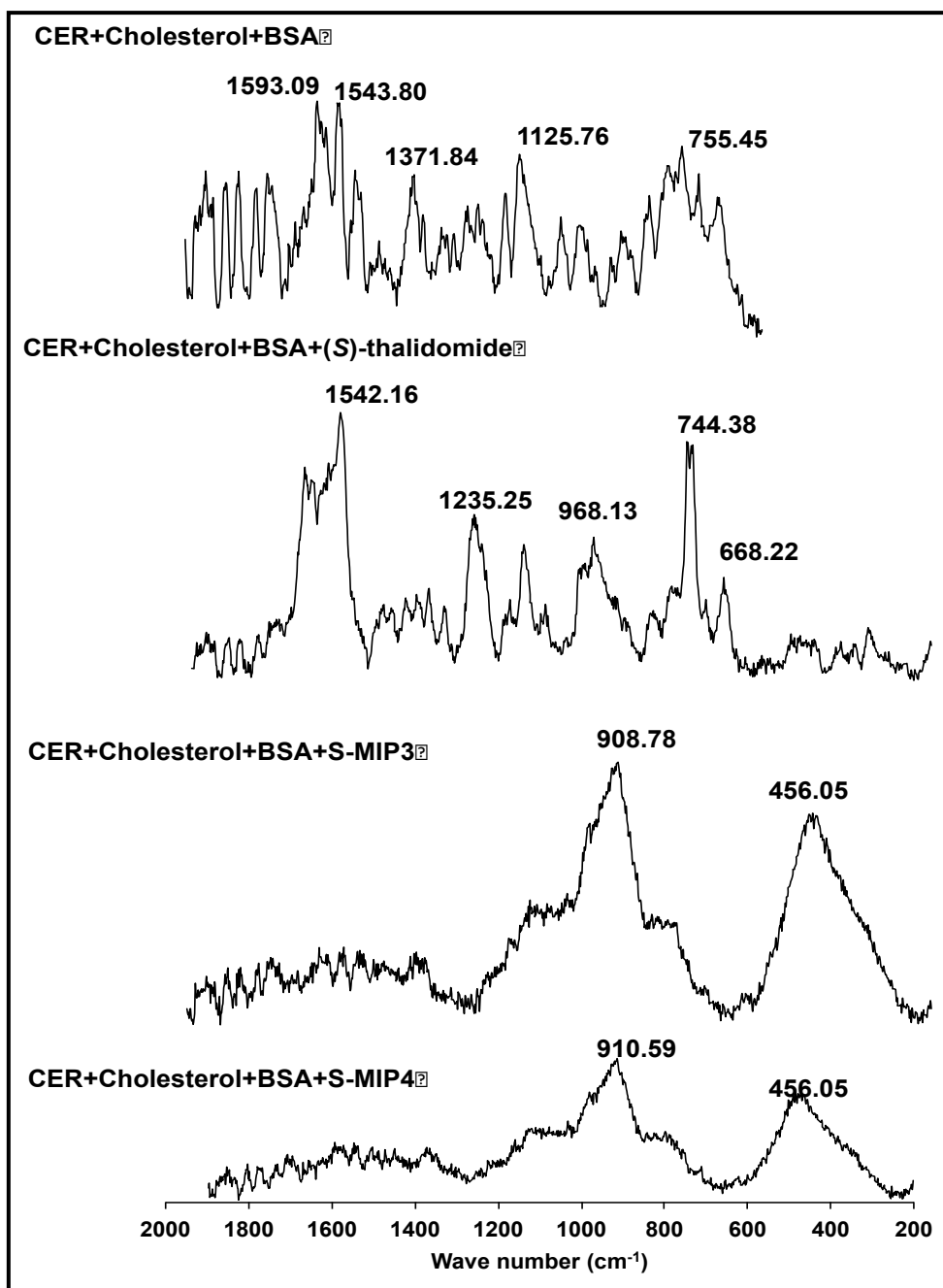
Figure 4.13: The characteristics of Raman spectrum of the ceramide (CER), cholesterol, and bovine serum albumin (BSA) mixture and the incubated mixture with the (*S*)-thalidomide on the adsorption of the imprinted nanoparticles. The concentration of the (*S*)-thalidomide was 50 μg mL^{-1}.

4.5 Conclusion

In this study, the determination of AFM images and Confocal Raman spectra were performed, which the measurement provided the information. The AFM showed the assemblies of the template (*R*)-thalidomide and (*S*)-thalidomide into three-dimensional structures of the imprinted sites of MIPs corroborating to success of the synthesis for the specific cavities that confirmed by the topographical images. The biological interaction of thalidomide could be detected onto the surface of the thin-film and the surface charge distribution plays a crucial role in orientation of the template-MIP assembly in the polymer materials that showed from the different force values depend on the movement of the cantilever onto the surface against the deflection and adhesion of the cantilever. For that reason, it had been successfully to prepare MIPs films on to the glass substrate by using MIP nanoparticles as the stamp in the polymer coating.

In addition, the interactions of the chiral pharmaceutical compounds in the recognition system onto the coated films containing the RMIPs and SMIPs were established with SERS techniques. A SERS technique also increases the sensitivity of Raman spectra which could separate the differentiation of both the enantiomers.

CHAPTER 5

THE STUDY OF MIP NANOPARTICLES SUPPORTED FILMS LAYER COATED INTERDIGITATED ELECTRODE AND THE APPLICATION FOR ANALYSIS OF THALIDOMIDE ENANTIOMERS IN THE BLOOD

5.1 Background

5.1.1 Interdigitated capacitance electrode (IDC)

Sensors based on microchanels with a planar interdigitated gold electrode array were studied. An interdigitated gold microelectrode provided the specific characteristics. The interdigitated gold electrode array consisted of a planar glass supported with a gold electrode that consisted of a ten-finger print. It was suitable for miniaturized sensor arrays. The principle of the capacitance detection was based on changes to the electrical resistance between two parallel electrodes from the reaction into solution (Gebbert *et al*., 1992). The conductivity decreased with an increase of a bound analyte. When different amounts of analytes were bound to a planar gold electrode, differences occurred in the resistance signal. This phenomenon caused a change in electro-conductivity due to changes in ion transfer. The capacitor consisted of an insulating material called a dielectric according to equation (1). The diffusion due to electromigration of the analyte can also be calculated according to equation (2)

to study the rate of the analyte bound/unbound to a planar gold electrode (Nilsson, 1977).

$$\text{C (capacitor)} = \frac{\text{Capacitive resistance} \times 2}{3.14 \times f} \qquad \text{-----------------------(1)}$$

$$D = \frac{D_0 M(T)^{1.75}}{RT} \times \frac{101 \times 10^3}{CP_{sat}} \qquad \text{-----------------------(2)}$$

Where,

f = Frequency (60,000 Hz)

C = Resistance from IDC electrode

D = Molar mass of diffractivity of the thalidomide enantiomer (m^2/s)

D_0 = Diffractive coefficient of the water-vapor-air mixture (2.5×10^{-5})

M = Molecular weight of the thalidomide molecule (M = 258 g/mol).

P_{sat} = Saturated vapor pressure, Pa (7.21 mmHg)

R = Gas constant (R = 8.314 JK^{-1} mol^{-1})

T = Temperature, K

In this study, the focus was on the development of an MIP based IDC sensor array for the detection of a specific enantiomer of a drug in a biological sample. Due to micropatterining-based electrochemical sensor systems have become attractive for excellent affinity separation and quantitative detection (Aherne *et al*., 1996). The applications of the inter-digital capacitance (IDC) transducer combined with the MIP as a sensor layer included the medical, biological (Ibrahim *et al*., 2013) environmental

diagnostics (Suedee *et al*., 2006), (Jungreuthmayer *et al*., 2012) and for the detection of mango volatiles (Hawari *et al*., 2013). There has been an increased attention to integrate the IDC gold electrodes with the MIP layers that can be used to produce a sensitive chemical sensor system for detecting drugs such as fenvalerate and pazufloxacin and other small molecules such as glucose. Applications combining MIPs and micropatterning technology have been proposed that have high selectivity and affinity for a selective binding to analytes from within a biological mixture containing structurally similar compounds. Thin films of an imprinted polymer were produced as a layer that was coated onto an IDC electrode that was used to improve the ability of the materials to analyze binding in biological fluids. The advantage of the analysis method by IDC is a label-free, inexpensive, and promising detection method that is performed in the presence of an electrical field and allows for the detection and quantification of target molecules in complex mixtures. Nevertheless, the disadvantages associated with interdigitated electrodes are its limitations in the production of a short and reproducible distance between the two conductors, and sensitivity to changes in the bulk solution. To overcome this problem, a reference cell without a recognition element can be used to compare with the recognition materials modified onto the electrode. Figure 5.1 shows the electrical circuit of IDC in this study having a comb-type pattern of gold electrode.

Figure 5.1: A comb-type of IDC electrode having gold pattern as electrical circuit on a glass substrate (Suedee *et al.*, 2006).

Method for the measurement of the molar mass of the thalidomide enantiomer through the flow cell system that has a comb type IDC electrode 10 finger prints as a transducer, The advantages of finger prints in the circuit of IDC were easily to detect the sample inside the small chamber and the parallel circuit can significantly increase the sensitivity with-out increasing the device size. (Tarikul *et al.*, 2015). The measurement of the resistance signal on the interaction between the molecularly imprinted polymer and the analyte was performed by an ohmmeter. The diffusion of the enantiomer drug to the imprinted layer could be measured under the same condition as those for the non-imprinted polymer. A method for analysis by sensor measurements of both the thalidomide enantiomers that had been exposed to the biological matrix compound of whole blood samples, cholesterol, bovine serum albumin (BSA), and ceramide has been studied. This can be achieved by generating a recognition site in the polymeric matrix by molecular imprinting technique. Therefore, the MIP nanoparticles have been prepared with the recognition sites for the

(*R*)-and (*S*)-thalidomide within a polymeric crosslinked chains, which subsequent coating on the IDC for resistance response measurements. The application of resistance measurements due to diffusion pathway and template accessibility to the imprint site give rise to the interaction of MIP-template complex in the imprinted cavity stereoisomers of thalidomide in solution and increase the resistance signal and the consistency of resistance response on the insulating layer, so called polarization resistance.

5.2 The objectives of this study

The objective of this chapter was to develop thalidomide enantiomer sensor based on molecularly imprinted polymer onto interdigitated transducer system for application to assess the interaction between thalidomide enantiomers in the presence of protein matrixes.

- To examine the recognition ability of both the (*R*)- and (*S*)-thalidomide on the molecularly imprinted nanoparticles supported with thin films using an interdigitated gold electrode

- To study the molecular interaction of the thalidomide enantiomers with and without a mixture of whole blood samples or a mixture of cholesterol, bovine serum albumin (BSA) and ceramide.

5.3 Materials and methods

5.3.1 Chemicals and reagents

Methacrylic acid (MAA), 1-vinyl-2-pyrrolidone (NVP)*, N,N′*-(1,2-dihydroxyethylene) bisacrylamide (DHEBA), (*S*)-(-)-thalidomide (99%), (*R*)-(+)-thalidomide (99%) were from Aldrich Chemical Company (Milwaukee, WI, USA). 2,2´-Azobisisobutyronitrile (AIBN) was obtained from Waco chemical company (Ozaka, Japan) and kind gift from Prof. Peter A. Lieberzeit for which many thanks. Sodium phosphate dibasic (Na_2HPO_4) and sodium phosphate monobasic dihydrate ($NaH_2PO_4.2H_2O$) were from the Sigma Aldrich Company (Milwaukee, WI, USA). All other solvents used were of analytical reagent grade and were used without further processing.

5.3.2 Biological compound

The study of the binding of thalidomide enantiomers to the imprinted polymer layer in the presence of bovine serum albumins, cholesterol, ceramide and blood sample have been carried out, which produce the information about the natural interaction of the biomolecules. To determine the resistance signals of the insulating layer on IDC, the selection of biological matrix consisting of the bovine serum albumins, cholesterol, ceramide because of the mimicking physiological effect of these compounds in this work.

5.3.2.1 Ceramide

Ceramide from the bovine brain (98% TLC) was from Sigma Aldrich Company (Milwaukee, WI, USA).
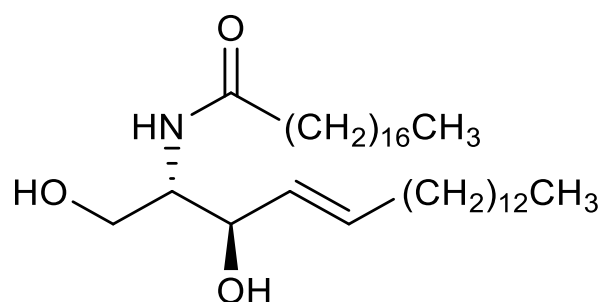
Figure 5.2: Chemical structure of ceramide.

5.3.2.2 Albumin from bovine serum

Bovine serum albumin (BSA) was from the Sigma Aldrich Company (Milwaukee, WI, USA).
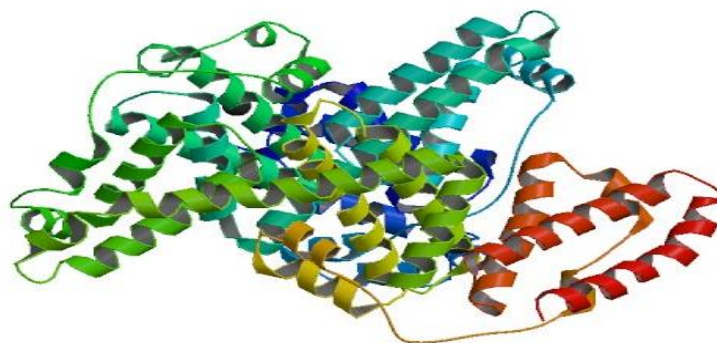
Figure 5.3: Chemical structure of bovine serum albumin (BSA).

(http://www.rcsb.org/pdb/explore/explore.do?structureId=4F5S)

5.3.2.3 Cholesterol

Cholesterol was from the Sigma Aldrich Company (Milwaukee, WI, USA).
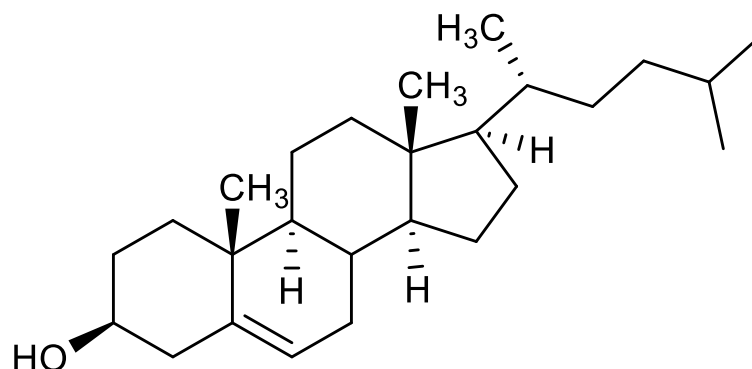
Figure 5.4: Chemical structure of cholesterol.

5.3.2.4 Human blood sample

Figure 5.5: Human blood samples from healthy volunteers.

5.3.3 Preparation of the MIP nanoparticle-layer

Precise control over the distribution of the particle size in the pre-polymer mixture was essential for reducing any defect in the resultant sensor layer. It has been found that the formation of the sensitive layer was achieved by controlling the shape and size from the imprinted nanoparticles that had the distribution of the particle size and a particle size of about 300 nm was used to ensure a greater density with the particle adhesion is improved. The procedures for preparing a pre-polymer of either of the two different types of MIP nanoparticles were carried out by using the monomer mixtures as shown in Table 5.1 except for the absence of a template. The monomeric mixtures were sonicated for 30 min, followed by addition of the initiator (0.73 mmol). These monomeric mixtures were purged with nitrogen gas for 1 min, and the mixture was pre-polymerized at 70 °C until the gel point was reached in about 5-10 min. The gel (1:2, v/v) was diluted with water, and then 50 µL of solution were then dropped onto the surface of the electrode. A 25 µL of the suspension was admixed with the pre-polymer coated onto the electrode, and polymerized at 60 °C overnight. The nanoparticles that remained on the surface of the film were removed from the coated film by using distilled water. A non-imprinted nanoparticle was also dropped onto the coated film by the same procedure for the imprinted nanoparticles.

Table 5.1: The composition of the pre-polymer polymer layer.

Components	Amount
MAA	0.60 *mmol*
NVP	0.20 *mmol*
DHEBA	0.05 *mmol*
AIBN	0.02 *mmol*
Acetonitrile: water (3:1)	800 µL

5.3.4 Set-up of IDC sensor and measurements

The preparation of a pre-polymerised layer onto an interdigitated electrode was as follows. MAA (50 mg, 0.6 mmol) NVP (20 mg, 0.2 mmol), and DHEBA (10 mg, 0.05 mmol) were dissolved in 800 µL of acetonitrile: water at a ratio of 3:1 (v/v), followed by the addition of AIBN (3 mg, 0.02 mmol). These monomeric mixtures were purged with a stream of nitrogen gas for 1 min and pre-polymerised mixture at 75 °C for 2 hour in a water-bath. Nanoparticles of either the (*R*)- or (*S*)-thalidomide imprinted polymer (RMIPs or SMIPs) after they were admixed with the polymeric mixture were dropped onto the pre-polymerised layer and placed in an oven for 24 hour. The interdigitated gold electrode and wire connections with electrode-contacts were merged with a 16 mm × 13 mm, 3 mm poly (dimethylsiloxane) pad. The silicone pad of 11 mm × 9 mm × 1 mm had holes for the sample inlet with a 1 mm diameter outlet that were drilled through the cavity with a total internal volume of 90 µL. A perspex housing-box size was 3.5 cm × 4.5 cm × 0.4 cm. The flow analysis system of the sensor consisted of a liquid port for delivery of a water sample from a sample-

reservoir, a peristaltic pump, operated at a continuous flow rate of 0.1 ml min^{-1}, that was driven by a peristaltic pump (MCP-Process Series, Ismatec SA, Wertheim-Mondfeld, Germany). The sensor output signals were monitored using an ohmmeter (Tonghui, Taipei, Taiwan) from the sensor display on the PC laptop screen (Figure 5.6). For the initial measurement, the electrical resistance of the sensors was measured with the bare gold electrode as a reference. The detection of the samples was carried out at room temperature (28 ± 1 $^{\circ}$C). The sensor signal of the MIP-based IDC sensor was measured as a function of the changes to the resistance of the polymer after exposure to the (*R*)-thalidomide or (*S*)-thalidomide with concentrations that ranged from 0.025-100 μgmL^{-1}. A control experiment was carried out with the corresponding NIP. The signal response towards the concentrations of the analyte was reported as a resistance (*R*), where *R* was the average resistance response after the addition of known amounts of the thalidomide enantiomer. Every experiment was carried out in triplicate to obtaining mean values and the standard deviation (SD).
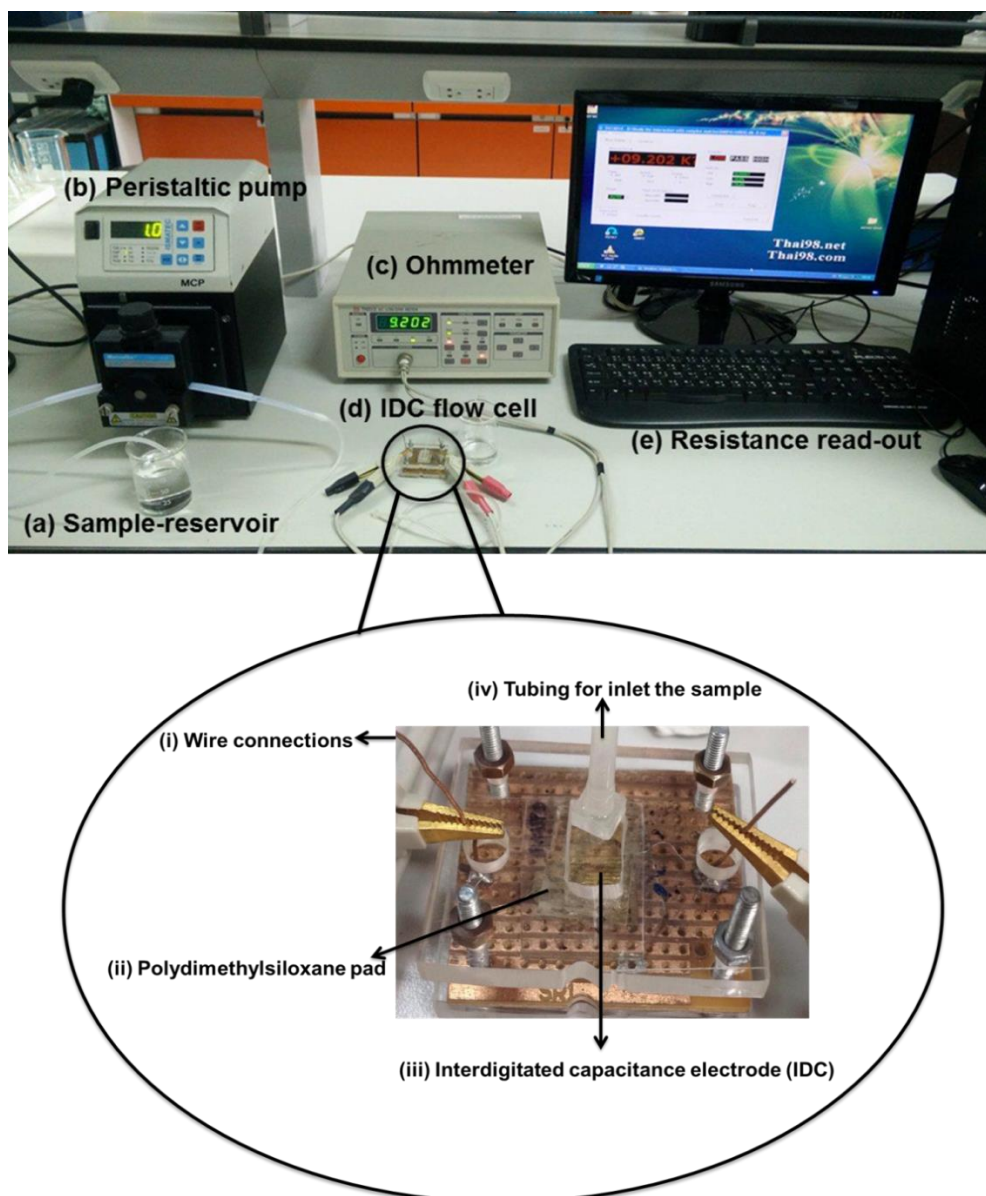
Figure 5.6: The sensor set-up of the MIP-based IDC consisted of a liquid port for delivery of a water sample from a sample-reservoir (a) and the online system connections with a peristaltic pump (b), a low ohm meter (c) and the flow cell (d) equipped with MIP layer coated onto the electrode. The resistance signals were read-out by computer software (e). The expanded images show the sampling cell of MIP layer chip consisting of (i) wire connection (ii) polydimethylsiloxane pad (iii) IDC electrode (iv) tubing for inlet the sample.

5.3.5 Methodology

5.3.5.1 Atomic force microscopy (AFM)

To examine the characteristics of the (*R*)-thalidomide and (*S*)-thalidomide imprinted films on the IDC. A Dynamic Force microscope: DFM (SPA400, SEIKO Inc., Chiba, Japan) was used to measure the surface morphology of the imprinted films after detecting the resistance signal onto the electrode. The nanoparticles of the film were measured in air at room temperature ($25 \pm 1°C$). The AFM tip Si_3N_4 consisted of a pyramidal shape with a nominal tip radius of 10 nm, and a spring constant of 20 N/m. The resulting images were scanned over 500 nm^2 with 256 x 256 pixels, and a scan speed of 1 Hz. The topography at the selected area of the imprinted nanoparticles was attached onto thin-film and the imprinted nanoparticles were attached with the biological matrix after sensor measurement that was first imaged by DFM, and the measurements of the force-distance were transferred from the AFM contact mode and the force analysis was obtained on the nanoparticle-MIP films in the same area. All experiments of images were achieved using the force measurement software SPI4000 Nano Navi SPA400.

5.3.5.2 Confocal Raman Spectroscopy

A confocal Raman spectroscopy (NT-MDT, NTEGRA spectra, Bosco, Russia) was used to investigate the vibrations of a single enantiomer of the thalidomide. The imprinted polymer nanoparticles were coated onto films of the pre-polymer, the imprinted films of (*R*)- or (*S*)-thalidomide was then used to identify the structure of the reactivity of drug enantiomer that interacted by a self-assembly process after the drug was exposed to the biological material: bovine serum albumin, ceramide, choresterol. The Raman-AFM consisted of an excitation light source at 632.8 nm (50mW, He-Ne laser), that delivered 3 mW to the analyte, using a 100 x objective lens (Olympus, Japan) with a spot size of approximate 333 nm. A monochromator grating of 1200 grooves/mm was employed together with an air-cooled charge-coupled device (CCD) detector that recorded the Raman signal at the operating temperature of −60 °C. Multiple spectra were acquired with an acquisition time of 60 s (exposure time of 10 s, and accumulated time 6 N). The reflection image was detected for all the samples from the photo multiplier tube: the PMT within the wavelength of the Raman spectrum. The PMT image was scanned at 1 μm with 256 x 256 pixels, and the resolution was approximately 3.9 nm/pixels under ambient conditions. We focused on a fingerprint region of approximately $100 - 2000 \text{ cm}^{-1}$, where most of the characteristic vibrational bands of the thalidomide were found. One microliter of sample was dropped onto the silver substrate that worked as the Surface Enhanced Raman Spectroscopy (SERS) substrate. The sample was driven in at room temperature for 1 h, prior to measurement. The silver thin film was prepared by using

the RF magnetron sputtering (model), with a thickness of 200 nm, and an RF power of 150W, an Ar flow rate of 20 sccm.

5.4 Results and discussions

5.4.1 The characteristic of MIPs onto IDC electrode

The MIP-based IDC was used for resistance measurements resulted in the shift of a signal between the two conductors of the gold electrode which the recognition element of imprinted nanoparticles supported onto thin films immobilized between them which is necessarily desirable and robust material. The thin-film integrated nanoparticles for immobilization onto the electrode required close contact to the transducer system to be useful for application as a sensor. The SEM images of the obtained MIP nanoparticle-films after washing the nanoparticles onto the coated films with particle sizes of 300 nm (see Figure 3.6) were examined, as the MIP nanoparticles template. The results showed planar surfaces of the interdigitated gold electrode and a very thin-film in Figure 5.7. It was noted that the coated particles were appropriately formed and that two key factors were to control the particle size distribution in the slurry and the selection of the solvent. Figure 5.7 illustrated the SEM images of the (*R*)-thalidomide-imprinted nanoparticle (Figure 5.7 (I) and (*S*)-thalidomide imprinted nanoparticle (Figure 5.7 II) supported by the thin film coating onto the IDC. RMIP1 and RMIP2 and also SMIP1 and SMIP2 had cavities on the surface with a specific shape that allowed the RMIP1 or SMIP1 nanoparticles to be removed from the films. For NIP nanoparticles on thin-films, they showed the particle

appeared on the coated thin-films supported on the IDC. From the NIP2 we see that the particles are almost spherical in shape with irregular surface and embedded inside the film. The film is highly non-specific particles was remained onto the thin-films, as can be seen in Figure 5.7 (III). The effect of the nanotopography of the core shell, MIP1 and MIP2 for either templates due to poly(styrene) during the formation of the chemically modified layer that was formed with the same composition as the MIP. Therefore they produced low stress and led to the greatest planarity of the MIP nanoparticle-film layer compared to the other formulations. In the case of the MIP3 and MIP4 for either two templates after extraction of the nanoparticles, the drug was adsorbed onto the selective pattern causing a complete covered surface, this is because of the very low force required to maintain low static removal rates by the non-core-shell upon the deposition of the low dielectric film on gold electrode. However, the surface of the coated electrode with the junction regions showed overlapping of the insulating layer. This was the changes of the nanoscale dimension that affected the nanotopography on the IDC.

(I)
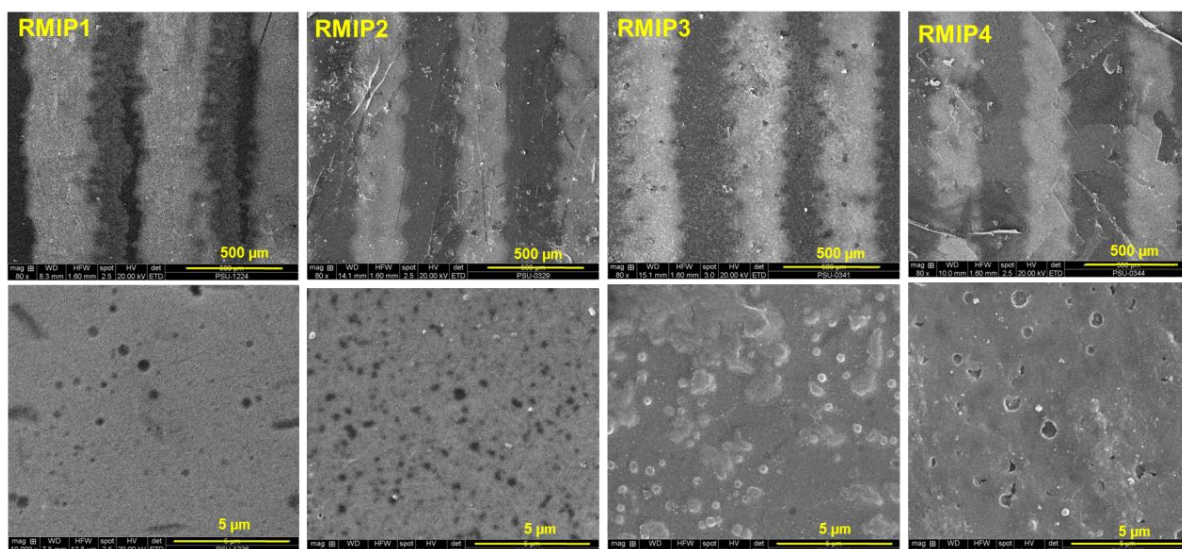
Figure 5.7 (I): SEM images of the (*R*)-thalidomide imprinted nanoparticles supported by the thin-film coating onto the IDC gold electrode with the pores of MIP nanoparticles on porous materials. (Top: 10 x magnifications, bottom: 100 x magnification).

(II)
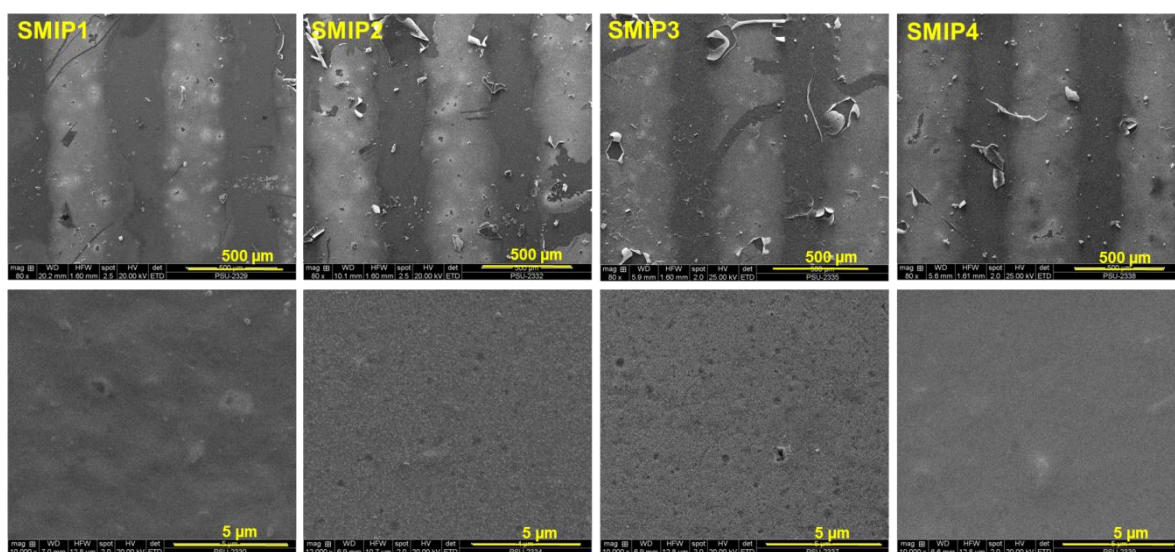
Figure 5.7 (II): SEM images of the (*S*)-thalidomide imprinted nanoparticle supported by the thin-film coating onto the IDC gold electrode (Top: 10 x magnification, bottom: 100 x magnification).

(III)
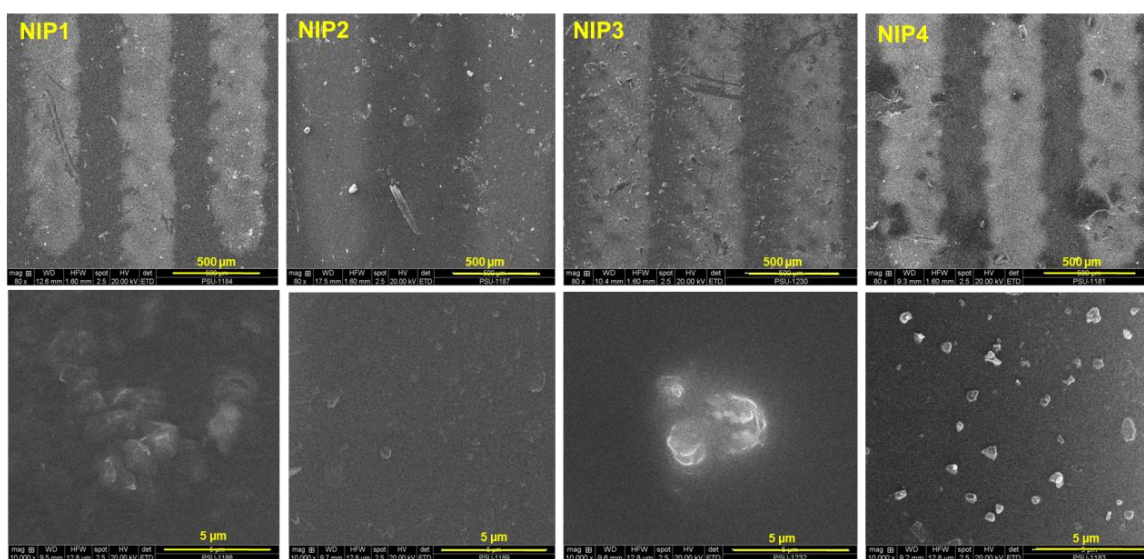
Figure 5.7 (III): SEM images of the non-imprinted nanoparticles supported by the thin-film coating onto the IDC gold electrode (Top: 10 x magnification, bottom: 100 x magnification).

5.4.2 IDC Sensor measurements

The IDC sensor measurements of the MIP nanoparticle-films on the IDC that contained varying functional monomers among the core-shell and non-core-shell MIPs were verified. To present the phenomenon of the resistance signal on different concentrations of thalidomide enantiomers, we used excel software to plot scientific concentration numbers of logical at x-axis. Figure 5.8 shows the sensors response at a fixed concentration of (R), and (S)-thalidomide enantiomer without the biological compounds of the RMIP and SMIP formulations, respectively on IDC. It seems that the introduction of the RMIP1 core-shell increased the densities of the layer-coating. This was desirable in order to produce a higher planarization, and allowed for the dielectric matrixes and the highest sensitivity for the drug-MIP interactions with a high specificity compared to the corresponding NIPs because RMIP1 showed the excellent interaction with the (R)-thalidomide. The sequentially dropped analytes (0.025-100 μg/mL) allowed for signal responses that was initially high and dropped off at the beginning of the addition of the analyte beyond 20 μg/mL. This indicated that the imprinted polymer coated with nanoparticles stamped. In contrast, the non-core-shell, SMIP3 and SMIP4 that contained the same monomeric precursor as the RMIPs showed a smaller signal response of the template. The non-core-shell MIP mostly showed electrical resistance responses as a function of the concentration of the enantiomer on the IDC. This is attributed to the MIP-template interactions which showed a reasonable signal response with an increase in the enantiomer concentration, but leveled off at between 30-100 μg/mL (Figure 5.8). In addition, the RMIP1 nanoparticle-film layer fixed onto the electrically active parts of the gold layer

produced uniform features. It was also preserved due to the strength of the structure between the insulating layers and nanoparticles stamped. The fine-tuning of the morphology of the nanoparticles and the precise control of the chemical properties in the nanoscale dimension by adjusting the functional monomer within the MIP binding sites was extremely important to ensure the uniform features of the coating layer of the nanoparticles. Indeed, the former material contained a core-shell of poly (styrene), that the cast film allowed for both the gold and insulator combined for the conducting properties, but removal of the contamination between the channel. As shown in the SEM image, in Figure 5.7, the structure and electrical characteristics of such a material through introduction of the insulating layer that was important for the signal from the interaction of the MIP-template that allowed for an improved performance of the circuit. Therefore, the fabrication of the nanoscale embedded structure onto the nanoparticles led to a three-dimensional device of the drug-MIP inside a nanoscale film attached to the IDC for application as an electronic sensor. The results showed that the approach had the potential to distinguish between chiral entities of thalidomide. In addition, the imprinted nanoparticles supported thin films on the gold electrode had been examined for the resistance measurement in the presence of MIP-IDC sensor response to the analyte. To examine the selectivity and sensitivity of the thalidomide imprinted polymer in the presence of a complex matrix. A control experiment was also performed with the non-imprinted polymer on the IDC. The effects on the sensor of a spiked sample with standard thalidomide are also compared. Figure 5.9 shows the typical sensor response at a fixed concentration of the (R), and (S)-thalidomide enantiomer in the concentration range of 0.025-100 μg ml^{-1} with the incubated mixture of cholesterol, bovine serum albumin (BSA), and ceramide at 1 mg

mL^{-1} in the flow through flow cell by using the peristaltic pump. As can be seen from Figure 5.9, the MIP1 and MIP2 of (R)-thalidomide and (S)-thalidomide sensor gives a signal response that depended on the concentration of the thalidomide, in the range of 0.025-100 µg mL^{-1}. In contrast the reference sensor showed only a slight response towards the thalidomide enantiomer solution in the phosphate buffer solutions (pH 7.4). RMIP1 and SMIP2 provided a stable resistance signal; moreover, the data showed that the resistance signal curve of the NIP3-R and NIP3-S provided a high resistance signal because of the effect of the non-specific binding of the biological compounds onto the thin film. The sensor effect was not influenced by the complex matrix of the measurement. A non-specific effect was obtained. In this study, the development of a MIP biochip for the detection of thalidomide in the presence of complex matrix was examined. The SMIP-IDC sensor showed a rapid shift in the resistance that was dependent on the concentrations of the thalidomide. The ability of the artificial recognition material to recognize the presence of defined organized structures on the enantiomers molecular surface allowed for an interaction and MIP binding sites that recognized on the film of polymer.
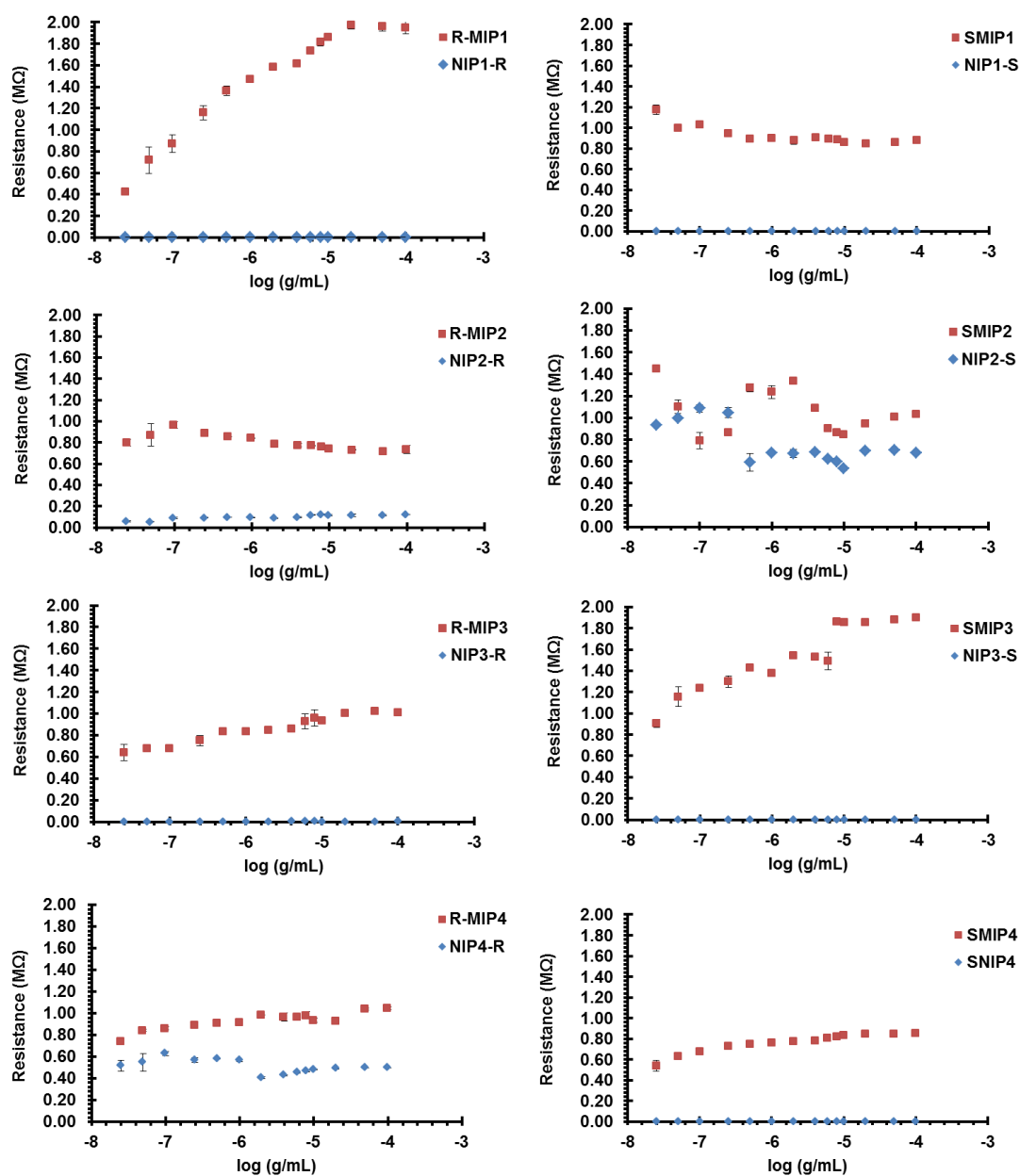
Figure 5.8: The effect of concentrations of (*R*), and (*S*)-thalidomide enantiomers on the resistance signals for the respective imprinted nanoparticles on a thin-film coating IDC. (Mean ± SD, n=3).
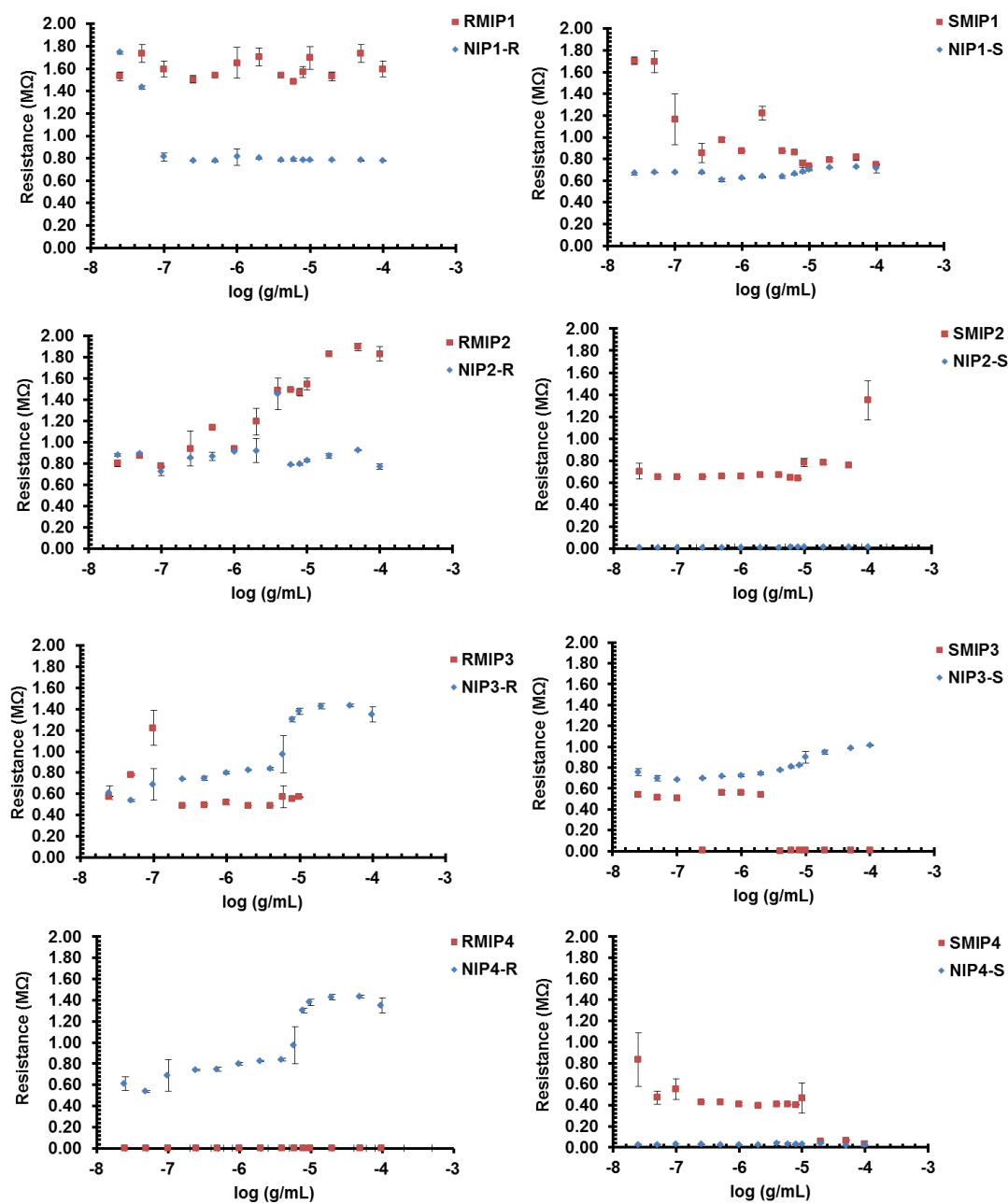
Figure 5.9: The effect of the additional lipid-protein component, on the resistance signals for the respective imprinted nanoparticle by a thin film layer on the IDC electrode. (Mean ± SD, n=3).

5.4.2.1 Molar mass transfer of thalidomide onto IDC electrodes

To understand the ability of the enantiomer drugs to penetrate from their specific cavities and provide the electrical resistance signals on an IDC, the mass transfer calculation was carried out; we expected that the analyte can diffuse through the MIP-IDC sensor layer. According to equation (2) we used that equation to calculate the mass transfer. Table 5.2 illustrates the data of the mass transfer on the IDC that was achieved from the properties of a chiral drug attached onto a synthetic surface of nanoparticles. The rates of the diffusion of the enantiomer drug of the RMIP1 in the absence of a protein matrix was lower than for the other formulations and provided the highest shift of the resistance signal. In the case of RMIP3 in the presence of a protein-lipid component the mass transfer increased 2 times. Moreover, the diffusion of the RMIP4 is a consequence from adhesive force of enantiomer drugs penetrate on the surface against the outer layer that had only a low space to rebind with the analyte. It can be seen clearly that in the presence of the core-shell of the poly(styrene) within the composition of the synthetic polymer (MIP1, MIP2) there was a shift of the mass transfer to lower values yet a considerable increase in its selectivity. It was evident that the transfer of low movement occurred and provided a more specific binding of the enantiomer drug, whereas at a higher concentration of thalidomide (20 µg mL^{-1}) a lower specific binding of the two enantiomers occurred together with the effect on the equilibrium. For the two different types of SMIPs, both with and without a protein matrix it was found that the resistance signal in the presence of the protein-lipid component decreased yet provided for the transfer of a higher diffusion coefficient, especially for SMIP3. Consequently, the selectivity

values of SMIP were to some extent influenced by the presence of the protein-lipids. These results showed that the optimal rate of transfer of the enantiomers onto a planar substrate might be due to a good binding of the desirable compounds to the miniaturized sensor.

Table 5.2: The data for the selectivity from mass transfer of thalidomide enantiomers between MIPs and NIPs by resistance measurement on IDC.

Formulations	Molar mass (m^2/s) $\times 10^5$					
	Without the protein-lipid mixture					
	NIP-R	RMIP	Selectivity (NIP/MIP)	NIP-S	SMIP	Selectivity (NIP/MIP)
F1	829±116	1.23±0.024	731.95±86.20	49100±2740	2.72±0.040	18048.36±748.16
F2	20.8±0.476	3.08±0.019	6.74±0.20	3.58±0.049	2.24±0.053	1.60±0.03
F3	807±0.126	2.62±0.199	308.42±22.42	1660±298	1.31±0.018	1296.55±211.40
F4	5.35±0.067	2.52±0.101	2.12±0.06	2360±748	3.00±0.042	845.02±256.97

Pvalues were < 0.001 for all formulations.

Table 5.3: The data for the selectivity from the mass transfer of thalidomide enantiomers between MIPs and NIPs exposed for resistance measurement on IDC with the protein-lipid mixture.

Formulations	Molar mass $(m^2/s) \times 10^5$					
	With the protein-lipid mixture					
	NIP-R	RMIP	Selectivity (NIP/MIP)	NIP-S	SMIP	Selectivity (NIP/MIP)
F1	3.14±0.006	1.55±0.048	2.03±0.06	3.4±0.014	3.21±0.138	1.06±0.05
F2	2.80±0.128	1.33±0.010	2.11±0.08	138±0.739	3.10±0.148	44.45±2.34
F3	1.87±0.034	4.98±0.016	0.37±0.01	2.70±0.172	479±40.30	0.01±0.00
F4	7970±10.00	18400±5.33	0.43±0.00	65.4±25.6	5.95±0.115	12.24±4.28

Pvalues were < 0.001 for all formulations.

5.5 CONCLUSIONS

In summary, the MIP as chemical probes on the IDC sensor could distinguish thalidomide enantiomer from the biomolecular domains including ceramide, bovine serum albumin, and cholesterol. Thus, it is extremely beneficial for the application of this analytical system to quantify analytes in real-life samples. Moreover, the IDC is one effective approach to miniaturize the MIP serves as sensing element that will allow for the detection of analyte in small sample volumes without reducing the sensitivity and selectivity. The IDC based on MIP for stereochemical detection using MIP biomimesis configuration system when integrated with the microfluidics systems of flow-cell, that sample delivery can achieve further improvements to the overall stability and reproducibility of the IDC. The interdigiated gold electrodes can be prepared in the introduction of MIP nanoparticles into the films of polymer and integrated into the microdetection device for electronic and sensing analysis.

MIP based IDC sensor was determined with resistance signal, which various chemical functionalities and the format of MIP nanoparticles. The reference sensor showed only a slight response towards the thalidomide enantiomer solution in the phosphate buffer solutions (pH 7.4). RMIP1 provided a rapid change in the resistance signal that was dependent on the concentrations of the thalidomide at low concentrations. The resistances respond effect was not influenced by the complex matrix inside the solution of the measurement. The design and development of a MIP biochip could recognize the structures on both the enantiomers at the surface that had the interaction onto the coated thin-film in IDC. In addition, excellent binding of the

specific enantiomer to the imprinted sites of the coated thin-film affect to mass transfer into the polymer layer in the presence of complex matrix.

CHAPTER 6

ATOMIC FORCE MICROSCOPY STUDIES FOR INVESTIGATION OF INTERACTION ON THE MIP LAYER AND COATING IDC ELECTRODE

6.1 Background

Atomic force microscopy (AFM) is a three-dimensional topographic technique with a high atomic resolution to measure surface roughness. It was invented in 1986 as the first new extension of scanning probe microscopy (Binnig *et al*., 1986). AFM is a kind of scanning probe microscope (SPM), and the interaction occurs between an AFM tip (Figure 6.1) and the atoms of the sample surface (Figure 6.2). The tip is attached to a very flexible cantilever. Laser light is reflected from the cantilever and detected by a photodiode. The tip is brought to contact or near-contact with the surface of interest. Scanning over the surface, AFM system records the deflection of the cantilever, due to very small forces between the atoms of the probe and the surface, with sub-nanometer precision. The deflection signal is recorded digitally, and can be visualized on a computer in real-time.

Figure 6.1: AFM tip (Si, N-type).
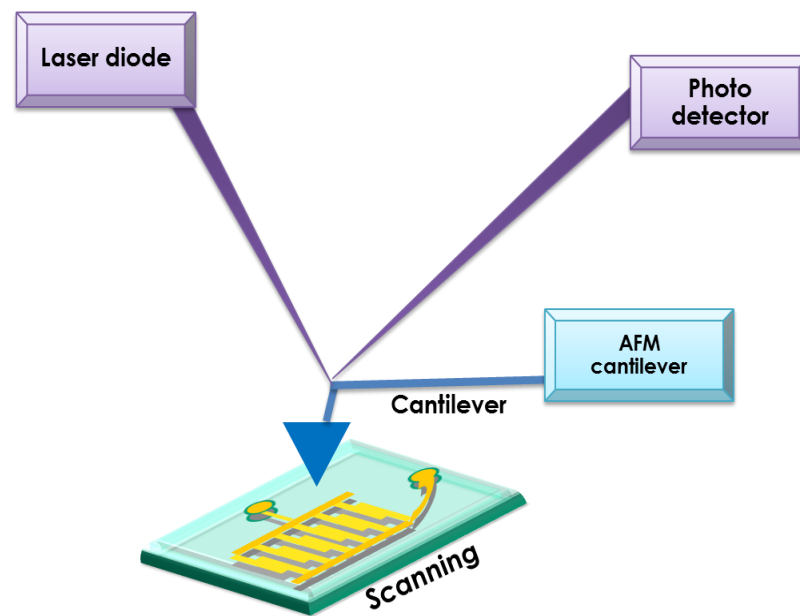
Figure 6.2: A typical Atomic Force Microscopy detection scheme.
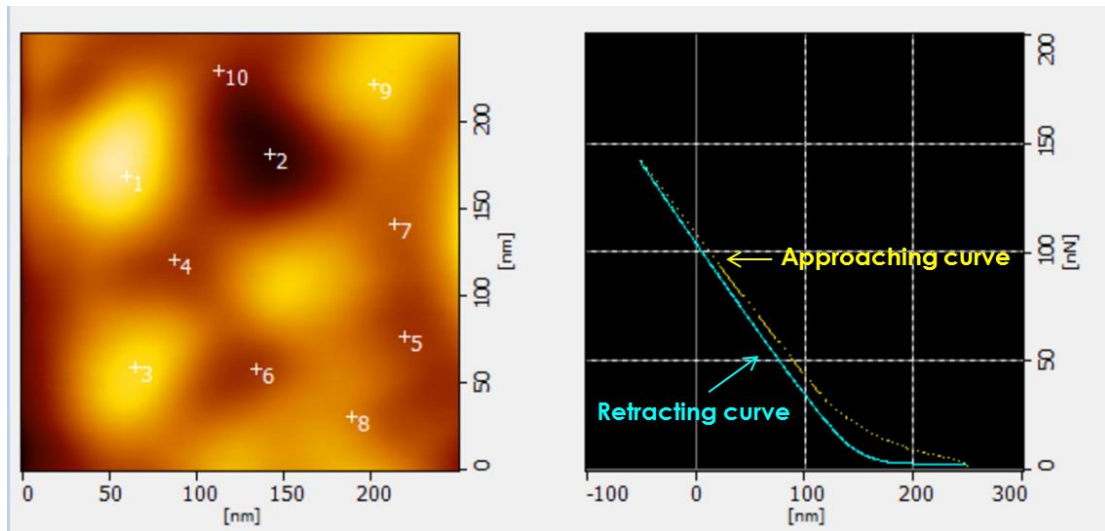
Figure 6.3: A typical force-distance curve recorded by AFM in force contact mode.

6.2 Objectives

The purposes of this study are to evaluate the application of MIP layer chip that has the chiral inversion of thalidomide enantiomers in the presence of bovine serum albumin that interacted with cholesterol and ceramide by using the AFM.

- To evaluate the characteristics of the MIP films by using AFM, to gain an insight into how the enantiomers of thalidomide interact with the MIP thin film and for the assessing of the structure of thalidomide in the presence of biomolecule such as rubber latex.

- To determine the stereoselective properties of thalidomide enantiomer by using chiral-HPLC method and IDC sensor chip measurement

- To validate the separation of thalidomide enantiomer in the presence of blood sample by using chiral-HPLC.

- To examine RMIP1 and SMIP1 can be used for sensing element for analytical sensor.

The protocol for sensor in analytical application after sensor measurement and the surface properties of MIP-film coating on IDC was examined by AFM, Raman spectroscopy. We employ MIP1 as a sensing element on an IDC sensor where is the same as the IDC sensor system for accessing the chiral molecule and biological binding site in the previous chapter. Method validation of MIP based IDC sensor has been carried out on the IDC measurement correlation with linearity, limit of detection (LOD), limit of quantification (LOQ), stability of sensor, and precision.

6.3 A study of the characteristic of MIPs films after detection the resistance signals

6.3.1 AFM images

To verify the characteristic morphology of the nanoparticles imprinted on the support thin films was examined. Figure 6.4 shows the 3D images of the (*R*)-thalidomide imprinted films (a-d) and the (*S*)-thalidomide imprinted films (e-h) on the IDC electrode after detection of the resistance signal by varying thalidomide concentrations in the range 0.025-100 µg mL^{-1}. The AFM images that determined the effects on the thalidomide adsorption patterns. For evaluation of the surface morphology after interaction between analyte and MIP were obtained in AFM images, from the all non-imprinted nanoparticle thin film supports (Figure 6.5). AFM images showed topography of all the MIPs on the IDC electrode, with less than 1.448 nm (NIP2-R) of averages root-mean-square (r.m.s.) roughness for a 500×500 nm^2 surface area. When the thalidomide was adsorbed onto the films they produced non-specific sites and shapes. The analyte flowed through the surface if it did not fit with the specific area, so the resistance was low. In conclusion, the characteristics of the imprinted nanoparticles showed much rougher areas and imprinted pattern of template with 13.41 nm (r.m.s.) roughness of S-MIP1. The thalidomide adsorbs onto the imprinted sites, leading to the formation of different morphological films depending on the shape of the imprinted structure. The circle line highlights the imprinted sites that were available to interact with the thalidomide enantiomer. The specific analyte can be fitted with the imprinted site and produce a high value for the resistance signal.

a) R-MIP1 b) R-MIP2 **RMIP**

c) R-MIP3 d) R-MIP4

SMIP

e) S-MIP1 f) S-MIP2

g) S-MIP3 h) S-MIP4
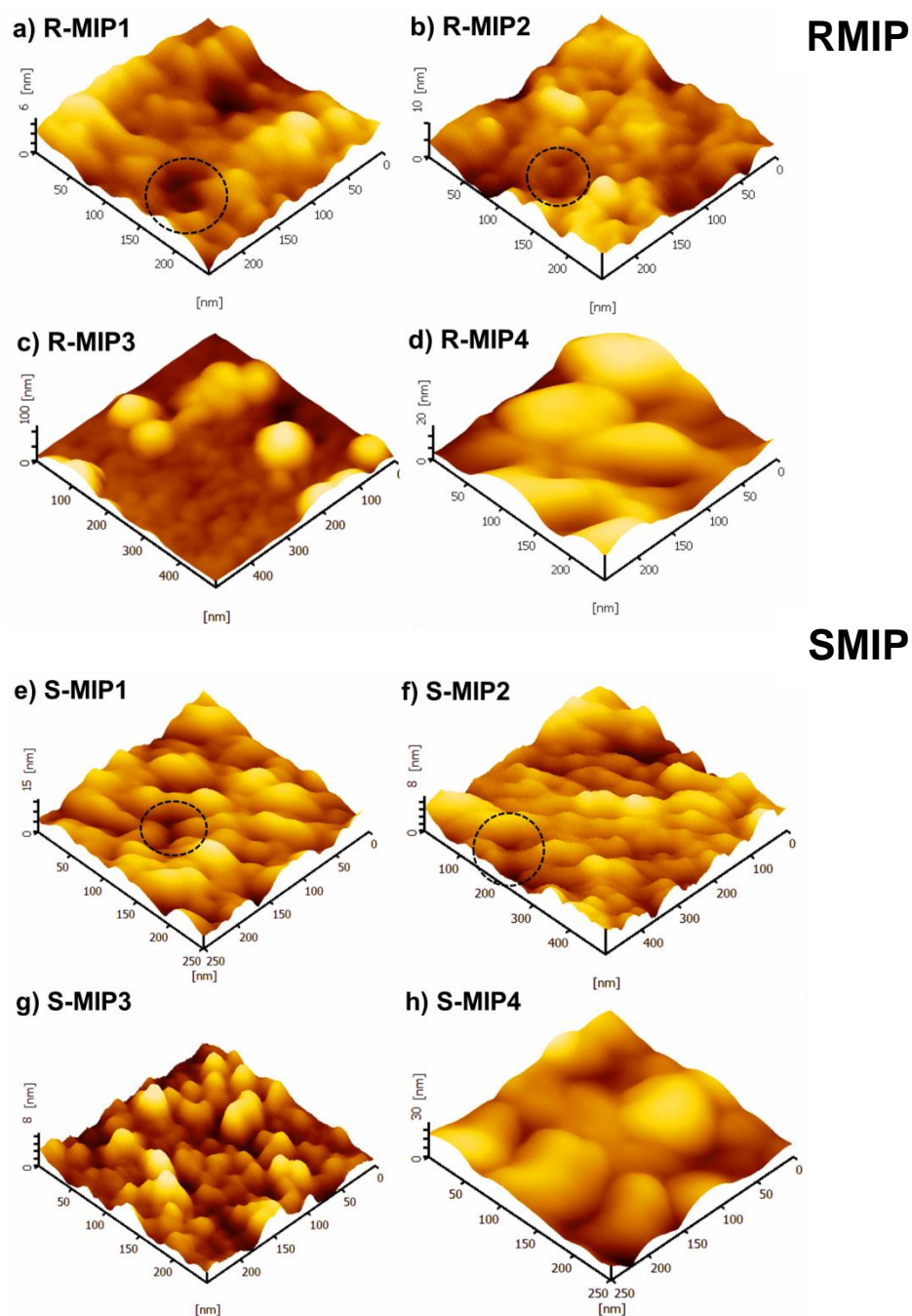
Figure 6.4: AFM images of various (*R*)-thalidomide imprinted films and (*S*)-thalidomide imprinted films exposed to the template. The image size of the analytes was 250 × 250 nm. The black circle represents the imprinted features of MIP nanoparticle as the stamp.
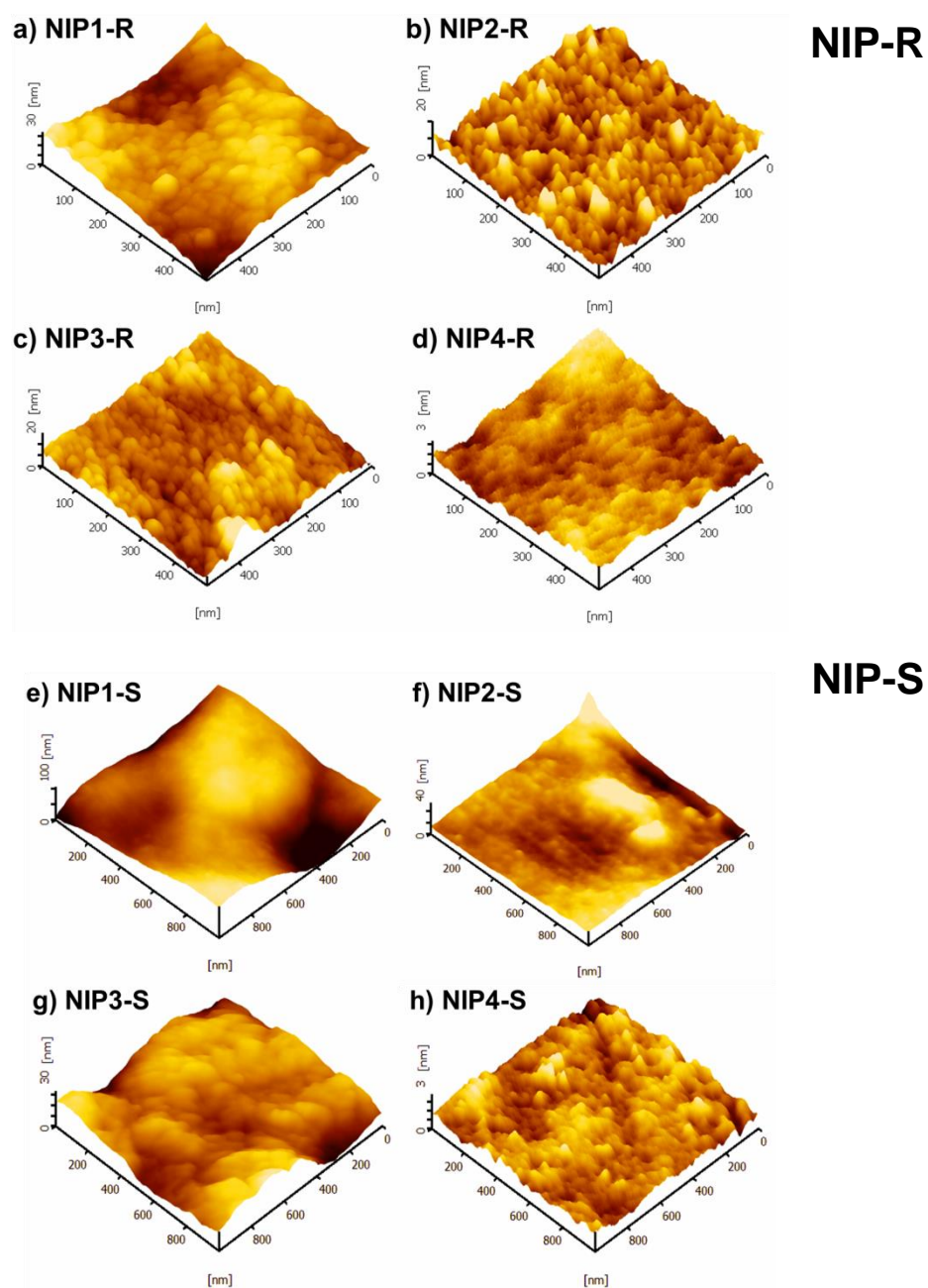
Figure 6.5: AFM images of the corresponding non-imprinted control polymers exposed to (*R*)-thalidomide and the (*S*)-thalidomide on the IDC for resistance measurement. The image size of (*R*)-thalidomide as the analyte was 500×500 nm and for (*S*)-thalidomide as the analyte was 1000×1000 nm.

6.3.2 Force measurement

In this experiment, AFM was used to probe the mechanical properties of thalidomide enantiomer that interacted with the specific binding site. The imprinted and non-imprinted thin films of the RMIP and SMIP were exposed to force measurement. Different molar ratio of MAA and NVP were used in the polymerization processes of the MIPs and NIPs samples. Figure 6.6 displays the force curve values of the coated thin films observed in the force curves supported on the RMIP (a) and SMIP (b) layers. Figure 6.6 (a&b) shows the force values of MIPs for both templates that were prepared by using different functional monomers. The force measurements were carried out on the surface of the thin films after the tip was close to the surface. The force curves describe the changes in the mechanical property of the films that the tip can move on to the depth site of the imprinted sites as can be seen in RMIP1 and SMIP1 that provided different force values when compared with the non-imprinted films. The largest force for (R)-thalidomide on R-MIP4 (70.53 Nn) was achieved while the R-MIP1 gave less force values of 43.88 nN after the resistance measurement on IDC with the matrix. For (S)-thalidomide as the template, force value of S-MIP1 (69.80) was highest and was smallest for S-MIP3 (64.55), among the other MIPs. For NIP the force values obtained show the different trend when compared with MIPs. The force values were different because the surface of the imprinted and non-imprinted polymer had different morphologies and arrangement of the molecules.
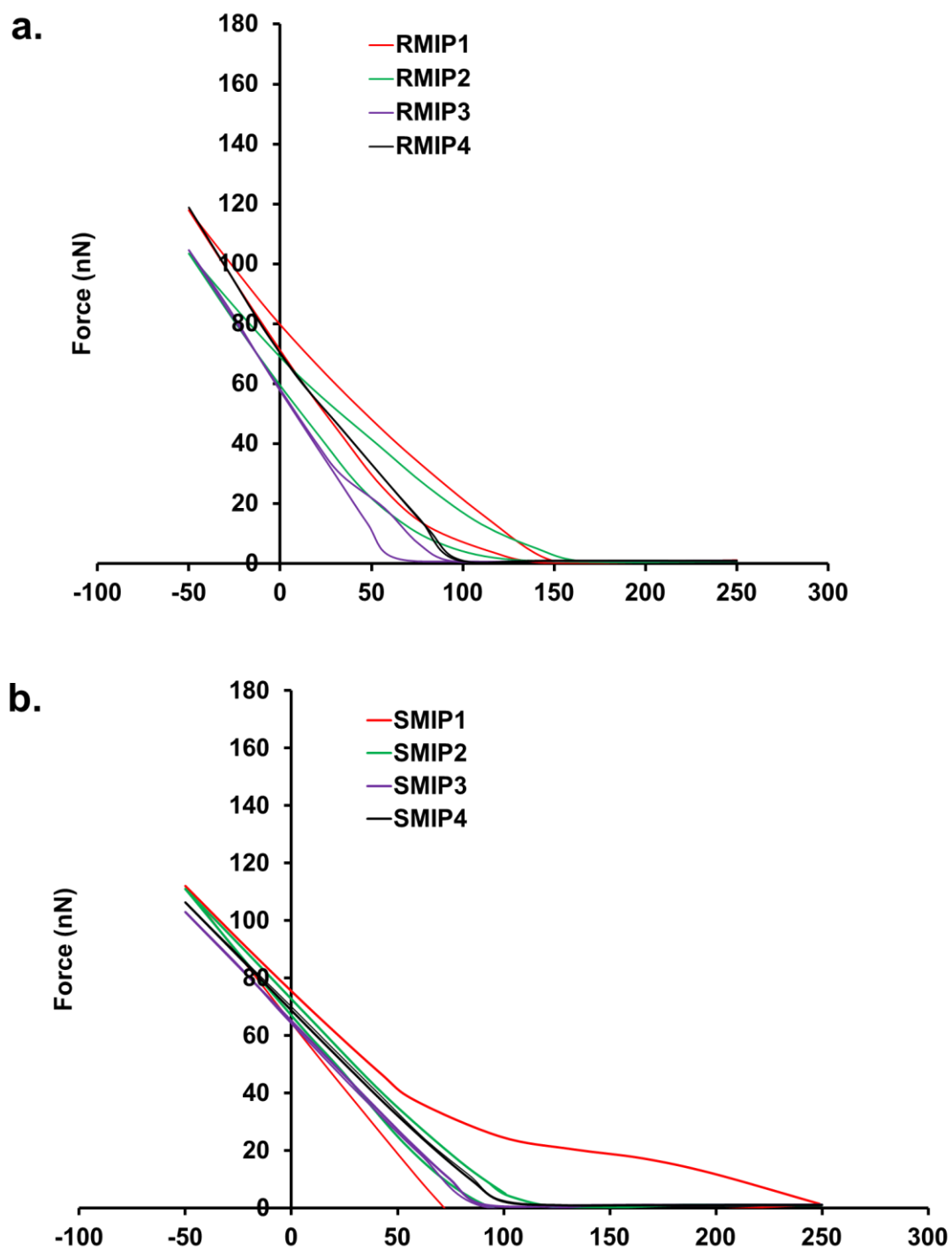
Figure 6.6: Force curves of the thin films observed for various (a) RMIP nanoparticles and (b) SMIP nanoparticles.
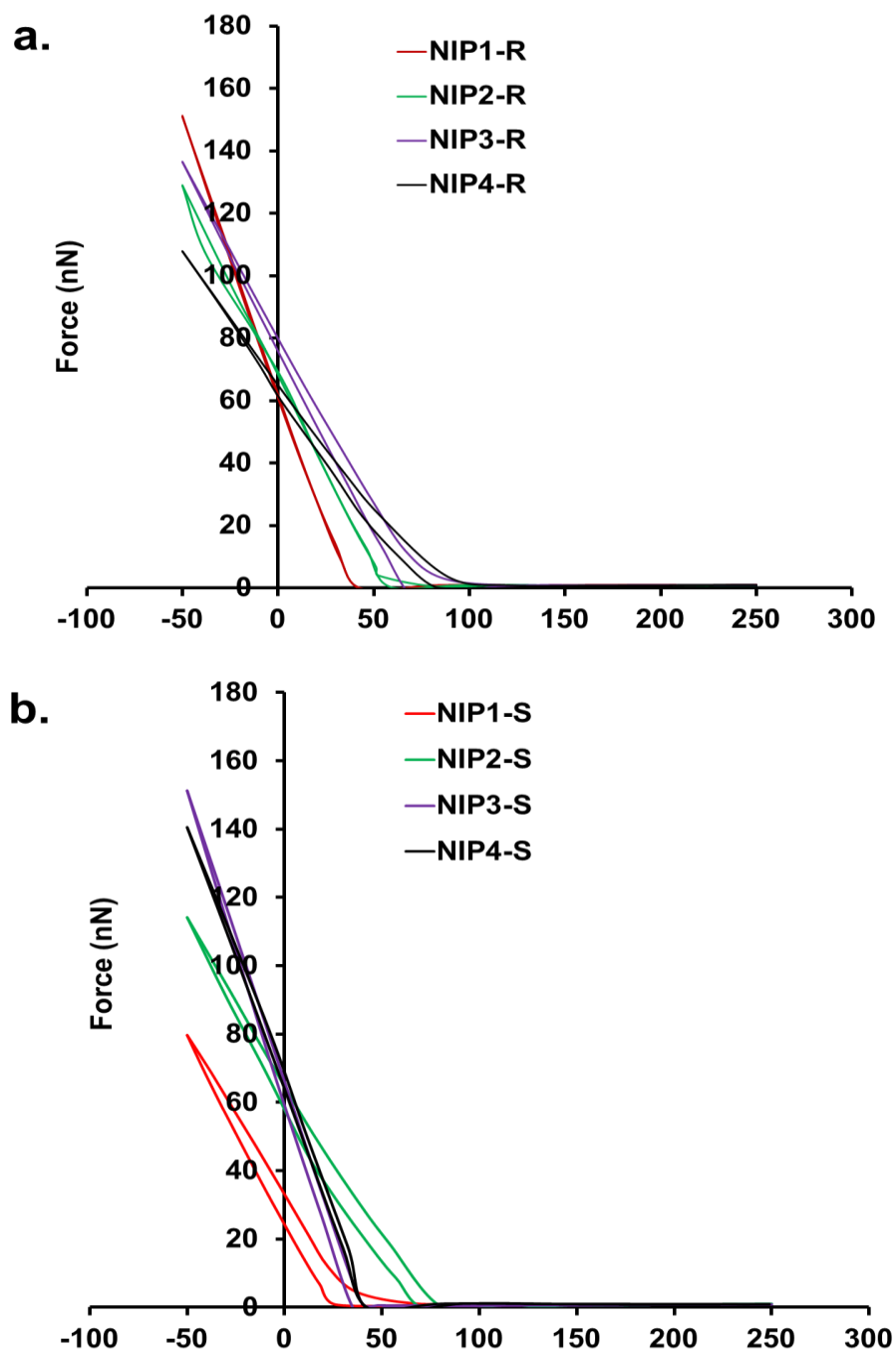
Figure 6.7: Force curves of the thin films observed for various (a) NIP-R nanoparticles and (b) NIP-S nanoparticles.
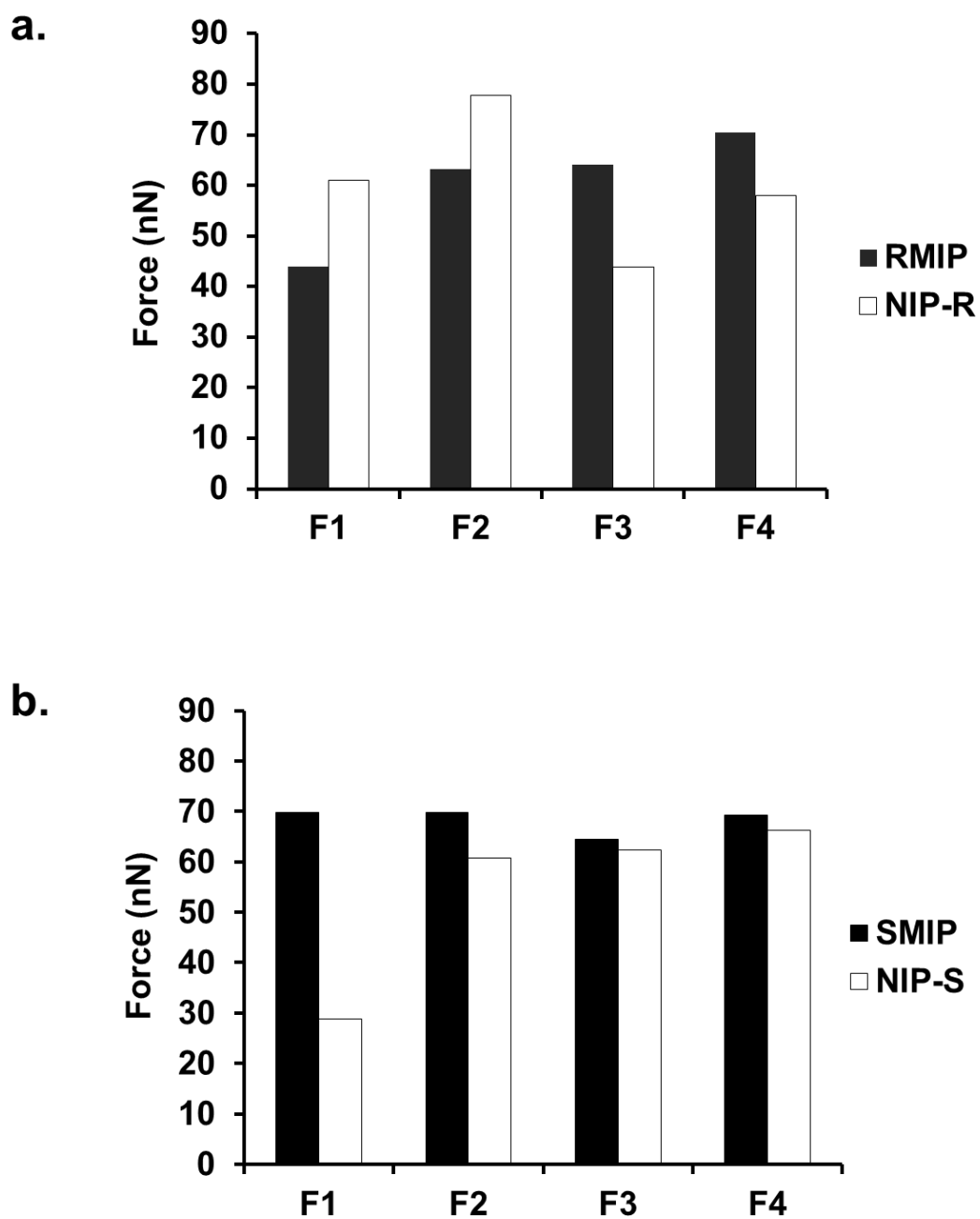
Figure: 6.8: The force values of various (a) RMIPs nanoparticles and (b) SMIPs as the film coating, compared with the non-imprinted polymer**.**

6.4 A study of the interaction of the IDC-MIP films with biological compounds (cholesterol, bovine serum albumin (BSA), and ceramide)

6.4.1 Topography images

In this experiment an attempt of examining AFM images of MIP layer chip was made to understand the mechanism of interaction of thalidomide with biological compounds that were involved with the non-covalent interactions. In this work, we used Atomic force microscopy (AFM) because it enabled a direct observation of the topographic surfaces and 3D images on a nanometer scale and could detect any spatial interactions of the protein matrix. The 3D images of the surface were taken with the Dynamic Force microscope: DFM. The mechanism of interaction of thalidomide with biological compounds that had a specific cavity on the imprinted films was explored. Futher, BSA, ceramide, cholesterol (at concentrations 1 mg mL^{-1}) and blood mixture were mixed to drop onto the surface of the (*R*)-thalidomide imprinted films-supported on the IDC electrode that the template was exposed to sensor. Figure 6.9, AFM image of RMIP1 shows the cavity size of 150 nm. The thalidomide and biological compounds adsorbed freely onto the imprinted films, which led to the formation of different morphological films resulting in the force raised. The AFM images of RMIP3 show large molecules (200 nm) assembled on the surface after dry in air, as nucleation of the growth aggregates did not occur as confirmed by the resistance measurement, showing the resistance signal because of the strong interaction between the thalidomide and the imprinted site by self-assembly process. With the RMIP2, the molecules of the matrix did not completely cover the electrode. This procedure led to

the binding of both the thalidomide enantiomers into the matrix molecules. The AFM images showed the formation of a thin film, with a number of molecular interaction embedded into its structure, and some regions that remained uncovered with molecules but showed the imprinted cavities. Both the particle sizes and the large or small particles attached were directly dependent on the interaction of the imprinted films and protein-lipid compounds. Biological compounds showed molecules as self-assembly or the interference of the lipid component on IDC. The self-organization caused the different binding site characteristic for RMIP3 films from those for the RMIP2, and RMIP4. In addition, a large number of the attached spheres, or particles were observed, that were related to the remaining thalidomide molecules that formed after washing. Increasing the molecules adsorbed onto the film was observed, and they provided a lower resistance signal when compared with RMIP1, due to the availability of specific imprinted cavities of thalidomide. It was able to detect the analyte of thalidomide enantiomer molecule and provide higher values for the resistance signals.
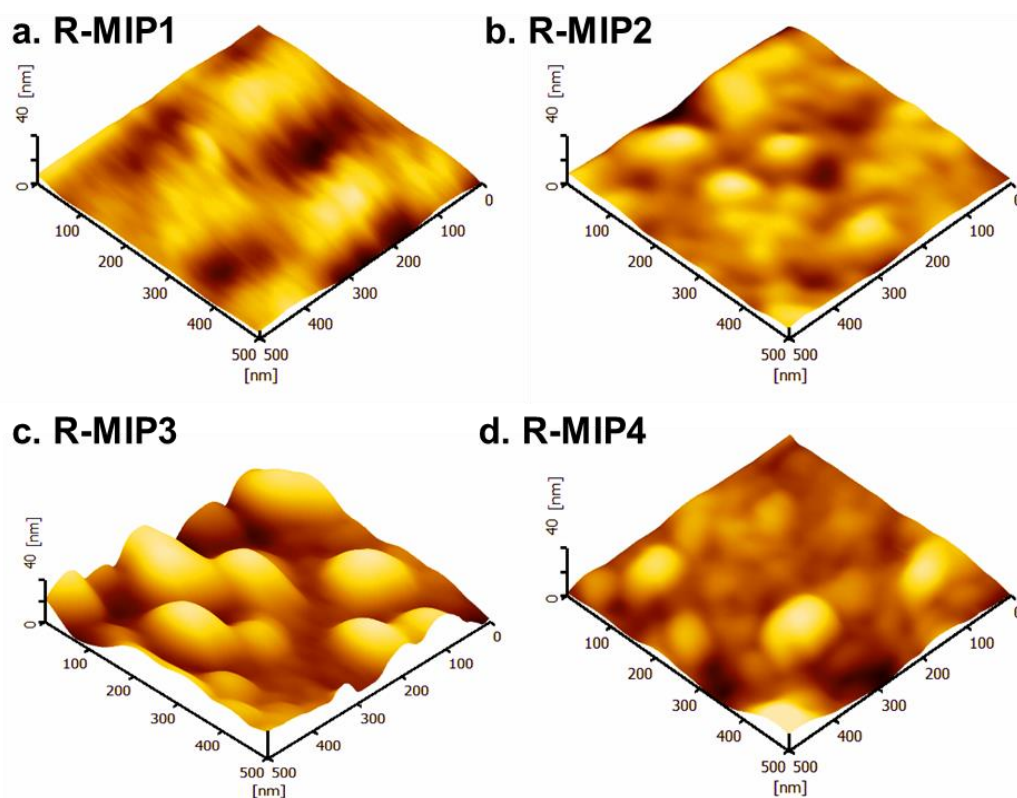
Figure: 6.9: Tapping mode 3D topographical AFM images of the (*R*)-thalidomide imprinted films of the IDC electrode: (a) RMIP1; (b) RMIP2; (c) RMIP3 and (d) RMIP4 in the presence of (*R*)-thalidomide into the nanoparticles with lipid protein and human blood mixture exposed on the surface of the coated films onto the IDC gold electrode.
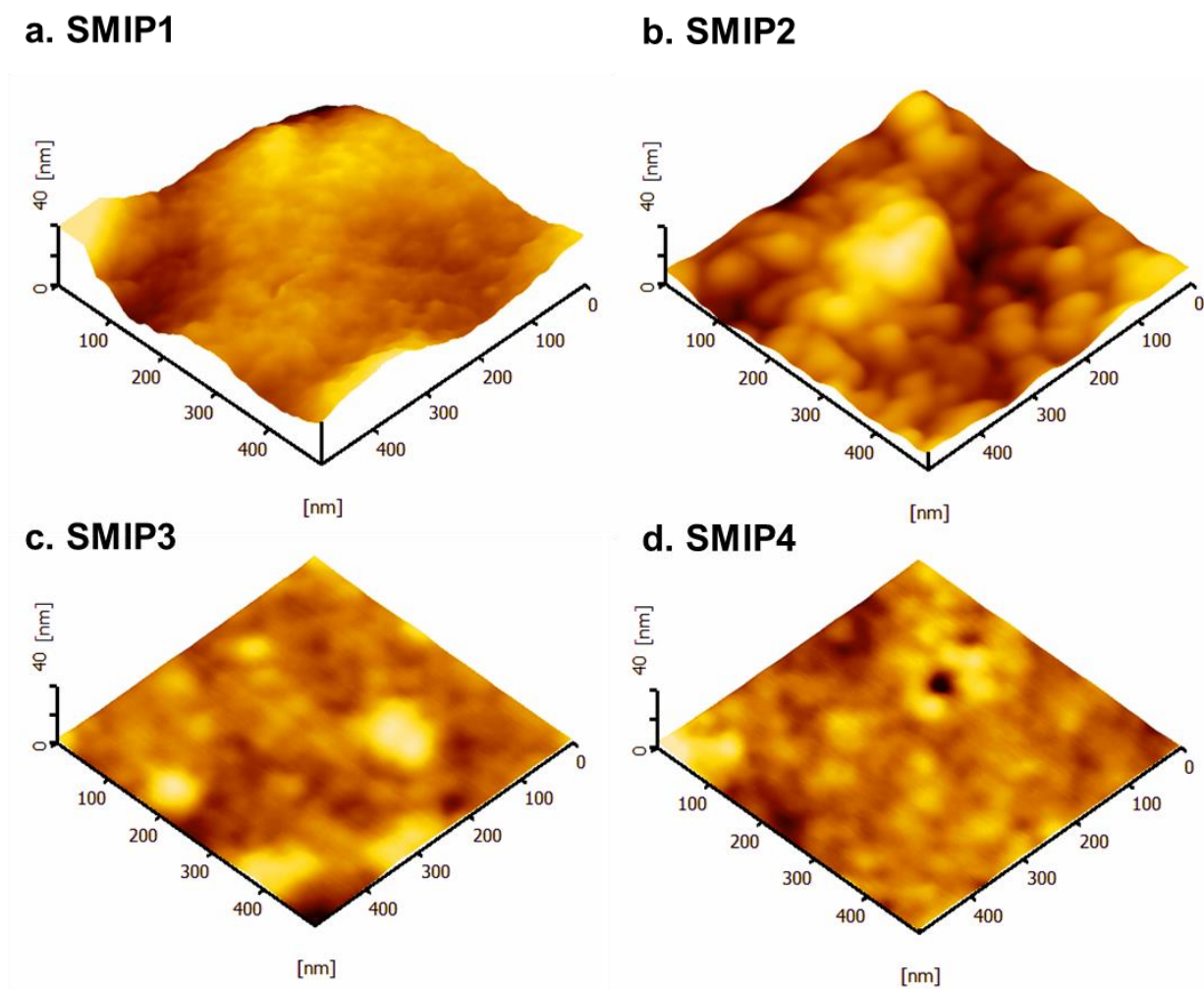
Figure: 6.10: Tapping mode 3D topographical AFM images of the (*S*)-thalidomide imprinted films of the IDC electrode: (a) SMIP1; (b) SMIP2; (c) SMIP3 and (d) SMIP4, in the presence of (*S*)-thalidomide into the nanoparticles with lipid protein and human blood mixture exposed on the surface of the coated films onto the IDC gold electrode.

6.4.2 Force measurement

For the AFM images in Figure 6.9 & 6.10, the imprinted cavities observed on the surface of polymer films were examined for the force. Figure 6.11 & 6.12 shows a contact-mode AFM, in which the corresponding force lines were based on the retractable curve for the RMIP. Typical force curve for the RMIP1 on the surface is shown with a force value of 91.96 nN on the surface before being pushed upward by the surface. The RMIP3 showed the force values of 112.99 nN because the tip was strong retracted due to the interaction of the (*R*)-thalidomide enantiomer molecules that were absorbed onto the surface of the thins films, and the tip then relaxes and subsequently is pulled down from the surface. Thus, the force curves showed different behavior of the interfacial layer on the protein-lipid domain that corresponded to the different surfaces with respect of the functionality monomeric precursor.
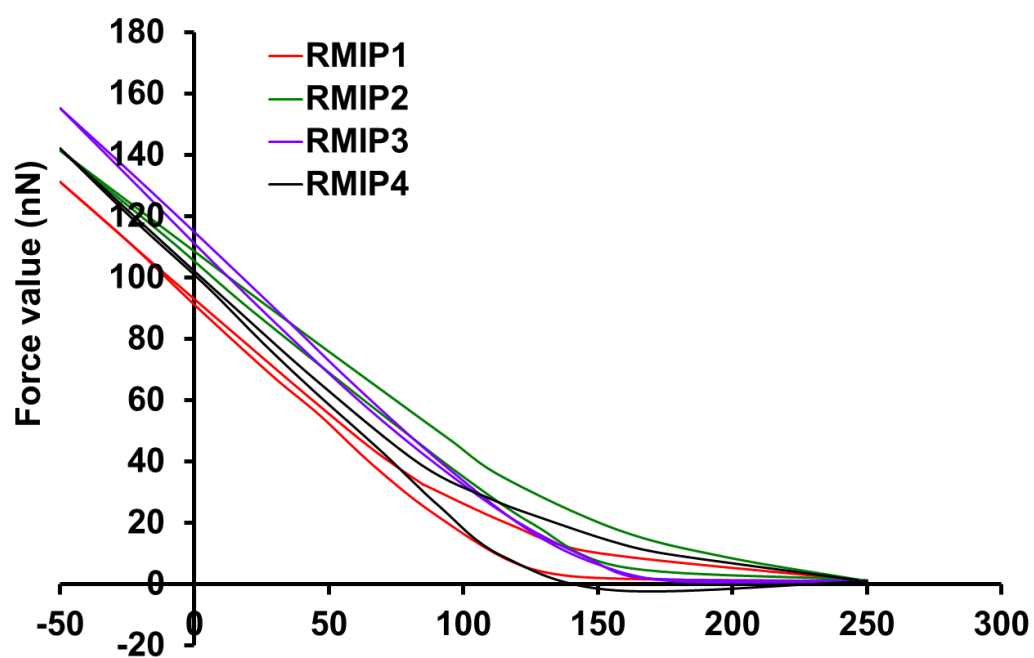
Figure: 6.11: Force analysis of the (*R*)-thalidomide imprinted nanoparticles films expose to the biological compounds.
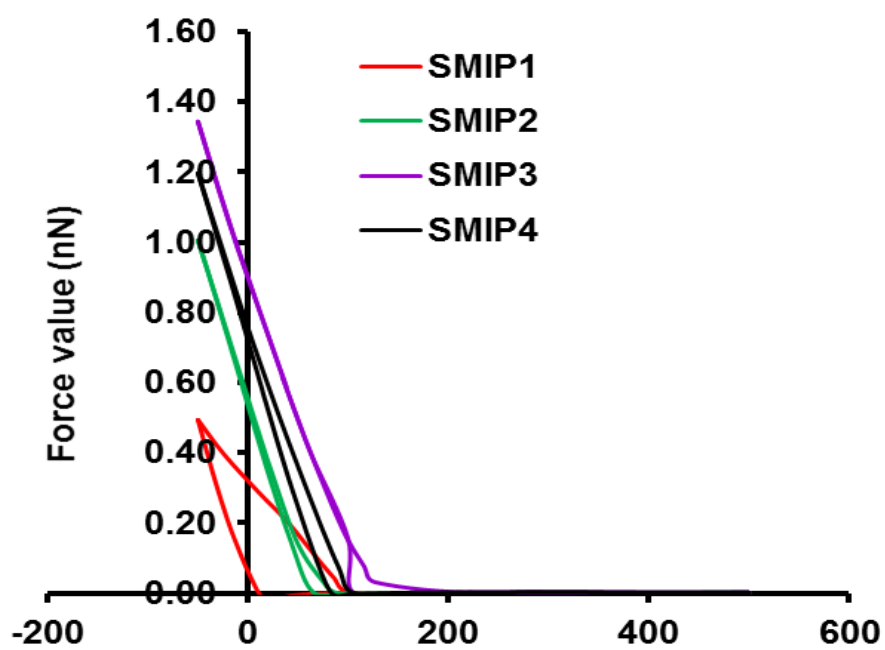
Figure: 6.12: Force analysis of the (*S*)-thalidomide imprinted nanoparticles films expose to the biological compounds.
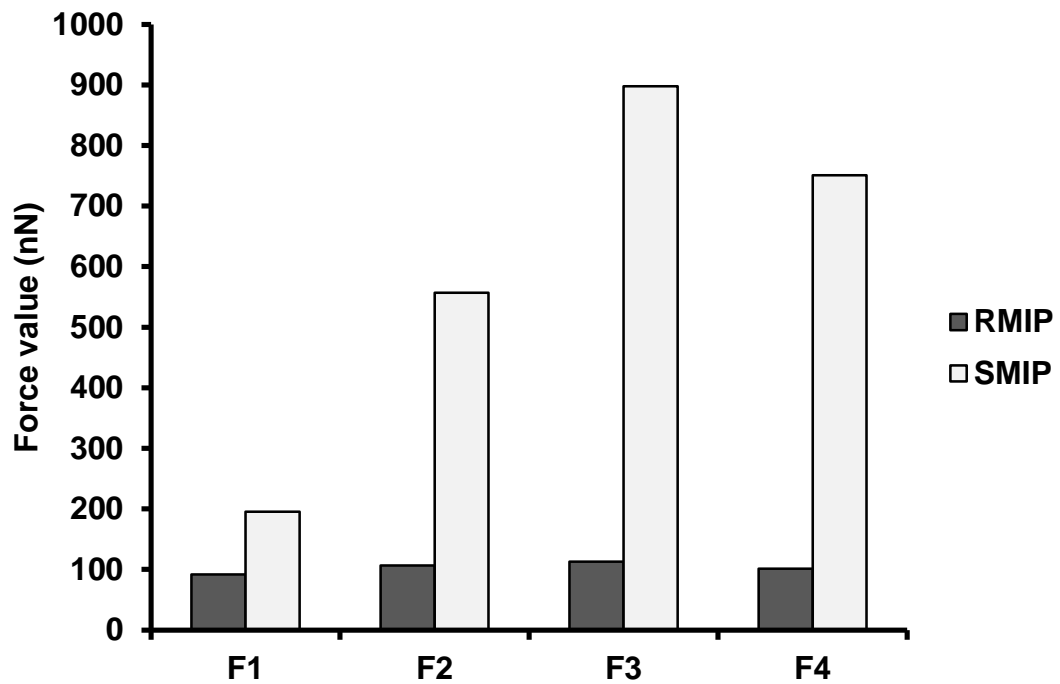
Figure: 6.13: (Shade bar graph) The force values in the nN scales. RMIP1 (F1) = 91.96 nN, RMIP2 (F2) = 106.55 nN, RMIP3 (F3) = 112.99 nN, and RMIP4 (F4) = 100.99. (Filled bar graph) The force values SMIP1 (F1) = 195. 16 nN, SMIP2 (F2) = 557.07 nN, SMIP3 (F3) = 897.86 nN, and SMIP4 (F4) = 750.67 nN).

6.5 Investigation of molecular recognition of thalidomide enantiomers in the presence of biological sample and IDC sensor detection

Many methods have been developed to quantify thalidomide, the reported methods included with MS (mass spectrometry) (Bai *et al*., 2013) capillary electrophoresis (Weinz and Blaschke 1995) and HPLC (Meyring *et al*., 2000), (Reepmeyer *et al*., 1996), (Murphy *et al*., 2007) detection. However, increasing the performance recognition of the potential importance of stereoselectivity in thalidomide pharmacology has more important and led to many investigators to separate its enantiomers. In this study, molecularly imprinted polymer was applied to recognize the thalidomide enantiomer before separation and quantitation by using chiral HPLC method. The miniature IDC sensors of thalidomide imprinted nanoparticles were fabricated for estimation of the enantiomers.

6.6 Methodology

    6.6.1 Chemicals and reagents

(*S*)-(-)-thalidomide (99%), (*R*)-(+)-thalidomide (99%) were from Aldrich Chemical Company (Milwaukee, WI, USA). Ceramide from bovine brain (98% TLC) Bovine serum albumin (BSA) and cholesterol were from Sigma Aldrich Company (Milwaukee, WI, USA).

6.6.2 Apparatus and analysis by using high performance liquid chromatography technique (HPLC)

The amount of the thalidomide enantiomers concentrations were analyzed by HPLC method using with chiral CBH column. The chromatographic system comprised a Thermo HPLC system, equipped with a variable wavelength UV detector. A 150 x 4 mm Chiral-CBH column (Chromtech, UK) was used. The detection wavelength was 225 nm and separation was performed at ambient temperature. The flow rate was set at 0.9 mL/min for every analysis. The mobile phase was 10 mM phosphate buffer (pH 5.5) containing 50 mM disodium EDTA and 2 % (v/v) acetonitrile.

6.6.3 Apparatus and analysis by using IDC-sensor electrode

Nanoparticles of either the (R)-or (S)-thalidomide imprinted polymer (RMIPs or SMIPs) and pre-polymerised layer onto interdigitated gold electrode that attached with the silicone consisted of a liquid port for delivery of a water sample from a sample-reservoir, a peristaltic pump, and a continuous flow rate of 0.1 mL min^{-1}, which is driven by a peristaltic pump (MCP-Process Series, Ismatec SA, Wertheim-Mondfeld, Germany). The sensor output signals were monitored using ohmmeter (TH 2515 DC, Tonghui, and Taipei, Taiwan) from the sensor display on the PC laptop screen. The detection of the samples was carried out at room temperature (28 ± 1 ˚C). The signal of the MIP-based sensor was measured as a function of the changes to the resistance of the polymer after exposure to (R)-thalidomide or (S)-thalidomide with

concentrations that ranged from 0.025-100 µg mL^{-1} were mixed with protein matrix of cholesterol, bovine serum albumin (BSA), and ceramide at concentration 1 µg mL^{-1}. A control experiment was carried out with the corresponding NIP. The signal response towards the concentration of the analyte was reported as a resistance (R), where R was the average resistance response after the addition of known amounts of the thalidomide enantiomer. Every experiment was carried out in triplicate for obtaining mean values and standard deviation (SD).

6.7 Method validation by using HPLC technique

6.7.1 Linearity and range

The standard calibration curves were constructed separately for the (R)-, (S)-thalidomide using single enantiomers. The stock solution of thalidomide was prepared by dissolving the drug in the acetonitrile:water 1:1 ratio to make the concentration of 1 mg mL^{-1}. The standard solutions of thalidomide were ranged in 0.5-8 µg mL^{-1}. The calibration curve was plotted from the relationship between peak area and concentration of the standards thalidomide.

6.7.2 Limit of detection (LOD) and limit of quantification (LOQ)

Limit of detection was determined from the least concentration giving an S/N level >3, being a peak different from baseline noise. The lower limit of quantitation

(LOQ) was determined from the lowest concentration calculated with precision and accuracy values.

$$LOD = \frac{3\sigma}{S} \qquad\text{--------------------- (6.1)}$$

$$LOQ = \frac{10\sigma}{S} \qquad\text{--------------------- (6.2)}$$

Where; σ is the standard deviation of the response.

S is the slope of the calibration curve.

6.8 Method validation by using IDC sensor

6.8.1 Linearity and range

The standard solutions of thalidomide were ranged in 0.025-100 μg mL^{-1}. The solutions of each concentration of thalidomide were flow through the flow-cell and a calibration curve was plotted from the relationship between resistance signal and concentration of the standards thalidomide.

6.8.2 Limit of detection (LOD) and limit of quantification (LOQ)

Calibration curves were constructed from the resistance signal of the standard solutions (25 ng mL^{-1}), from which the limit of quantification (LOQ) and limit of detection (LOD) were calculated using equation (1) and (2).

$$LOD = y_B + 3s_B \qquad \text{----------------------- (6.3)}$$

$$LOQ = y_B + 10s_B \qquad \text{------------------------(6.4)}$$

Where $\quad s_B$ is the standard error of the y estimate

y_B the intercept from the regression equation

6.8.3 Precision

The precision was evaluated through repeatability and expressed by relative standard deviation (RSD). Three different concentrations (2, 4, and 6 µg ml^{-1}) of each drug were prepared in the acetonitrile: water 1:1. Each concentration was prepared in sets of three and each one was flow through the flow cell in triplicate.

6.9 Result and discussions

6.9.1 Calibration curve of (*R*)-, (*S*) and (*rac*)-thalidomide by using HPLC technique
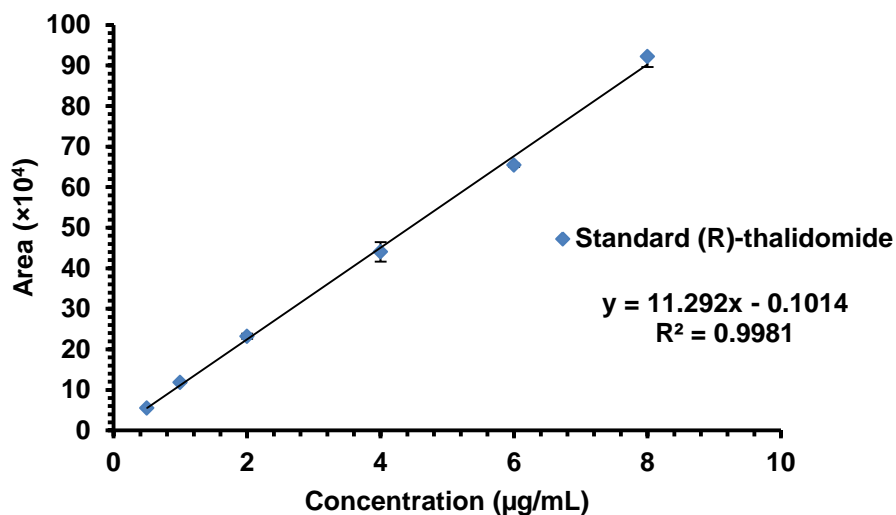
Figure 6.14: The linearity of standard (*R*)-thalidomide at the concentration range 0.5-8 µg mL^{-1} was examined on HPLC CBH chiral column.
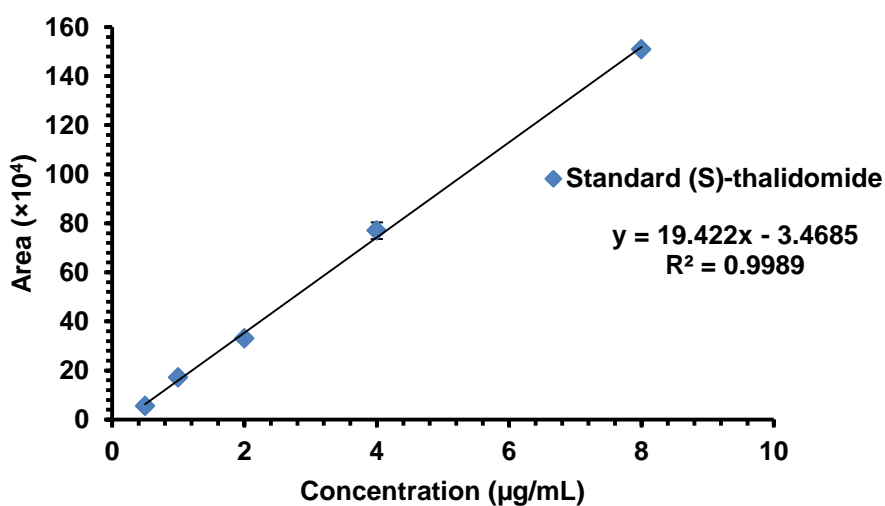
Figure 6.15: The linearity of standard (*S*)-thalidomide at the concentration range 0.5-8 µg mL^{-1} was examined on HPLC CBH chiral column.
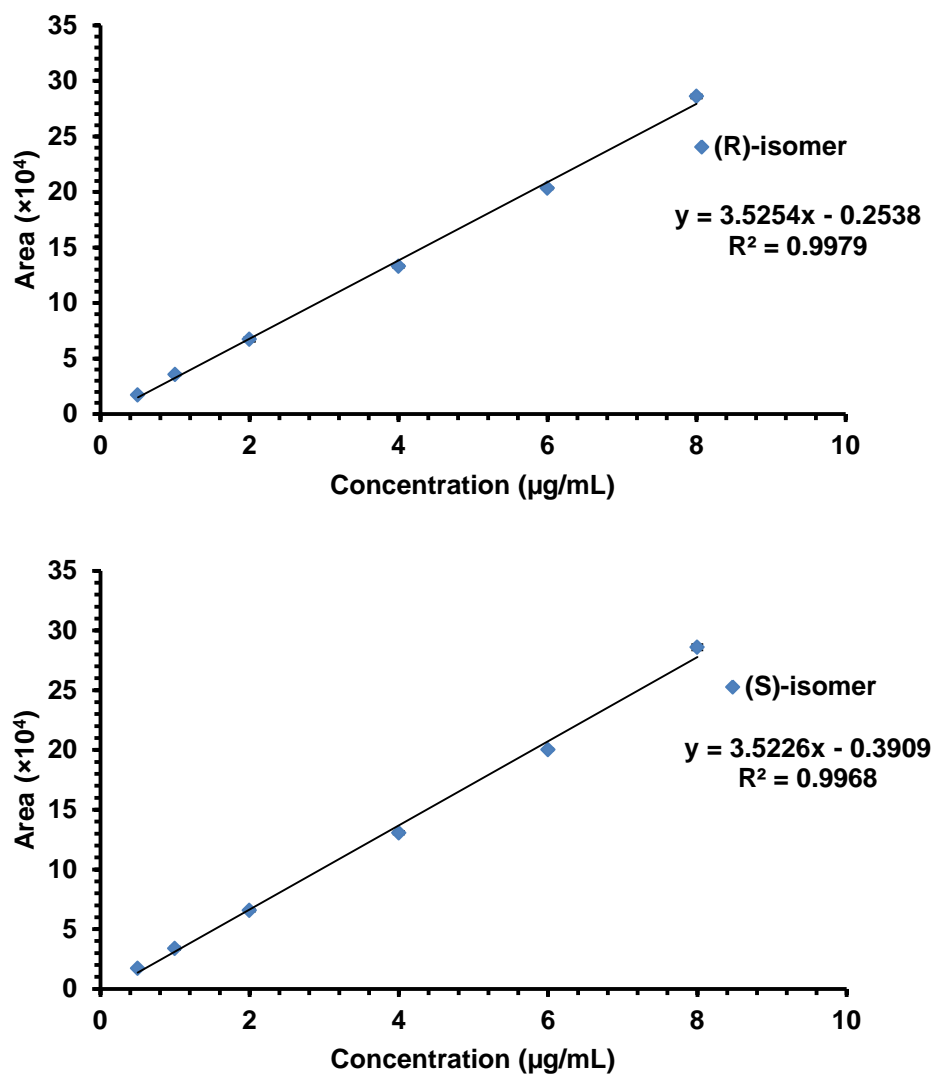
Figure 6.16: The linearity of standard *rac*-thalidomide at the concentration range 0.5-8 µg mL^{-1} was examined on HPLC using CBH chiral column.

Table 6.1: The linearity and sensitivity of the thalidomide enantiomers were analyzed by HPLC method.

Thalidomide enantiomer	Linearity	LOD* (ng mL^{-1})	LOQ** (ng mL^{-1})	%RSD
R-thalidomide	0.998	5.31	17.71	5.30
S-thalidomide	0.998	1.54	5.15	1.80

* LOD is the lower limit of detection

**LOQ is the lower limit of quantification

6.9.2 Method validation by using IDC sensor technique

6.9.2.1 Calibration curve of (R)-, (S)-thalidomide

Method validation is validated to verify that an analytical methodology when employing the MIP-base IDC sensor for thalidomide enantiomers analyses and further application is accurate, specific range that an analyte will be analyzed. Standard solution of (*R*) and (*S*)-thalidomide concentrations in the range of 0.025 to 100 μg mL^{-1} were analyzed through the flow cell with and without the biological matrix. The analyte resistances were calculated from analyte flow through the flow cell and provide the resistance signal. In this method, using the thalidomide imprinted nanoparticles onto stamp thin films onto IDC sensor is employed for determination of the analytes in the presence and absence of biological compound with enantiomer drugs. MIP-IDC sensor-based assay was performed for measuring the analyte, and

studied its analytical performance. MIP-IDC miniature sensor array allows for a rapid and simple continuous thalidomide enantiomer assessment. Figure 6.14 shows the linearity of standard (*R*)-thalidomide at the concentration range 1-10 µg mL^{-1} were examined on imprinted nanoparticles supported thin films of RMIP1 formulation. The linearity was obtained with correlation (*R^2*) of 0.987 for the concentrations range of 1-10 µg mL^{-1}. In case of the linearity of standard (*S*)-thalidomide were examined that shown in Figure 6.15. The signals were corresponding to the concentration of thalidomide at range 0.05-8 µg mL^{-1} and provided correlation coefficient 0.985. The assay data covered a linear range of 0.025 to 100 µg mL^{-1} according to Table 6.2. The analytical detection limit, calculated using a signal-to-noise ratio of 3, were 0.6 ng ml^{-1} in the absence of matrix.
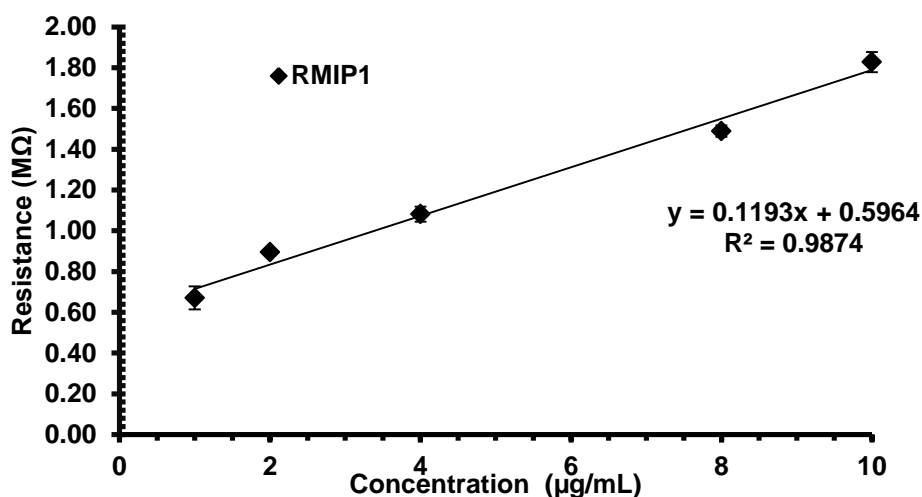
Figure 6.17: The linearity of standard (*R*)-thalidomide at the concentration range 1-10 µg mL^{-1} was examined on imprinted nanoparticles supported onto the thin films of RMIP1.
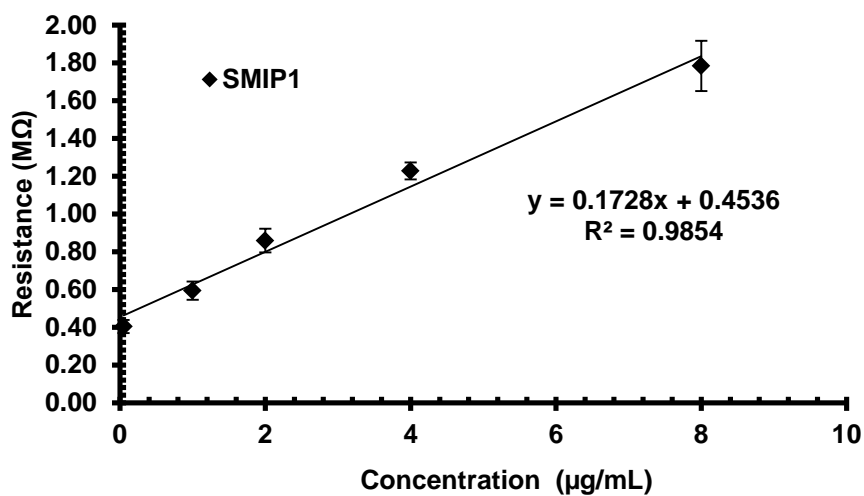
Figure 6.18: The linearity of standard (*S*)-thalidomide at the concentration range 0.05-8 μg mL^{-1} were examined on imprinted nanoparticles supported thin films of SMIP1 formulation.

Table 6.2: The linearity and sensitivity of the thalidomide enantiomers were analyzed by IDC sensor method.

substance	Thalidomide enantiomer	Linearity	LOD* (ng mL^{-1})	LOQ** (ng mL^{-1})	%RSD
without matrix	*R*-thalidomide	0.987	0.761	1.146	9.04
	S-thalidomide	0.985	0.619	1.003	0.86
with matrix	*R*-thalidomide	0.990	6.399	21.273	0.80
	S-thalidomide	0.996	0.538	0.634	0.63

* LOD is the lower limit of detection

**LOQ is the lower limit of quantification

6.9.2.2 Calibration curve of (R)-, (S)-thalidomide with protein matrix

The sensitivity of thalidomide imprinted polymer was applied to detect the analyte inside the biological compound. The principal intention of the MIP-IDC sensor is to minimize the matrix effects. Evaluation of the matrix effect on IDC measurement was carried out to verify the performance of the IDC-based assay of both (*R*)-thalidomide and (*S*)-thalidomide. For this purpose we used biological of ceramide, BSA, and cholesterol sample with a standard solution of thalidomide at concentration levels of 0.025-100 μg mL^{-1}. Figure 6.19 shows the linearity of standard (*R*)-thalidomide mixed with protein matrix (BSA:ceramide:cholesterol 1:1:1) at the concentration 1 mg mL^{-1} were examined on imprinted nanoparticles supported thin films of RMIP1 formulation. RMIP1 exposed to protein matrix provided correlation coefficient (R^2) 0.990. Figure 6.20 show the linearity of standard (*S*)-thalidomide mixed with protein matrix (BSA:ceramide:cholesterol 1:1:1 at the concentration 1 mg mL^{-1}) were examined on imprinted nanoparticles supported thin films of SMIP1 formulation. SMIP1 exposed to protein matrix provided the correlation coefficient (R^2) 0.996. The method showed high sensitivity and low detection limit at 6.4 ng mL^{-1} with the biological complex. Consequently, the measurements of thalidomide in the presence of interferences were performed by the developed MIP-IDC assay method.
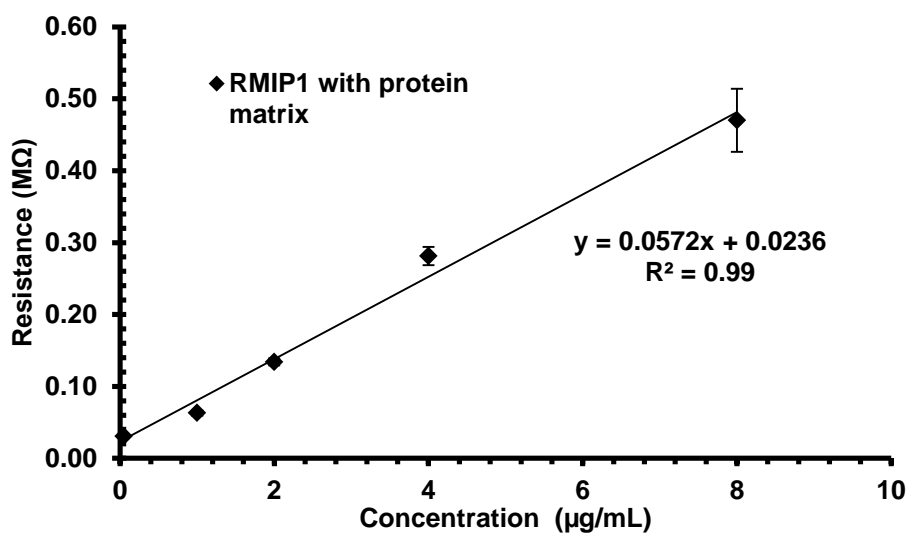
Figure 6.19: The linearity of standard (*R*)-thalidomide mixed with protein matrix (BSA:ceramide:cholesterol 1:1:1 at the concentration 1 mg mL^{-1}) at the concentration range 0.05-8 µg mL^{-1} were examined on imprinted nanoparticles supported thin films of RMIP1 formulation.
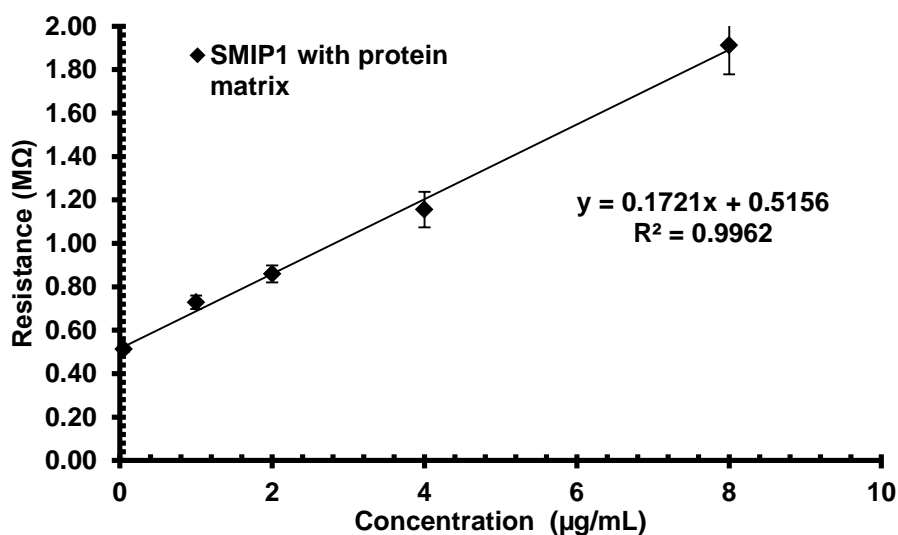
Figure 6.20: The linearity of standard (*S*)-thalidomide mixed with protein matrix (BSA:ceramide:cholesterol 1:1:1 at the concentration 1 mg mL^{-1}) at the concentration range 0.05-8 µg mL^{-1} were examined on imprinted nanoparticles supported thin films of SMIP1 formulation.

6.10 CONCLUSIONS

To determine real analysis and dynamic concentration range, we have developed very simple, rapid lab on chip capable of detection the thalidomide enantiomers in the presence of biological compounds by employing resistance measurement of molecularly imprinted nanoparticle thin-films onto the IDC electrode. The interdigitated capacitive electrode (IDC) allows the detection *via* the interactions of the imprinted polymer and the enantiomer of thalidomide through the microfluidic network caused the rapid resistance changes at the low concentration. The MIPs nanoparticles coated thin-films were used to examine the binding interaction of both templates to the imprinted sited in the presence and absence of biological compounds with blood sample. The characteristic properties of the coated thin-films displayed the thalidomide adsorbs onto the surface, leading to the formation of different morphological films, as determined by AFM images and provide a high value for the resistance signal. In addition, the pattern of nanosized scale were observed, that were related to the thalidomide molecules and biological compounds remained onto the film. However, it was able to measure the thalidomide enantiomer molecule inside the interference compounds consisted of lipid and proteins and provide the resistance signals shift. Thus, the force curves showed changes of the interfacial layer on the protein-lipid domain that resembled to the different properties of the coated thin-film.

The fabricated sensor was successfully applied to evaluate the thalidomide enantiomers. The assay data covered a linear range of 0.025 to 100 µg mL^{-1}. The analytical detection limit was 0.6 ng ml^{-1} in the absence of matrix. The method showed high sensitivity and low detection limit at 6.4 ng mL^{-1} with the biological

complex. The results showed that MIP had the high sensitivity and selectivity on IDC for sensor measurement.

CHAPTER 7

SURFACE ENHANCED RAMAN SPECTROSCOPY STUDIES FOR EVALUATION OF INTERACTION ON MIP-FILMS IDC ELECTRODE

7.1 Background

Raman spectroscopy is very useful in drug analysis due to advantages such as its ease of use, and minimal sample handling (Ellis *et al*., 1989). Raman spectroscopy can also be used to identify the structure drug isomer and its interaction with the other materials, which is highly useful for advanced material and study in biological function. In the present work, we examined the effect of biological compounds using Raman spectroscopy for the detection of effluent matrixes onto the imprinted nanoparticles supported by the thin films. In this experiment, surface enhanced Raman scattering was used to magnify the Raman intensity at the silver electrode surface (Fleischmann *et al*., 1974). Experimental Raman spectroscopy is a simple and rapid analytical technique for determining the vibrations of the thalidomide enantiomer (Cipriani *et al*., 2008).

7.2 Objectives

The intentions of this study are to evaluate the rotational, vibrational, and discriminate the chiral inversion of thalidomide enantiomers in the presence of bovine serum albumin that interacted with cholesterol and ceramide by using the SERS.

7.3 SERS on MIPs Films

The Raman spectra of the (*R*)-imprinted thin films and the (*S*)-imprinted thin films before and after the expose to the protein-lipid component with and without human blood mature illustrated in Figure 7.1 and Figure 7.2. As shown in Figure 7.1 it was evident that there was a Raman shift between the standard solution of the thalidomide wavenumbers and those imprinted thin films of each formulation. Vibrations of the substituted benzene ring appeared in the 1051.97 cm^{-1} region of the (*R*)-thalidomide standard solution. The vibration of the substituted benzene ring of the sample at the frequencies were 846.30, 837.19, and 817.09 cm^{-1} on the surface of the RMIP1, RMIP3, and RMIP4 spectra, respectively, that can be attributed to the structure of (*R*)-thalidomide but the RMIP2 formulations showed no stretching modes of benzene. There is also an additional peak at 1450.93 cm^{-1} in the (*R*)-thalidomide that represented CH bending. The spectrum of the RMIP1, RMIP2, RMIP3, and RMIP4 appeared at 1567.85, 1598.99, 1566.20, and 1529.95 cm^{-1} respectively. There is one band of the RMIP2 spectrum in the 1300–1400 cm^{-1} range at 1310 cm^{-1} that was assigned to the carbonyl and C-N-C stretching related to the ring. In the case of the SMIP formulations a comparison with the (*S*)-thalidomide is shown in Figure 7.2,

The vibration of the substituted benzene ring appeared in the 1003.08 cm^{-1} region of the (*S*)-thalidomide standard solution. The broad spectrum at 839.01, 842.66, 840.84 and 844.48 cm^{-1} of SMIP1, SMIP2, SMIP3 and SMIP4 spectra, respectively belong to the ring deformation and cyclic C-C-C stretching. The broad peak of the spectrum was due to the conformational changes of the thalidomide that were absorbed by the imprinted nanoparticle onto the supporting thin films. The 1508.44 cm^{-1} peak as usually indicative of CH$_2$ deformation or C-H stretching that appeared in the spectrum of the (*S*)-thalidomide. There was low frequency at 1500-1600 cm^{-1} in all the SMIP formulations spectrum that was due to too weak interactions. It did not appear as a sharp peak. Raman spectroscopy has been used to characterize the vibrational modes of thalidomide, which provided the information of the interaction of the thalidomide with recognition site of the supporting thin films on IDC. The resulting different spectra provided information on the thalidomide configuration achieved by the imprinted thin films.
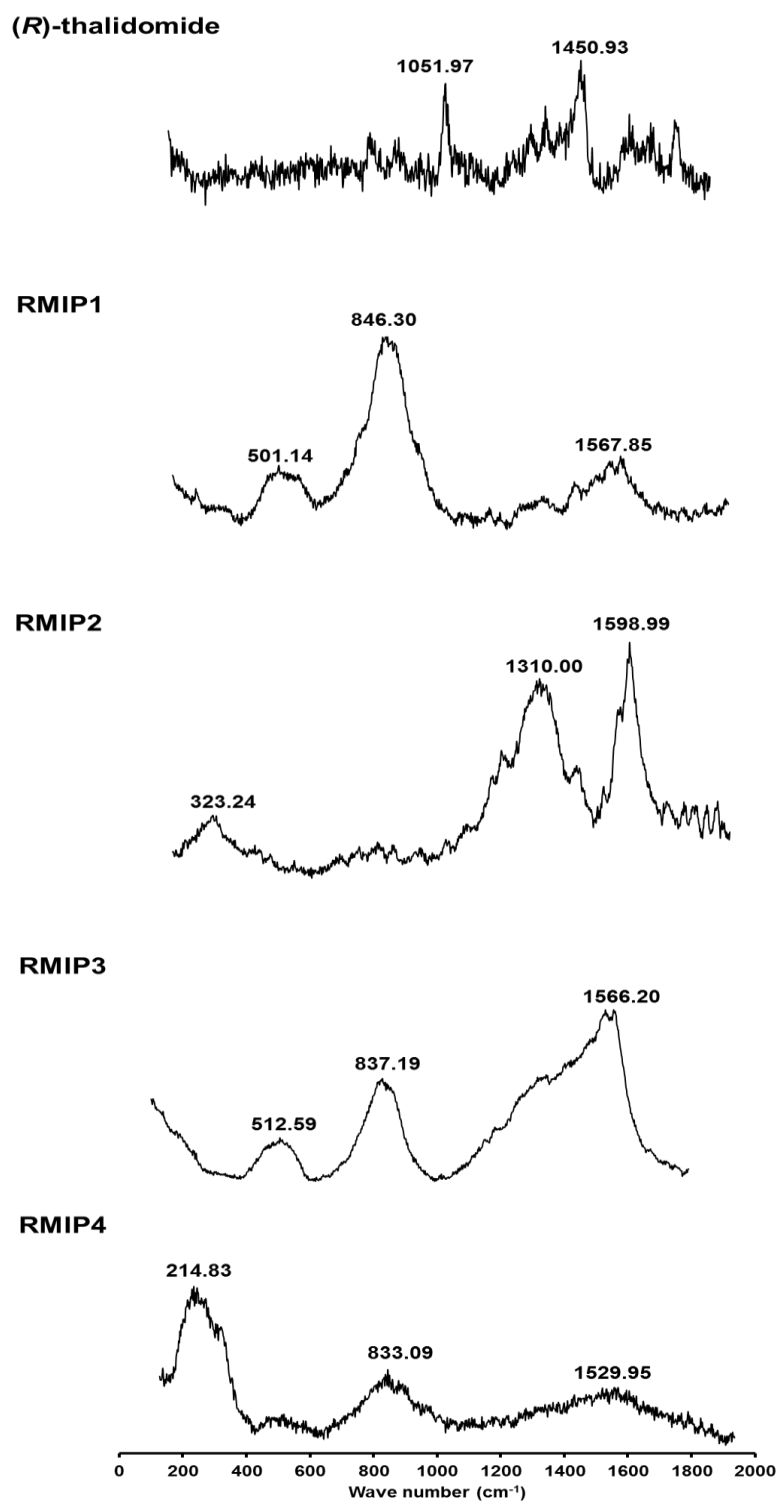
Figure: 7.1: Raman spectra of various (*R*)-thalidomide MIP nanoparticles embedded thin-film and Raman spectra of (*R*)-thalidomide for comparison.
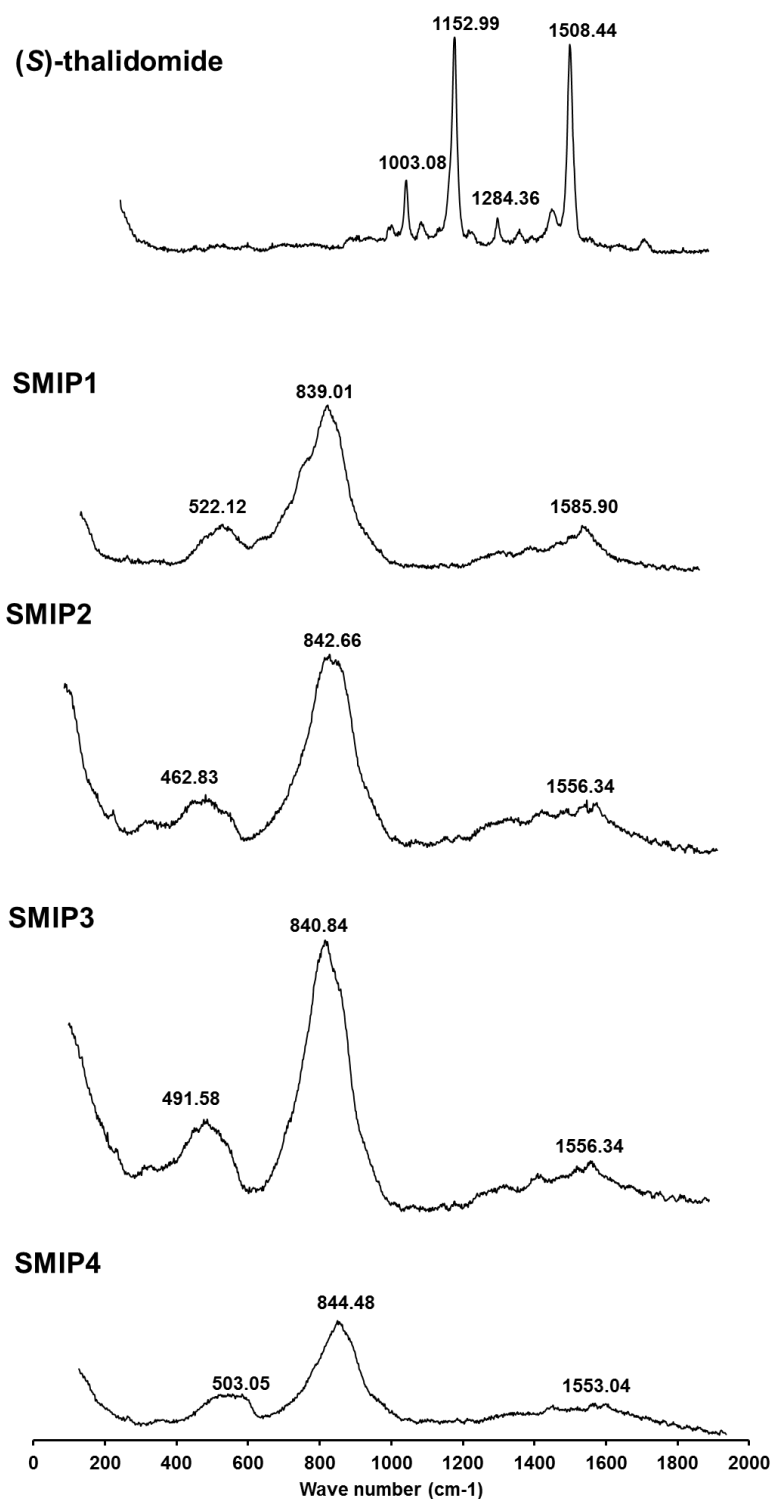
Figure: 7.2: Raman spectra of various (*S*)-thalidomide MIP nanoparticles embedded thin-film and Raman spectra of (*S*)-thalidomide for comparison.

7.4 The interaction of MIPs films exposed to the biological matrix

7.4.1 Raman spectra of biological matrix

SERS experiment identified and characterized for the Raman vibrations of a thalidomide imprinted polymer layer onto a thin film that included the biological matrixes consisting of BSA, cholesterol, ceramide, and human blood mixture. In the standard solution of (*R*)-thalidomide, (*S*)-thalidomide including with and without blood and the addition of BSA, ceramide and cholesterol were dropped onto the imprinted nanoparticle-films at the IDC electrode. The Raman intensity is illustrated in Figure 7.3, from the comparison; it was evident that there was very close wavenumbers between the thalidomide enantiomer and cholesterol. The aromatic ring and cyclic molecules of thalidomide that showed the stretching modes at the 1182.58, 1058 cm^{-1} region of the thalidomide structure and the blood this attributed to the aromatic stretch of a substituted benzene ring. In the Raman spectrum of thalidomide with blood mixture, there was a broad band in the 1300-1350 cm^{-1} region. There was the Raman peak at 1308.09 cm^{-1} for the (*R*)-thalidomide and 1330.44 cm^{-1} for the (*S*)-thalidomide with the blood component. The peak at 1308.09 and 1330.44 cm^{-1} may be assigned to carbonyl and C-N-H stretching. The peaks at 1594.08 and 1592.45 cm^{-1} were assigned to CH_2 deformation or amide stretching on the thalidomide molecule in the presence of the human blood. In this experiment, we compared each of the protein matrix structure in Figure 7.3. There are peak at 1300-1400 cm^{-1} that attributed to the BSA and ceramide and those appeared at 1303.17 cm^{-1} and 1367.76 cm^{-1} which was assigned to carbonyl and C-N-C stretching. The 1453.51 cm^{-1} and 1441.80 cm^{-1} peaks

were indicative of CH$_2$ deformation and amide stretching that can be observed in the ceramide and cholesterol spectrum. There were 1600–1700 cm^{-1} regions at 1594.44, 1644.63, and 1668.96 cm^{-1}, that were assigned to carbonyl group. We can apply to use Raman spectroscopy to confirm the interaction between thalidomide enantiomer and MIPs exposed to a blood and protein-lipid mixture, that led to the perturbation in the blood caused potential corrosion of molecule, resulting in the resistance polarization corresponding to the change of force values on the surface.
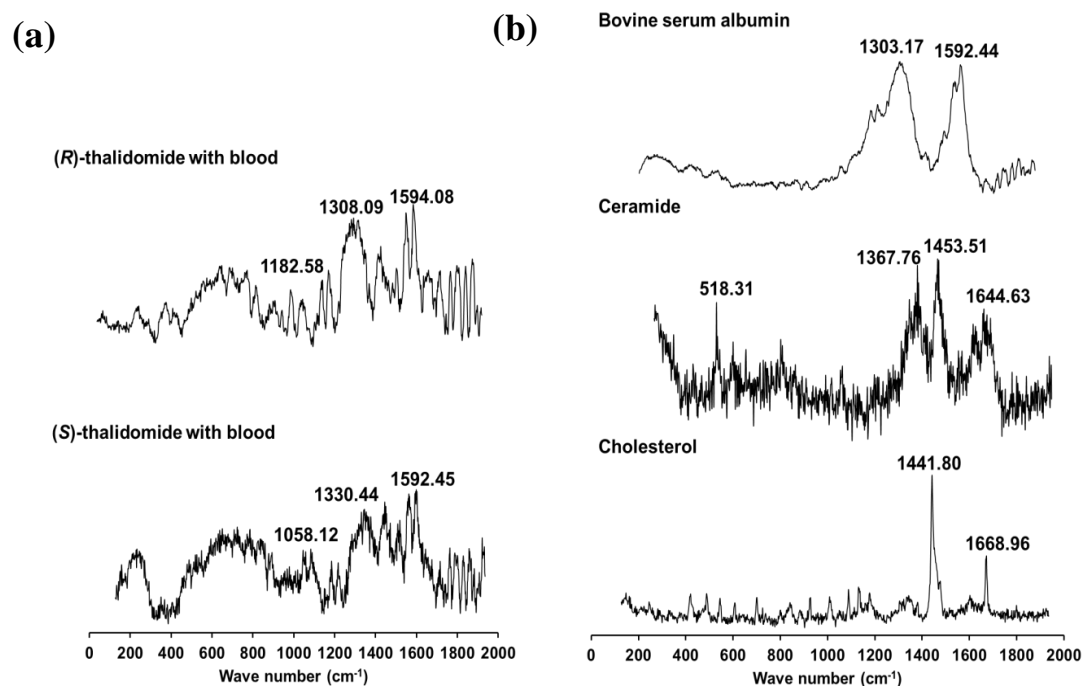
Figure: 7.3: (a) Raman spectra of (*R*)-thalidomide and (*S*)-thalidomide incubated with human blood mixture (left) and (b) Raman spectra of the individual biological compound: bovine serum albumin (BSA); ceramide (CER); and cholesterol.

7.4.2 The molecular sizes of the (*R*)- and (*S*)-thalidomide on the imprinted polymer at blood interface detected by SERS

To study the structure of the enantiomers in the presence of the protein matrix that can be induced by the imprinted cavity on the supported thin films, Raman AFM was used for this purpose. For typical Raman spectrum of investigation, the coated thin films were scanned at three areas and this provided the Raman spectrum for each MIP and the corresponding NIPs (see Figure 7.4 (a). In Figure 7.4 (b), the pointed area was used to examine the imprinted size of the thalidomide molecules accommodated into the bovine serum albumin with the cholesterol and ceraminde upon the attachment of the blood on the MIP coated at IDC.

Table 7.1: The molecular sizes of the (*R*)- and (*S*)-thalidomide in the presence of the bovine serum albumin, ceramide and cholesterol on the interspace of the pore obtained for MIPs exposed to the blood with respect to different functional monomer precursors.

Molecular size of thalidomide (Å)	F1	F2	F3	F4
RMIP	1.04±0.21	1.22±0.29	1.62±0.30	1.74±0.30
SMIP	1.88±0.20	0.74±0.17	1.60±0.32	1.80±0.16

The molecular sizes of thalidomide enantiomer for the RMIPs and SMIPs at the blood exposure were shown in Table 7.1 on the IDC electrode. The RMIP1 provided the smallest size of the thalidomide molecules on the coated thin films and the blood on the surface that was 1.04 ± 0.21 Å. In the case of the SMIP formulation SMIP2 demonstrated the smallest size of the thalidomide molecules in an order of 1 Å. The small sizes of the drugs adsorbed between the nanospaces onto the coated thin films consisted of imprinted nano-cavities, and hence a greater surface area with an enhanced better in-depth structure. The analyte can be better adsorbed onto the coated thin-films that resulted in a high resistance signal of the analytes at the MIP nanoparticles imprinted film on IDC. Both the thalidomide enantiomers were appeared into the nanopores of MIP nanoparticles with different sizes as shown in Table 7.1.

7.4.3 MIPs films exposed to the biological matrix

Figure 7.4a shows the Raman spectrum of the (R)-imprinted films onto the IDC electrode with biological compounds. There are low-frequency peaks that may were ascribed to vibrations of the substituted-benzene portion that appeared at 849.94, 857.22, and 839.01 cm^{-1} in the RMIP1, RMIP2 and RMIP4 on Raman spectra. The 510.68 and 504.96 cm^{-1} peaks were assigned to the ring deformation in the RMIP1 and RMIP4. The broad and high intensity spectrum containing one band in the 1500-1600 cm^{-1} regions at 1551.39, 1592.44, 1597.35, and 1594.39 cm^{-1} was identified for stretching of carbonyl group of the amide on (R)-thalidomide structure. Figure 7.5a shows the Raman spectrum of the (S)-imprinted films onto the IDC sensor in the presence of biological compounds, the Raman spectrum of (S)-thalidomide showed a sharp peak at 1003.08, 1152.99, 1284.36, and 1508.44 cm^{-1} related to the stretching of aromatic ring, CH bending, ring, C-N-C or C-C stretching and CH_2 deformation, respectively. SMIP1 and SMIP4 showed a low intensity of the Raman peak due to less or the absence the thalidomide molecules onto the pores in the interspace and the MIP binding sites. The SMIP2 showed a high intensity wave number at 877.20 cm^{-1} related to the vibrations of the substituted-benzene portion and the low intensity peak at 1561.27 cm^{-1}, similar as the SMIP3 showed a low intensity peak at 839.01 cm^{-1}. In addition SMIP2 had a high intensity peak with a broad peak at 1561.27 cm^{-1}, that occurred on the surface of the supporting thin films, there was the interaction between MIP and the thalidomide enantiomer via hydrogen bond interaction.

(a)
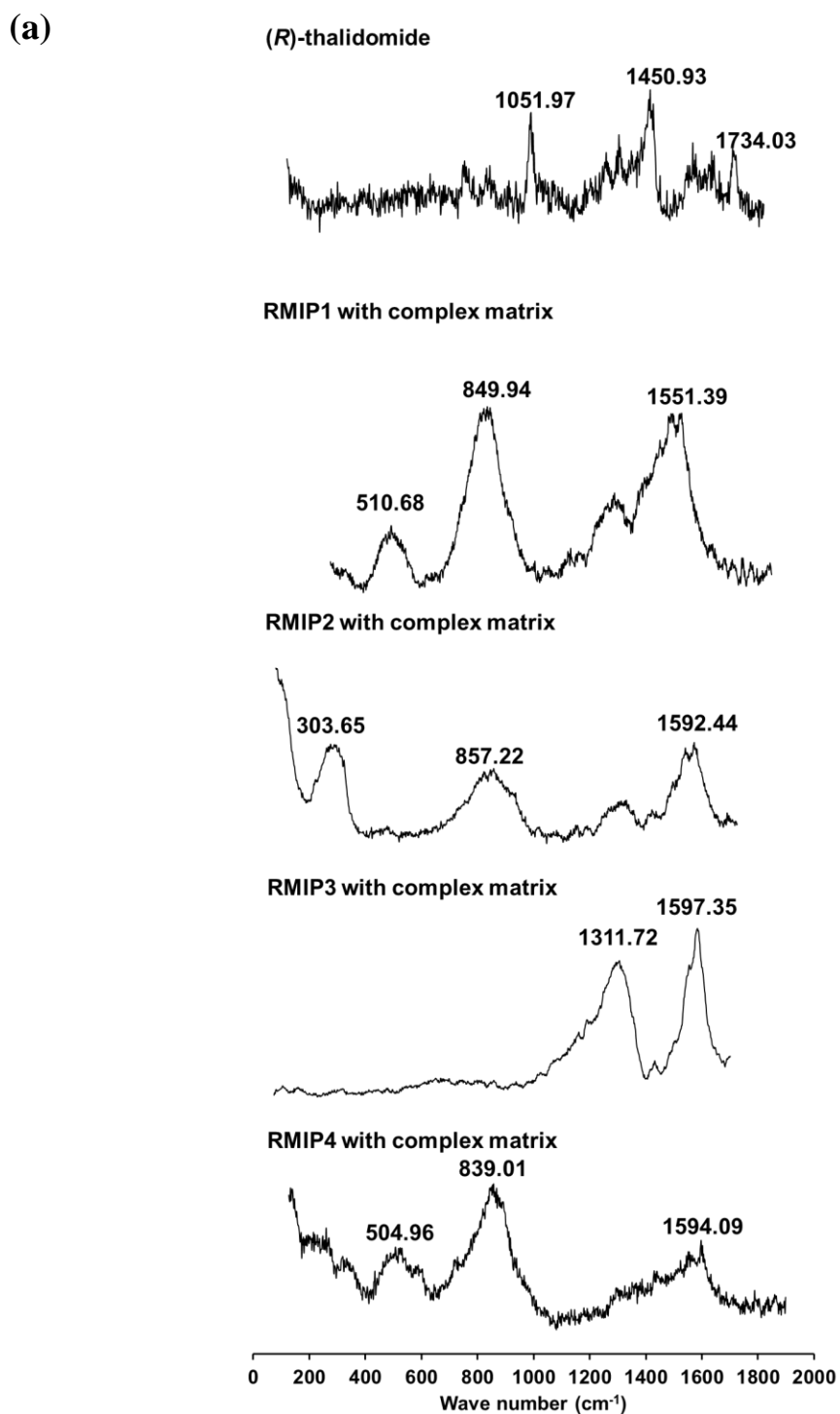
Figure: 7.4: (a) Raman spectrum of (*R*)-thalidomide attached on the imprinted films occurred upon exposure on various MIP layer chips to bovine serum albumin (BSA), ceramide (CER), cholesterol and with blood mixture.

(b)
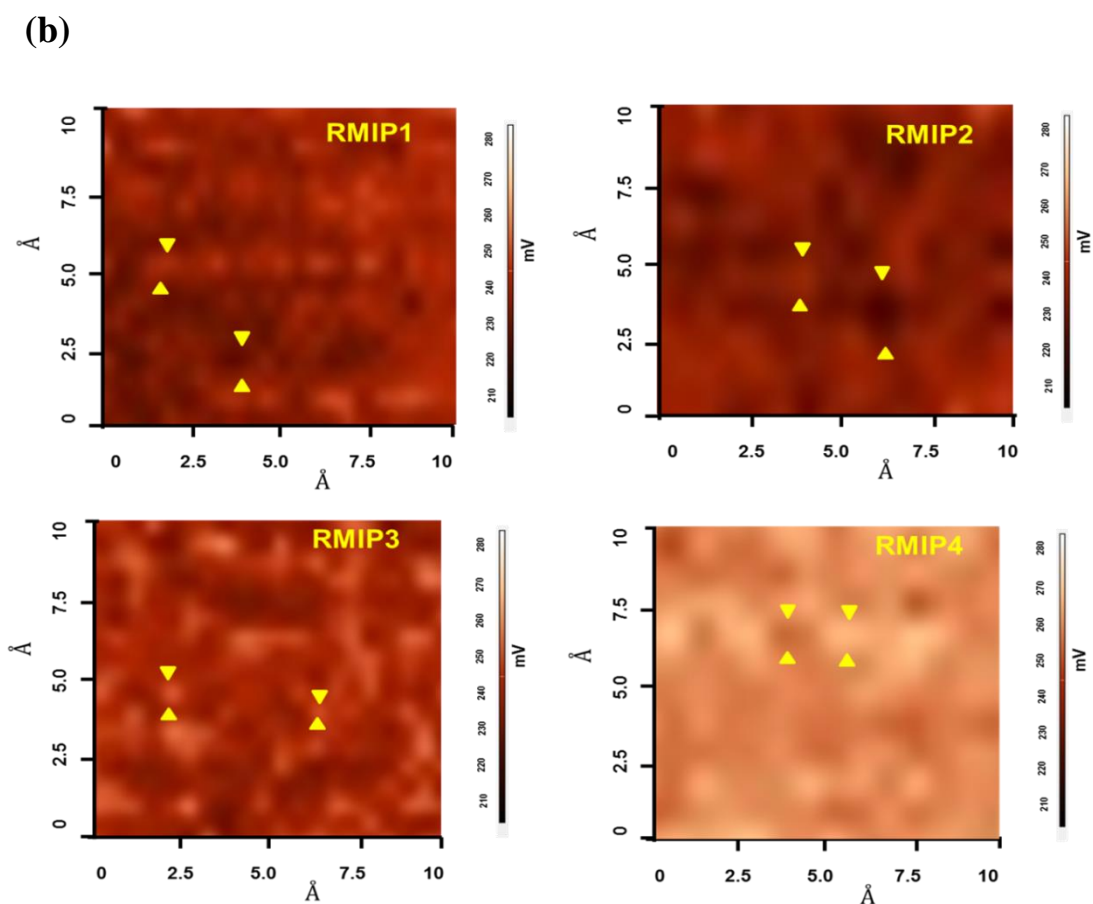
Figure: 7.4: (b) AFM images of RMIP showing the particular site of the enantiomer drug located on the layer coating with the imprinted nanoparticles stamped in the porous material interface with the lipid-lipid-protein component at the ambient temperature.
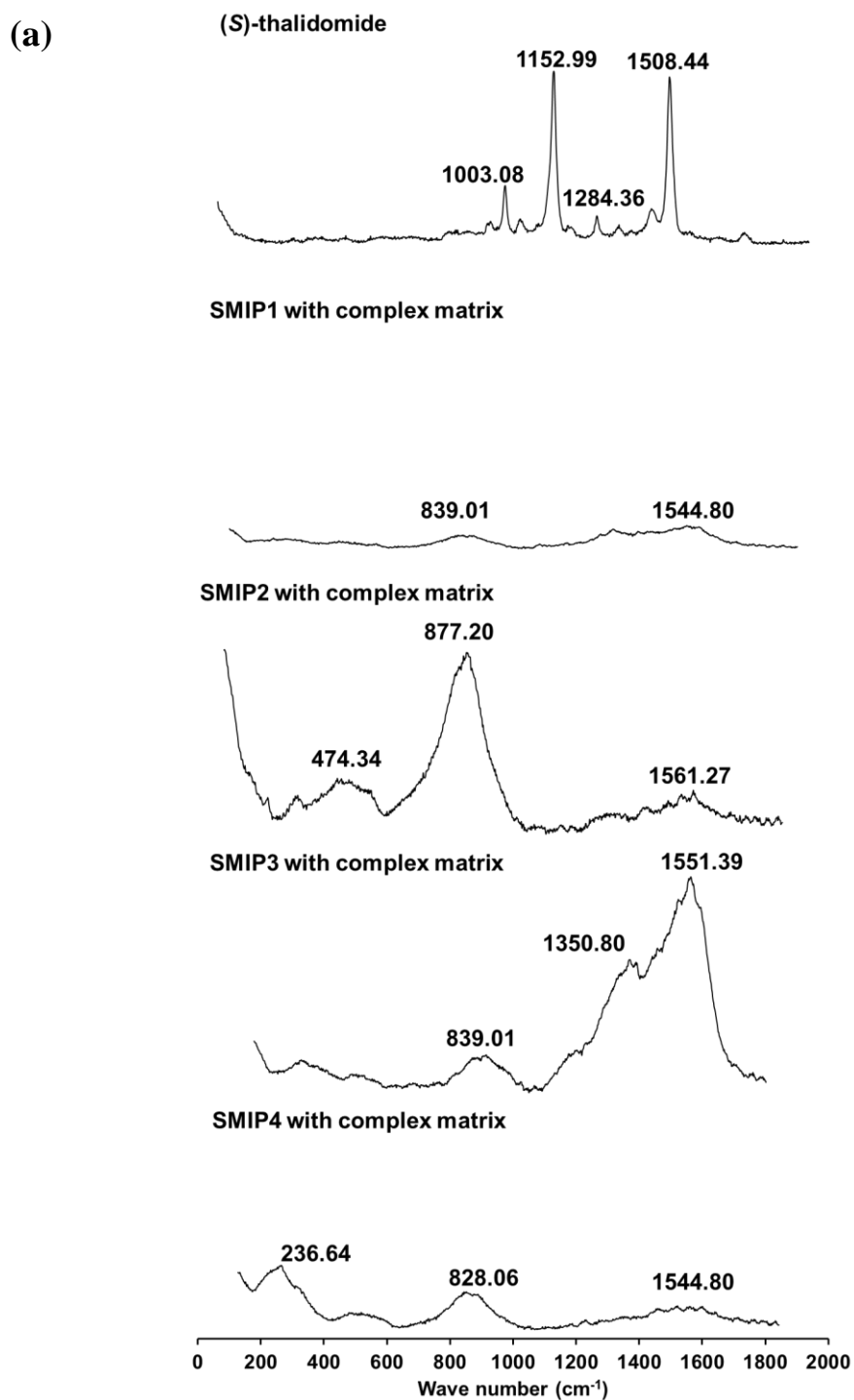
Figure: 7.5: (a) Raman spectrum of the (*S*)-thalidomide attached to the imprinted films coating upon exposed to biological compounds [bovine serum albumin (BSA), ceramide (CER), cholesterol and with blood mixture] on various MIP layer chips.

(b)
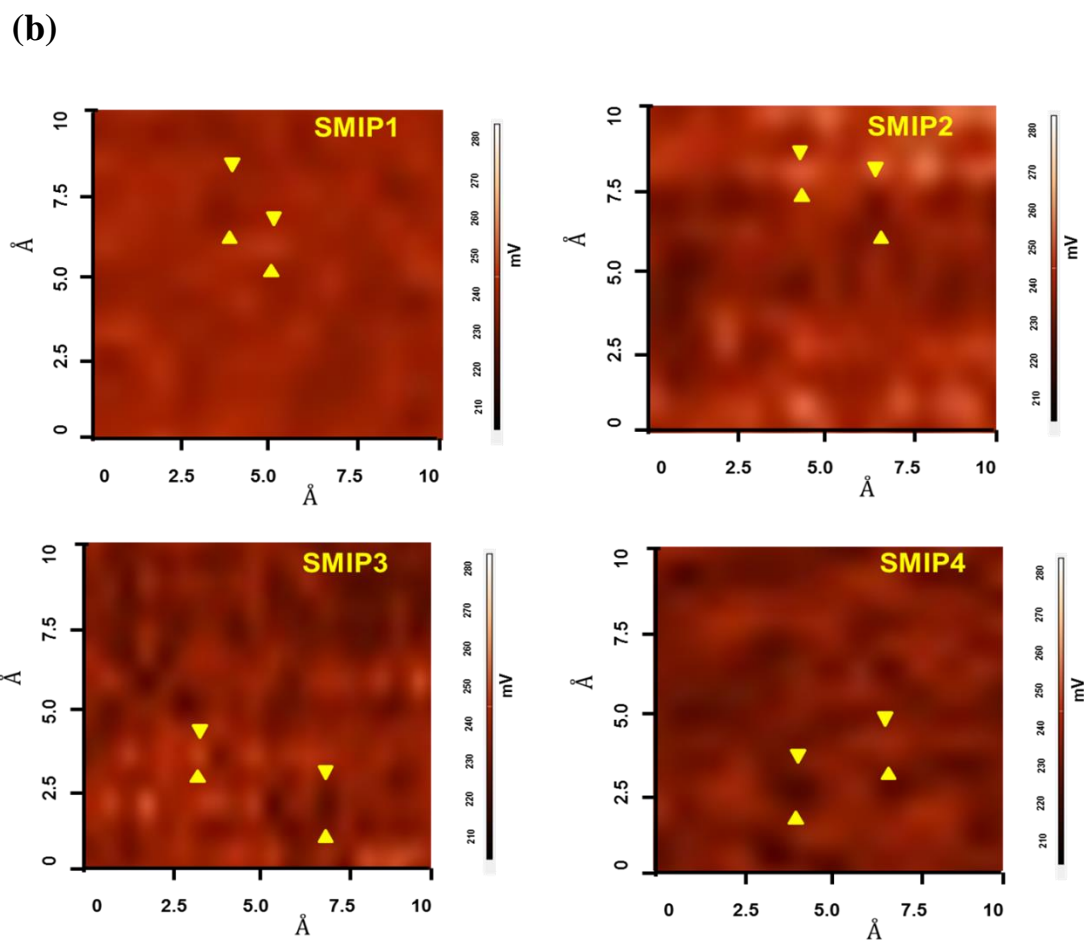
Figure: 7.5: (b) AFM images of SMIPs on the surface of IDC, showing the specific areas of the particular site of the enantiomer drug located onto the imprinted polymer in the porous material interface upon the lipid-lipid-protein interaction.

7.5 CONCLUSIONS

SERS is a technique that can significantly enhance the weak Raman scattering signal on the silver substrate which provided an enhanced Raman signal. The developed MIPs nanoparticles coated onto thin-films of IDC electrode could selectively adsorb and distinguish (*R*)-thalidomdie and (*S*)-thalidomdie. Thus, we possibly will apply to use Raman spectroscopy to confirm the interactions between thalidomide enantiomer and MIPs exposed to a blood and protein-lipid mixture due to the high selectivity and binding capability of MIPs together with high sensitivity of SERS detection.

CHAPTER 8

CONCLUSIONS

In this research study, the design and development of (*R*), and (*S*)-thalidomide imprinted polymer nanoparticles and their use for application in selective recognition and sensor of chiral drugs was done. This thesis has several studies that focused on the investigation of the recognition of MIPs systems and the polymerization condition and the effects for obtaining the desirable particle size. The selectivity and capacity of the resulting MIP nanoparticles was used to the selective enrichment for the specific enantiomer from the solution.

Firstly, the synthesis of chiral binding sites during polymerization process of the imprinted MIP nanoparticles has been successfully produced. The selectivity of both the imprints is found two factors; the different mole ratio of two functional monomers component and the poly (styrene) as a seed core particles during polymer formation. For the rebinding of the template enantiomer on MIP nanoparticles for single enantiomer, it performed high selectivity within 24 hour that still provided high accessible distribution of thalidomide enantiomer of stereogenic entities to the imprinted cavities due to the interaction with complementary of functional groups containing on configurational biomimetic layer. The size of the pre-formed MIPs particles, after homoginization was 1-5 μm that exhibited the stable shape and size in the presence of PVA or PCL-T stabilizer.

Secondly, the assessment of the recognition ability for the artificial thalidomide imprinted polymers on MISPE had been successfully done, after the

separation before using a chiral HPLC method to measure the amount of stereoisomer species in an aqueous environment or the solvent mixture and the blood samples.

Thirdly, we described the development of thalidomide sensor for detection of the chiral drug enantiomers at low concentration in the buffer and whole blood sample based on microcontact imprinting technique. The molecularly imprinted polymer (MIP) nanoparticles were used as a stamp in a film of non-conducting polymer. Additionally, SERS was used to identify and characterize for the Raman spectra of a thalidomide imprinted polymer coating onto the glass substrate and the gold electrode that confirms the interactions between thalidomide enantiomer and MIPs exposed to the blood and the protein-lipid mixture together with the determination of thalidomide enantiomers when released in the biological fluid. Upon the IDC sensor measurement in the resistance polarization, that corresponded to the change of force values of one of thalidomide enantiomer on the surface. The surface of IDC sensor and surface-enhanced Raman scattering (SERS) can provide the detection of low concentrations in thalidomide enantiomers and the characterization in nanosized pore and surface topography of the polymer coating that protected the racemization of thalidomide enantiomers and to provide an excellent resistant signals and high selectivity, showing the robustness of devices. The MIP used in this study was proposed to monitor drug delivery of thalidomide enantiomers in blood sample and ease and rapid method for accelerating of clinical application.

In conclusion, the main aspects to achieve the artificial materials of the thalidomide enantiomers were used as a stationary phase in solid phase extraction and supported onto the coated thin films of interdigitated electrode. The critical key includes: (1) the selection of two functional monomers, (2) the

size and morphology of MIPs, (3) the poly (styrene) seed as core shell, and (4) the micropatterning for thalidomide enantiomers detection system. Consequently, for the future work chiral functional monomer for MIP synthesis should be used that can be used to screening of ligand binding and uses of thalidomide enantiomers in the biological matrix. The advantages of configurational biomimesis-MIP nanoparticles that have the high surface area provides the best accessibility at the specific binding sites that were related to the geometry of the MIP nanoparticles stamped into thin-film represent high sensitivity and robustness should be further developed the portable device or a lab-on-chip for real-time monitoring for analytical application. The MIP sensors have potential for study drug delivery application and to detect the enantiomers for clinical studies.

APPENDIX

A.1. Chromatogram of Standard (*R*)-thalidomide enantiomer at 8 μg mL^{-1}.

a. Standard (*R*)-thalidomide at 8 μg/mL
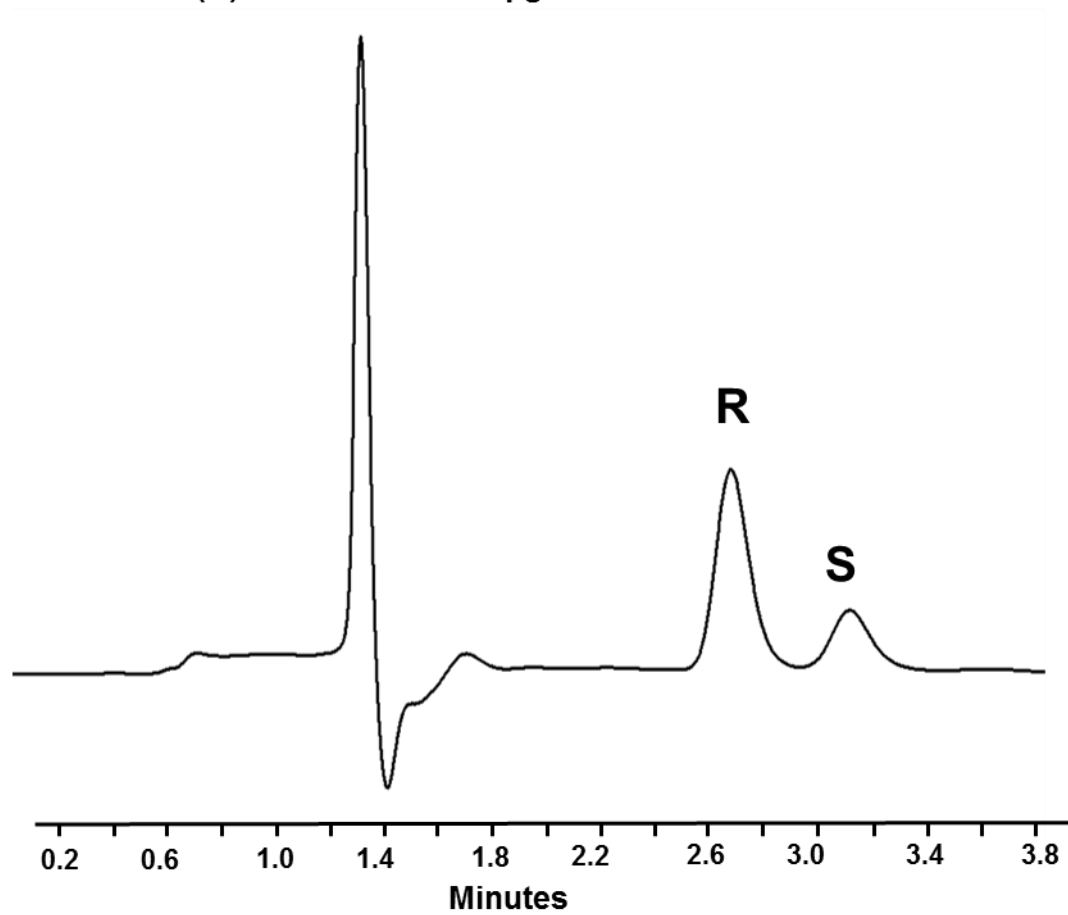
A.2. Chromatogram of Standard (*S*)-thalidomide enantiomer at 8 μg mL^{-1}.

b. Standard (*S*)-thalidomide at 8 μg/mL
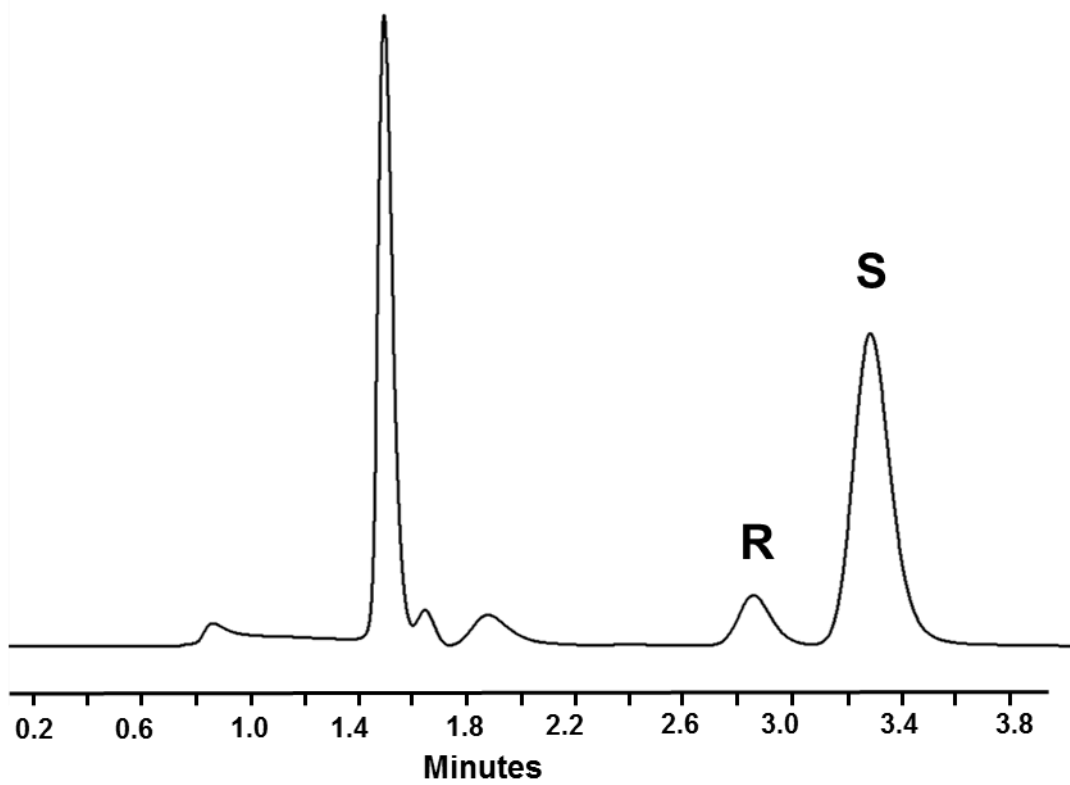
REFERENCES

Ahuja, S. 1997. The Important of Chiral Separations in Pharmaceuticals, In: The Impact of Stereochemistry on Drug Development and Use, Aboul-Enein, H. and Wainer I.W (eds.), Wiley-Interscience Publication, John Wiley & Son, Inc. New York. 312-315.

Allender, C., Heard, C. M. and Brian, K. 1997. Mobile Phase Effects on Enantiomer Resolution using Molecularly Imprinted Polymers. *Chirality*. 9: 238-242.

Andersson, L. 1996. Application of Molecular Imprinting to the Development of Aqueous Buffer and Organic Solvent Based Radioligand Binding Assays for (*S*)-Propranolol. *Analytical Chemistry*. 68: 111.

Arshady, R. and Mosbach, K. 1981. Synthesis of Substrate-Selective Polymers by Host-Guest Polymerization. *Makromol Chem*. 182: 687-692.

Aweeka, F., Trapnell, C., Chernoff, M., Jayewardene, A., Spritzler, J., Bellibas, S. E., Lizak, P. and Jacobson, J. 2001. Pharmacokinetics and Pharmacodynamics of Thalidomide in HIV Patients Treated for Oral Aphthous Ulcers: ACTG Protocol 251. *The Journal of Clinical Pharmacology*. 41: 1091-1097.

Bai, N. A. N., Cui, X.-Y., Wang, J. I. N., Sun, C.-G., Mei, H.-K., Liang, B.-B., Cai, Y. U. N., Song, X.-J., Gu, J.-K. and Wang, R. U. I. 2013. Determination of Thalidomide Concentration in Human Plasma by Liquid Chromatography-Tandem Mass Spectrometry. *Experimental and Therapeutic Medicine*. 5: 626-630.

Bajwa, S. Z., Mustafa, G., Samardzic, R., Wangchareansak, T. and Lieberzeit, P. A. 2012. Nanostructured Materials with Biomimetic Recognition Abilities for Chemical Sensing. *Nanoscale Research Letters*. 7: 1-7.

Binnig, G., Quate, C. F. and Gerber, C. 1986. Atomic Force Microscope. *Physical Review Letters*. 56: 930-933.

Birnbaumer, G. M., Lieberzeit, P. A., Richter, L., Schirhagl, R., Milnera, M., Dickert, F. L., Bailey, A. and Ertl, P. 2009. Detection of Viruses with Molecularly Imprinted Polymers Integrated on a Microfluidic Biochip using Contact-less Dielectric Microsensors. *Lab on a Chip*. 9: 3549-3556.

Cacho, C., Turiel, E., Martín-Esteban, A., Pérez-Conde, C. and Cámara, C. 2003. Clean-up of Triazines in Vegetable Extracts by Molecularly-Imprinted Solid-Phase Extraction Using a Propazine-Imprinted Polymer. *Analytical and Bioanalytical Chemistry*. 376: 491-496.

Chang, L., Ding, Y. and Li, X. 2013. Surface Molecular Imprinting onto Silver Microspheres for Surface Enhanced Raman Scattering Applications. *Biosensors and Bioelectronics*. 50: 106-110.

Christopher, L. J., Estroff, L. A., Kriebel, K. J., Nuzzo, G. R., and Whitesides., M. G. 2005. Self-Assembled Monolayers of Thiolates on Metals as a Form of Nanotechnology. *ChemIcal Reviews*. 105: 1103−1169.

Cipriani, P. and Smith, C. Y. 2008. Characterization of Thalidomide using Raman Spectroscopy. *Spectrochimica Acta Part A: Molecular and Biomolecular Spectroscopy*. 69: 333-337.

Ding, X. and Heiden, P. A. 2014. Recent Developments in Molecularly Imprinted Nanoparticles by Surface Imprinting Techniques. *Macromolecular Materials and Engineering*. 299: 268-282.

Dufrene, Y. F. 2009. Atomic Force Microscopy: A Powerful Molecular Toolkit in Nanoproteomics. *Proteomics*. 9: 5400–5405.

Ellis, G., Hendra, P. J., Hodges, C. M., Jawhari, T., Jones, C. H. and Le Barazer, P. 1989. Routine Analytical Fourier Transform Raman Spectroscopy. *Analyst*. 114: 1061-1066.

Eriksson, T., Björkman, S., Fyge, Å. and Ekberg, H. 1992. Determination of Thalidomide in Plasma and Blood by High-Performance Liquid Chromatography: Avoiding Hydrolytic Degradation. *Journal of Chromatography B*. 582: 211-216.

Eriksson, T., Björkman, S. and Höglund, P. 2001. Clinical Pharmacology of Thalidomide. *European Journal of Clinical Pharmacology*. 57: 365–376.

Findeisen, A., Wackerlig, J., Samardzic, R., Pitkänen, J., Anttalainen, O., Dickert, F. L. and Lieberzeit, P. A. 2012. Artificial Receptor Layers for Detecting Chemical and Biological Agent Mimics. *Sensors and Actuators B*: *Chemical*. 170: 196-200.

Fotiadis, D., Scheuring, S., Müller, S. A., Engel, A. and Müller, D. J. 2002. Imaging and Manipulation of Biological Structures with the AFM. *Micron*. 33: 385-397.

Fuchs, Y., Soppera, O. 2012. Photopolymerization and Photostructuring of Molecularly Imprinted Polymers for Sensor Applications—A Review. *Analytical. Chemistry*. 717. 7-20.

Fujita, J., Mestre, J. R., Zeldis, J. B., Subbaramaiah, K. and Dannenberg, A. J. 2001. Thalidomide and Its Analogues Inhibit Lipopolysaccharide-Mediated Induction of Cyclooxygenase-2. *Clinical Cancer Research*. 7: 3349.

Gao, F. X., Ma, X. T., He, X. W., Li, W. Y. and Zhang, Y. K. 2013. Smart Surface Imprinting Polymer Nanospheres for Selective Recognition and Separation of Glycoprotein. *Colloids and Surfaces A: Physicochemical and Engineering Aspects*. 433: 191-199.

Gebbert, A., Alvarez-Icaza, M., Stoecklein, W. and Schmid R. D. 1992. Real-Time Monitoring of Immunochemical Interactions with a Tantalum Capacitance Flow-Through Cell. *Analytical Chemistry*. 64: 997-1003.

Ghosh, S., Chakraborty, I., Chakraborty, M., Mukhopadhyay, A., Mishra, R. and Sarkar, D. 2016. Evaluating the Morphology of Erythrocyte Population: An Approach Based on Atomic Force Microscopy and Flow Cytometry. *Biochimica et Biophysica Acta BBA-Biomembranes*. 1858: 671-681.

Haginaka, J., Takehira, H., Hosoya, K. and Tanaka, N. 1998. Molecularly Imprinted Uniform-Sized Polymer-Based Stationary Phase for Naproxen: Comparison of Molecular Recognition Ability of the Molecularly Imprinted Polymers Prepared by Thermal and Redox Polymerization Techniques. *Journal of Chromatography A*. 816: 113-121.

Haginaka, J., Takehira, H., Hosoya, K. and Tanaka, N. 1999. Uniform-Sized Molecularly Imprinted Polymer for (*S*)-naproxen Selectively Modified with Hydrophilic External Layer. *Journal of Chromatography A*. 849: 331-339.

Haginaka, J. and Sanbe, H. 2000. Uniform-Sized Molecularly Imprinted Polymers for 2-arylpropionic Acid Derivatives Selectively Modified with Hydrophilic External Layer and Their Applications to Direct Serum Injection Analysis. *Analytical Chemistry*. 72: 5206-5210.

Hall, R. H. 2002. Biosensor Technologies for Detecting Microbiological Foodborne Hazards. *Microbes and Infection*. 4: 425-432.

Hamidi, M., Azadi, A. and Rafiei, P. 2008. Hydrogel Nanoparticles in Drug Delivery. *Advanced Drug Delivery Reviews*. 60: 1638-1649.

Han, L., Daniel, D. R., Maye, M. M. and Zhong, C.-J. 2001. Core−Shell Nanostructured Nanoparticle Films as Chemically Sensitive Interfaces. *Analytical Chemistry*. 73: 4441-4449.

Haupt, K. and Mosbach, K. 2000. Molecularly Imprinted Polymers and Their Use in Biomimetic Sensors. *Chemical Reviews*. 100: 2495-2504.

Haupt, K. 2003. Peer Reviewed: Molecularly Imprinted Polymers: The Next Generation. *Analytical Chemistry*. 75: 376A-383A.

Hawari, H. F., Samsudin, N. M., Shakaff, A. Y. M., Wahab, Y., Hashim, U. and Zakaria, A. 2013. Highly Selective Molecular Imprinted Polymer (MIP) based Sensor Array using Interdigitated Electrode (IDE) Platform for Detection of Mango Ripeness. *Sensors and Actuators B: Chemical*. 187: 434-444.

Hinterdorfer, P. and Dufrene, Y. F. 2006. Detection and Localization of Single Molecular Recognition Events Using Atomic Force Microscopy. *Nature Methods*. 3: 347-355.

Hosoya, K., Yoshizako, K., Tanaka, N., Kimata, K., Araki, T. and Haginaka, J. 1994. Uniform-Size Macroporous Polymer-based Stationary Phase for HPLC Prepared through Molecular Imprinting Technique. *Chemistry Letters*. 23: 1437-1438.

Hosoya, K., Yoshizako, K., Shirasu, Y., Kimata, K., Araki, T., Tanaka, N. and Haginaka, J. 1996. Molecularly Imprinted Uniform-Size Polymer-Based Stationary Phase for High-Performance Liquid Chromatography Structural Contribution of Cross-linked Polymer Network on Specific Molecular Recognition. *Journal of Chromatography A*. 728: 139-147.

Hoshino, Y., Kodama, T., Okahata, Y. and Shea, K. J. 2008. Peptide Imprinted Polymer Nanoparticles: A Plastic Antibody. *Journal of the American Chemical Society*. 130: 15242-15243.

Hoshino, Y., Koide, H., Urakami, T., Kanazawa, H., Kodama, T., Oku, N. and Shea, K. J. 2010. Recognition, Neutralization, and Clearance of Target Peptides in the Bloodstream of Living Mice by Molecularly Imprinted Polymer Nanoparticles: A Plastic Antibody. *Journal of the American Chemical Society*. 132: 6644-6645.

Hugel, T. and Seitz, M. 2001. The Study of Molecular Interactions by AFM Force Spectroscopy. *Macromolecular Rapid Communications*. 22: 989-1016.

Hulanicki, A., Glab, S. and Ingman, F. 1991. Chemical Sensors Definitions and Classification. *Pure and Applied Chemistry*. 63: 1247-1250.

Ibrahim, M., Claudel, J., Kourtiche, D. and Nadi, M. 2013. Geometric Parameters Optimization of Planar Interdigitated Electrodes for Bioimpedance Spectroscopy. *Journal of Electrical Bioimpedance*. 4: 13-22.

Igor, M. and Tigran, A. 2015. Control of a Two-Body Precision Turntable Electromechanical System in the Presence of Friction. Biophotonics for Medical Applications. *IFAC-Papers Online*. 48-25: 283–286.

Joshi, V. P., Kulkarni, M. G. and Mashelkar, R. A. 2000. Enhancing Adsorptive Separations by Molecularly Imprinted Polymers: Role of Imprinting Techniques and System Parameters. *Chemical Engineering Science*. 55: 1509-1522.

Jungreuthmayer, C., Birnbaumer, G. M., Ertl, P. and Zanghellini, J. 2012. Improving the Measurement Sensitivity of Interdigital Dielectric Capacitors (IDC) by Optimizing the Dielectric Property of the Homogeneous Passivation Layer. *Sensors and Actuators B: Chemical*. 162: 418-424.

Kasas S, Dietler G. 2008. Probing Nanomechanical Properties from Biomolecules to Living Cells. *Pflugers Arch-European Journal of Physiology*. 456: 13–27.

Kim, D. T., Blanch, H. W., Radke, C. J. 2002. Direct Imaging of Lysozyme Adsorption onto Mica by Atomic Force Microscopy. *Langmuir*. 18: 5841-5850.

Kirsch, N., Hedin-Dahlström, J., Henschel, H., Whitcombe, M. J., Wikman, S. and Nicholls, I. A. 2009. Molecularly Imprinted Polymer Catalysis of a Diels-Alder Reaction. *Journal of Molecular Catalysis B: Enzymatic*. 58: 110-117.

Kor, K. and Zarei, K. 2016. Development and Characterization of an Electrochemical Sensor for Furosemide Detection Based on Electropolymerized Molecularly Imprinted Polymer. *Talanta*. 146: 181-187.

Kriz, D., Ramstroem, O., Svensson, A. and Mosbach, K. 1995. A Biomimetic Sensor Based on a Molecularly Imprinted Polymer as a Recognition Element Combined with Fiber-Optic Detection. *Analytical Chemistry*. 67: 2142-2144.

Kryscio, D. R., Peppas, N. A. 2009. Mimicking Biological Delivery Through Feedback-Controlled Drug Release Systems based on Molecular Imprinting. *AIChE Journal*. 55: 1311-1324.

Kumar, S., Witzig, T. E. and Rajkumar, S. V. 2004. Thalidomide: Current Role in the Treatment of Non-plasma Cell Malignancies. *Journal of Clinical Oncology*. 22: 2477-2488.

Last, J. A., Russell, P., Nealey, P. F. and Murphy, C. J. 2010. The Applications of Atomic Force Microscopy to Vision Science. *Investigative Ophthalmology & Visual Science.* 51: 6083-6094.

Latif, U., Mujahid, A., Afzal, A., Sikorski, R., Lieberzeit, P. A. and Dickert, F. L. 2011. Dual and Tetraelectrode QCMs using Imprinted Polymers as Receptors for Ions and Neutral Analytes. *Analytical and Bioanalytical Chemistry*. 400: 2507-2515.

Li, W. H. and Stöver, H. D. H. 1998. Porous Monodisperse Poly(divinylbenzene) Microspheres by Precipitation Polymerization. *Journal of Polymer Science, Part A: Polymer Chemistry*. 36: 1543-1551.

Li, X., Liu, X. and Wang, J. 2003. Thalidomide Downregulates the Expression of VEGF and bFGF in Cisplatin-resistant Human Lung Carcinoma Cells. *Anticancer Research*. 23: 2481-2487.

Li, J., Chen, Z. and Li, Y. 2011. A Strategy for Constructing Sensitive and Renewable Molecularly Imprinted Electrochemical Sensors for Melamine Detection. *Analytica Chimica Acta*. 706: 255-260.

Lian, W., Liu, S., Yu, J., Xing, X., Li, J., Cui, M. and Huang, J. 2012. Electrochemical Sensor based on Gold Nanoparticles Fabricated Molecularly Imprinted Polymer Film at Chitosan-Platinum Nanoparticles/Graphene–Gold Nanoparticles Double Nanocomposites Modified Electrode for Detection of Erythromycin. *Biosensors and Bioelectronics*. 38: 163-169.

Lieberzeit, P. A., Afzal, A., Glanzing, G. and Dickert, F. L. 2007. Molecularly Imprinted Sol–Gel Nanoparticles for Mass-Sensitive Engine Oil Degradation Sensing. *Analytical and Bioanalytical Chemistry*. 389: 441-446.

Lieberzeit, P. A., Afzal, A., Rehman, A. and Dickert, F. L. 2007. Nanoparticles for Detecting Pollutants and Degradation Processes with Mass-Sensitive Sensors. *Sensors and Actuators B: Chemical*. 127: 132-136.

Liu, F., Liu, X., Ng, S.-C. and Chan, H. S.-O. 2006. Enantioselective Molecular Imprinting Polymer Coated QCM for the Recognition of l-tryptophan. *Sensors and Actuators B*: *Chemical*. 113: 234-240.

Liu, B., Cang, H. and Jin, J. 2016. Molecularly Imprinted Polymers Based Electrochemical Sensor for 2, 4-Dichlorophenol Determination. *Polymers*. 8: 309 (1-9).

Lockman, P. R., Mumper, R. J., Khan, M. A. and Allen, D. D. 2002. Nanoparticle Technology for Drug Delivery Across the Blood-Brain Barrier. *Drug Development and Industrial Pharmacy*. 28: 1-13.

Lynd, N. A. and Hillmyer, M. A. 2005. Influence of Polydispersity on the Self-Assembly of Diblock Copolymers. *Macromolecules*. 38: 8803-8810.

Lyon, A. W., Duran, G. and Raisys, V. A. 1995. Determination of Thalidomide by High Performance Liquid Chromatography: Methodological Strategy for Clinical Trials. *Clinical Biochemistry*. 28: 467-470.

Mairhofer, J., Roppert, K. and Ertl, P. 2009. Microfluidic Systems for Pathogen Sensing: A Review. *Sensors*. 9: 4804-4823.

Martín-Esteban, A. 2013. Molecularly-Imprinted Polymers as a Versatile, Highly Selective Tool in Sample Preparation. *TrAC Trends in Analytical Chemistry*. 45: 169-181.

Mayes, A. G. and Mosbach, K. 1996. Molecularly Imprinted Polymer Beads: Suspension Polymerization Using a Liquid Perfluorocarbon as the Dispersing Phase. *Analytical Chemistry*. 68: 3769-3774.

Mayes, A. G. and Whitcombe, M. J. 2005. Synthetic Strategies for the Generation of Molecularly Imprinted Organic Polymers. *Advanced Drug Delivery Reviews*. 57: 1742-1778.

McBride, W. G. 1977. Thalidomide Embryopathy. *Teratology*. 16: 79-82.

McConathy, J. and Owens, M. J. 2003. Stereochemistry in Drug Action. *Primary Care Companion to The Journal of Clinical Psychiatry*. 5: 70-73.

Meyring, M., Chankvetadze, B. and Blaschke, G. 2000. Simultaneous Separation and Enantioseparation of Thalidomide and its Hydroxylated Metabolites Using High-Performance Liquid Chromatography in Common-size Columns, Capillary Liquid Chromatography and Nonaqueous Capillary Electrochromatography. *Journal of Chromatography A*. 876: 157-167.

Mirzajani, R., Ramezani, Z. and Kardani, F. 2017. Selective Determination of Thidiazuron Herbicide in Fruit and Vegetable Samples using Molecularly Imprinted Polymer Fiber Solid Phase Microextraction with Ion Mobility Spectrometry Detection (MIPF-SPME-IMS). *Microchemical Journal*. 130: 93-101.

Mosbach, K. and Ramson, O. 1996. The Emerging Technique of Molecular Imprinting and Its Future Impact on Biotechnology. *Bio/Technology*. 14: 163-170.

Mustafa, G., Hussain, M., Iqbal, N., Dickert, F. L. and Lieberzeit, P. A. 2012. Quartz Crystal Microbalance Sensor based on Affinity Interactions between Organic Thiols and Molybdenum Disulfide Nanoparticles. *Sensors and Actuators. B*: *Chemical*. 162: 63-67.

Mustafa, G. and Lieberzeit, P. A. 2014. Molecularly Imprinted Polymer-Ag$_2$S Nanoparticle Composites for Sensing Volatile Organics. *RSC Advances*. 4: 12723-12728.

Murphy, S., Boyle, F. M., Davey, R. A. and Gu X-Q, Mather L. E. 2007. Enantioselectivity of Thalidomide Serum and Tissue Concentrations in a Rat Glioma Model and Effects of Combination Treatment with Cisplatin and BCNU. *Journal of Pharmacy and Pharmacology*. 59: 105-114.

Muller D. J. 2008. AFM: A Nanotool in Membrane Biology. *Biochemistry*. 47: 7986-7998.

Nestora, S., Merlier, F., Prost, E., Haupt, K., Rossi, C. and Tse Sum Bui, B. 2016. Solid-Phase Extraction of Betanin and Isobetanin from Beetroot Extracts Using a Dipicolinic Acid Molecularly Imprinted Polymer. *Journal of Chromatography A*. 1465: 47-54.

Nilsson G. E. 1977. Measurement of Water Exchange through Skin. *Medical and Biological Engineering and Computing*. 15: 209-218.

Oberländer, J., Jildeh, B. Z., Kirchner, P., Wendeler, L., Bromm, A., Iken, H., Wagner, P., Keusgen, M. and Schöning, J. M. 2015. Study of Interdigitated Electrode Arrays Using Experiments and Finite Element Models for the Evaluation of Sterilization Processes. *Sensors*. 15: 26115-26127.

Owens, P. K., Karlsson, L., Lutz, E. S. M., Andersson, L. I. 1999. Molecular Imprinting for Bio-and Pharmaceutical Analysis. *Trends in Analytical Chemistry*. 18: 146-154.

Polreichova, M., Latif, U. and Dickert, F. L. 2011. Functionalized Polymers as Receptors for Detection of Cells. *Australian Journal of Chemistry*. 64: 1256-1260.

Poma, A., Guerreiro, A., Whitcombe, M. J., Piletska, E. V., Turner, A. P. F. and Piletsky, S. A. 2013. Solid-Phase Synthesis of Molecularly Imprinted Polymer Nanoparticles with a Reusable Template-"Plastic Antibodies". *Advanced Functional Materials*. 23: 2821-2827.

Reddy, S. M., Sette, G. and Phan, Q. 2011. Electrochemical Probing of Selective Haemoglobin Binding in Hydrogel-Based Molecularly Imprinted Polymers. *Electrochimica Acta*. 56: 9203-9208.

Reepmeyer, J. C. 1996. Separation of *R*- and *S*-Thalidomide by Reversed-Phase HPLC with β-cyclodextrin in the mobile phase. *Chirality*. 8: 11-17.

Sambe, H., Hoshina, K. and Haginaka, J. 2007. Molecularly Imprinted Polymers for Triazine Herbicides Prepared by Multi-Step Swelling and Polymerization Method: Their Application to the Determination of Methylthiotriazine Herbicides in River Water. *Journal of Chromatography A*. 1152: 130-137.

Sampaio, E. P., Sarno, E. N., Galilly, R., Cohn, Z. A. and Kaplan, G. 1991. Thalidomide Selectively Inhibits Tumor Necrosis Factor Alpha Production by Stimulated Human Monocytes. *The Journal of Experimental Medicine*. 173: 699.

Sanbe, H. and Haginaka, J. 2003. Restricted access media-molecularly imprinted polymer for propranolol and its application to direct injection analysis of β-blockers in biological fluids. Analyst. 128: 593-597.

Schirhagl, R., Lieberzeit, P. A. and Dickert, F. L. 2010. Chemosensors for Viruses Based on Artificial Immunoglobulin Copies. *Advanced Materials*. 22: 2078-2081.

Schirhagl, R. 2014. Bioapplications for Molecularly Imprinted Polymers. *Analytical Chemistry*. 86: 250-261.

Sellergren, B. and Andersson, L. 1990. Molecular Recognition in Macroporous Polymers Prepared by a Substrate Analogue Imprinting Strategy. *Journal of Organic Chemistry*. 55(10): 3381-3383.

Sener, G., Ozgur, E., Yılmaz, E., Uzun, L., Say, R. and Denizli, A. 2010. Quartz Crystal Microbalance based Nanosensor for Lysozyme Detection with Lysozyme Imprinted Nanoparticles. *Biosensors and Bioelectronics*. 26: 815-821.

Sener, G., Uzun, L., Say, R. and Denizli, A. 2011. Use of Molecular Imprinted Nanoparticles as Biorecognition Element on Surface Plasmon Resonance Sensor. *Sensors and Actuators B: Chemical*. 160: 791-799.

Singh, R., Verma, R., Kaushik, A., Sumana, G., Sood, S., Gupta, R. K. and Malhotra, B. D. 2011. Chitosan-Iron Oxide Nano-Composite Platform for Mismatch-Discriminating DNA Hybridization for Neisseria Gonorrhoeae Detection Causing Sexually Transmitted Disease. *Biosensors and Bioelectronics*. 26: 2967-2974.

Silvestri, D.; Borrelli, C.; Giusti, P.; Cristallini, C.; Ciardelli, G. 2005. Polymeric Devices Containing Imprinted Nanospheres: A Novel Approach to Improve Recognition in Water for Clinical Uses. *Analytica Chimica Acta*. 542: 3-13.

Sokolov, I. 2007. Atomic Force Microscopy in Cancer Cell Research. Edited by Hari Singh Nalwa and Thomas Webster. *American Scientific Publishers' Inc*. ISBN: 1-58883-071-3. 1-17.

Sontimuang, C., Suedee, R. and Dickert, F. 2011. Interdigitated Capacitive biosensor based on Molecularly Imprinted Polymer for Rapid Detection of Hev b1 Latex Allergen. *Analytical Biochemistry*. 410: 224-233.

Subrahmanyam, S., Guerreiro, A., Poma, A., Moczko, E., Piletska, E. and Piletsky, S. 2013. Optimisation of Experimental Conditions for Synthesis of High Affinity MIP Nanoparticles. *European Polymer Journal*. 49: 100-105.

Suksuwan, A., Lomlim, L., Rungrotmongkol, T., Nakpheng, T., Dickert, F. L. and Suedee, R. 2015. The Composite Nanomaterials Containing (*R*)-thalidomide-Molecularly Imprinted Polymers as a Recognition System for Enantioselective-Controlled Release and Targeted Drug Delivery. *Journal of Applied Polymer Science*. 132: 41930 (1-21).

Suedee, R., Srichana, T., Chotivatesin, R. and Martin, G. P. 2002. Stereoselective Release Behaviors of Imprinted Bead Matrices. *Drug Development and Industrial Pharmacy*. 28: 545-554.

Suedee, R., Srichana, T., Sangpagai, C., Tunthana, C. and Vanichapichat, P. 2004. Development of Trichloroacetic Acid Sensor Based on Molecularly Imprinted Polymer Membrane for the Screening of Complex Mixture of Haloacetic Acids in Drinking Water. *Analytica Chimica Acta*. 504: 89-100.

Suedee, R., Intakong, W. and Dickert, F. L. 2006. Molecularly Imprinted Polymer-Modified Electrode for On-line Conductometric Monitoring of Haloacetic Acids in Chlorinated Water. *Analytica Chimica Acta*. 569: 66-75.

Sun, L., Sun, X., Zheng, Y., Lin, Q., Su, H. and Qi, C. 2017. Fabrication and Characterization of Core-Shell Polystyrene/polyaniline/Au Composites and their Catalytic Properties for the Reduction of 4-nitrophenol. *Synthetic Metals*. 224: 1-6.

Tamayo, F. G., Casillas, J. L. and Martin-Esteban, A. 2003. Highly Selective Fenuron-Imprinted Polymer with a Homogeneous Binding Site Distribution Prepared by Precipitation Polymerisation and Its Application to the Clean-Up of Fenuron in Plant Samples. *Analytica Chimica Acta*. 482: 165-173.

Tamayo, F. G., Casillas, J. L. and Martin-Esteban, A. 2005. Clean Up of Phenylurea Herbicides in Plant Sample Extracts Using Molecularly Imprinted Polymers. *Analytical and Bioanalytical Chemistry*. 381: 1234-1240.

Tamayo, F. G., Casillas, J. L. and Martin-Esteban, A. 2005. Evaluation of New Selective Molecularly Imprinted Polymers Prepared by Precipitation Polymerisation for the Extraction of Phenylurea Herbicides. *Journal of Chromatography A*. 1069: 173-181.

Teo, S. K., Colburn, W. A. and Thomas, S. D. 1999. Single-Dose Oral Pharmacokinetics of Three Formulations of Thalidomide in Healthy Male Volunteers. *The Journal of Clinical Pharmacology*. 39: 1162-1168.

Teo, S. K., Colburn, W. A., Tracewell, W. G., Kook, K. A., Stirling, D. I., Jaworsky, M. S., Scheffler, M. A., Thomas, S. D. and Laskin, O. L. 2004. Clinical Pharmacokinetics of Thalidomide. *Clinical Pharmacokinetics*. 43: 311-327.

Terzopoulou, Z., Papageorgiou, M., Kyzas, G. Z., Bikiaris, D. N. and Lambropoulou, D. A. 2016. Preparation of Molecularly Imprinted Solid-Phase Microextraction Fiber for the Selective Removal and Extraction of the Antiviral Drug Abacavir in Environmental and Biological Matrices. *Analytica Chimica Acta*. 913: 63-75.

Vaihinger, D., Landfester, K., Kräuter, I., Brunner, H. and Tovar, G. E. M. 2002. Molecularly Imprinted Polymer Nanospheres as Synthetic Affinity Receptors Obtained by Miniemulsion Polymerisation. *Macromolecular Chemistry and Physics*. 203: 1965-1973.

Vargesson, N. 2015. Thalidomide-induced Teratogenesis: History and Mechanisms. *Birth Defects Research Part C: Embryo Today: Reviews*. 105: 140-156.

Vlatakis, G., Andersson, L. I., Miller, R. and Mosbach, K. 1993. Drug Assay using Antibody Mimics Made by Molecular Imprinting. *Nature*. 361: 645-647.

Wackerlig, J. and Lieberzeit, P. A. 2015. Molecularly Imprinted Polymer Nanoparticles in Chemical Sensing Synthesis, Characterisation and Application. *Sensors and Actuators, B: Chemical*. 207: 144-157.

Wangchareansak, T., Sangma, C. 2013. Self-assembled Glucosamine Monolayers as Biomimetic Receptors for Detecting WGA Lectin and Influenza Virus with a Quartz Crystal Microbalance. *Analytical and Bioanalytical Chemistry*. 405: 6471-6478.

Weinz, C. and Blaschke, G. 1995. Investigation of the in vitro Biotransformation and Simultaneous Enantioselective Separation of Thalidomide and its Neutral Metabolites by Capillary Electrophoresis. *Journal of Chromatography B: Biomedical Sciences and Applications*. 674: 287-292.

Whitcombe, M. J., Rodriguez, M. E., Villar, P. and Vulfson, E. N. 1995. A New Method for the Introduction of Recognition Site Functionality into Polymers Prepared by Molecular Imprinting: Synthesis and Characterization of Polymeric Receptors for Cholesterol. *Journal of the American Chemical Society*. 117: 7105-7111.

Wulff, G and Sarhan, A. 1972. Use of Polymers with Enzyme-Analogous Structures for the Resolution of Racemates. *Angewandte Chemie International Edition in English.* 11: 341–342.

Wulff, G. 2013. Fourty Years of Molecular Imprinting in Synthetic Polymers: Origin, Features and Perspectives. *Microchimica Acta.* 180: 1359-1370.

Xu, Z. X., Gao, H. J., Zhang, L. M., Chen, X. Q. and Qiao, X. G. 2011. The Biomimetic Immunoassay Based on Molecularly Imprinted Polymer: A Comprehensive Review of Recent Progress and Future Prospects. *Journal of Food Science.* 76: R69-R75.

Yager, P., Edwards, T., Fu, E., Helton, K., Nelson, K., Tam, M. R. and Weigl, B. H. 2006. Microfluidic Diagnostic Technologies for Global Public Health. *Nature.* 442: 412-418.

Yang, M., Guo, Y., Wu, Q., Luan, Y. and Wang, G. 2014. Synthesis and Properties of Amphiphilic Nonspherical SPS/PS Composite Particles by Multi-step Seeded Swelling Polymerization. *Polymer.* 55: 1948-1954.

Ye, L., A. G. Cormack, P. and Mosbach, K. 1999. Molecularly Imprinted Monodisperse Microspheres for Competitive Radioassay. *Analytical Communications.* 36: 35-38.

Ye, L., Weiss, R. and Mosbach, K. 2000. Synthesis and Characterization of Molecularly Imprinted Microspheres. *Macromolecules.* 33: 8239-8245.

Yoshimatsu, K., Reimhult, K., Krozer, A., Mosbach, K., Sode, K. and Ye, L. 2007. Uniform molecularly imprinted microspheres and nanoparticles prepared by precipitation polymerization: The control of particle size suitable for different analytical applications. *Analytica Chimica Acta.* 584: 112-121.

Zhang, J. H., Jiang, M., Zou, L., Shi, D., Mei, S. R., Zhu, Y. X., Shi, Y., Dai, K. and Lu, B. 2006. Selective Solid-phase Extraction of Bisphenol A Using Molecularly Imprinted Polymers and its Application to Biological and Environmental Samples. *Analytical and Bioanalytical Chemistry*. 385: 780-786.

Zorita, S., Boyd, B., Jönsson, S., Yilmaz, E., Svensson, C., Mathiasson, L. and Bergström, S. 2008. Selective Determination of Acidic Pharmaceuticals in Wastewater Using Molecularly Imprinted Solid-phase Extraction. *Analytica Chimica Acta*. 626: 147-154.

VITAE

Name   Miss Sirirat Rakkit

Student ID   5610730005

Educational Attainment

Degree	Name of Institution	Year of Graduation
Bachelor of Science (Chemistry)	Prince of Songkla University	2010

Scholarship Awards during Enrolment

1. National Research University (NRU), Prince of Songkla University

2. Drug Delivery System Excellence Center (DDSEC), Grant of Faculty of Pharmaceutical Sciences, Prince of Songkla University.

List of Publication and Proceeding

Proceeding

Srichana, R. and Rakkit, S. 2012. Manipulation of Template-Monomer Complexation onto a Solid Particle within an Organic Polymer Environment. Oral presentation at The 2nd Current Drug Development (CDD), Phuket Graceland Resort & Spa, Phuket, Thailand, May 2-4.

Suedee, R., Rakkit, S., and Treetong, A. 2014. Preparation and Characterization of Selective Patterning of Thalidomide Enantiomers by Molecular Imprinting Technique. Poster presentation at The 3rd Current Drug Development (CDD). Pavilion Queen's Bay Krabi Ao Nang Beach, Thailand, May 1-3.

Rakkit, S., Srichana, R. and Treetong. A. 2016. AFM and Raman-AFM for Characterization of Thalidomide Imprinted Polymer Nanoparticles Supported Thin Films. Poster presentation at Thailand-Japan (NIMS) Collaborative Seminar 26th-27th May, Dusit Thani Bangkok, Thailand.

Rakkit, S., Srichana, R. and Treetong. 2016. (*R*)-, and (*S*)-thalidomide Imprinted Polymer Nanoparticles as Thin Films Supported onto Interdigitated Capacitive Electrode for Analytical Application. Oral and poster presentation at Asian Graduate Congress on Pharmaceutical Technology, National University of Singapore, Singapore, July 10-13.

Rakkit, S., Srichana, R. and Treetong. 2016. Thalidomide Imprinted Nanoparticles on Thin-Film Layers of Interdigitated Capacitive Electrode for Sensor Application. Poster presentation at Nano Thailand 2016, the greenery resort Khao Yai, Nakhon Ratchasima, Thailand, November 27-29.

Publication

Jaiswal, L., Rakkit, S., Pochin, K., Jaisamut, P., Tanthana, C., Tanmanee, N., Srichana, T. and Suedee, R. 2015 A thalidomide templated molecularly imprinted polymer that promotes a biologically active chiral entity tagged in colon carcinoma cells and protein-related immune activation. *Process Biochemistry*. 50: 2035-2050.

Exhibition

Srichana, R., Rakkit, S. and Naklua, W. 2015. Sensor for Use in Online Detection of Rubber Latex-associated Allergen Protein. Poster presentation at Seoul International Invention Fair 2015" (SIIF 2015). Coex exhibition hall, Seoul, Korea, November 26-29.

Awards

Srichana, R., Rakkit, S. and Naklua, W. 2015. Silver prize for poster presentation, Sensor for Use in Online Detection of Rubber Latex-associated Allergen Protein at Seoul International Invention Fair 2015 (SIIF 2015). Coex exhibition hall, Seoul, Korea, November 26-29.

Rakkit, S., Srichana, R. and Treetong. 2016. The best poster award presentation, (*R*)-, and (*S*)-thalidomide Imprinted Polymer Nanoparticles as Thin Films Supported onto Interdigitated Capacitive Electrode for Analytical Application at Asian Graduate Congress on Pharmaceutical Technology, National University of Singapore (NUS), Singapore, July 10-13.